TECHNISCHE UNIVERSITÄT MÜNCHEN

WACKER-Lehrstuhl für Makromolekulare Chemie

Rational Design, Synthesis, Characterization and Application of Carbene-Centered Pincer Complexes for Small Molecules Conversion

Andriy Plikhta

Vollständiger Abdruck der von der Fakultät für Chemie
der Technischen Universität München zur Erlangung des akademischen Grades eines
Doktors der Naturwissenschaften genehmigten Dissertation.

Vorsitzender: Prof. Dr. Tom Nilges

Prüfer der Dissertation:

1. Prof. Dr. Dr. h.c. Bernhard Rieger
2. Prof. Dr. Klaus Köhler

Die Dissertation wurde am 08.06.2016 bei der Technischen Universität München eingereicht und durch die Fakultät für Chemie am 12.12.2016 angenommen.

Technische Universität München

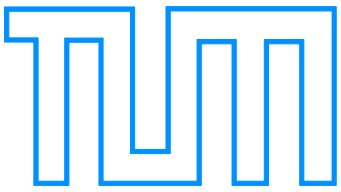

WACKER Lehrstuhl für Makromolekulare Chemie

Rational Design, Synthesis, Characterization and Application of Carbene-Centered Pincer Complexes for Small Molecules Conversion

Rationales Design, Synthese, Charakterisierung und Anwendung von Carben-Zentrierten Pinzerkomplexen für die Umsetzung Kleiner Moleküle

Dissertation

Zur Erlangung des akademischen Grades eines

Doktors der Naturwissenschaften

vorgelegt von

Andriy Plikhta

Garching bei München, Mai 2016

Für
meine Eltern

Die vorliegende Arbeit entstand in der Zeit von August 2010 bis Januar 2014 am WACKER-Lehrstuhl für Makromolekulare Chemie unter der Betreuung von Prof. Dr. Dr. h.c. Bernhard Rieger.

Acknowledgments

I want to express special gratitude to Dr. Dr. h.c. Bernhard Rieger for taking me to his working group and for his contribution to my professional development, for the support, guidance, confidence, interesting discussions, and fascinating area of research. I want to thank Dr. Carsten Troll for his help in solving practical problems and organizational issues.

My special thanks go to Dr. Sergei Vagin for fruitful discussions, criticism and strong support. I highly appreciate the fact that I had an opportunity to adopt his experience and skills to solve problems in the field of preparative chemistry, as well as in work with analytical equipment.

I am grateful for a generous scholarship from the Konrad-Adenauer-Foundation, whose ideological and financial support became a strong foundation for my development.

Also the words of gratitude relate to all colleagues and employees of WACKER-Chair of Macromolecular Chemistry for the pleasant working atmosphere, valuable advice, communication and good mood.

I am infinitely grateful to my parents Plikhta Natalia and Plikhta Nikolay as well as to my dear friends for invaluable support and understanding during the whole graduate education and doctoral dissertation. Without you I would not be able to come to everything, what has been achieved.

List of General Abbreviations

[bmim]	1-n-butyl-3-methylimidazolium
CO	carbonyl or carbon monoxide
COD	cycloocta-1,5-diene
D	*cis*-donor
DMSO	dimethyl sulfoxide
DMF	dimethyl formamide
E	*trans*-donor
EA	elemental analysis
ESI MS	Electrospray ionization mass spectrometry
FG	functional group
GC	gas chromatography
HBPin	pinacolborane
IL	ionic liquid
IR	infrared
L	ligand
M	metal
MS	mass spectrometry
[NEt_4]	tetraethylammonium
[NBu_4]	tetra-n-butylammonium
NHCs	N-heterocyclic carbenes
NMP	N-methyl-2-pyrrolidone
NMR	nuclear magnetic resonance
NPs	nanoparticles
scCO_2	supercritical carbon dioxide
[Tf_2N]	bis(trifluoromethylsulfonyl)imide
TGA	thermogravimetric analysis
THF	tetrahydrofuran
TMDS	tetramethyldisiloxane
TOF	turn over frequency
TON	turn over number
X	anion (unless otherwise specified)
XRD	X-ray diffractometry

Table of Contents

Abstract

The thesis presents an extensive work starting from the analysis of recent achievements in the field of organometallic pincer chemistry and ending up with the development of the synthesis of pincer ligands, their metal complexes as well as the investigation of chemical properties of well-defined rhodium organometlallics. In Chapter I the latest state-of-the-art in cooperative mechanisms, hemilability, and ionic liquid-based hydroformylation is reviewed in detail. Herein, the focus was set on the cooperative ability of the ligands to promote homogeneous CO_2 hydrogenation. Additionally, further uses of CO_2 as chemical C^1-feedstock or supercritical CO_2 (*sc*CO_2) as carrier for the reagents and products in the hydroformylation reaction are summarized in last subsection.

The easy formation of stable carbene complexes based on tridentate ligands by simple addition of the metal precursor to the (benz)imidazolium salts has been already recognized by Lee *et al*. and other research groups. Although several reports on the synthesis of tridentate chelates containing carbene donor functionalities have been published lately, the field of carbene-centered pincer ligand systems has developed rather slow, probably due to the synthetic issue. Therefore, we underline the importance of the organic synthesis in the rational catalyst design. Now the pincer NHC-centered complexes are almost not studied as catalysts for the homogeneous processes. Through our work and reports of Lee *et al.*, Hahn *et al.*, and Fryzuk *et al.* on the [n,n]-membered carbene-centered complexes we point out the significant interest in the synthetic accessibility of the carbene-centered ligand architectures containing the methylene- and ethylene-bridged auxiliary donor functionalities as well as the hybrid motifs containing basic functionalities and their applications in the conversion of small molecules (Scheme A1).

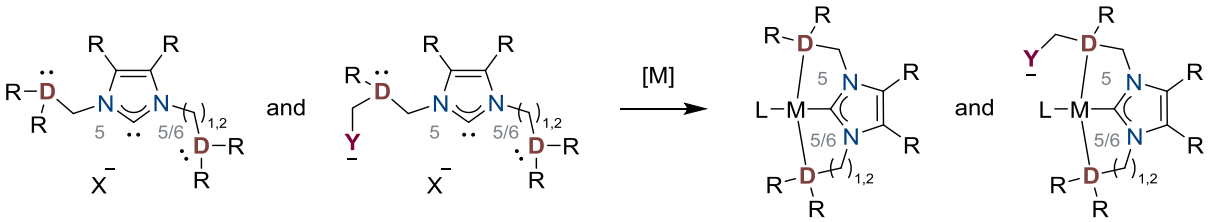

Scheme A1. NHC-centered ligands – promising motifs for organometallic catalytic systems

In Cahpter II, the synthesis of tridentate carbene-centered bisphosphine ligand precursor and its complexes are described. The developed four-step synthetic strategy of a new $PC^{BIm}P$ pincer ligand represents the derivatization of benzimidazole in the first and third positions by

(diphenylphosphoryl)methylene synthone, followed by phosphine deprotection and subsequent insertion of a noncoordinating anion. From the experimental study, the readership will note an important role of tosylate derivatives for the *N*-functionalization of heterocycles and learn how to use the oxygen atom phosphine protection for the synthesis of fragile ligand architectures. The obtained ligand precursor undergoes complexation, with $PdCl_2$ and [μ-$OCH_3Rh(COD)]_2$ smoothly forming the target organometallics [($PC^{BIm}P$)$Pd^{II}Cl$][PF_6] and [($PC^{BIm}P$)$Rh^{I}(L)$][PF_6] under mild hydrogenation conditions. A more detailed study of the rhodium complexes [($PC^{BIm}P$)$Rh^{I}(L)$][PF_6] reveals significant thermal stability of the ($PC^{BIm}P$)Rh moiety in the solid state as well as in solution. We raised the question about its reactivity against small molecules such as H_2, CO, CO_2 and ethylene. The chemical behavior of 1,3-bis(diphenylphosphinomethylene)benzimidazol-2-ylrhodium acetonitrile hexafluorophosphate has been screened under decarbonylation, hydrogenation, and hydroboration reaction conditions. Thus, the rhodium and palladium complexes based on $PC^{BIm}P$ ligands are sufficiently stable and reactive compounds, with the potential to be applied in catalysis.

New hybrid carbene-centered $NC^{BIm}P$ pincer ligands and their rhodium complexes containing heteroatomic pendant domains are described in chapter III . The developed modular four-step synthetic approaches enable the tuning of the arm length of phosphorus ligand fragment as well as the variation of pendant functional groups in the ligand structure. The ligand precursors smoothly undergo complexation with [μ-$OCH_3Rh(COD)]_2$ forming the corresponding mononuclear [5,5]- and [5,6]-membered $NC^{BIm}P$ rhodium organometallics under mild hydrogenation conditions. Based on x-ray single crystal analysis it was observed that the domains are situated in direct proximity to the free coordination site of the metal center, as expected. The [5,5]- and [5,6]-membered $^{MeO}NC^{BIm}P$ rhodium(I) complexes proved to be active hydroboration catalysts.

The described findings will help to better understand the chemistry of the [5,5]- and [5,6]-membered carbene-centered complexes and become a solid foundation for further developments in this field.

Chapter 1: Theoretical Background

Literature Review: Rational Design and Synthesis of Pincer-Derived Catalysts. Homogeneous Conversion of CO_2

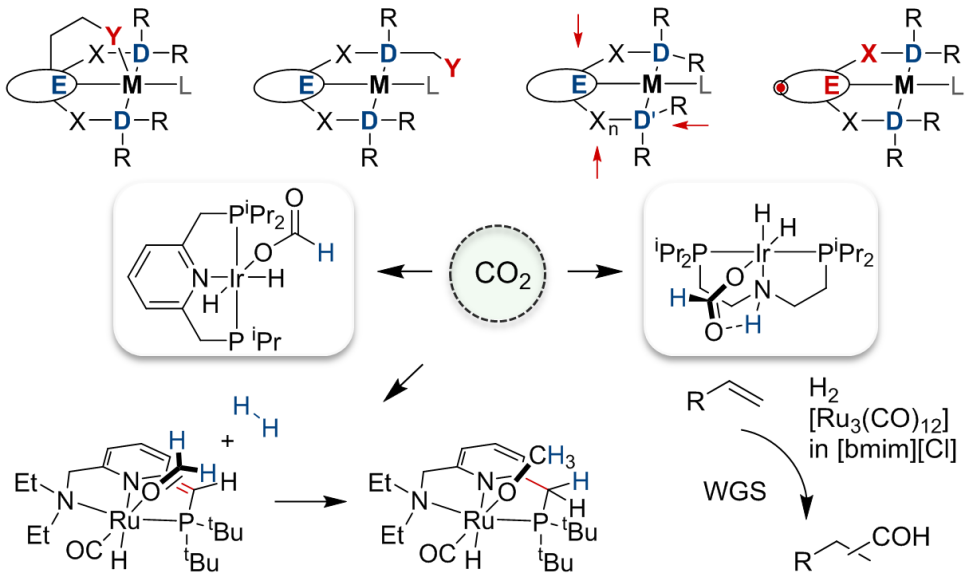

1 Pincer ligands: structure, synthesis, application and stability

The catalysis is one of the most rapidly developing fields of the modern chemistry. Nearly 90% of all industrial processes are carried in the presence of the catalysts and their potential is nowhere near exhausted.[1] Recently the special attention is paid to the problems of small molecules activation. The integration and recycling of biatomic and triatomic compounds CO_2, N_2, O_2, H_2O etc. into industrial processes as cheap ubiquitous resources is one of the top priorities of the industrial chemistry and the challenge for the contemporary. The inertness and high stability of N_2, CO_2 and H_2O are the stumbling block for the development of the atom-efficient methods of their conversion into valuable products.

The rational design of the catalytic systems directed on the simplicity of the synthesis, enhancement of selectivity and efficiency push the boundaries in homogeneous catalysis. Herewith, the focus is made on the incorporation of the additional functionality in the molecular structure of catalysts; unlock synergetic effects; search for the conditions for reaction proceeding through non-conventional mechanistic pathways; implementation of multicomponent and conjugated chemical processes, investigation of reactivity of the metals in their unstable and extreme oxidation states; and also high-throughput-screening.

The tridentate ligand platform has established itself as a privileged ligand for preparation of the metal complexes and catalytic studies. Pincer ligands coordinate to the metals mainly in a meridional bonding mode, although the facial coordination also takes place (Figure 1.1).[2] The complexes based on them show not only excellent stability within the range of high temperatures up to 250 °C,[3] but are also convenient for characterization. The chemical properties of pincer complexes are specified according to the three main parameters: metal nature, nature of coordinating atoms and structure of the organic ligands. The last ones change the steric and electronic character of the metal center, its catalytic activity and selectivity. Both *trans*- and *cis*-coordinating group (E and D, Figure 1.1) can be represented by a variety of the elements, such as B, C, N, O, Si, P, S etc. Depending on the charge, the ligands are divided into neutral, anionic and cationic.

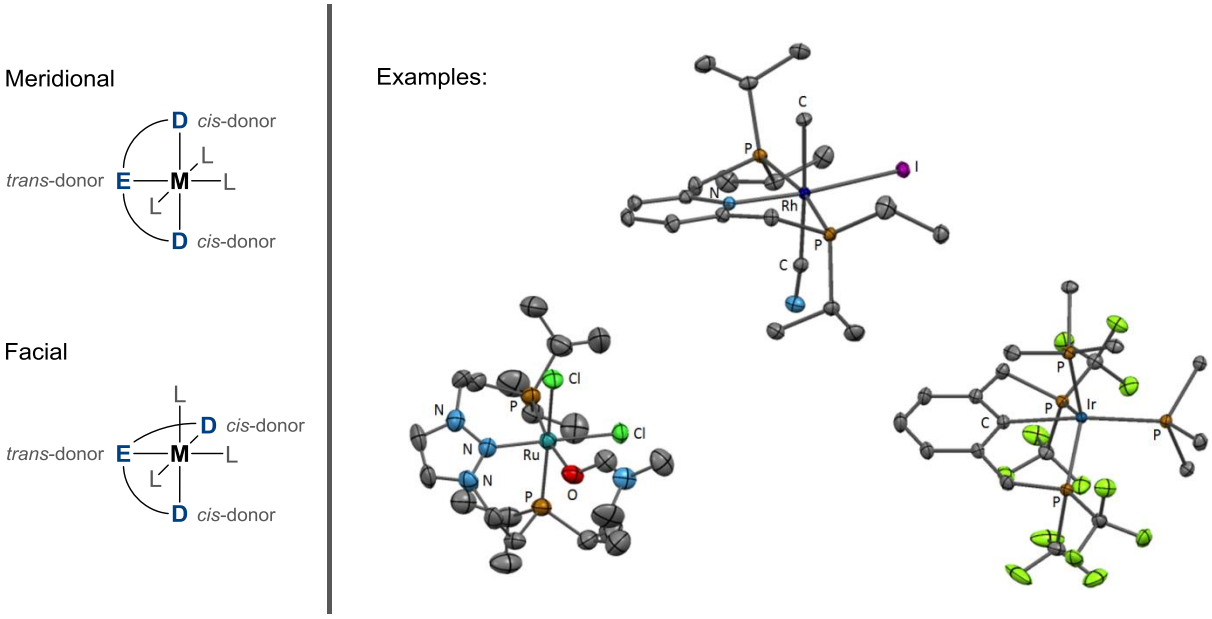

Figure 1.1. Schematic representation of meridional and facial bonding modes of DED-pincer ligands and the crystal structures of *mer*-[(PNP)RhCH$_3$ICN],[4] *fac*-[(PNP)Ru(Cl)$_2$DMF][Br],[5] and *fac*-[(PCP)Ir(DFMP)$_2$][6]

The σ-donor and π-acceptor properties of the central coordinating atom (E) have significant impact on the opposite coordinated ligand (L). This effect, called as *trans*-effect, involves the competitive electronic interaction of the opposite groups *via* p- and d-orbitals of the metal (Figure 1.2). Thus, if E is more σ-electron-donating in comparison to L, the stronger E–M bond is formed. Herewith, the M–L bond weakens due to the increase of electron density on metal caused by the E group (Figure 1.2, a).

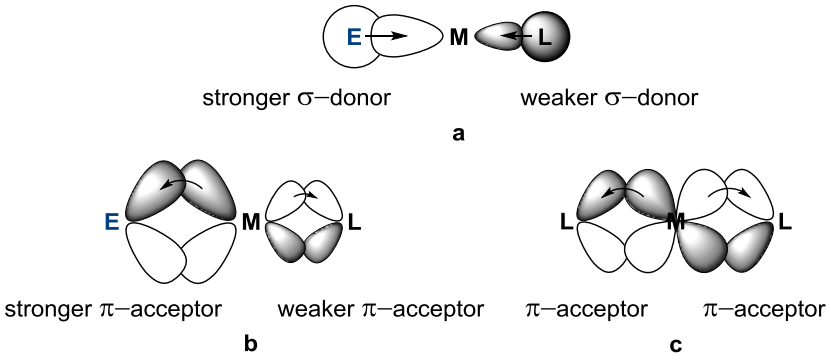

Figure 1.2. Competitive σ- and π-interactions causing the *trans*-effect

In the same way, the E group, being stronger π-acceptor, attracts the electrons from d-orbital of the metal (metal-ligand-backbonding) increasing the E–M bond strength. The lack of electron density on the metal d-orbital results in lesser electron donation from M to L and, consequently, in destabilization of the M–L bond (Figure 1.2, b). Two ligands having the

same σ-donor and π-acceptor properties equally weaken their bonds to the metal (Figure 1.2, c). The general scheme of variable parameters of a pincer system is represented in the Figure 1.3.[7] The fine tuning of these factors that control activation and conversion of the substrate molecules on the catalytic centers requires new approaches in design and preparation of tridentate structures.

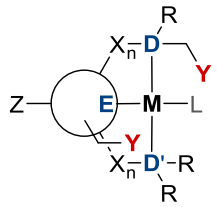

Structure	Group	Parameters
	X	Cooperativity, indirect steric control, electronic tuning
	Y	Cooperativity, solubility
	Z	Remote electronic and steric tuning solubility, immobilization
	E	Control over electron density, lability, cooperativity
	D	Steric and electronic control, chirality, lability

Figure 1.3. General features of pincer complexes

The synthesis of the pincer complexes can be performed in different ways. The most general approach is the modification of the central molecular fragment with the subsequent addition of auxiliary donor groups and complexation of the metal (Scheme 1.1, a). The advantage of this approach is in universalism of its application for preparation of the majority of molecular architectures. Another concept gives the opportunity to introduce the central coordinating atom E on the final step of the molecule construction (Scheme 1.1, b). This strategy is used mainly for the synthesis of the boron-,[8] carbon-,[9] and silicon-centered[10] heterocyclicles. Some heterocyclic ligand backbones can be formed in one step by a modular principle. The most eloquent example is the implementation of a click reaction for the preparation of triazole moiety, which is based on copper-catalysed azide-alkyne Huisgen cycloaddition.[11] This methodology developed by Gandelman *et al*. has been proved to be very useful for the generation of tailor-made symmetric and asymmetric ligands (Scheme 1.1, c). Moreover, the post-modification of pincer complexes leading to the generation of triazolidene carbenes as central motifs can be performed.[12]

Scheme 1.1. General synthetic approaches to pincer compounds

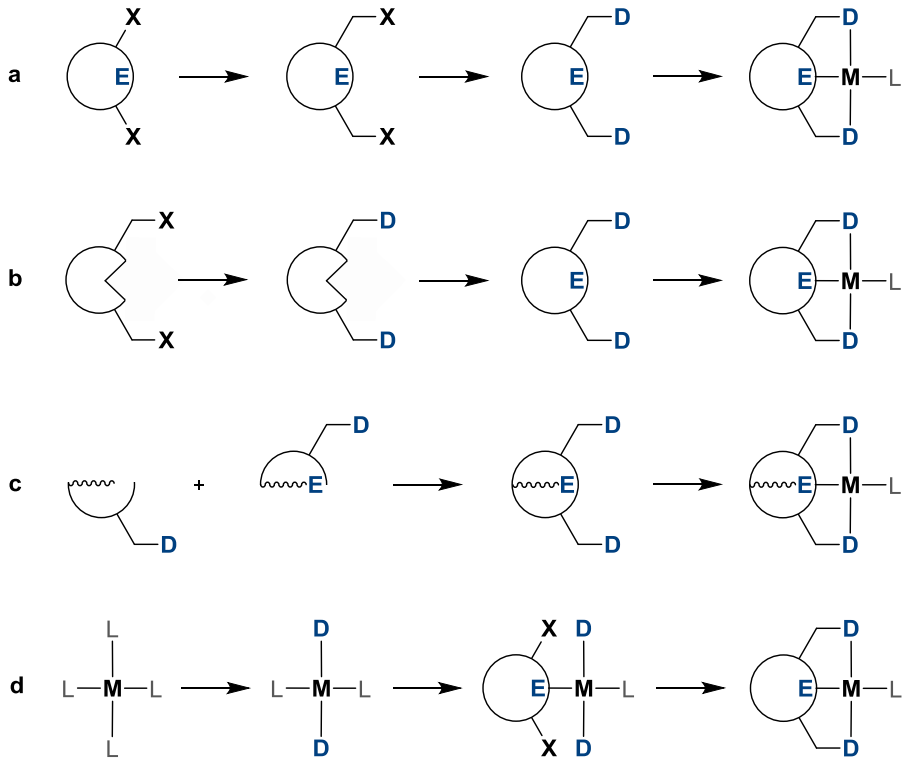

A further efficient synthetic method for the preparation of phenylene-based organometallic structures is the "electrophilic ligand introduction route". It represents the condensation of coordinated ligands on the metal templates with the formation of the target metalorganics (Scheme 1.1, d)[13, 14]

Pincer ligand complexes of ruthenium, palladium, rhodium, and iridium as catalysts are receiving widespread attention, because of their outstanding ability to activate stable C–X (X = H, C, O, N, F) bonds. These transition metals have been shown to facilitate such important catalytic reactions as acceptorless dehydrogenation and dehydroaromatization of alkanes,[7, 15-19] transfer (de)hydrogenation,[20, 21] alkane metathesis,[22] alkohol and amine (de)hydrogenation,[21, 23-27] ester synthesis,[28] hydrogenation of esters[29] and biomass-derived cyclic diesters,[30] carbothiolation,[31, 32] decarbonylation,[33-35] and carbon dioxide (CO_2) hydrogenation (Scheme 1.2).[36-40]

Scheme 1.2. Selected pincer complex-catalyzed transformations

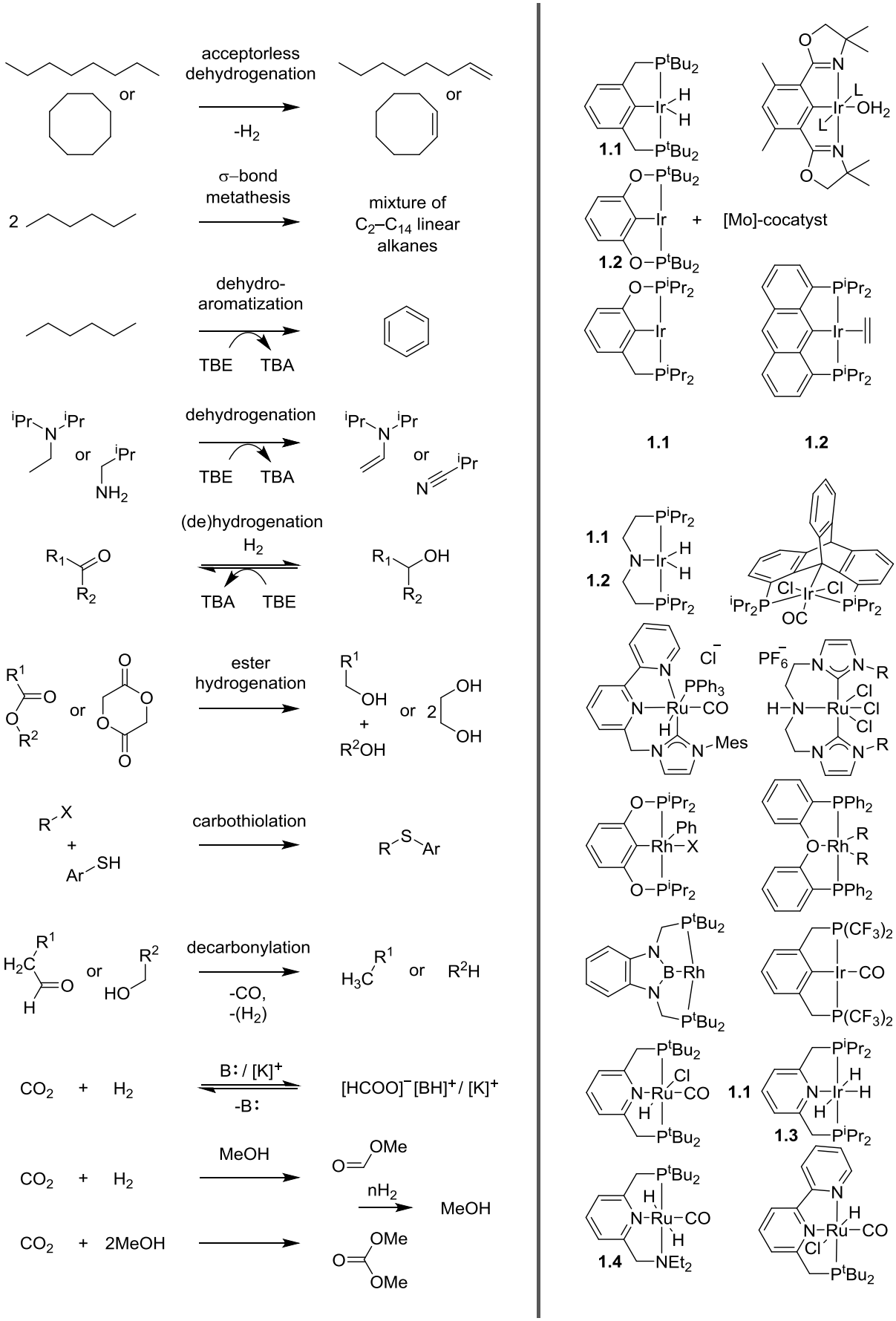

Pincer complexes-mediated transformations of hydrocarbons and oxo compounds are not the only subject of intensive study, but also synthesis of nitrogen-based chemicals shifts into focus. The oxidative addition of ammonia to the transition metal complexes, forming amido-hydride complexes, is a potential entry point for the catalytic hydroamination reactions. This step was elucidated by Hartwig *et al*. in 2005 on the example of iridium complex based on electron donating aliphatic PCP backbone.[41] Later on, Milstein *et al.* reported an N–H activation process *via* metal-ligand cooperation by dearomatized [($PN^{Py}P$)Rh^{I}(L)] and [($PN^{Py}N$)Rh^{I}(L)] metallocycles.[42] Significant achievements also include: hydrogenation of urea and amide derivatives leading to alcohols and amines by using [($N^{Py}N^{Py}P$)Ru^{III}H(CO)] catalyst,[43, 44] deamination of primary amines by water to alcohols mediated by acridine-based [(PNP)RuH(CO)Cl] system,[45] and direct synthesis of amides from alcohols and amines catalysed by [($NN^{Py}P$)Ru^{III}H(CO)] complex.[46] Furthermore, pincer systems show remarkable activity in hydroboration,[47-49] hydrosilylation,[50, 51] and hydrovinylation[52] of unsaturated hydrocarbons. A large number of palladium pincers have been reported to be efficient catalysts for Heck, Suzuki-Miyaura, Sonogashira, Hiyama, Stille, and Negishi cross-coupling reactions, as well as aldol condensation, Michael, and Kharasch addition[53-55] Nevertheless, the question about mechanistic aspects of coupling reactions involving palladium-based pincers *via* classical Pd^{0}/Pd^{II} catalytic cycle or Pd^{II}/Pd^{IV} redox process remains open and is still a matter of debate. Several studies led to the conclusion that pincer complexes are not active species, but serve as dispensers for reactive palladium catalysts. They undergo degradation under harsh reaction conditions with the formation of decomposition products such as palladium clusters or nanoparticles.[54]

Although, as has already been mentioned, the pincer complexes are considered as stable metalorganic compounds, some of them undergo degradation under relatively mild conditions. Known decomposition pathways include cleavage of phosphines, ligand dissociation, irreversible ligand oxidative addition or the transfer of an activated substrate to the ligand leading to its destruction. Thus, upon investigation of the thermal reactivity of carbene-centered phenylene-bridged [($PC^{Im}P$)Rh^{I}(L)] complex, Fryzuk *et al.* detected a ligand rearrangement process resulting from intramolecular P–C bond cleavage between the aryl linker and one of the phosphine donors.[56] Such decomposition takes place under quite mild reaction conditions at 60 °C in a non-polar solvent. The formation of more stable planar [5,6]-membered [($C^{Ar}C^{Im}P^{iPr}$)Rh^{I}(P^{iPr})] metallocycle with a lesser degree of system strain was confirmed by crystallographic analysis (Scheme 1.3, compound **1.5**).

Willis *et al.* observed a new deactivation pathway for the [(POP)Rh^{I}(L)] system studying the alkynes carbothiolation mechanism. It has been found that nucleophilic attack of the thio group on sp^2-hybridized carbon atom of POP ligand takes place after activation of S–C bond of the substrate molecule at 120 °C. As a result, the tridentate backbone transfroms into two bidentate ligands: aryl thioether and phosphine aryl oxide (Scheme 1.3, compound **1.6**).[31]

Scheme 1.3. Examples of pincer complexes decomposition

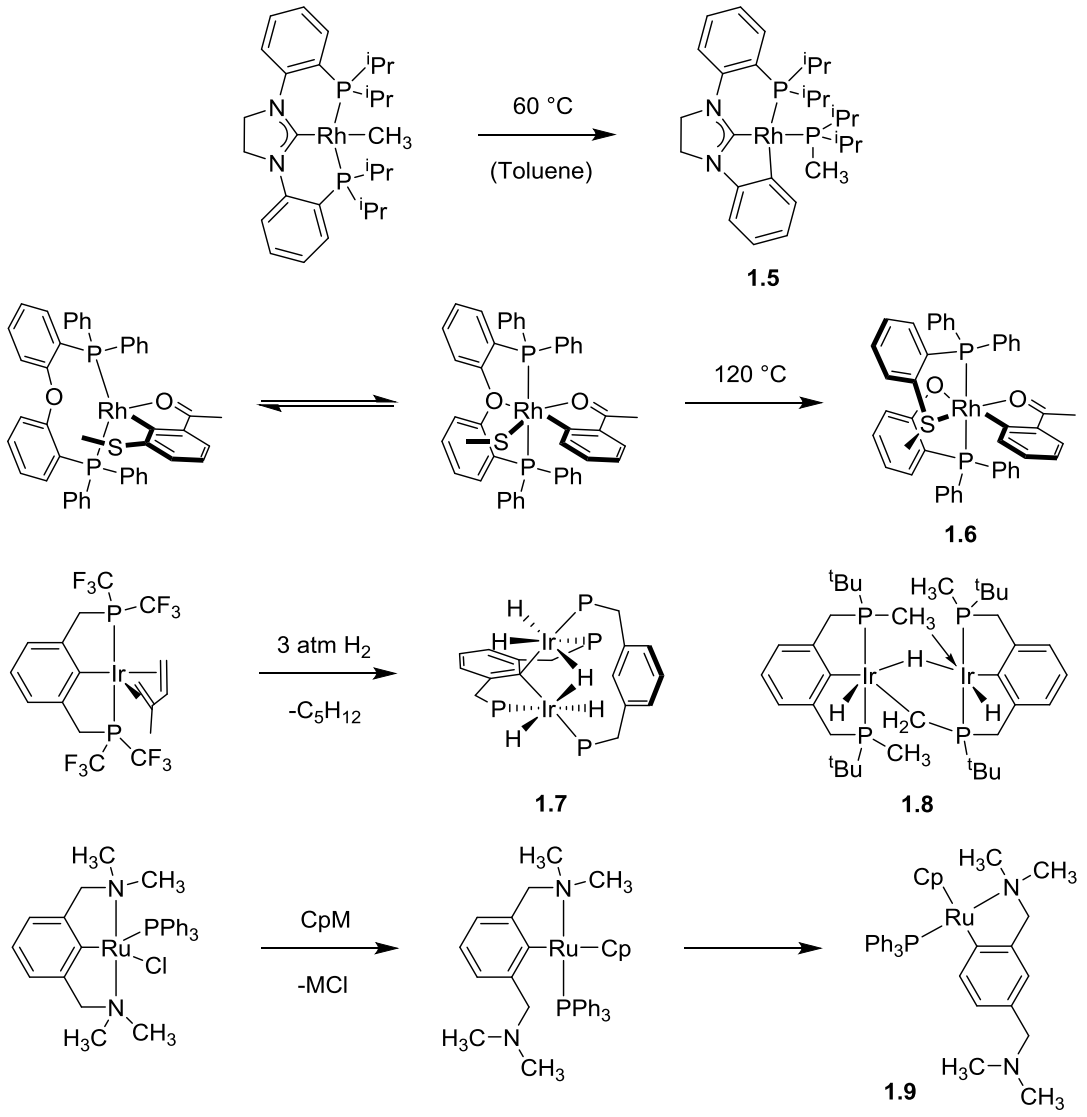

Roddick *et al.* describe unusual rearrangement of the [(^{CF_3}PCP^{CF_3})Ir^{I}L] complex. Its reaction with hydrogen at ambient temperature resulted in the formation of aryl-bridged bimetallic compound **1.7**. The reason for this is supposedly a lack of steric bulkiness of CF_3-substituted pincer ligand.[33] Low steric hindrance also contributes to the formation of dimeric iridium hydride complex **1.8**, due to C–H bond activation of a phosphinomethyl group.[57] Weak coordination of supporting NR_2 ligands can be a reason for destabilization of the whole

complex structure resulting in a "shift" of Ru–C^{Ar} bond from position 1 to position 3 on an aromatic ring of $NC^{Ar}N$ ligand (compound **1.9**), as it was shown by G. van Koten *et al.*[58]

2 Rational complexes design for cooperative metal-ligand interactions

While irreversible structural ligand changes are regarded as undesirable processes leading to deactivation of catalytic active species, reversible interactions of pincer ligands with metal centers and substrate molecules often result in extraordinary reactivity of pincer complexes. Such cooperative behaviour of tridentate ligands has already been applied successfully in homogeneous catalytic approaches and became one of the most important topic in the field.

2.1 Cooperative heterolytic substrate activation

Spectator ligands act as static and inert organic scaffolds and usually do not interact with substrate molecules. Actor ligands, by contrast, are actively involved in a conversion of substrates and can facilitate reactions proceeding through non-conventional pathways. Such cooperative catalysis is widely represented in biological systems.[59-62] It has been only recently recognized that rational design of actor ligands can provide an opportunity to discover new types of reactivity of the complexes.

Tridentate PNP system based on 2,6-lutidine is cooperatively active and most widely studied. Its distinctive feature is easy deprotonation of methylene group located between aromatic moiety and phosphine rest. Cleavage of a proton leads to dearomatization of the heterocylce along with acquiring by central nitrogen atom more pronounced electron-donor properties (Scheme 1.4, a). Carbon atom of the methylene fragment acts as reactive center of the ligand during the reaction. Dearomatized [(PNP)Ru$(L)_2$] complexes are able to add hydrogen, water, CO_2,[63] alkohols, boranes, aromatic[64] and carbonyl compounds.[65] A number of new reactions described in the Scheme 1.2 have been implemented using this type of interaction. Similar dearomatization has been found also for nitrogen-bridged pincers.[66] The ethylene linkers of aliphatic PNP pincer systems can also be converted into unsaturated groups, however, cooperative interaction by central nitrogen atom is more typical for these complexes (Scheme 1.4, c).[67] It is also worth noting a conceptually different mode of metal-ligand cooperation that involves "long-range" interaction between acridine C9 position and metal center. Heterolytic splitting of hydrogen on acridine-based ruthenium complex results in dearomatization of central acridine ring along with change of PNP ligand configuration from meridional to facial (Scheme 1.4, d).[68, 69]

Scheme 1.4. Reversible heterolytic addition of hydrogen through aromatization-dearomatization of pyridine and acridine moieties (a, d). Amine-amide interconversion of ruthenium pincer complex (c). Heterolytic addition of HCl across M−C(sp^3) bond in iridium pincer complex (b).[70, 71]

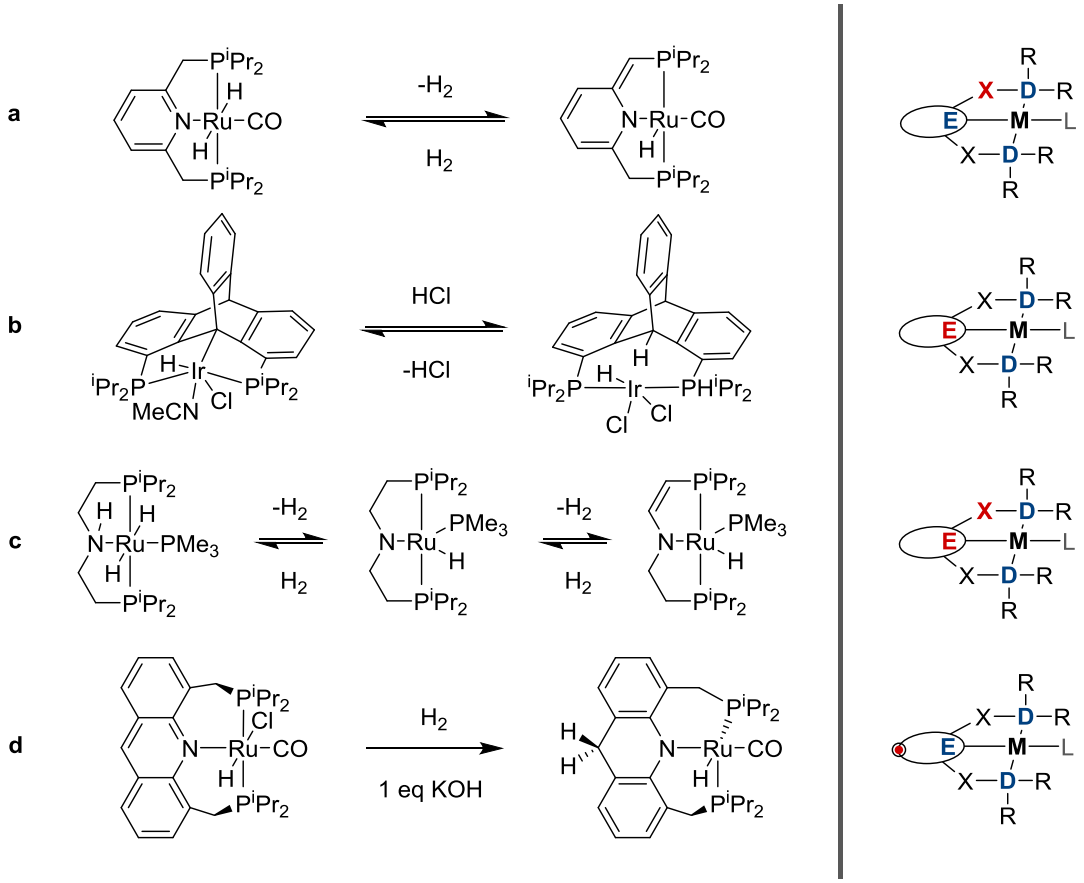

2.2 Hemilability

Multidentate ligands, which contain different coordinating functionalities in their molecular structure such as soft and hard donors, have been defined as hybrid or heteroditopic ligands. They attract much interest first and foremost because of their characteristic adaptive coordination behaviour, which was termed as hemilability or flexidenticity. Hemilabile ligands do not only provide free coordination sites at the metal center because of their reversible coordination, but are also able to stabilize reactive intermediates during the reaction.[72] The association-dissociation reversibility is a hemilability criterion and is a consequence of small difference in energy between "open" and "closed" states. Both nature of coordinating atom and metallocycle ring strain determine E/D–M bond strength. The last can be set by varying the length and rigidity of the linker X.[73, 74] Selective dissociation of central ligands as well as "side-arms" can be predefined from the very beginning during the design of target complex. Hemilability of ligand as well as cooperative heterolytic substrate activation

described in Section 2.1 determines mainly the reactivity of the complex first coordination sphere.

Scheme 1.5. Concept of tunable hemilability to induce cooperative reactivity. Selected examples of hemilabile pincer ligands[75-77]

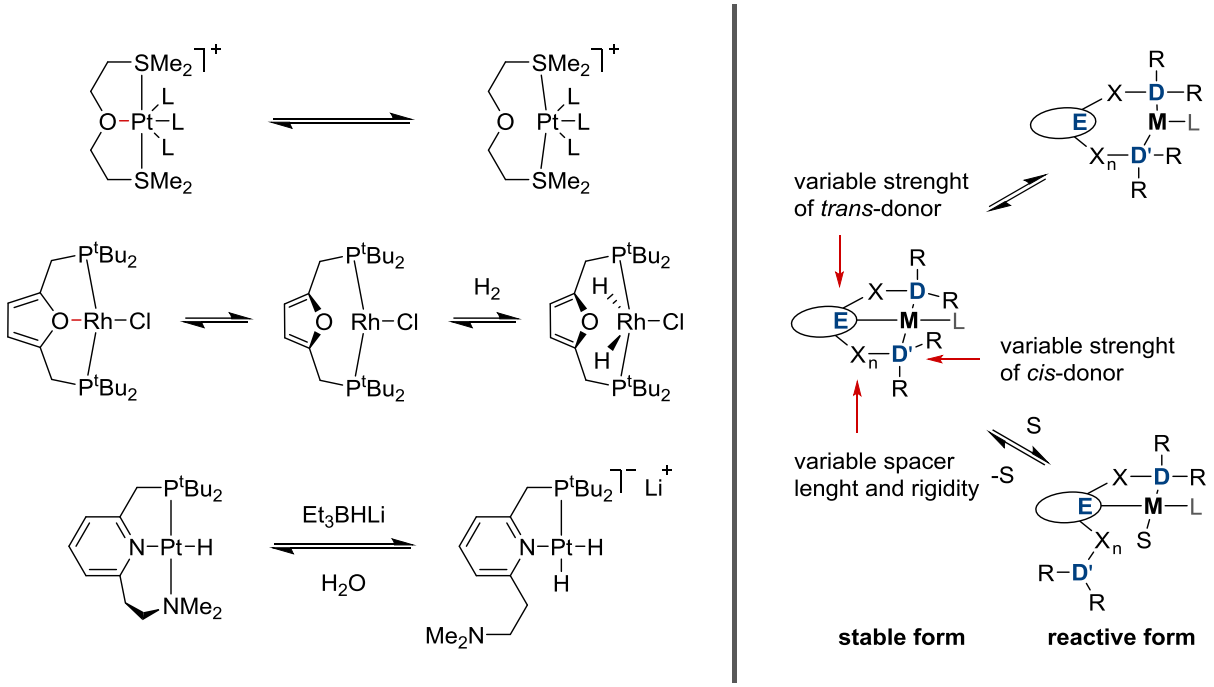

Braunstein and Naud distinguish three types of hemilability: spontaneous dissociation of ligand arm with formation of free coordination site (type I), competing intramolecular displacement of donor D by other donor D` (type II), and substitution of donor D by external reagent S (type III).[75] Some tridentate complexes based on ligands, which represent different types of flexidenticity, are given in Scheme 1.6.

Scheme 1.6. Types of hemilability

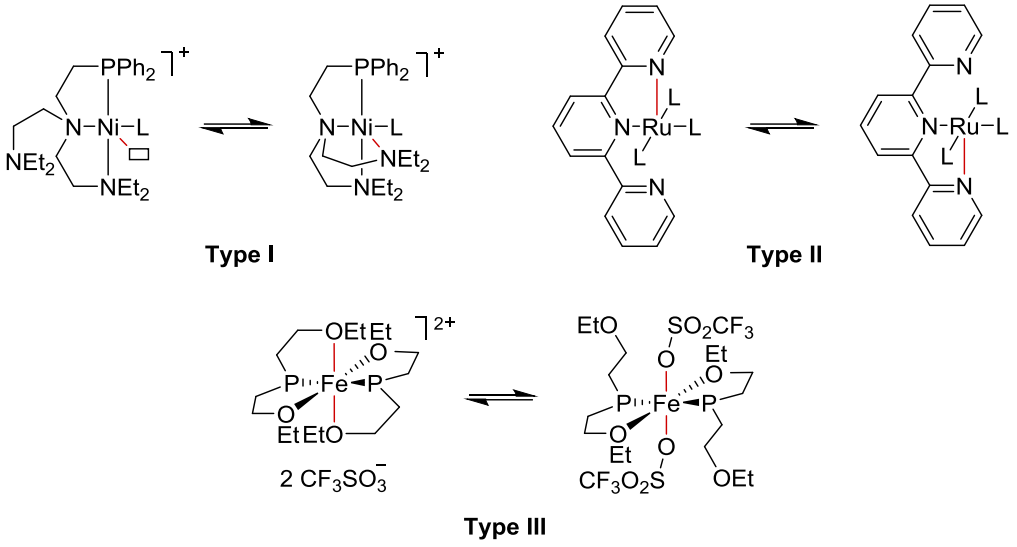

2.3 Complexes containing appended functionality

Additional functional groups can be introduced into a ligand framework to engage further reactivity of pincer complexes. These groups are represented by hydroxy, amino, sulpho, oxo, carboxy, pyrido, boronato, and phosphinoxy functionalities. Like aromatization-dearomatization described above, keto-enol and amino-imino tautomerisms play an important role in metal-ligand reactivity. [67, 78, 79] *Brønsted/Lewis* basic/acidic domains can be attached to E, D, or X pincer ligand moiety and set both coplanar and perpendicular to a plane of a complex. Depending on a length of the linker, functional groups can be coordinated at metal center or not bound to a metal directly, but suspended above it, in close proximity to a metal free coordination site. Non-coordinated functional groups particularly determine directing character of ligand secondary coordination sphere.[80]

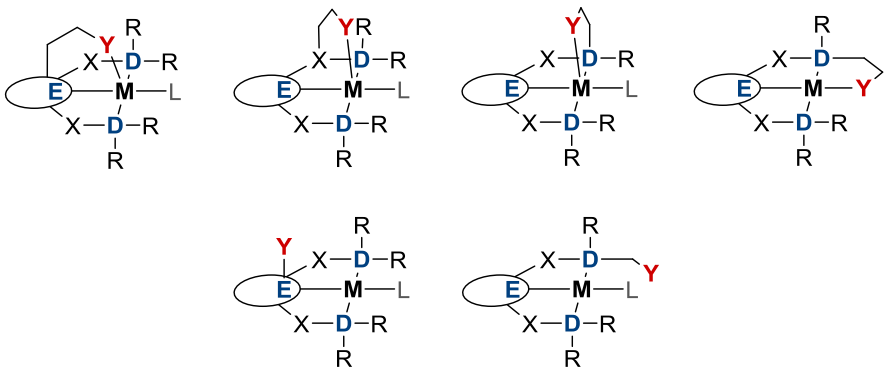

Figure 1.4. Positioning of heteroatomic domain in a structure of pincer complex

The role of such pendant domains in the substrate activation was first shown by Shvo *et al*. on the example of bifunctional ruthenium catalyst bearing monodentate cyclopentadienone ligand.[81-84] For bidentate ligands, Crabtree *et al*. has demostrated the heterolytic activation of hydrogen by a bidentate NCIr system furnished with an amine group.[85, 86] Other mono and bidentate ligands of this type can be also found in the literature.[87-92] For pincer chelates, a simple ruthenium complex bearing two distal pyridine goups was presented by Wright and coworkers for the first time.[93] In series of publications, C. M. Moore and N. K. Szymczak reported the significant interactions between functionalized terpyridine ligand frameworks and the substrate emphasizing the ability of the secondary coordination sphere to participate cooperatively in binding small molecules.[79, 80, 94, 95] The same principle of cooperative substrate-directed interactions was implemented by Gelman *et al*. on a new three-dimensional shaped (PC^{sp3}P)M pincersystem,[71] by Britovsek *et al*. on diaminoterpyridine-substituted platinum(II)methyl complex,[96] and other research groups.[97, 98] Further selected conceptual

patterns of mono-, bi- and tridentate organometallics containing pendant electron rich heteroatomic centers are shown in the Figure 1.5.

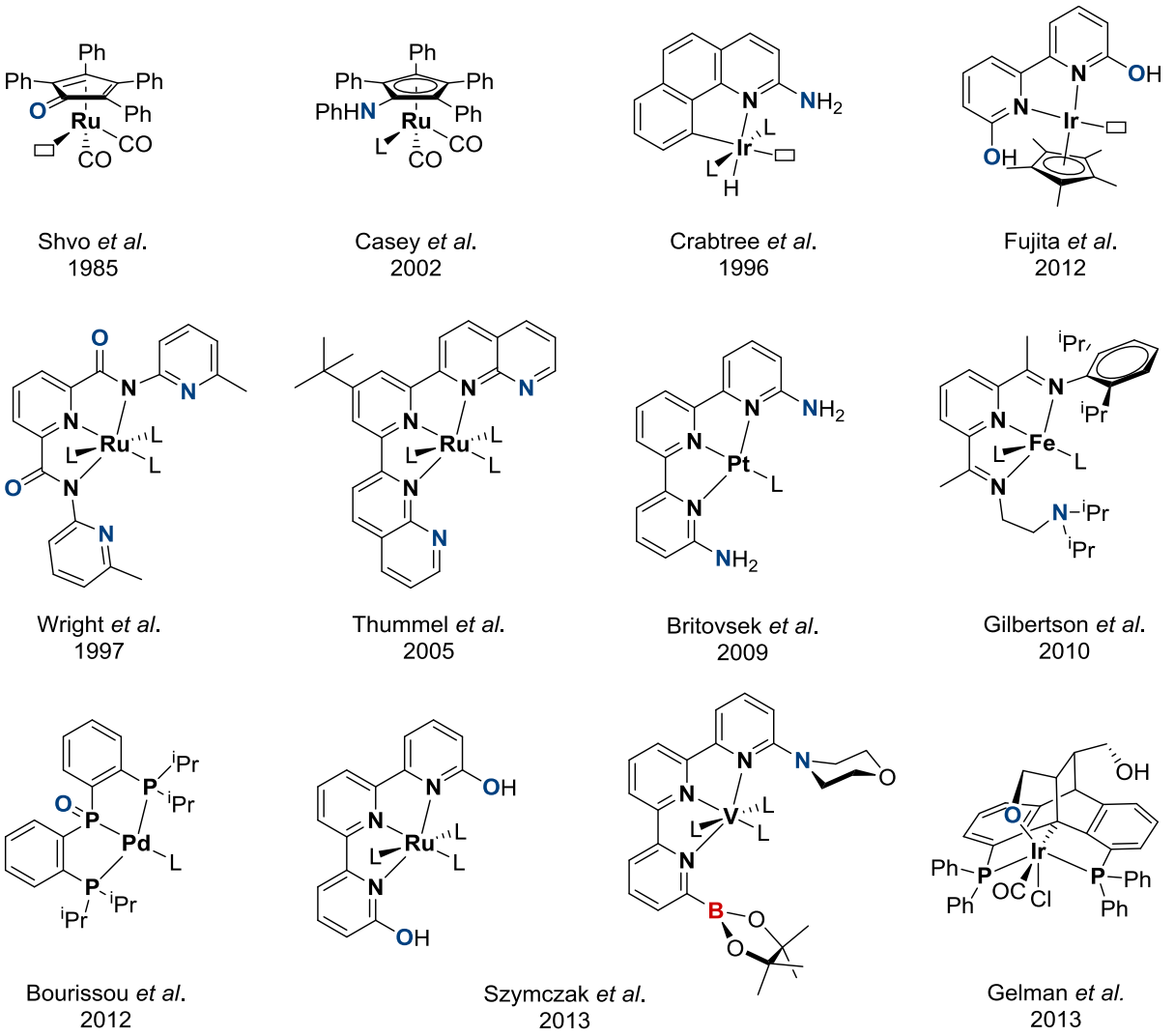

Figure 1.5. Selected examples of mono-, bi- and tridentate metal complexes bearing heteroatomic domains

The cooperativity of the systems based on other heterocycles is somewhat less studied, although they may also demonstrate interesting catalytic reactivity.

3 Selected aspects of CO_2 conversion

Among all greenhouse gases in the atmosphere, CO_2 plays a special role due to the magnitude of its anthropogenic emissions. There are three main ways which carbon dioxide management should be based on: capture, storage and its chemical utilization. The use of CO_2 as a raw material in production of fuels and materials is the only profitable technological solution for CO_2 emissions control. From an economic perspective, CO_2 is widely available, inexpensive and non-toxic compound. The most promising are processes of direct CO_2 hydrogenation to

formic acid, formaldehyde, methanol and methane (Scheme 1.7). The last ones have been considered as chemical energy storage media due to their high energy content.

Scheme 1.7. Elementary steps in homogeneous CO_2-reduction[99]

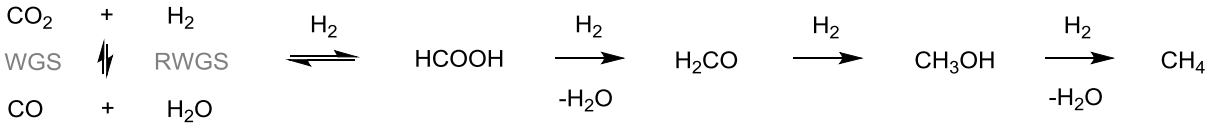

The exothermic reduction of CO_2 to methane and water has been already known since 1910 as Sabatier reaction. Methanation of CO_2 proceeds on Ni, Pd, Ru, and Rh heterogeneous catalysts at temperatures 300-400 °C. In 2012, the process has been launched on a commercial scale in a pilot project "Power-to-Gas" by ZSW research centre (Germany), and it is the world's largest installation of this type with up to 300 m^3/day methane production capacity.[100] Industrial heterogeneous synthesis of methanol from CO_2 (CAMERE process) was carried out using $Cu/ZnO/ZrO_2/Ga_2O_3$ (5/3/1/1) catalyst at 250 °C. It represents a combination of Reverse-Water-Gas-Shift reaction with syngas methanation.[101] The Reverse-Water-Gas-Shift reaction being a reversible exothermic and exergonic process is considered as an entry point for CO_2 conversion into more reactive carbon monoxide and for syngas production.

3.1 Homogeneous hydrogenation of CO_2

Mononuclear complexes of late transition metals were used as catalysts in vast number of studies on activation and homogeneous hydrogenation of CO_2.[102-105] Carbon dioxide possessing *Lewis*-acidic carbon atom and weak *Lewis*-basic oxygen atoms coordinates to metals in different ways forming both M–C and M–O bonds (Figure 1.6).[106, 107]

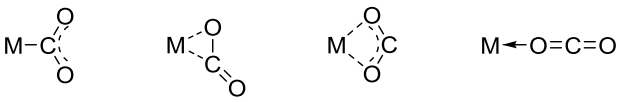

Figure 1.6. Coordination modes of CO_2 to the metal center

In the light of recent achievements, it is obvious that key-factors that determine the outstanding catalytic activity in the hydrogenation of CO_2 are not only the optimal selection of metal or electronic properties of ligands, but also their cooperation ability. Thus, Nozaki *et al*. has obtained extremely high TON (3 500 000) and TOF (150 000 h^{-1}) values for the potassium formate synthesis from CO_2 at 120 °C using $[(PN^{Py}P)Ir^{III}H_3]$ complex.[108] As can be seen from the proposed mechanism, exposure of trihydride complex **1.3** to 1 atm CO_2 leads to

an equilibrium between **1.3** and [(PN^{Py}P)Ir^{III}H$_2$(OOCH)] **1.10** at 25 °C. The formato ligand occupies *cis* position to the nitrogen atom of the pyridine ring. In the next step, elimination of formate anion from **1.10**, accompanied by deprotonation of the methylene bridge of the ligand and subsequent dearomatization of the pyridine ring, gives amidoiridium dihydride compound **1.11** (Scheme 1.8, a). Authors concluded that deprotonative dearomatization accelerates formate dissociation increasing the catalytic activity. It is this synergetic behaviour that determines an unprecedentedly high performance of some pincer catalysts. Hazari *et al.* also demonstrated the feasibility of another cooperative activation route for CO_2 reduction. They have shown by DFT calculations that intramolecular hydrogen bond in complex **1.13** facilitates CO_2 insertion (Scheme 1.8, b).

Scheme 1.8. Plausible mechanisms for CO_2 hydrogenation using [(PN^{Py}P)Ir^{III}H$_3$][108] **1.3** and [(PNP)Ir^{III}H$_3$][109] **1.12** complexes

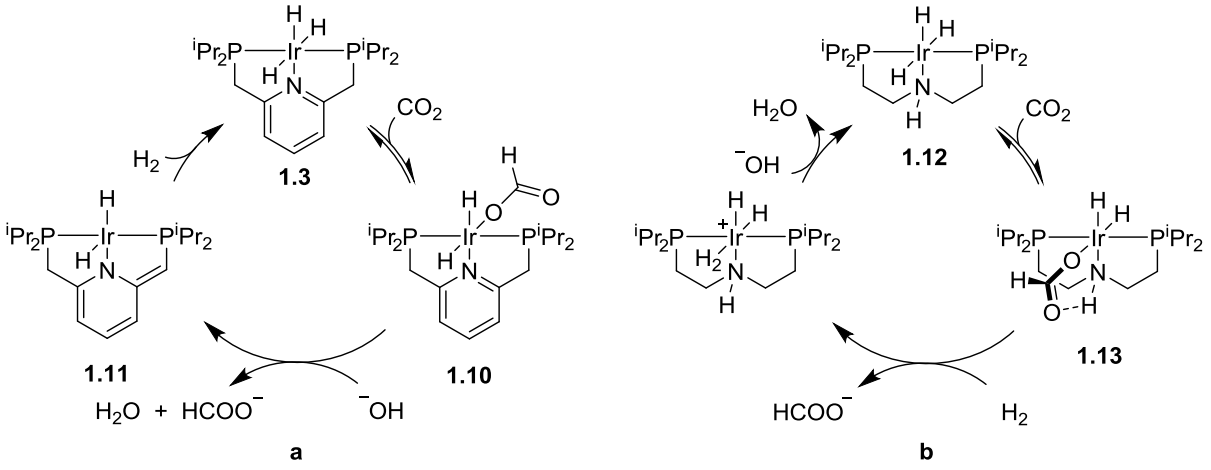

Lower activity of TON (59 000) and TOF (30 000 h^{-1}) was measured for analogous [(PC$^{m\text{-}phenylene}$P)IrH$_2$] system. For this complex no rearomatization was yet detected. High performance of iridium complex **1.3** is comparable with activity of heterogeneous systems and therefore provides opportunities for its application in industrial scale.

Homogeneous catalysts, which suffer from thermal instability, deliver formic acid derivatives in most cases,[108, 110-125] however at significantly reduced reaction temperatures in comparisson to heterogeneous processes. Intramolecular hydrogenation of HCOO$^-$ moiety is considered as the key-step in the entire reduction sequence and is currently not yet feasible, as it can be seen from the literature. Recently, Milstein *et al.* has reported on pincer-type ruthenium-based homogeneous catalysts that afford hydrogenation of organic formates, carbonates and carbamates to methanol.[126] In fact, this approach represents an alternative route of carbon dioxide hydrogenation to methanol, because these intermediate compounds can be readily

formed from CO_2 and CO (Scheme 1.2). This reaction is selective and proceeds under mild neutral conditions in the temperature range from 50 °C to 150 °C. The TON values reach up to 4400 for dimethyl carbonate and 4700 for methyl formate. Authors postulated following reaction mechanism, which involves metal-ligand cooperation by rearomatization of heteroaromatic $PN^{Py}P$ pincer ligand and hydride transfer to the carbonyl group (Scheme 1.9).

Scheme 1.9. Homogeneous hydrogenation of CO_2-derived methyl formate

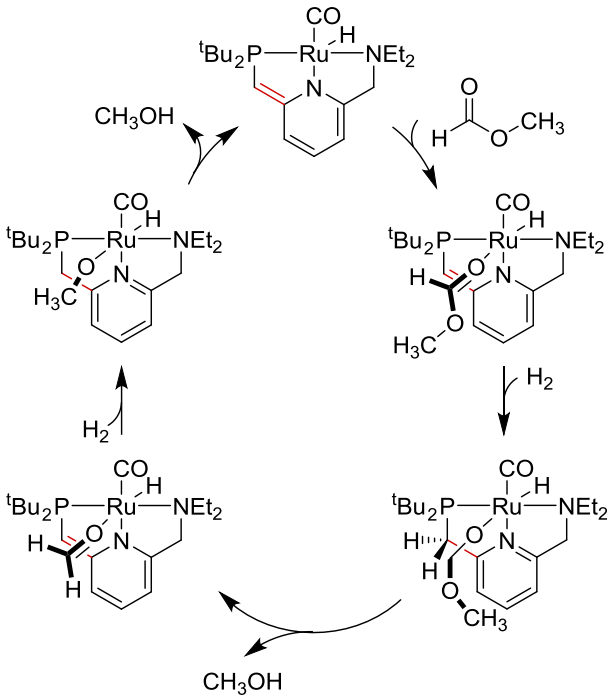

In comparison to the proposed direct hydrogenation of CO_2, which contemplates elimination of a bad leaving HO^- group in form of H_2O, the C–O cleavage is favored by formation of alkohols or amines from carbonates, formates and carbamates. In addition, decarbonylation of substrates was also observed. Thus, reaction of $[(PN^{Py}P)RuH_2(CO)]$ **1.4** with 2.5 equiv. of dimethyl carbonate at 50 °C resulted in formation of dicarbonyl complex $[(PN^{Py}P)RuH(CO)_2]$, methyl formate and methanol. Although, more studies are needed for mechanistic interpretation, it is evident that ruthenium basically facilitates rearomatization of metallocycle and acts as an oxophilic center, to which substrate is bound *via* oxygen atom of the carbonyl group. On the other hand, crucial hydride transfer to carbon atom occurs through heterolytic cleavage of hydrogen by coordinated substrate molecule and methylene fragment of the ligand. Therefore, it is to expect that other heterocyclic metalorganic systems, facilitating similar heterolytic addition of dihydrogen, might show high activity in conversion

of CO_2 and CO_2-derived products as well. However, an efficient direct catalytic reduction of CO_2 to methanol or methane has not yet been achieved despite of major activities in this field.

3.2 Ionic liquids

Liquid organic salts below 100 °C, defined as ionic liquids (ILs), are promising non-conventional green solvents, which attract more and more interest for homogeneous multiphasic applications. They are constituted by a wide range of asymmetric organic cations such as imidazolium, pyridinium, morpholinium, ammonium or phosphonium as well as by inorganic or organic anions like halogenides, perfluorinated borates and phosphates, sulphonates, carbonates, and carboxylates. Their physicochemical properties are related to those of cations and anions. Solubility, stability, thermomorphic behavior, density, viscosity, and polarity are key physicochemical features of ILs. On the other hand, their recyclability, cost, and toxicity have to be considered before applying them in catalysis, especially for industrial purposes. Herein, their decomposition pathways and toxicities[127] remain as issues to be studied in detail. Some of the advantages of using ILs in catalysis are their negligibly low vapor pressure, relatively high thermal stability, task-specific structure variability, and ability to immobilize the catalyst.

3.2.1 Ionic liquids in transition metal catalyzed hydroformylation.

The role of ILs in homogeneous processes using CO_2 can be demonstrated on the transition metal catalyzed hydroformylation.[128] Hydroformylation, also known as oxo process or oxo synthesis, is the most powerful synthetic industrial tool where an alkene is converted in a highly valuable aldehyde through a homogeneous procedure.[129] During this process, a new C–C bond is formed using CO and H_2 as reagents, which affords a linear and a branched product with the use of a transition metal catalyst as depicted in Scheme 1.10.

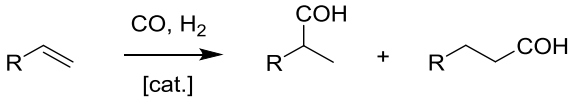

Scheme 1.10. Typical hydroformylation of an alkene

The mechanism of hydroformylation in a biphasic medium is analogous to that in organic solvents. The progress on the ILs-based hydroformylation covering the period from 1972 to 2008 has been reviewed by Dyson and Geldbach[130] as well as in publications from Haumann, Riisager, and Rieger[128, 131, 132] to the full extend. The interest on their industrial application is reflected by the number of patents reported from 1993-2009.[133-145] Their use as solvents in catalysis is also well-documented for other catalytic reactions.[146-150] Hydroformylation with

Ru complexes has been investigated in recent years due to the concerns on the efficient use of CO_2 as C^1-feedstock in industrial processes (Scheme 1.11).

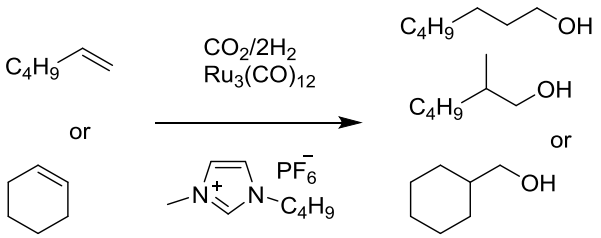

Scheme 1.11. The hydroformylation of alkenes in ILs using CO_2 as a C^1-feedstock

Additionally, the use of *sc*CO_2 in multiphasic ionic liquid-based hydroformylation catalysis has become an attractive approach.

A different reaction mechanism has been proposed for the hydroformylation of alkenes using ruthenium clusters as catalytic precursors and CO_2 as educt. During the search for new environmentally friendly alternatives for the hydroformylation, CO_2 has been found to be a good nontoxic reagent to produce alcohols and/or aldehydes. The first tests on hydroformylation with CO_2 as carbon source in ILs were reported by Tominaga *et al.*[151] His previous work on the hydroformylation of alkenes using metal halides and multinuclear ruthenium complexes as catalyst precursors[152] prompted him to look for alternative polar solvents to *N*-methyl-2-pyrrolidone (NMP), which has a high boiling point and, therefore, complicates the isolation of hydroformylation products. In addition, terminal alkenes in NMP afforded the corresponding alkanes due to the reduction of the educt before the hydrogenation took place. Herein, ILs were seen as an alternative solvent to overcome those difficulties. Accordingly, a biphasic system would reduce the undesired alkene hydrogenation and improve the chemoselectivity toward hydroformylation. Moreover, the catalytic species could remain in the ionic liquid layer with the possibility of reusing it several times. Hydroformylation with CO_2 using the most effective catalyst precursors ($H_4Ru_4(CO)_{12}$ or $Ru_3(CO)_{12}$) consists in two steps: conversion of CO_2 to CO *via* a reverse-water-gas-shift reaction and subsequent reaction of the latest with alkenes through a hydroformylation mechanism. For the first step, tetranuclear ruthenium species have been detected in the reaction medium and these are assumed to be responsible for the reduction of CO_2 to CO, as depicted in Scheme 1.12.[153, 154]

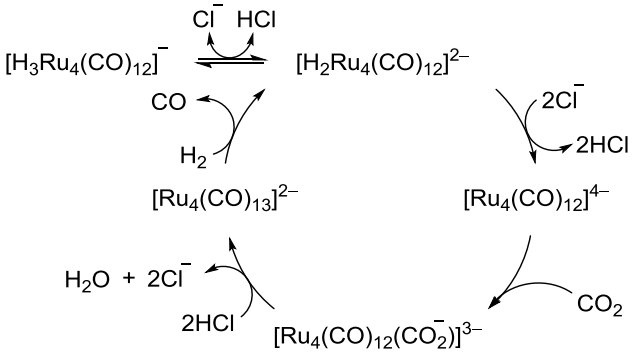

Scheme 1.12. Ruthenium-catalyzed reduction of CO_2 to CO

A key step in the mechanism requires the successive elimination of the coordinated hydrogens in the hydride complex $[H_2Ru_4(CO)_{12}]$, which is promoted by the chloride anions from the corresponding ionic liquid. Subsequent electrophilic attack of protons to tetranuclear ruthenium $[Ru_4(CO)_{12}(CO_2^-)]$ converts CO_2 to CO. According to investigations followed by Tominaga, the halide anions are sufficiently strong to abstract a proton from metal hydride complexes in nonaqueous solvents. Therefore, the reaction rate depends on the proton affinity of such anions. This is supported by the observed effect of anions: the yield of hydroformylation increases in the order Cl > Br > I.

For the second step of the hydroformylation of alkenes with CO_2 catalyzed by ruthenium complexes, the reactivity of CO with cyclohexene in the presence of metal halides has been studied to determine the possible mechanism.[154] The observations by electrospray-ionization mass spectrometry suggested that this step is catalyzed by a combination of mono- and tetranuclear ruthenium complexes ($[RuCl_3(CO)_3]$ and $[H_3Ru_4(CO)_{12}]$). Moreover, $[(cyclohexene)RuCl_2(CO)_3]$ was also observed in the reaction solution. This step involves the coordination of substrates to the mononuclear species, followed by insertion of CO and the hydrogen donation from the tetranuclear species. These observations can be extrapolated to the reactions in ILs. Table 1.1 shows some examples of hydroformylation of alkenes with CO_2 using multinuclear ruthenium complexes and different ILs.

The seminal investigations conducted by Tominaga *et al*. have been used to develop a new strategy for the hydroaminomethylation of olefins. Srivastava *et al*. reported the first example of a one-pot protocol which includes the hydroformylation of alkenes and a subsequent reductive amination which leads to secondary and tertiary amines with good yields[155]. This reaction was carried out in the presence of $Ru_3(CO)_{12}$, CO_2 and an ionic liquid (benzyltriethylammonium chloride).

Table 1.1. CO_2-Hydroformylation of alkenes using $Ru_3(CO)_{12}$ as catalyst precursor[a]

Substrate	Reaction medium	Conversion/Yield[b]	Ref.
1-Hexene	[bmim][Cl]/Toluene	97/84, 0, 11	151, 156
1-Hexene	[bmim][BF_4]/Toluene	96/63, 0, 26	151
1-Hexene	[bmim][PF_6]/Toluene	95 /3, 0, 86	151
1-Hexene	[bmim][Cl]/[bmim][NTf_2][c]	94/82, 0, 9	157
1-Hexene	[bmim][Cl]/[bmim][BF_4][c]	95/71, 0, 9	157
1-Hexene	[bmim][Cl]/[bmim][PF_6][c]	94/50, 0, 7	157
Cyclohexene	[bmim][Cl]/Toluene	80/76, 0, 3	156
α-Methylstyrene	[bmim][Cl]/Toluene	78/50, 0,22	156
α-Methylstyrene	[bmim][Cl]/Benzene	88/62, 2, 22	156
Styrene	[bmim][Cl]/Toluene	100/47, 0, 49	156
Styrene	[bmim][Cl]/Benzene	100/60, 0, 38	156

[a] $p(CO_2/H_2)$ [bar] = 40/40 and T [ºC] = 140 ºC, unless noted; [b]Alcohol, aldehyde, and alkane, respectively; [c] T [ºC] = 160 ºC.

Recently, Porcheddu has demonstrated that formic acid can be used as feedstock in the hydroformylation of alkenes.[158] This procedure avoids all the safety issues related to the use and management of gaseous reagents and facilitates the performance of small scale reactions. However, the reactions have to be conducted in two separated reaction chambers to obtain good yields. The production of CO_2 and H_2 is done in one of the chambers in the presence of a small amount of sodium formate and lithium chloride. The second chamber contains the desired educt and a mixture of ILs ([bmim][Cl]/[bmim][Tf_2N]) to accomplish the hydroformylation. Both chambers contain $Ru_3(CO)_{12}$ as catalyst precursor and heated at the same temperature. Several alkenes were reported to afford the corresponding alcohol through this procedure with high regioselectivity. Some examples are (conversion; yield; *n/iso* ratio): 1-hexene (95; 74; 85/15), 2-methyl-1-hexene (95; 71; 100/0), vinylcyclohexane (94; 81; 82/18), and α-methylstyrene (97; 71; 100/0).

Hydroformylation of alkenes was one of the first catalytic reactions investigated in *sc*CO_2 due to its industrial importance. The conception of using *sc*CO_2 in the hydroformylation of alkenes came as a solution for the high energy-consuming distillations to separate the desired products from the catalyst in the reaction medium.[159-163] Moreover, such distillations have to be often carried out above the decomposition temperature of the catalyst.

Due to the sharp changes in solubilities of dissolved species with density of the supercritical medium, *sc*CO_2 was seen as a solvent for hydroformylation that would facilitate such separations by easy pressure alterations to control fluid density and, in turn, catalyst or product solubility. Additionally, *sc*CO_2 is an environmentally friendly solvent which is miscible with gases such H_2 and CO.

One of the first studies on the use of *sc*CO_2 in hydroformylation was reported by Rathke *et al*. in the late 1980s.[164] Their research can be considered the first systematic study with the aim of understanding the equilibrium and dynamic processes in the hydroformylation of propylene in *sc*CO_2 catalyzed by a dicobalt octacarbonyl complex. Sometime later, several methods were described in the literature involving changes in the temperature and/or pressure in the *sc*CO_2-based hydroformylation reactors to separate the products from the catalyst. However, a separation procedure that occurs under the reactions conditions was more desirable, so that it could be adapted for use in flow systems. Cole-Hamilton *et al*. proposed at first a solution by introducing a highly active catalyst which was poorly soluble in *sc*CO_2.[165] The products could be removed by fluxing them into a second autoclave at low temperature and decompressing the system.

ILs were seen as a solution for these processes due to their poor solubility in *sc*CO_2 (as a result of their ionic character and negligible vapor pressure) and the high solubility of *sc*CO_2 in certain ILs, as observed by Brennecke *et al*.[166] In addition, the ability of CO_2 to induce liquid/liquid-phase separations of ILs and organics have also been studied and it depends on the solubility of CO_2 in the ionic liquid and the hydrogen bonding interactions between the latest and organics.[166-168] Therefore, pure organic compounds could be extracted from the catalyst-containing ionic liquid phase by using *sc*CO_2. There are further remarkable properties of *sc*CO_2-ionic liquid systems: they remain biphasic even at high operating pressures and the presence of *sc*CO_2 decreases the viscosity of the original ILs enhancing the mass transfer and solubility of permanent gases in the liquid phase.[169] This reduction of potential mass transfer barriers can lead to increased reaction rates and selectivities. Additional studies about the interactions of CO_2 or *sc*CO_2 in ILs and their effects have been published elsewhere.[170-173]

It is important to note that symmetric solid organic salts can also be applied in biphasic hydroformylation of olefins by setting their melting point using *sc*CO_2 or even low to moderate CO_2 pressures. As an example, Leitner *et al*. showed that the prototypical hydroformylation of 2-vinyl-naphthalene in $[NBu_4][BF_4]$ is possible by inducing its melting point depression with CO_2.[174] Thus, the melting point of $[NBu_4][BF_4]$ can be significantly lowered from 156 °C to 36 °C at 150 bar, whereas $[NEt_4][CF_3SO_3]$ (m.p. 102 °C) turns to the liquid state already at 20 °C at 35 bar CO_2. This methodology has the potential to expand the number of organic melts by using easy accessible and cheaper symmetric ionic salts as an alternative to ILs.

Cole-Hamilton *et al*. reported the first continuous flow process with immobilization of the catalyst in ILs and extraction with *sc*CO_2.[175] This process showed that the catalyst was stable

during 30 h due to the lack of ligand oxidation. A general design of the applied system for the hydroformylation is depicted in Figure 1.7. This consists of two separated vessels. On the first one, an ionic catalyst is immobilized in the ionic liquid in a stirred reactor.

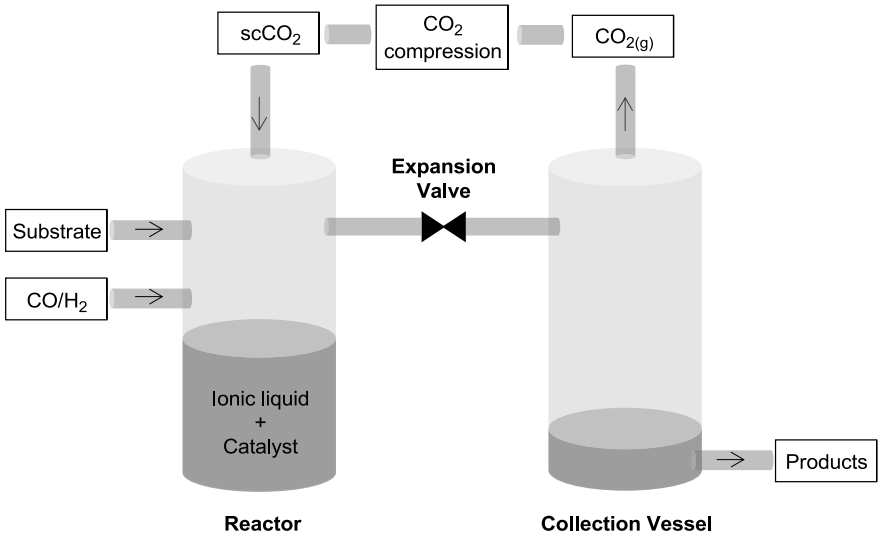

Figure 1.7. General representation of a continuous flow system for hydroformylation in the presence of ILs and using *sc*CO_2 as the transport vector

The desired alkene, CO/H_2, and *sc*CO_2 are introduced continuously at determined rate, coming from separated feeds. The reaction takes place under homogeneous conditions. The expected products and *sc*CO_2 are transferred to a second vessel where they are subject to product separation from the gases by simple expansion. The desired products precipitate immediately due to the poor solvating capacity of the expanded CO_2 under ambient conditions. The catalyst and the ionic liquid stay in the reactor and CO_2 can be recycled. Moreover, CO_2 can be also used as a switchable water additive to allow homogeneous hydroformylation to take place in a monophasic form and to separate the products in a biphasic version.[176] This new technique presented by Jessop *et al.* does not suffer from the traditional mass transfer limitations because the reaction is conducted in a monophasic medium. As noticed by Leitner *et al.*, the right combination of immobilization techniques with modern engineering solutions will cope the still remaining challenges in hydroformylation.[177]

ILs can also participate as ligands when they are used as reaction medium. Formation of *N*-heterocyclic carbene Rh-complexes can take place during the catalysis in imidazolium-based ILs in accordance with several reports about the room temperature C−H activation at the C2/C4 position of imidazolium cations. Evidences for the complexation of Rh with carbenes

in ionic liquid supported oxo synthesis have been reported more intensively in recent years.[178, 179] For instance, the formation of transient carbene species in the ILs-supported hydroformylation of 1-octene was first observed by Dupont *et al*.[179, 180] Based on D/H exchange experiments, it was concluded that NHCs derived from imidazolium moieties are produced in typical [bmim]-based catalytic systems. Moreover, phosphine ligands play an essential role in the creation of carbene species and the presence of weak bases, such as methanol, favors the complexation. Such Rh-NHC complexes do not cause any significant changes in the catalytic activity or selectivity and the NHCs can be displaced by other substrates present in the reaction mixture.

Chapter 2: The Symmetric Carbene-Centered Complexes

Toward New Organometallic Architectures: Synthesis of Carbene-Centered Rhodium and Palladium Bisphosphine Complexes. Stability and Reactivity of $[(PC^{BIm}P)Rh^{I}(L)][PF_6]$ Pincers

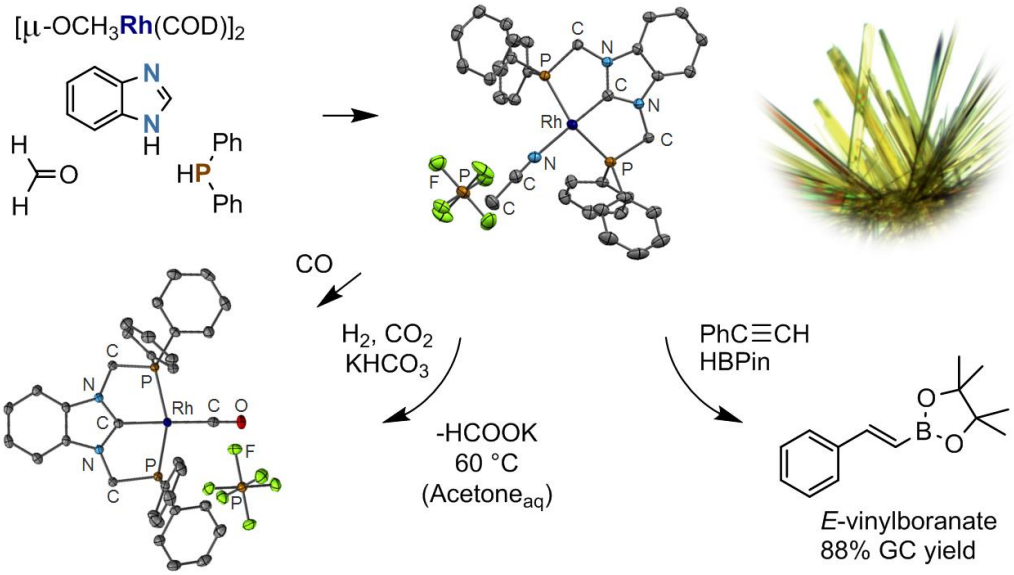

1 Introduction

Research on N-heterocyclic carbenes (NHCs) is an exponentially growing area nowadays. Owing to their easy accessibility, strong coordinating character, oxidation resistance, and high thermal stability of their metal complexes, the NHCs serve as a powerful tool in different research fields[181-185] and are promising ligands for industrially relevant areas.[184, 186-189] Metal−carbene bonds in transition-metal NHC organometallics determine their remarkable catalytic performance in olefin metathesis,[182, 190] hydrogenation reactions,[191, 192] hydroformylation[128] and others.[185, 193] In spite of the broad structural diversity of known NHCs, a search for new architectures and their application fields continues steadily.[187, 191, 194-197] Carbene-based pincer complexes[198, 199] have shown their high potential for various catalytic reactions such as C−C and C−X couplings[54, 184, 200] or alkene isomerization,[201] but examples of their application as catalysts are still rather rare. Notably, the nature of tridentate equatorial ligands allows strong retention of the metal core, resulting in a high thermodynamic stability of the pincers[202] and opens a range of novel catalytic approaches. Moreover, in some cases, the ligand constitution has a crucial impact on the behavior of the catalytic active species, enabling new reaction pathways through ligand−metal cooperation.[67, 69, 203, 204] At the same time, the role of five-membered heterocyclic ligands, their electronic properties, their reactivity, and in particular their cooperative interactions in catalytic processes are of significant interest and have not been studied yet to the full extent. Therefore, we focused our attention on the synthetic accessibility and reactivity of the carbene-centered pincer complexes.

While the [5,5]-membered boron,[8, 34, 35] [6,6]/[5,5]-membered nitrogen,[5 205, 206] [5,5]-membered silicon,[10, 207] [5,5]-triazole,[11] triazolylidene,[12] and [6,6]-(benz)imidazolium[50, 56, 208, 209] carbon-centered phosphine-functionalized pincer complexes were discovered during the past decade, the carbene-based [5,5]-(benz)imidazolium type has remained a challenge (Figure 2.1).[210]

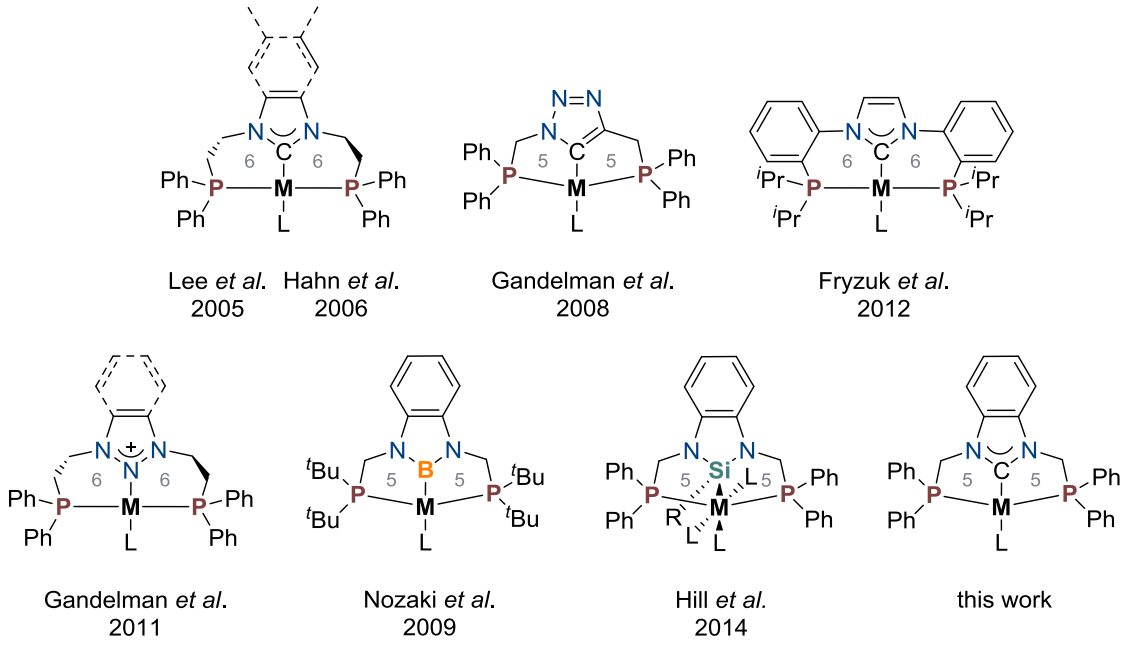

Figure 2.1. Recent developments in heterocyclic-based bisphosphine metal complexes.[211]

In this chapter, we report for the first time the synthesis of a cationic phosphine-functionalized methylene-bridged tridentate benzimidazolin-2-ylidene ligand precursor, its $(PC^{BIm}P)Pd^{II}$ and $(PC^{BIm}P)Rh^{I}$ complexes, as well as the stability study of $(PC^{BIm}P)Rh^{I}$ and evaluation of its chemical behavior in various environments. By combining the features of both the strong σ-donating properties of NHC-moiety and tridentate equatorial complexation mode of the ligands, we present a new tool for organometallic chemistry.

2 Results and discussion

The accessibility of [5,5]-membered $PC^{BIm}P$ metal complexes has been a challenge because of the complexity of the synthesis of a 1,3-bis(diphenylphosphinomethylene)benzimidazolium architecture rather than metal insertion. According to the retrosynthetic analysis represented in Scheme 2.1, the target ionic ligand precursor can be obtained in four steps, starting from commercially available benzimidazole, diphenylphosphine, and formaldehyde. Upon analysis of the critical points of the retrosynthesis, it should be noted that we were not able to perform N-alkylation of benzimidazole in the third position using CH_2Cl_2, CH_2ICl, and CH_2Br_2. This would allow consecutive halogen substitution in the halogenomethylenebenzimidazole moiety by the diphenylphosphine group with formation of the target molecule. The strong electron-acceptor properties of phosphine oxides as well as the steric influence of the tosylate leaving group, which determines the reactivity of the p-toluenesulfonyl derivative,[212] were considered to build a methylene bridge between phosphorus and nitrogen heteroatoms.[210, 213] Therefore,

methylenediphenylphosphinoxide synthone was chosen for N-quarternization. Another problematic issue was deprotection of phosphine oxide, leading to the target molecule. Such reduction takes place normally under relatively harsh conditions but theoretically was evident, proceeding from numerous reports: $AlH(^{i}Bu)_2$,[214] AlH_3,[215] $MeX/LiAlH_4$,[216] $PhSiH_3$,[217, 218] $SiHCl_3$,[219-221] $Ti(O^{i}Pr)_4$/poly(methylhydrosiloxane) (PMHS),[222] $Ti(O^{i}Pr)_4/HSi(OEt)_3$,[223] [Cu]/(PMHS or tetramethyldisiloxane (TMDS).[224] Herein, interaction of another reactive molecule site during the synthesis was expected as well.

Metal insertion was aimed to be performed through the direct metalation of phosphine-functionalized benzimidazolium salt using the appropriate rhodium(I) methoxide or metal chloride precursor. Diphenyl substituents were chosen considering their less steric bulkiness compared to ^{i}Pr and ^{t}Bu. In this work, we set our choice on the normal carbene motif, blocking the fourth and fifth positions by an aromatic ring to prevent the abnormal coordination mode.[225-227] Although, it was expected, that the abnormal carbenes might form more reactive catalytic species.[228-230]

Scheme 2.1. Retrosynthetic analysis of target phosphine-functionalized methylene-bridged benzimidazolinium salts.

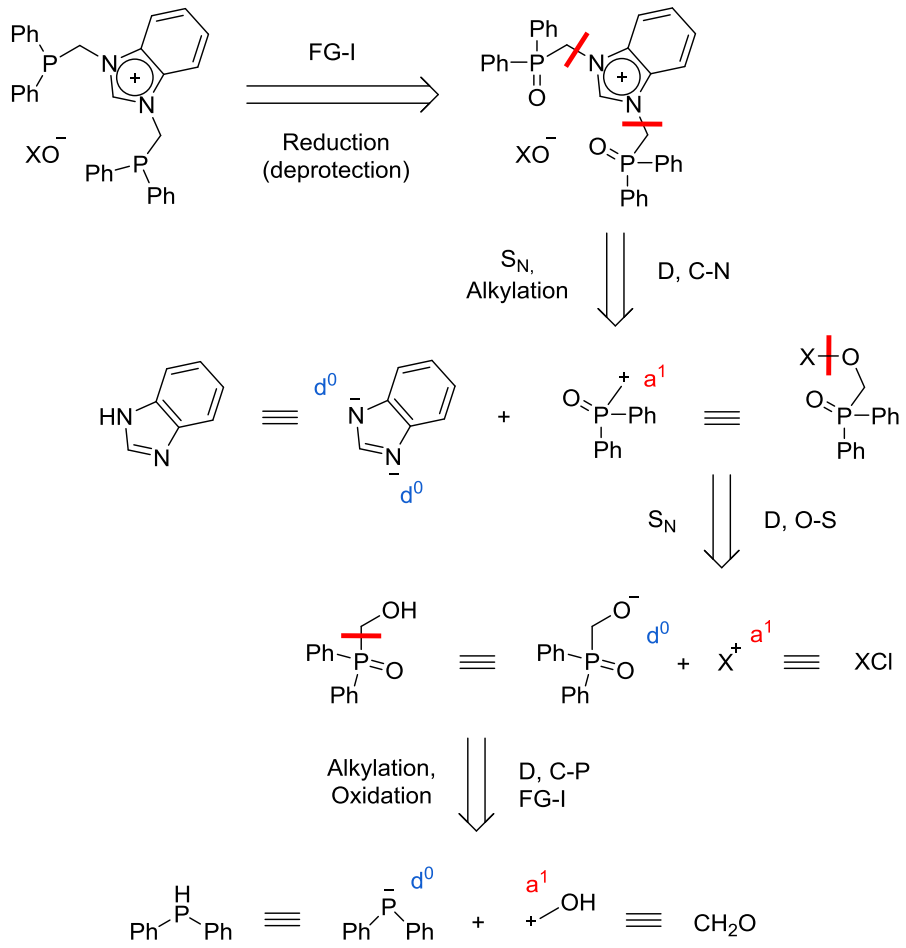

[(Diphenylphosphoryl)methyl]-4-methylbenzenesulfonate (**2.1**) can be obtained with moderate yields according to the previous works.[212] We have significantly optimized and modified the synthesis of **2.1** to the gram scale with an overall yield of 71% [see the Experimental Section (ES)]. While the first alkylation of benzimidazole gives an almost quantitative yield of 1-[(diphenylphosphoryl)methylene]benzimidazole (**2.2**) in the presence of K_2CO_3 in dimethyl sulfoxide (DMSO), the second alkylation step could be performed only under neat conditions, slightly over the melting point of **2.1**. The obtained diphenylphosphoryl derivative 1,3-bis[(diphenylphosphoryl)methylene]benzimidazolium 4-methylbenzylsulfonate (**2.3**) was then reduced using a $Ti(O^iPr)_4$/PMHS system.[222, 231] This reaction is conducted by simultaneous hydrogenation of the benzimidazolium fragment giving 1,3-bis(diphenylphosphinomethylene)benzimidazoline (**2.4**). The phosphine deprotection is highly dependent on reaction conditions. Thus, conducting the reaction over more than 3 h or increasing the temperature over 70 °C led to the formation of several byproducts in most of

the cases, because of decomposition of the reaction product. Interestingly, the use of $HSiCl_3$ as a reducing agent[226] led to hydrogenation of the only cationic moiety without P–O bond reduction under mild conditions. By testing several known synthetic dehydrogenation approaches[196, 232-237] we have found that the most successful was the use of nonmetal containing reagents, viz., triphenylcarbenium derivatives.[238, 239] Thus, the target 1,3-bis(diphenylphosphinomethylene)benzimidazolium salt was obtained in one step by hydride abstraction from **2.4** with the simultaneous introduction of a noncoordinating hexafluorophosphate counterion (Scheme 2.2). Because of the ring-opening polymerization of tetrahydrofuran (THF) caused by $[(C_6H_5)_3C][PF_6]$, low temperatures (–78 °C) and short reaction times (30 min) are required.

Scheme 2.2. Synthesis of **2.5**.

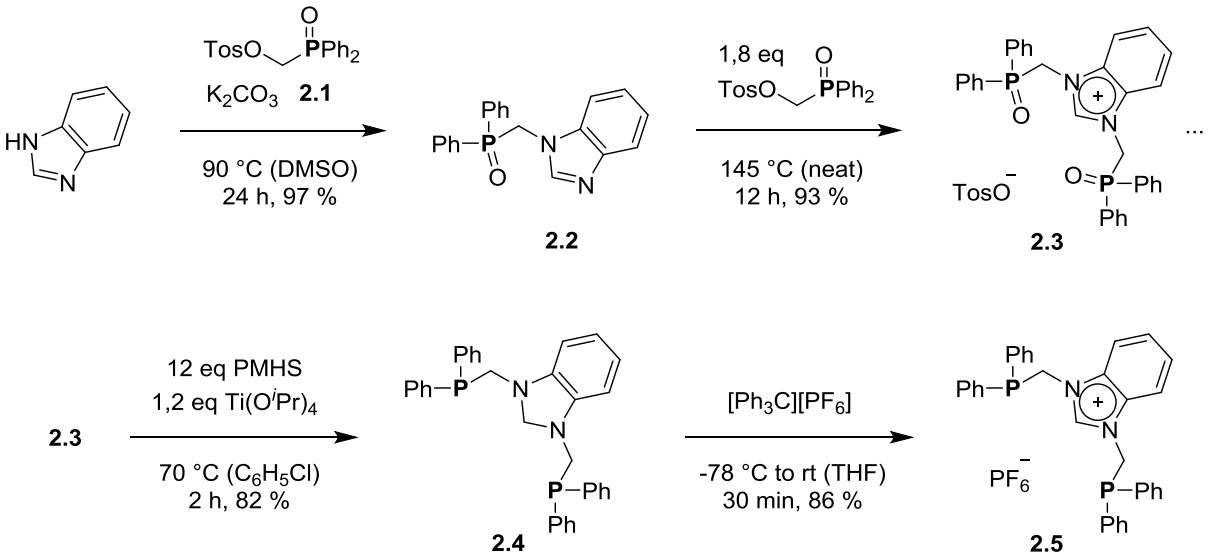

The structure of the ligand precursor 1,3-bis(diphenylphosphinomethylene)benzimidazolium hexafluorophosphate (**2.5**) was confirmed by NMR spectroscopy, mass spectrometry (MS) and elemental analysis (EA). Several characteristic chemical shift values of ^{1}H, ^{31}P, ^{13}C nuclei should be pointed out for this compound. In the ^{31}P NMR, a sharp singlet for the two equivalent phosphorus atoms is observed at –14.05 ppm, along with a typical septet for phosphorus atom of the non-coordinated PF_6 group in the upfield region at –144.0 ppm ($J^{P\text{-}F}$ = 706.7 Hz). Two equivalent methylene groups appear as a doublet at 5.15 ppm ($J^{2,H\text{-}P}$ = 5.4 Hz), and the singlet of the acidic proton was detected at 8.69 ppm in CD_3CN in the ^{1}H NMR spectrum. The signals of C2, as well as carbon atoms of the methylene bridges were found at 140.61 ppm (t, $J^{3,C\text{-}P}$ = 3.9 Hz) and 47.55 ppm (d, $J^{2,C\text{-}P}$= 20.9 Hz) in the ^{13}C NMR spectrum

(CD_3CN) respectively. An X-ray single crystal analysis established the structural details of the methylene-bridged ligand precursor **2.5**, confirming formation of the desired proligand. The results are consistent with those reported for the PBP X-ray structure (Figure 2.2).[8]

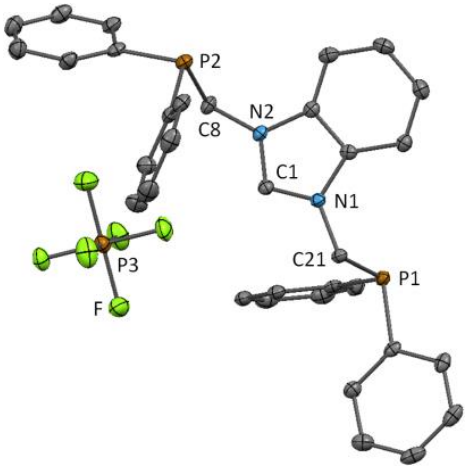

Figure 2.2. Crystal structure of **2.5** (50% displacement ellipsoids; hydrogen atoms were omitted for clarity). Selected interatomic distances (Å): N1–C1, 1.3323(19); N2–C1, 1.3296(19); N1–C21, 1.4646(18); N2–C8, 1.4674(18); P1–C21, 1.8736(15); P2–C8, 1.8686(15); angles (deg): C1–N2–C8, 125.46(12); C1–N1–C21, 126.71(12); N1–C21–P1, 113.21(10); N2–C8–P2, 112.25(10)

The obtained organic salt **2.5** undergoes complexation with $[\mu\text{-}OCH_3Rh(COD)]_2$ smoothly through deprotonation of the benzimidazolium moiety, forming the target organometallic product $[(PC^{BIm}P)Rh^{I}(solvent)][PF_6]$ (**2.6**) under mild hydrogenation conditions (Scheme 2.3). The use of simple inorganic metal halides like $PdCl_2$ as precursors for the synthesis of $PC^{BIm}P$-based organometallics was also tested. The palladium complex 1,3-bis(diphenylphosphinomethylene)benzimidazol-2-ylpalladium chloride hexafluorophosphate (**2.7**) was obtained by direct complexation without the addition of a base according to analogous procedures.[11, 208]

The structures of $(PC^{BIm}P)Rh^{I}$ complexes **2.6a** and **2.6b**, as well as $(PC^{BIm}P)Pd^{II}$ complex **2.7** were confirmed by NMR, MS, IR and X-ray techniques (see ES). The following NMR chemical shifts give exhaustive evidence for complexation of these transition metals. Thus, the signal corresponding to the two phosphorus atoms shifts from –14.05 ppm (ligand precursor) to 45.84 ppm (d, $J^{P\text{-}Rh}$ = 152.8 Hz) for the rhodium complex **2.6b** and to 38.16 ppm (singlet) for the palladium complex **2.7** in the ^{31}P NMR spectrum. The methylene protons were detected at 4.97 ppm (vt, $J^{H\text{-}P}$ = 3.0 Hz) for **2.6b** and at 5.45 ppm (vt, $J^{H\text{-}P}$ = 3.3 Hz) for **2.7** in the ^{1}H NMR spectrum, while the characteristic singlet of the acidic proton H2 at 8.69

ppm disappears in both cases during the reaction. The doublets related to the carbon atoms of the methylene bridges shift and split to virtual triplets from 47.55 ppm (d, J^{C-P}= 20.9 Hz) in the ligand precursor to 51.43 ppm (vt, J^{C-P}= 16.8 Hz) for **2.6** and 52.43 ppm (vt, J^{C-P} = 17.8 Hz) for **2.7**, as observed by ^{13}C NMR. In addition, the C2 atom signal is shifted to the downfield from 140.61 ppm (t, $J^{2,C-P}$ = 3.9 Hz) to 198.96 ppm (dt, J^{C-Rh} = 51.2 Hz, $J^{2,C-P}$ = 11.9 Hz) for **2.6b** and 178.82 ppm (t,$J^{2,C-P}$ = 5.8 Hz) for **2.7**.

Scheme 2.3. Synthesis of **2.6a**, **2.6b** and **2.7**

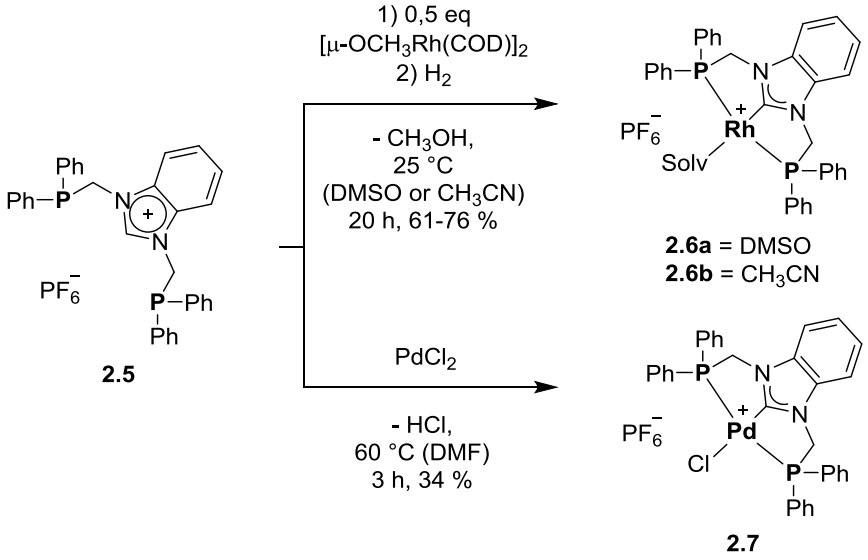

Single crystals suitable for X-ray crystallographic analysis were grown from DMSO/ethanol (Et_2O) and acetonitrile (CH_3CN)/Et_2O solutions. The structures of **2.6a**, **2.6b**, and **2.7** are presented in Figures 2.3 and 2.4.

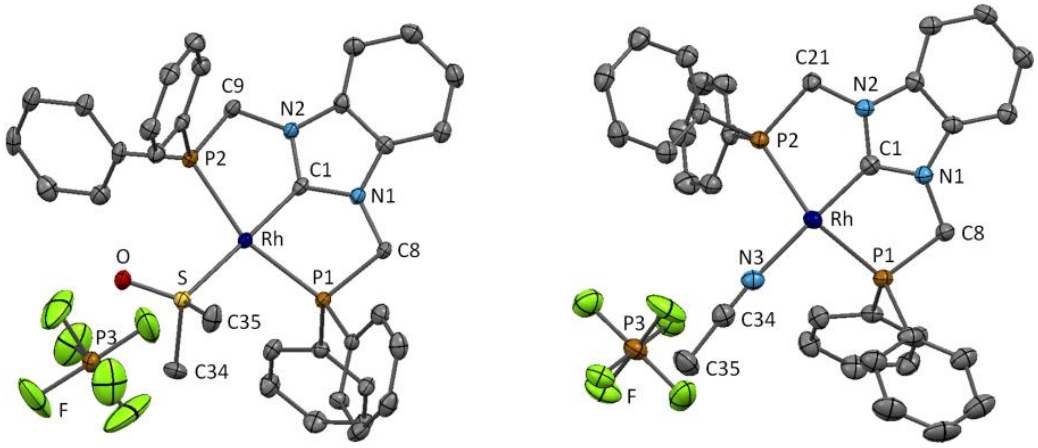

Figure 2.3. Crystal structures of **2.6a** (at the top) and **2.6b** (at the bottom) (50% displacement ellipsoids; hydrogen atoms were omitted for clarity). **2.6b**: Selected interatomic distances (Å):

Rh-N3, 2.091(3); Rh–C1, 1.933(3); Rh–P1, 2.2739(8); Rh–P2, 2.2976(8); N1–C1, 1.369(4); N2–C1, 1.365(4); N1–C8, 1.457(4); N2–C21, 1.457(4); P1–C8, 1.873(3); P2–C21, 1.860(3); angles (deg): N3–Rh–C1, 178.15(12); P1–Rh–P2, 155.28(3); N1–C1–N2, 106.0(3); torsion angles (deg): Rh–P1–C8–N1, -6.18; Rh–P2–C21–N2, 21.64

Hereby, because of the limited quality of the measured crystal, we do not discuss the molecular structure of **2.6a** in detail (for metrical data, see ES). A small fraction of the whole molecule disorder could not be resolved and yields residual electron densities of the second set of heavy atoms, which result in a checkcif A-alert.

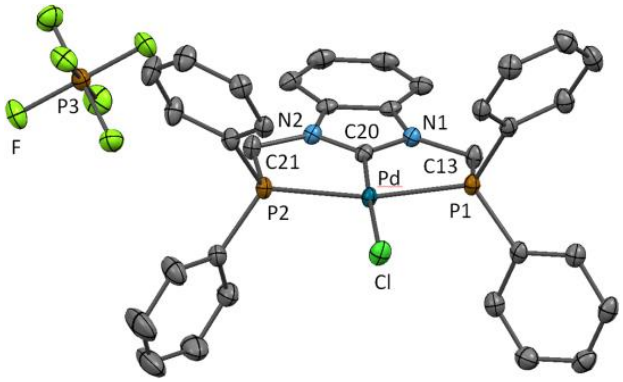

Figure 2.4. Crystal structure of **2.7** (50% displacement ellipsoids; hydrogen atoms were omitted for clarity). Selected interatomic distances (Å): Pd–Cl, 2.3381(5); Pd–C20, 1.9356(17); Pd–P1, 2.2924(5); Pd–P2, 2.3098(5); N1–C20, 1.346(2); N2–C20, 1.345(2); N1–C13, 1.457(2); N2–C21, 1.457(2); P1–C13, 1.8606(18); P2–C21, 1.8688(19); angles (deg): Cl–Pd–C20, 176.95(5); P1–Pd–P2, 162.76(2); N1–C20–N2, 108.06(14); torsion angles (deg): Pd–P1–C13–N1, 16.16; Pd–P2–C21–N2, –2.33

The $PC^{BIm}P$ pincer ligand coordinates meridionally upon reaction with the tested late-transition metal precursors. The rhodium and palladium adopt a distorted square-planar geometry, which is consistent with the reported $(PBP)Rh^{I}$ [34] and $(PCP)Pd^{II}$ [11] X-ray structures. The fourth coordination site is occupied by a loosely bound solvent molecule in **2.6a**, and **2.6b** or by a halogen atom in **2.7** *trans* to the carbene. The heterocyclic rings in methylene-bridged **2.6b** and **2.7** are not twisted from the rhodium and palladium planes as it was the case for the ethylene-bridged imidazole-centered[50, 208] or phenylene-bridged dihydroimidazole-based bisphosphine complexes[56] and coordinate in a planar fashion to the metal center. The geometry of complex **2.7** is consistent with the calculated 1,3-bis(diphenylphosphinomethylene)imidazol-2-ylpalladium chloride reported by Lee *et al*.[208]

In this work, we have mainly focused on rhodium complexes, although the $PC^{BIm}P$ palladium organometallic compounds undoubtedly deserve no less attention. Upon a study of the stability of **2.6a** and **2.7**, it was observed that the rhodium complexes were stable in the presence of moisture but underwent degradation in oxygen containing environments, while the palladium complex **2.7** remained stable under moisture and air over weeks in solution.

Thermogravimetric analysis (TGA) of substances **2.5** and **2.6a** in the solid state shows that complexation of the metal by organic salt **2.5** leads to some stabilization of the carbon-heteroatom-alternated molecule architecture. While the $PC^{BIm}P$ ligand precursor decomposes at an offset temperature of 221 °C with 97% mass loss, the rhodium complex undergoes degradation in three steps at 131, 258 and 513 °C with an overall mass loss of around 73% (Figure 2.5). The first degradation step up to 258 °C corresponds to the mass loss of coordinated DMSO (m/z 78; mass loss 9.29%), and subsequently other degradation products are released.

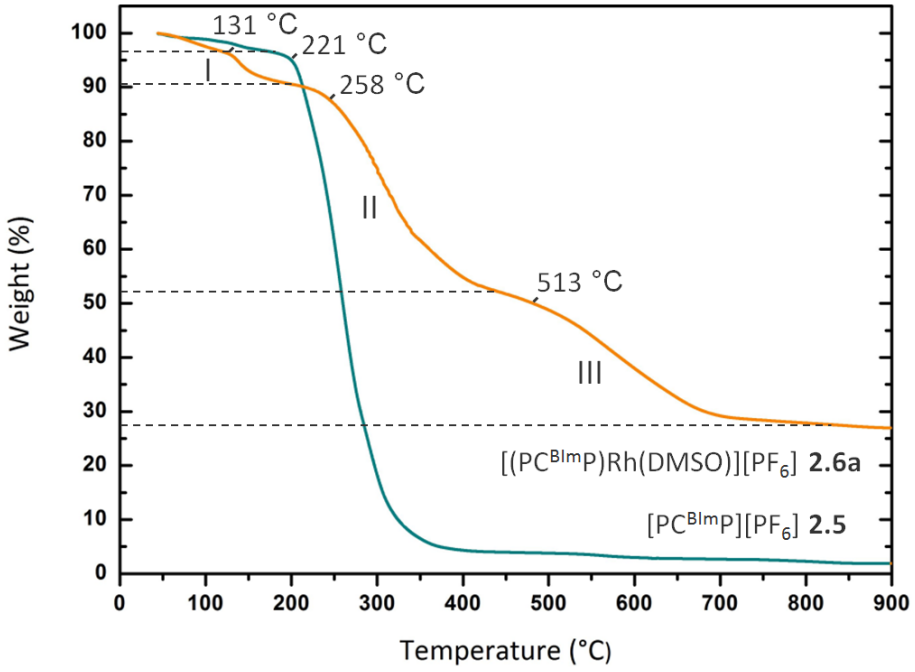

Figure 2.5. TGA of the $PC^{BIm}P$ ligand precursor **2.5** and the $(PC^{BIm}P)Rh^{I}$ complex **2.6a**.

Furthermore, we were interested in exploring the chemistry of organometallic compound **2.6b** and determining its stability and reactivity in various environments, taking into account possible side reactions

First, the interaction of **2.6b** with π-acceptor ligands was investigated (Scheme 2.4). The 16-electron square-planar rhodium carbonyl complex **2.8** was obtained by exposure of **2.6b** to a carbon monoxide (CO) atmosphere (1–10 bar) in PO. On the other hand, ethylene binds

reversibly to the rhodium atom in PO, dichloromethane (CH_2Cl_2), and THF at 25 °C, as observed by an in situ ^{31}P NMR experiment. After ethylene was added to the solutions of **2.6b**, a new doublet signal was detected at 61.29 ppm (d, $J^{P\text{-}Rh}$ = 137.6 Hz), evidencing the formation of 1,3-bis(diphenylphosphinomethylene)benzimidazol-2-ylrhodium ethylene hexafluorophosphate (**2.9**, see the ES). However, the ethylene-coordinated complex could not be isolated from those polar solvents.

Scheme 2.4. Reactions of CO and ethylene with **2.6b**. Conversion is estimated by ^{1}H and ^{31}P NMR spectroscopy

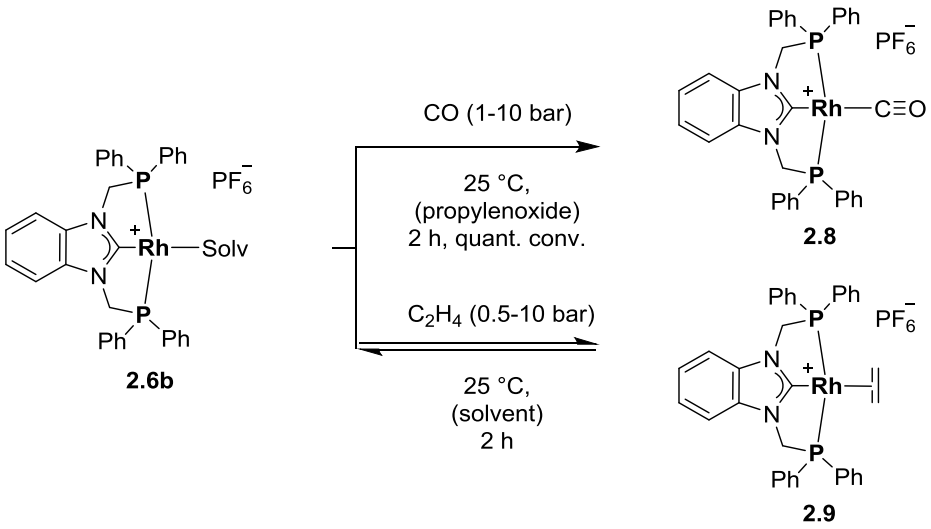

The coordination of CO causes the chemical shift of the phosphorus atoms from 45.84 ppm (d, $J^{P\text{-}Rh}$ = 152.8 Hz) for **2.6b** to 55.41 ppm (d, $J^{P\text{-}Rh}$ = 138.5 Hz) in the downfield of the ^{31}P NMR spectrum. In the ^{1}H NMR spectrum, the signal related to the methylene protons is also shifted downfield and appears at 5.37 ppm (vt, $J^{H\text{-}P}$ = 3.1 Hz). It is worth noting that the shift of all proton signals to the high-frequency field took place after CO was bound to the metal center, evidencing an overall decrease of the electron density around the hydrogen atoms. In addition, the ^{13}C NMR chemical shift of the C2 nucleus changed from 198.96 ppm (dt, $J^{C\text{-}Rh}$ = 51.2 Hz, $J^{2,C\text{-}P}$ = 11.9 Hz) to 197.21 ppm (dt, $J^{C\text{-}Rh}$ = 40.5 Hz, $J^{2,C\text{-}P}$ = 12.6 Hz), as well as the displacement of all quaternary carbon atoms signals ($C9^{all}$, C3a, C7a) to the upfield region was observed for complex **2.8**. The signals of all other carbon atoms shift in direction of high frequencies following the common tendency. The singlet of the carbon-13 atom of the carbonyl group was detected at 195.96 ppm.

The light-yellow crystals of **2.8** suitable for X-ray analysis were grown by the addition of diethyl ether to the reaction mixture. The solid-state structure of **2.8** (Figure 2.6) represents the expected distorted square-planar environment around rhodium. Powder IR spectroscopy

showed the characteristic CO stretching band at 1995 cm^{-1}. This value indicates a medium electron-donating character of the $PC^{BIm}P$ ligand, which is comparable with that of the phosphaferrocene-pyrrole-based pincer ligand (ν = 1990 cm^{-1}) reported by Mathey *et al*.[205]

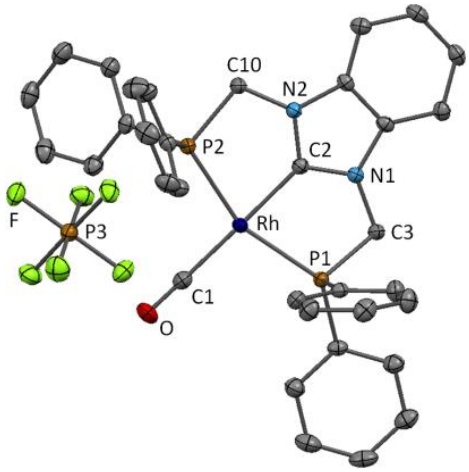

Figure 2.6. Crystal structure of **2.8** (50% displacement ellipsoids; hydrogen atoms were omitted for clarity). Selected interatomic distances (Å): Rh–C1, 1.8882(17); Rh–C2, 1.9994(15); Rh–P1, 2.3003(4); Rh–P2, 2.3093(4); N1–C2, 1.3521(19); N2–C2, 1.354(2); N1–C3, 1.4571(19); N2–C10, 1.4605(19); P1–C3, 1.8726(16); P2–C10, 1.8606(16); C1–O, 1.142(2); angles (deg): C1–Rh–C2, 178.80(7); P1–Rh–P2, 153.52(1); N1–C2–N2, 106.90(13); torsion angles (deg): Rh–P1–C3–N1, 24.38; Rh–P2–C10–N2, -5.34

The CO bond vibration of **2.8** is considerably higher than the values obtained for weak π-acceptor ligands $PC^{m\text{-phenylene}}P$[240] (ν = 1929 and 1943 cm^{-1}), $PC^{Im}P$[50] and PBP[34] (ν = 1933 cm^{-1}). According to received data of crystallographic analysis it can be stated that the reason of such high values of vibration frequency is pronounced π-backbonding to the carbene ligand. The orientation of benzimidazole ring co-planar to the plane defined by Rh–C1–C2–P1–P2 results in the efficient overlap of metal d_π orbital with the p_z orbital of the carbon. Nevertheless, the $PC^{BIm}P$ ligand possesses weaker π-acceptor properties than the nitrenium-based PNP ligand (ν = 2024 cm^{-1}),[5] which is considered to be a good π-acceptor. Dependence of electronic properties of ligands from their constitution can be quantitatively evaluated using characteristic carbonyl stretching frequencies, as shown on the example of series of known pincer complexes in the Figure 2.7.

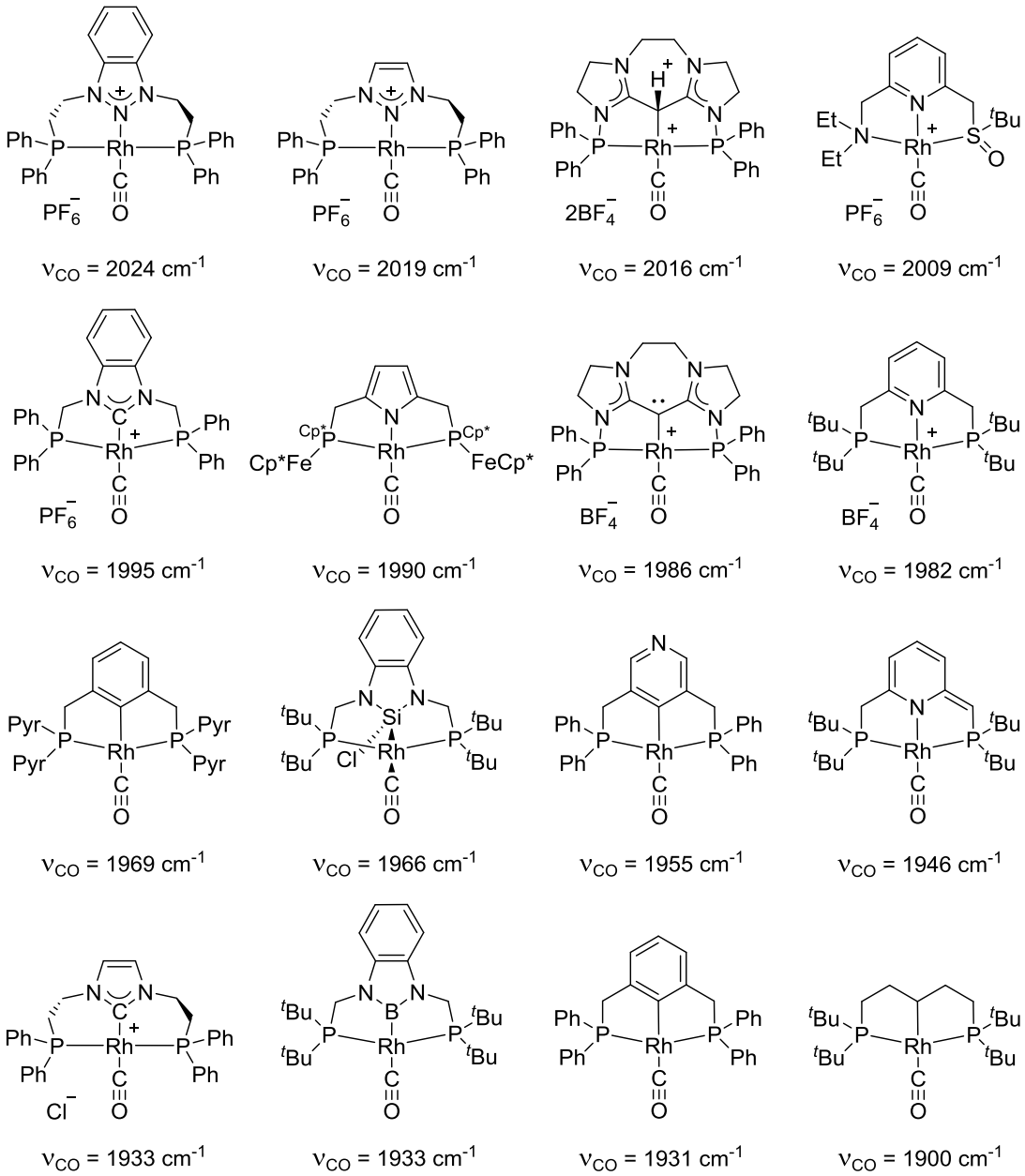

Figure 2.7. Selected bisphosphine rhodium carbonyl complexes and their characteristic carbonyl stretching frequencies. Compounds are arranged in order of increasing electron donating character of the ligands (from the upper left corner to the bottom right corner of the figure)

Compound **2.6b** shows very good solubility in CH_3CN, DMSO, dimethylformamide (DMF), acetone, CH_2Cl_2, chloroform, and PO; poor soluble in methanol, isopropyl alcohol, and THF; extremely sparingly solubility in n-butanol and other long chain alcohols, and no solubility in benzene, toluene, ethyl acetate, diethyl carbonate, cyclohexanone, diethyl ether, and hydrocarbons.

The thermal stability of [($PC^{BIm}P$)Rh^{I}(solvent)][PF_6] (**2.6b**) in solution is mainly determined by its anion stability[241, 242] and the ability of the organometallic cationic moiety to react with solvents at elevated temperatures, as we have seen from a number of tests. Thus, a series of experiments was conducted to evaluate the reactivity of **2.6b** against various substrates. Complex **2.6b** reacts with chloroform at 25 °C and CH_2Cl_2 at elevated temperatures, giving a range of various reaction products as a consequence of the oxidative addition of halogenated hydrocarbons[50] (Figure S2.10). Compound **2.6b** remained stable in CH_3CN under an argon atmosphere by heating to 120 °C over 20 h. A Further temperature increase up to 125–130 °C resulted in complete decomposition of the hexafluorophosphate anion and formation of several organometallic products containing the ($PC^{BIm}P$)Rh fragment (Figure S2.11). Considering the stability of the PF_6 anion, we observed that hexafluorophosphate was much more stable in basic environments. Thus, its decomposition was not visible in DMF at 150 °C after 17 h and in an n-octene/ammonia mixture at 180 °C after 12 h. No rearrangement of the rhodium complex due to P–C^{Ph} bond cleavage was observed through a study of its thermal stability in solution.

The stepwise heating of **2.6b** in CH_3CN in hydrogen atmosphere (1 bar) led to the formation of a new organometallic product [39.88 ppm (d, $J^{P\text{-}Rh}$ = 157.6 Hz; ^{31}P NMR] followed by slow deposition of rhodium black from solution during prolonged heating at 80 °C. The observed intermediate could not be isolated in the solid state via the fractional crystallization of components from the reaction mixture. Further attempts to obtain classical or nonclassical monometallic $PC^{BIm}PRh$ hydride species through the direct reaction of **2.6b** with hydrogen in suitable polar solvents were not successful. Nevertheless, the reaction of **2.6b** with 30 equiv of $KHCO_3$ in THF/H_2O under a H_2 atmosphere proceeds with quantitative conversion to the hydride-bridged dimer [($PC^{BIm}PRh^{I}$)$_2$(μ-H)][PF_6] (**2.10**), which is a rare example of a pincer-ligated bimetallic cluster (Scheme 2.5).[243] Such dimerization is evidently favored by insufficient steric hindrance of the phenyl substituents. The μ-hydride characteristic peak appears as a multiplet at –9.15 ppm; the eight protons of the methylene fragments show up as an unresolved multiplet at 4.79 ppm in the ^{1}H NMR spectrum. The ^{31}P NMR spectrum exhibits a doublet at 55.90 ppm (d, $J^{P\text{-}Rh}$ = 156.5 Hz) assigned to four phosphorus nuclei along with the typical multiplet of the PF_6 anion. The crystallographic analysis clearly confirms the dinuclear mono-hydride-bridged structure with the interrhodium distance of 2.807 Å and a Rh1–H1–Rh2 bond angle of 109.4(13)° (Figure 2.8). These values give evidence for significant metal–metal interaction in [($PC^{BIm}PRh^{I}$)$_2$(μ-H)][PF_6] analogous to homotypic

[(PC$^{m\text{-phenylene}}$PPt)$_2$(μ-H)][SbF$_6$] dimer and [(X(R$_3$P)$_2$Pt)$_2$(μ-H)]$^+$ clusters, for which the diminution of the Pt–H–Pt angle results in a stronger direct Pt–Pt overlap.[243, 244]

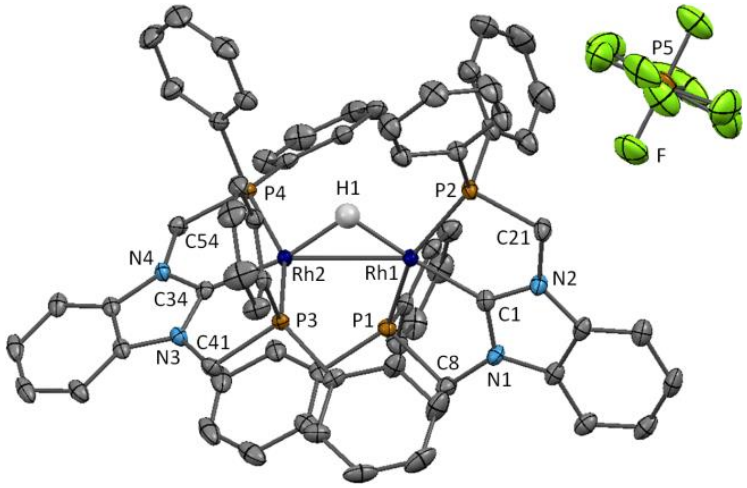

Figure 2.8. Crystal structure of **2.10** (50% displacement ellipsoids; hydrogen atoms except H1 were omitted for clarity). Selected interatomic distances (Å): Rh1–Rh2, 2.8075(2); Rh1–H1, 1.71(2); Rh2–H1, 1.73(2); Rh1–C1, 1.941(2); Rh2–C34, 1.937(2); Rh1–P1, 2.2905(5); Rh1–P2, 2.2379(5); Rh2–P3, 2.2823(5); Rh2–P4, 2.2311(5); N1–C1, 1.363(2); N2–C1, 1.369(3); N3–C34, 1.368(3); N4–C34, 1.367(3); N1–C8, 1.454(3); N2–C21, 1.456(2); N3–C41, 1.452(3); N4–C54, 1.457(3); P1–C8, 1.874(2); P2–C21, 1.867(2); P3–C41, 1.878(2); P4–C54, 1.878(2); angles (deg): Rh1–H1–Rh2, 109.57; Rh2–Rh1–C1, 156.86(6); H1–Rh1–C1, 167.7(8); Rh1–Rh2–C34, 150.23(6); H1–Rh2–C34, 170.7(8); P1–Rh1–P2, 154.36(2); P3–Rh2–P4, 153.88(2).

It is worth noting that the reaction of complex **2.6b** with HCOOK also produces **2.10** in the absence of hydrogen in THF, as revealed by ^{31}P NMR. This allows us to assume, that potassium bicarbonate is being hydrogenated to HCOOK at the first step and decomposes than on **2.6b** forming **2.10** (Scheme 2.5).

Not only is the excision of a carbonyl group from organic substrates considered as an important useful industrial catalytic approach for selective conversion of biorenewable materials or for energy applications,[24, 245] but it is also often mentioned as an undesirable reaction, leading to deactivation of an active catalyst through its complexation with a carbonyl group, for instance, in catalytic dehydrogenation.[24, 33, 246, 247] The activity of transition-metal pincer complexes in stoichiometric CO excision through C–H and C–C bond activation is pronounced and is reflected in numerous studies on [(PNP)RuH$_2$(H)],[248] [(PC$^{m\text{-phenylene}}$P)IrH$_2$],[21] [(^{CF_3}PC$^{m\text{-phenylene}}$P^{CF_3})Ir(L)],[33] [(PC$^{m\text{-phenylene}}$P)RhN$_2$],[249]

[(PN^{Py}P)RhH(C_6H_5)][PF_6],[247] and [(PBP)Rh].[34, 35] Therefore, we were interested in the reactivity of [(PC^{BIm}P)Rh^{I}(CH_3CN)][PF_6] **2.6b** against oxygen-containing substrates at elevated temperatures. According to the ^{31}P NMR screening experiments, heating of **2.6b** in β-propiolactone, THF, diethyl carbonate, DMF, acetone, methanol and aliphatic aldehydes (S14-21) ultimately results in C–H or C–C bond activation followed by formation of the [(PC^{BIm}P)Rh^{I}CO] moiety. Such thermally induced decarbonylation is accompanied in most cases by degradation of the PF_6 anion in neutral environments. The ^{31}P NMR monitoring of the reaction with undecanal exemplarily shows a slow transformation of **2.6b** to the carbonyl complex at 110 °C, while no formation of intermediary organometallics could be observed. Further development of this system, allowing regeneration of active (PC^{BIm}P)Rh species by CO dissociation from the complex, would open up applications in catalytic defunctionalization of organic compounds.

We also tested the catalytic hydrogenation of CO_2 (10–30 bar) and $KHCO_3$ with H_2 (10 bar) in THF/H_2O and acetone/H_2O solvent mixtures at 60 °C for 40 h. Complex **2.6b** produced potassium formate with very low catalytic activity in acetone/H_2O under such mild reaction conditions. No detectable decomposition of either [(PC^{BIm}P)Rh(L)] or [PF_6] was observed under a reducing atmosphere of H_2 in a basic environment. It is worth noting that **2.6b** has been converted quantitatively into **2.8** in an acetone/H_2O mixture during the reaction, as was confirmed by ^{31}P NMR analysis (Figure S2.24). A small amount of formed carbonyl complex **2.8** was also identified in ^{31}P NMR after the reaction of CO_2 and H_2 without the addition of $KHCO_3$. The use of the rhodium carbonyl complex **2.8** under the same hydrogenation conditions led again to conversion of potassium bicarbonate to potassium formate. Therefore, [(PC^{BIm}P)Rh^{I}CO][PF_6] can be seen as a resting state of the catalytic active species. Unfortunately, we could not find any traces of free CO in the gas phase over the reaction mixture using micro GC–MS and IR techniques (S2.27-2.28). It follows that decarbonylation of bicarbonate in aqueous acetone occurs stoichiometrically on complex **2.6b**, in accordance with observations made by Ozerov *et al*. (Scheme 2.5).[248]

Scheme 2.5. Formation of dinuclear rhodium-μ-hydride cluster **2.10** and hydrogenation of $KHCO_3$ and preliminary results of stoichiometric decarbonylation of substrates by **2.6b**.

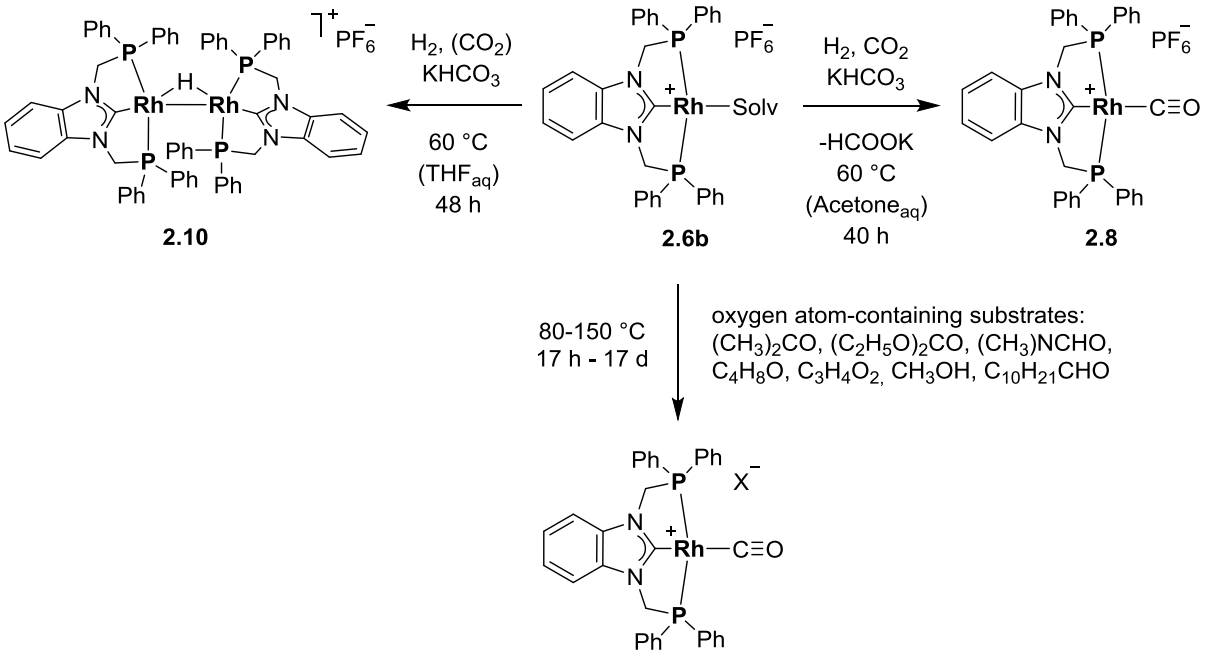

Blocking of coordination site located *trans* to the carbene as the result of the complexation with strongly coordinating CO ligand, and formation of dimeric complex are side reactions that may lead to significant reduction of the activity of the $[(PC^{BIm}P)Rh^{I}(L)][PF_6]$ catalytic species or to its complete deactivation. That is why we consider that primarily prevention of these side reactions is one of the principal objective of the efficient use and further study of $(PC^{BIm}P)Rh^{I}$ complexes in catalytic processes. It is expected that dimerization reaction can be prevented by changing of phenyl groups to more sterically crowded ^{i}Pr or ^{t}Bu rests. Strong coordination of CO to the metal provides much greater difficulties. The carbonyl group can be labilized by changing of rhodium oxidation state and electronic effect of coligands through the *trans*-effect. External influence of energy rich UV irradiation also can promote the elimination of CO from the complex. According to our preliminary experiments was shown that when complex **2.8** is irradiated all over the UV spectrum in CH_3CN, no disruption of Rh−CO bond, transition of CO to the gas phase and formation of **2.6b** took place. One of further possible approaches may be significant increase of the σ-type of M−CO bond and as the result activation of the carbonyl moiety. In this case activated carbonyl ligand can be exposed to nucleophilic attack and removed from the complex being incorporated as C^1 fragment into a molecule of a reaction product. One of alternative ways is changing of rhodium to other metal with less affinity for CO.

A series of experiments with Lewis basic and acidic reagents were conducted to find reactive forms of [($PC^{BIm}P$)$Rh^{I}(CH_3CN)$][PF_6]. Thereby, $NaO^{t}Bu$ reacts with **2.6b** forming a less polar organometallic compound containing no PF_6 counterion. According to the ^{1}H NMR analysis there is the presence of multiplets typical for protons of the benzimidazole fragment 6.94 ppm (m, 2H) and 6.62 ppm (m, 2H), methylene protons at 4.07 ppm (vt, 4H), and the signal in the negative region of the spectrum at –3.34 ppm (s, 1H). Two chemically equivalent phosphorus nuclei were determined at 50.10 ppm (d, J = 162.6 Hz, 2P) in ^{31}P NMR spectrum (Figure S2.29). This reaction product was not isolated in crystalline form and detailed studies have not been conducted because of the small amounts of the obtained compound.

When reacting [($PC^{BIm}P$)$Rh^{I}(CH_3CN)$][PF_6] with two equivivalents [$(C_6H_5)_3C$][PF_6] in Et_2O for two days two new organometallic compounds with the characteristic signals 48.86 (d, $J^{P\text{-}Rh}$ = 99.61 Hz, 2P) **2.11** and 42.29 ppm (d, $J^{P\text{-}Rh}$ = 74.40 Hz, 2P) **2.12** were observed in the ^{31}P NMR spectrum. According to the ^{1}H NMR analysis there is the presence of hydride (–15.22 ppm, dt) within one of the products. Subsequently was found that by varying of the nature of the solvent and the reaction time each of the observed compounds can be isolated. Thereby, conducting the reaction in THF for 15 minutes leads to a quantitative conversion to the hydride complex **2.11**. It is noteworthy that the signal of methylene protons splits into four virtual triplet in the range 5.62–5.19 ppm, which indicates significant violation of the symmetry of ($PC^{BIm}P$)Rh fragment (Figure S2.30). The analogous signal splitting pattern was observed for distorted trigonal-bipyramidal [(PBP)Rh^{III}HCl] and [(PBP)Rh^{III}(H)OTf] complexes by Nozaki *et al.*[34] The presence of the hydride and more than one PF_6 anions in the structure of the molecule, as well as a diamagnetic behaviour of the obtained compound give the reason to anticipate the change in the oxidation state of rhodium from I to III after the reaction.

The detailed study of redox reactivity of mononuclear [($PN^{Py}P$)Rh^{II}(L)][BF_4] complexes was recently reported by Feller *et al*. The author observed the oxidation of [($PN^{Py}P$)Rh^{I}Cl] (**2.13**) to the paramagnetic complex [($PN^{Py}P$)Rh^{II}Cl][BF_4] (**2.14**) without abstraction of chloride in the reaction with $AgPF_6$ in acetone. On the other hand, treatment of [($PN^{Py}P$)Rh^{I}Cl] with 1 equiv CF_3COOAg in the same solvent resulted in the abstraction of halogen atom rather than the oxidation of the metal (Scheme 2.6).

Scheme 2.6. Formation of mononuclear PN^{Py}P rhodium(II)chloride tetrafluoroborate **2.14** and PN^{Py}P rhodium(I) trifluoroacetate **2.15**

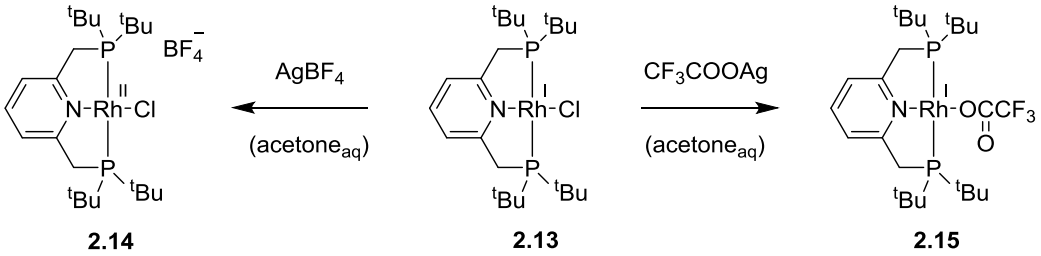

The relatively stable complex [(PN^{Py}P)Rh^{II}Cl][BF$_4$] (**2.14**) can be either reduced to Rh^{I} species (**2.13**) in the presence of PEt$_3$/H$_2$O or be oxidized to the Rh^{III} complex (**2.16**) in the reaction with PPh$_3$/H$_2$O. It is supposed that the oxidation occurs *via* formation of a neutral [(PN^{Py}P)Rh^{I}Cl] intermediate. The last undergoes than a protonation forming [(PN^{Py}P)Rh^{III}Cl(H)(CH$_3$CN)][BF$_4$] (**2.16**) (Scheme 2.7).[250]

Scheme 2.7. The redox reactivity of PN^{Py}P rhodium(II)chloride tetrafluoroborate **2.14**.

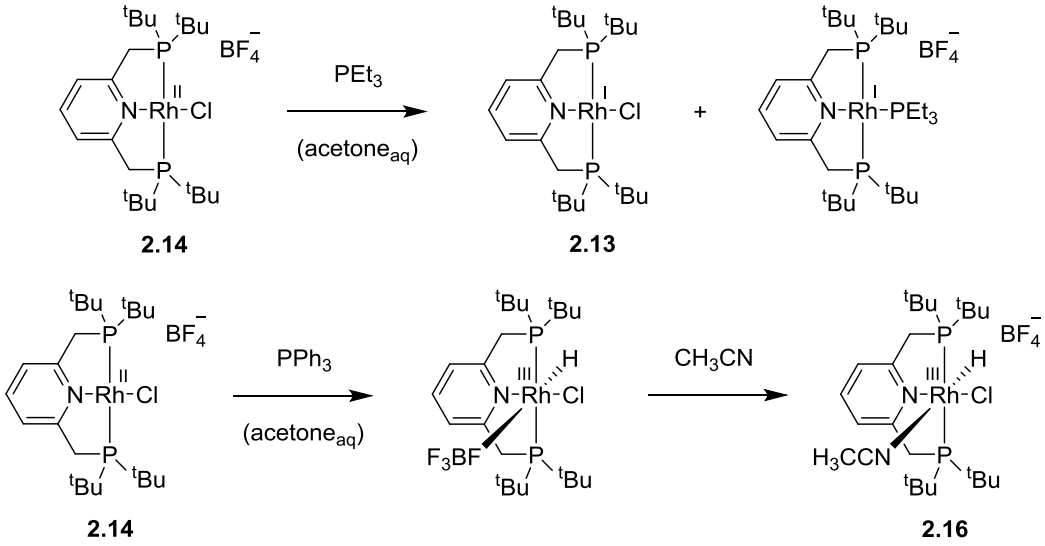

In our case, the prolonged reaction of **2.6b** with an oxidation reagent [(C$_6$H$_5$)$_3$C][PF$_6$][251] results in the formation of [(PC^{BIm}P)Rh^{III}(CH$_3$CN)$_3$]3[PF$_6$] **2.12** as it was confirmed by X-ray analysis (Figure 2.9). We also did not observe the formation of any paramagnetic species.

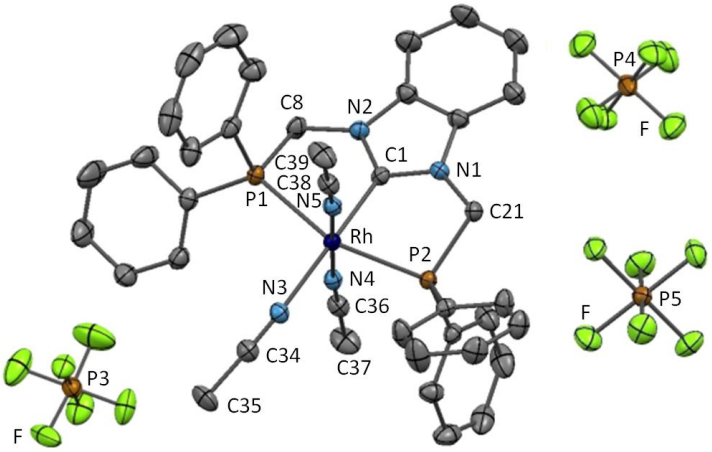

Figure 2.9. Crystal structures of **2.12** (50% displacement ellipsoids; hydrogen atoms were omitted for clarity). Selected interatomic distances (Å): Selected interatomic distances (Å): Rh–N3, 2.091(2); Rh–N4, 1.996(2); Rh–N5, 1.991(2); Rh–C1, 1.959(3); Rh–P1, 2.3584(7); Rh–P2, 2.3529(7); N1–C1, 1.338(3); N2–C1, 1.338(3); N1–C21, 1.452(3); N2–C8, 1.460(3); P1–C8, 1.844(3); P2–C21, 1.854(3); angles (deg): N3–Rh–C1, 176.65(9); P1–Rh–P2, 160.55(2); N1–C1–N2, 109.0(2); torsion angles (deg): Rh–P1–C8–N2, −22.31; Rh–P2–C21–N1, 26.33

The rhodium atom in the structure **2.12** is in a slightly distorted octahedral coordination environment. The Rh–C1 distance of 1.959(3) Å is 0.03 Å longer than the Rh–C1 bond distance in **2.6b** and the twist angle of 12.9° between the benzimidazole ring and the plane defined by Rh–N3–C1–P1–P2 is significantly bigger than that of **2.6b**. Compound **2.12** is a rare type of Rh^{III} complex, in which all three coordination sites are occupied by acetonitrile molecules.

In conclusion to the section describing stoichiometric transformations of carbene-centered pincer complexes should be noted that yet we have failed to demonstrate experimentally the possibility of elimination of H^+/H^- from methylene bridge of $PC^{BIm}P$ moiety. Removal of H^+/H^- would entail a change in the electronic structure of the ligand, which in turn would significantly affect on the chemical properties of organometallic compound. Such transformation is important for catalytic processes which are based on the principle of metal-ligand cooperativity.

In order to evaluate the catalytic activity of **2.6b**, we used borylation as a test reaction. In general, transition-metal-catalyzed hydroboration can be run through different mechanistic pathways.[252] Depending on the particular catalysts used, various target regio- and stereoselective products can be achieved. This assertion is demonstrably illustrated by a number of peculiar borylation approaches, such as the synthesis of (Z)-vinylboronates

promoted by [($PN^{Py}P$)$RuH_2(H)_2$],[47] dehydrogenative alkene borylation to (E)-vinylboronates using [(PSiP)Pd][OTf][253] or dehydrogenative alkyne borylation with [(SiNN)IrH$(HBPin)_2$],[48] [(NNN)$CoCH_3$]-catalyzed enantioselective hydroboration of alkenes,[254] and alkene isomerization-hydroboration.[255]

We have performed borylation with phenylacetylene and pinacolborane (HBPin) as a model reaction according to a common procedure. No reaction was observed between HBPin and phenylacetylene in THF at room temperature and 60 °C within 24 h in the absence of the rhodium complex **2.6b**. After the addition of **2.6b**, hydroboration proceeds catalytically with the selective formation of β-(E)-vinylboronate (88%, GC–MS). Besides the main product, β-(Z)-vinylboronate and α-vinylboronate along with hydrogenated α- and β-alkylboronates were identified in the GC–MS chromatogram and ^{1}H NMR spectra (Figures S2.33-2.35, and S2.37). The reaction occurs until full consumption of phenyl acetylene within less than 17 h (Scheme 2.7).

Scheme 2.7. E-Selective hydroboration of phenylacetylene with pinacolborane using **2.6b**. Conversions are estimated by ^{1}H NMR and GC–MS techniques.

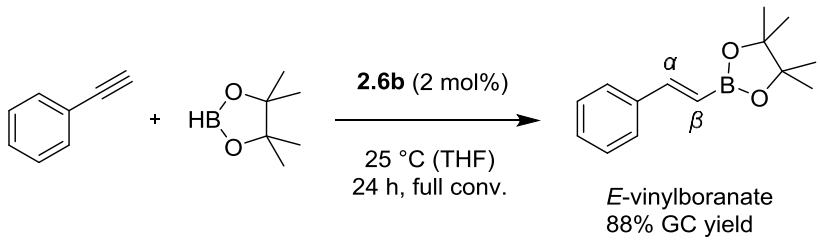

The predominant generation of a β-E-isomer proves that transformation on the rhodium center is controlled by steric. However, the 1,2-H migration, followed by η^1-Rh-vinylidene formation leading to β-(Z)-vinylboronate as the minor product, apparently also takes place, but is not prevalent in this case.[47, 256, 257] ^{31}P NMR spectra recorded after 2 and 31 h reveal the presence of **2.6b**, a new species with an intense characteristic doublet at 43.67 ppm (J^{Rh-P} = 157.9 Hz), and the previously described dimer **2.10** (Figure S2.36).

Chapter 3: The Asymmetric Functionalized Carbene-Centered Complexes

Synthesis and Characterization of Hybrid Carbene-Centered Asymmetric $[(NC^{BIm}P)Rh(L)][PF_6]$ Pincer-Complexes.

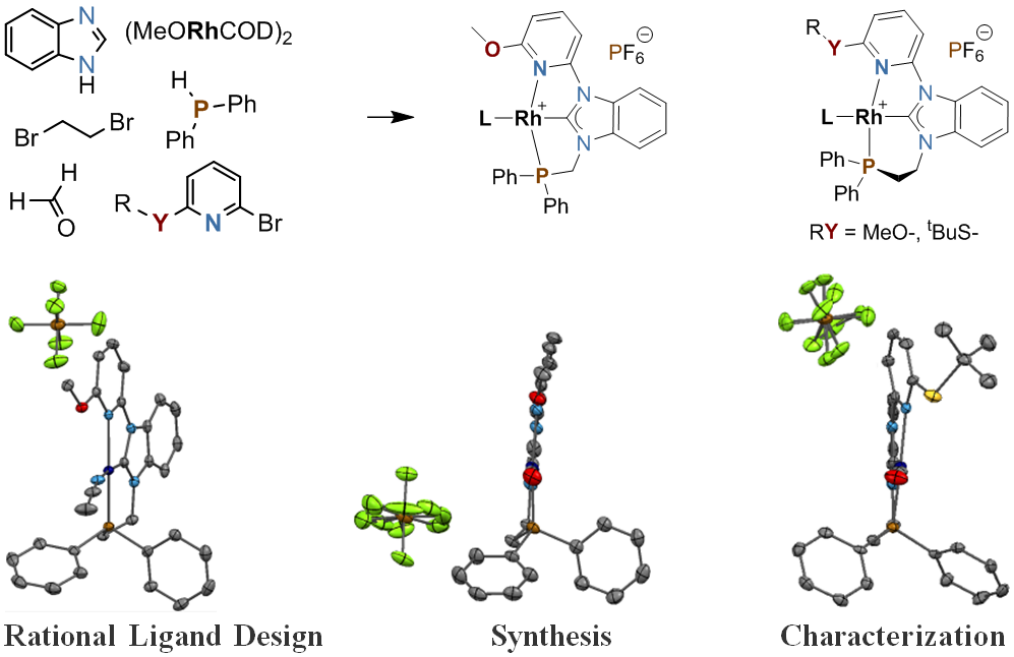

1 Introduction

The synthesis and characterization of organometallic compounds based on hybrid tridentate ligands bearing N-heterocyclic moieties and tethered with various linking groups have gained considerable research interest during last years, due to the strong σ-donating properties, oxidation resistance and remarkable stability of N-heterocyclic carbenes. A wide range of various well-designed hybrid pincer complexes has been reported up to date. In a vast majority of cases, the [5,5]- and [6,6]-membered pincer metallocycles have been chosen as principal objectives of the studies. Whereas, the examples of [5,6]-membered complexes remained rather rare. In some reports the last were mentioned as products of intramolecular ligand rearrangement of [6,6]-membered complexes.[56, 258] In other works, compounds with mixed ring sizes were designed purposefully and the hemilability was emphasized, as the main distinctive feature of these structures, determining the unique reactivity compared to their symmetric analoga.[259-269] Thus, Milstein *et al*. has clearly demonstrated the significant effect of the amine arm length on the reactivity of [5,5]- and [5,6]-membered ($PC^{Py}N$)Pt complexes.[261, 270] Among the asymmetric NHC-based [5,6]-membered architectures a number of works on hybrid ligands $C^{NHC}CP$[271] and complexes ($C^{NHC}NO$)Pd,[272] (NNC^{NHC})Ru,[30, 273] ($NC^{NHC}N$)Pd,[267] ($NC^{CHN}N$)Rh/Pd,[262] ($PC^{NHC}P$)Rh,[56] (PCP)Ni[274] should be emphasized (Figure 3.1). Many of them were found as promising active precursors for efficient catalytic transformations, such as Suzuki–Miyaura and Heck reactions, catalytic hydrogenation of esters and cyclic diesters.

Recently, the cooperative functionality became of great importance in the rational ligand design.[67, 74, 203, 204, 275-278] In view of this, we drew our attention to the possibility of incorporation of heteroatomic centers coplanar to the pincer chelate. In particular, we were interested in molecular architectures, in which a donor atom is not directly bound to the metal center,[109, 279, 280] but is appended above its free coordination site.[81, 203, 204, 277]

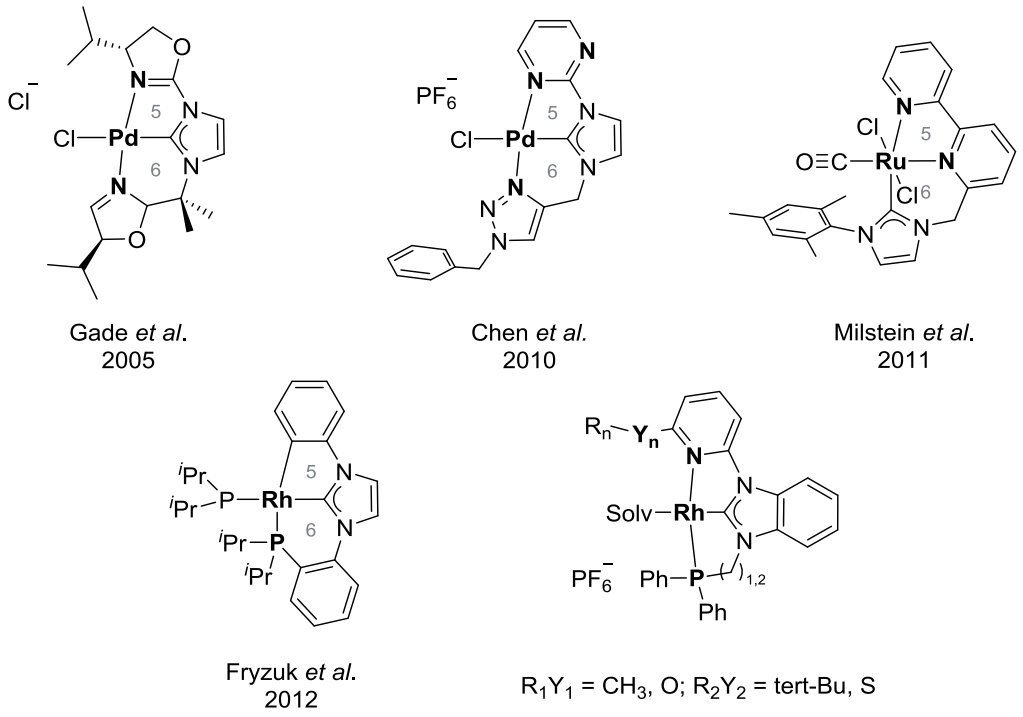

Figure 3.1. NHC-based [5,6]-membered metallocycles

In this chapter, the modular synthesis of new asymmetric [5,5]- and [5,6]-membered carbene-centered ligand systems bearing protected oxygen and sulfur pendent domains as well as first results of their coordination chemistry are described.

2 Results and discussion

The synthetic accessibility of [5,5]-membered $NC^{BIm}P$ architectures presented some difficulties due to the incorporation of a methylene group between phosphorus and nitrogen heteroatoms heretofore. Recently Hofmann *et al*., Lugan *et al*., and our research group have reported the phosphinomethyl-functionalization of N-heterocycles using phosphorylmethyl-4-methylbenzenesulfonates.[210, 213, 281, 282] We have planned the preparation of the target ionic $NC^{BIm}P$ ligand precursors in four steps starting from commercial available benzimidazole, pyridine derivatives, diphenylphosphine and formaldehyde, as shown in the retrosynthetic analyses represented in Schemes 3.1 and 3.2.

Scheme 3.1. Retrosynthetic analysis of target phosphine-functionalized methylene-bridged benzimidazolinium salts

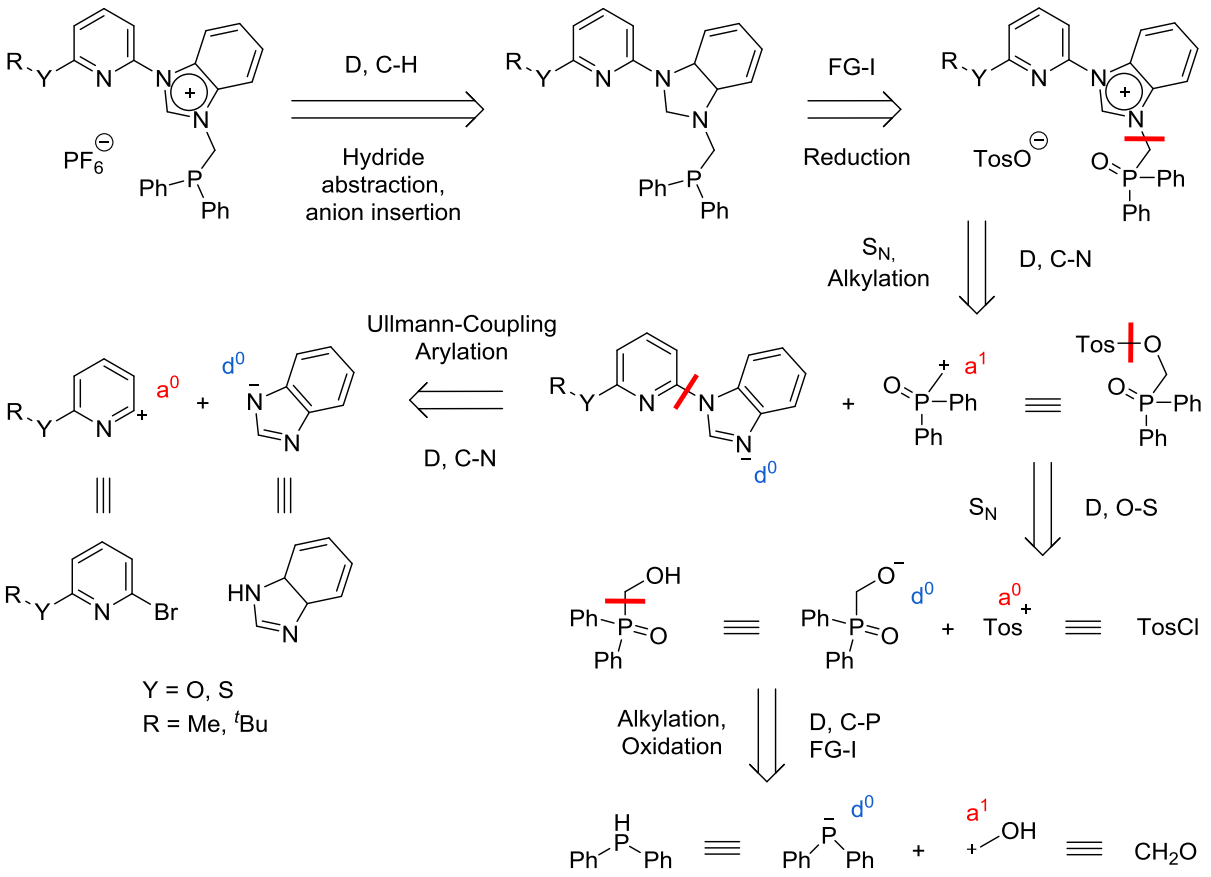

Scheme 3.2. Retrosynthetic analysis of target phosphine-functionalized ethylene-bridged benzimidazolinium salts

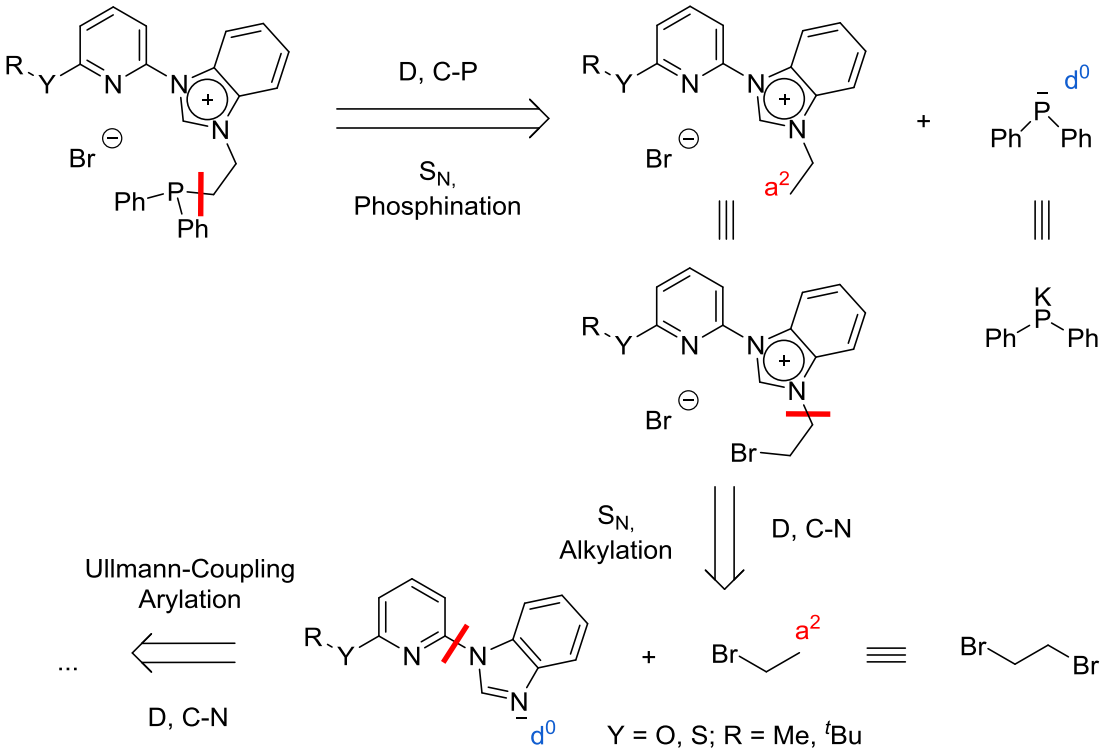

In the first step, 1-(6-alkylhalkogenopyridin-2-yl)benzimidazoles **3.1** and **3.5** were synthesized from 2-bromo-pyridine derivatives *via* an Ullmann coupling reaction with good yields (Scheme 3.3, 3.4). The second step could only be performed in melt at 127 °C affording compound **3.2**. The methylene-bridged phosphoryl derivative **3.2** was then reduced using 0.6 equiv $Ti(O^iPr)_4$ and 6 equiv PMHS.[222, 231] Herein, phosphine deprotection is conducted by simultaneous hydrogenation of the benzimidazolium fragment giving 1-((diphenylphopshino)-methylene)-3-(6-methoxypyridin-2-yl)benzimidazoline **3.3**. This reaction showed the formation of several by-products at longer reaction times (more than 3 h) or higher temperatures (above 70 °C). Interestingly, the reaction of compound **3.2** with excess of $HSiCl_3$[226] resulted in the hydrogenation of the benzimidazolium moiety without phosphine deprotection under mild conditions.

Scheme 3.3 Total synthesis of 1-((diphenylphopshino)methylene)-3-(6-methoxypyridin-2-yl)benzimidazolium hexafluorophosphate **3.4**

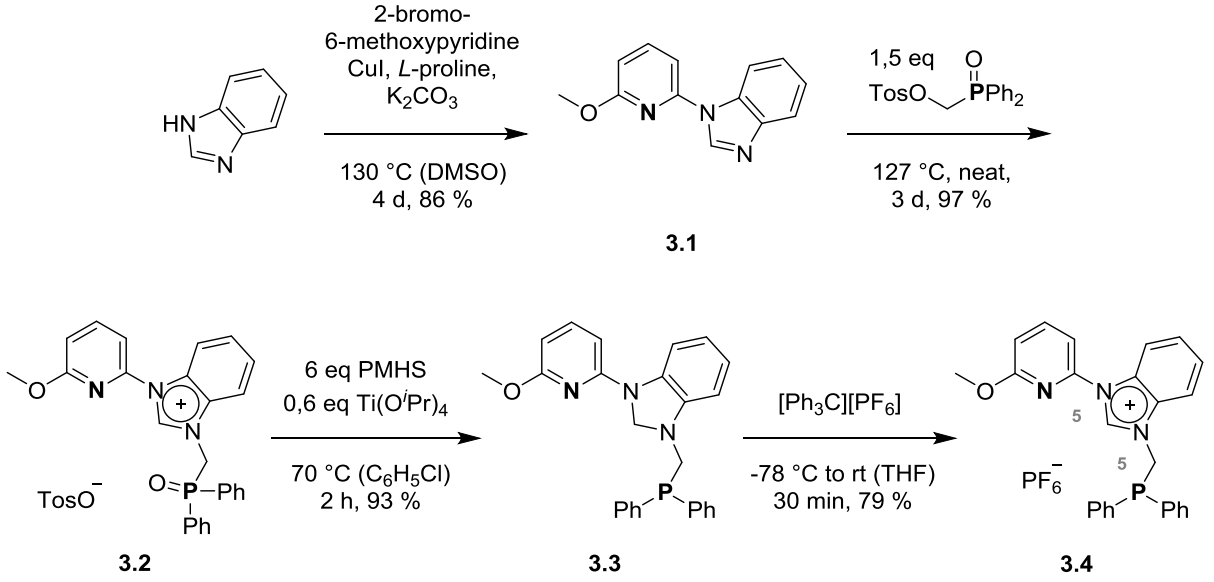

The formed benzimidazoline derivative **3.3a** subsequently undergoes a hydride abstraction leading to the organic salt **3.2a**, as it was revealed by ^{1}H NMR analysis (Scheme S3.2, Figure S3.1). In order to abstract a hydride from compound **3.3** various synthetic approaches were tested using inorganic and organic acids and the combination of them with CuI, $Ni(CH_3COO)_2$, $Zn(CH_3COO)_2$, $Pd(CH_3COO)_2$, $Fe(BF_4)_2{\cdot}6H_2O$, $Co(BF_4)_2{\cdot}6H_2O$, $Zn(BF_4)_2{\cdot}xH_2O$, under diverse reaction conditions (Schemes S3.3, S3.4).[196, 232-237] However, the most selective approach was the use of non-metal-containing reagents.[238, 239] Thus, the intermediate **3.3** was converted to the target 1-((diphenylphopshino)-methylene)-3-(6-methoxypyridin-2-yl)-benzimidazolium hexafluorophosphate **3.4** using triphenylcarbenium

hexafluorophosphate. To avoid the ring-opening polymerization of THF in the presence of $[(C_6H_5)_3C][PF_6]$ taking place at normal conditions the reaction was conducted at low temperatures within 30 min.

The synthesis of [5,6]-membered $NC^{BIm}P$ ligand precursors was implemented in a different way (Scheme 3.4). Both, methoxy- and tert-butyl thiol-derivatized bromides (**3.6a** and **3.6b**, respectively) were obtained by alkylation of pyridobenzimidazoles with 1,2-dibromoethane in bulk at moderate temperatures. The organic salts **3.8a** and **3.8b** were obtained after phosphination followed by anion exchange for hexafluorophosphate with good yields (see ES). It is noteworthy, that the transformation chains in whole, from starting materials to the final products, were conceptuated aiming steadily softening of reaction conditions to avoid possible decomposition.

Scheme 3.4 Total synthesis of 1-(2-(diphenylphopshino)ethyl)-3-(6-(tert-butylthio)pyridin-2-yl)benzimidazolium hexafluorophosphate **3.8b**. The methoxy derivative **3.8a** was prepaired according to analogous synthetic procedure (see ES).

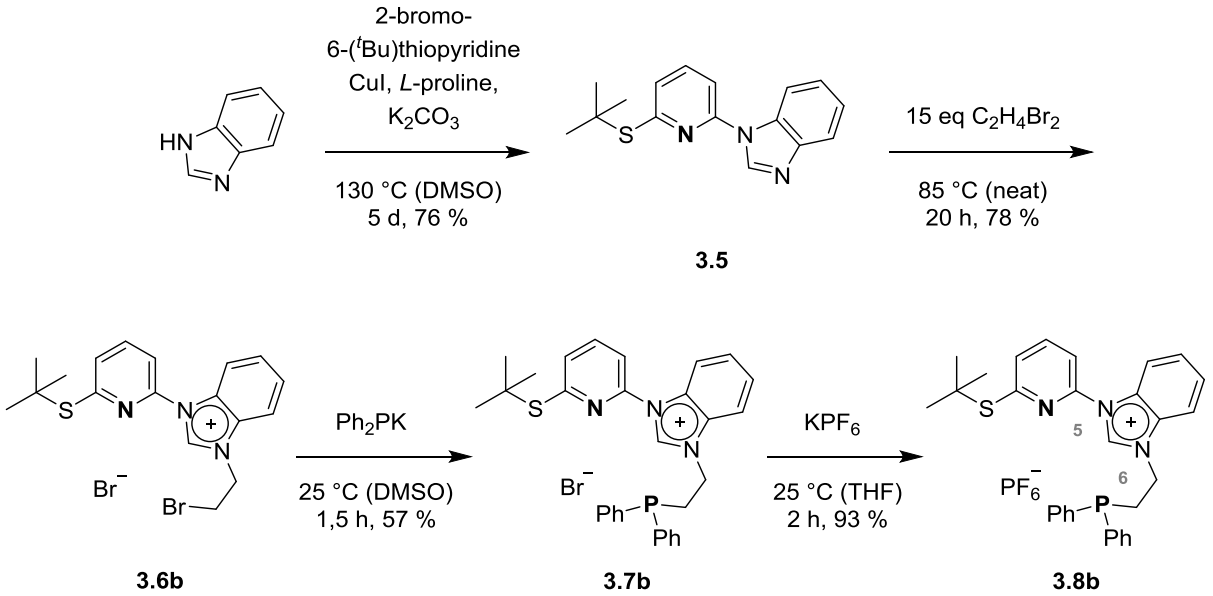

The compounds **3.4**, **3.8a**, **3.8b** were characterized by NMR spectroscopy, mass spectrometry and elemental analysis. In their ^{31}P NMR spectra, sharp singlets for phosphorus atoms were observed at −16.35 (**3.4**), −20.98 (**3.8a**), and −20.69 (**3.8b**) ppm, along with typical septet corresponding to the phosphorus nucleus of the non-coordinated PF_6 group in the upfield region at −144.00 ppm. A doublet corresponding to the methylene group of compo und **3.4** was observed at 5.34 ppm ($J^{2,H-P}$ = 5.5 Hz), and a singlet related to the acidic proton of the benzimidazolium moiety was detected at 9.07 ppm in the ^1H NMR spectrum ($CDCl_3$). The triplets corresponding to protons (H-13) of methylene groups bound to nitrogen atoms in both

3.8a and **3.8b** were detected at 2.89 ppm (J^3 = 7.2 Hz, CD_2Cl_2) and 3.00 ppm (J^3 = 7.2 Hz, d_8-THF) respectively. In addition, multiplets related to the H-14 methylene protons were observed at 4.85 ppm. The singlets of acidic protons H-2 were found at 9.61 ppm (s, CD_2Cl_2) for **3.8a** and 9.91 ppm (s, d_8-THF) for **3.8b**.

The ligand precursors **3.4**, **3.8a**, **3.8b** undergo complexation with [μ-$OCH_3Rh(COD)]_2$ through deprotonation of the benzimidazolium moiety. The subsequent mild hydrogenation at room temperature gives the target organometallic products [($NC^{BIm}P$)Rh(CH_3CN)][PF_6] **3.9**, **3.10a**, **3.10b** with moderate yields (Scheme 3.5). The hydrogenation has been performed to prevent the coordination of cyclooctadiene to the [($NC^{BIm}P$)Rh] moiety. The preliminary experiments have shown, that also the mononuclear $NC^{BIm}P$ iridium halogenide [($NC^{BIm}P$)IrClBr] **3.11** can be synthesized in the reaction of [μ-ClIr(COD)]$_2$ with **3.7a** and subsequent hydrogenation of formed intermediates under 10 bar H_2 atmosphere (Scheme S3.5)

Scheme 3.5. Synthesis of [5,5]- and [5,6]-membered $NC^{BIm}P$ rhodium(I) complexes **3.9**, **3.10a**, **3.10b**

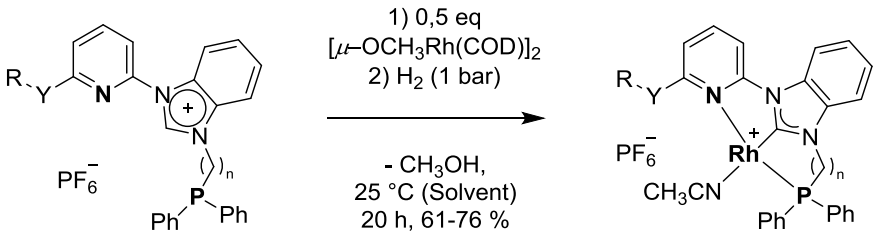

The ethylene-bridged complexes could be also prepared by complexation of bromide derivatives **3.7a** and **3.7b**, followed by subsequent anion exchange. The preliminary experiments have shown, that the mononuclear $NC^{BIm}P$ iridium halogenide **3.11** can be achieved in the reaction of [μ-ClIrCOD]$_2$ with **3.7a** and subsequent hydrogenation of formed intermediates under 10 bar H_2 atmosphere (see ES).

The observed changes in the NMR spectra after reaction gave evidence for the complexation of rhodium with the formation of **3.9**, **3.10a**, and **3.10b**. Thus, the signals related to phosphorus nuclei split to doublets and shift to 60.64 ppm ($J^{P\text{-}Rh}$ = 222.6 Hz) for **3.9**, 38.47 (d, $J^{P\text{-}Rh}$ = 187.4 Hz) for **3.10a**, and 39.84 (d, $J^{P\text{-}Rh}$ = 189.9 Hz) for **3.10b** in ^{31}P NMR spectrum. The dublets of methylene protons of complex **3.9** were detected at 4.98 ppm (d, $J^{2,H\text{-}P}$ = 6.4

Hz). The proton signals of ethylene bridges were observed at 2.83 ppm (m, 2H, H-13), 4.08 ppm (m, 2H, H-14)) for **3.10a** and at 2.91 (m, 2H, H-13), 4.21 (m, 2H, H-14)) for **3.10b** in ^{1}H NMR spectra. After complexation, the characteristic singlets of acidic protons H-2 corresponding to the free ligand precursors disappear in all cases.

Single crystals of methoxy-derivatized ethylene-bridged complex **3.10a** were grown from a CH_3CN/Et_2O solution. An X-ray diffraction study established its structural details and the tridentate nature of the ligand (Figure 3.2). The neutral $NC^{BIm}P$ pincer chelate bearing four different donor functionalities coordinates meridionally to the metal. The rhodium atom adopts a distorted square-planar coordination geometry, which is consistent with the reported [5,6]-membered $(CC^{Im}P)Rh^{I}$ X-ray structure.[56] The fourth coordination site is occupied by a weakly bound solvent molecule *trans* to the carbene. The benzimidazolyl moiety in the ethylene-bridged complex **3.10a** is not twisted out of N4–P1–Rh1–C1 plane unlike in the ethylene-bridged imidazole-centered [6,6]-membered symmetric analoga[5, 50, 208, 283] and coordinates to the metal center with an insignificant distortion of planarity. The five-membered metallacycle has a common geometry whereas the six-membered one adopts a boat-conformation with the C15 atom jutting out of plane. The distance of the methoxy oxygen O1 atom is 2.855(2) Å to the nitrogen atom N4 of the coordinated acetonitrile molecule and at 3.230(1) Å to the rhodium atom. These values correlate with the reported distances of oxo-[79] and amino-derivatized[97] symmetric (NNN)Ru complexes.

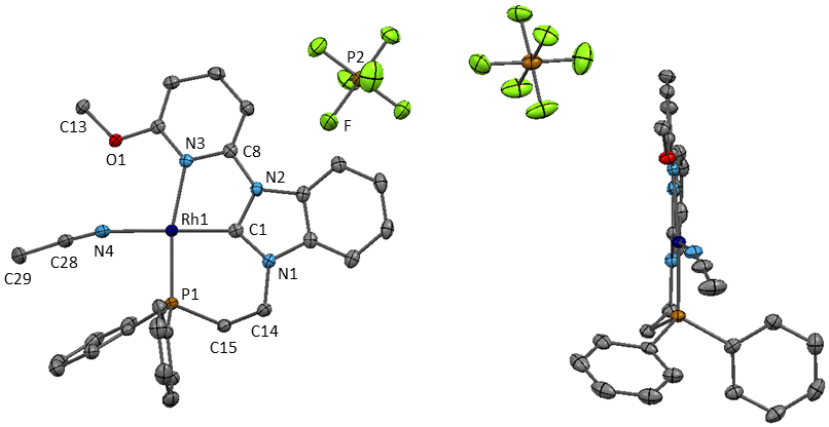

Figure 3.2. Molecular structure of $NC^{BIm}P$-rhodium(I) hexafluorophosphate **3.10a** with ellipsoids at 50% probability. Hydrogen atoms were omitted for clarity. Selected interatomic distances (Å): Rh1–C1 1.914(2), Rh1–P1 2.1826(3), Rh1–N3 2.133(1), Rh1–N4 2.073(1); angles (deg): C1–Rh1–N4 173.37(6), N3–Rh1–P1 168.06(4), C1–Rh1–P1 90.12(5), C1–Rh1–N3 78.56(6), N3–Rh1–N4 102.63(5), N4–Rh1–P1 89.05(4); torsion angles (deg): N1–C1–Rh1–P1 -4.9(2), N2–C1–Rh1–N3 7.6(1), C1–Rh1–P1–C15, 25.77(7)

We also were able to obtain colourless needle-shaped crystals of $NC^{BIm}P$ iridium halogenide complex from CH_3CN/Et_2O mixture suitable for X-ray crystallographic analysis. The solid state molecular structure of **3.11**, shown in Figure 3.3, represents a distorted square-pyramidal molecular architecture. The distances between O1–N4 atoms and O1–Ir1 atoms in compound **3.11** are 2.795 Å and 3.223 Å respectively. ^{1}H NMR analysis also confirms the formation of iridium complex **3.11**. The characteristic proton signals of ethylene bridge appear at 3.27 ppm (m, 2H, H-13), 4.83 ppm (m, 2H, H-14). In the ^{31}P NMR, singlet corresponding coordinated to the iridium phosphorus atom was found at –4.91 ppm.

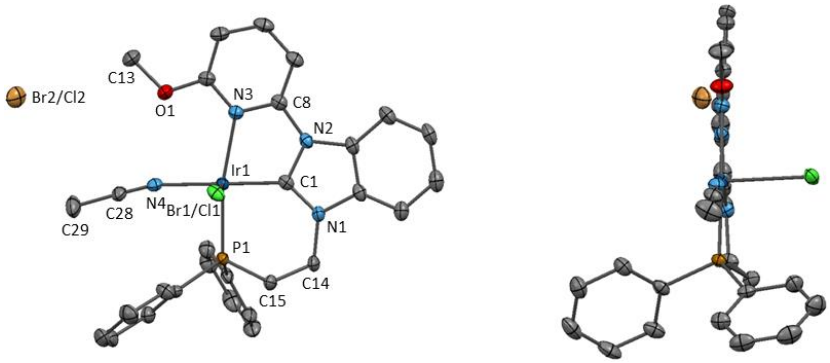

Figure 3.3. Molecular structure of [($NC^{BIm}P$)IrClBr] **3.11**

Treatment of the ethylene-bridged complexes **3.10a** and **3.10b** with 5 bar CO in propylene oxide for 2 h at 25 °C resulted in the formation of the corresponding 16-electron rhodium carbonyl complexes **3.13a** and **3.13b** (Scheme 3.6). The coordination of CO causes a slight shift of dublets related to the phosphorus nuclei to 37.26 ppm (d, $J^{P\text{-}Rh}$ = 161.7 Hz) for **3.13a** and to 38.33 ppm (d, $J^{P\text{-}Rh}$ = 161.6 Hz) for **3.13b** in the upfield of the ^{31}P NMR spectra.

Scheme 3.6. Reaction of carbon monoxide with [5,6]-membered $NC^{BIm}P$ rhodium(I) complexes **3.10a** and **3.10b**. Conversions are estimated by ^{1}H and ^{31}P NMR spectroscopy

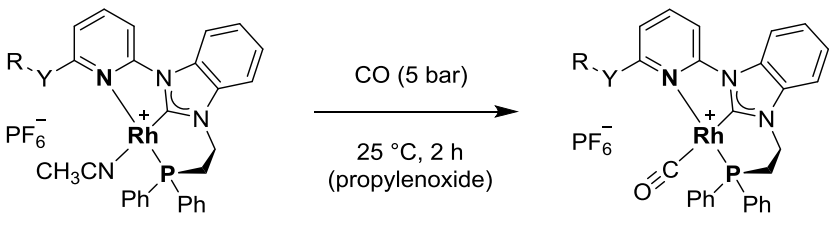

Dark red crystals of complex **3.13a** suitable for X-ray analysis were grown by addition of Et_2O to the reaction mixture, whereas compound **3.13b** could be isolated by crystallization from THF/pentane mixture. Both solid-state structures **3.13a** and **3.13b** show distorted

square-planar environment around rhodium (Figure 3.4). The O1 atom is located 2.696(3) Å from the C28 atom of coordinated CO and 3.187(2) Å from the rhodium center in **3.13a**. In the tert-butyl thiol derivative **3.13b**, the bonds distances S1–C28 and S1–Rh1 amount 2.986(4) Å and 3.497(2) Å, respectively. It is notable that the pyridyl rest in complex **3.13b** coordinates to the metal with a significant distortion of planarity, whereas the benzimidazolyl fragment is only slightly twisted out of the C17–P1–Rh1–C28 plane. The bond length N^{Py}–Rh increases from **3.13a** (2.133(2) Å) to **3.13b** (2.161(3) Å). A shift of the pendent tert-butyl thiol group at 18.04° (torsion angle of S1–C28–Rh1–N3) indicates a significant repulsion between alkylrest and CO moiety, while the torsion angle of O1–C28–Rh1–N3 in the methoxy derivative is only 0.4143°. Thus, as can be derived from obtained crystal structures the bulky ^{t}BuS-group leads to the weakening of N–Rh bond enhancing the degree of hemilability of pyridyl moiety.

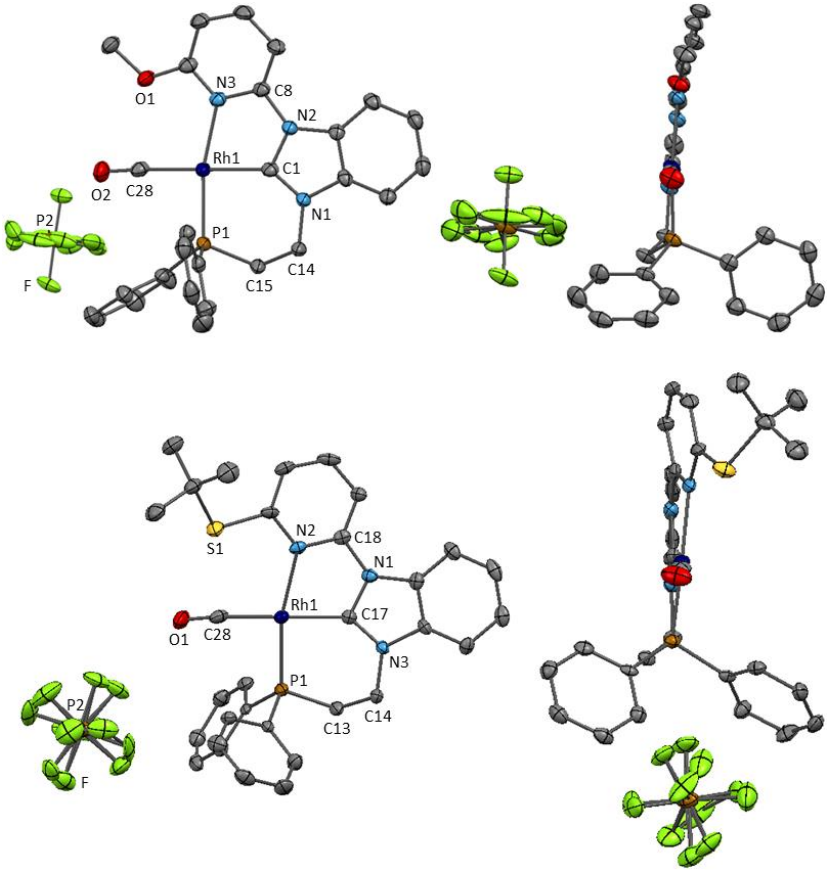

Figure 3.4. Molecular structures of [5,6]-membered methoxy-substituted **3.13a** and tert-butyl thiol-substituted **3.13b**. Hydrogen atoms were omitted for clarity. **3.13a**: Selected geometrical parameters (Å): Rh1–C1 2.005(3), Rh1–P1 2.2069(6), Rh1–N3 2.133(2), Rh1–C28 1.891(3); C1–Rh1–C28 179.5(1), P1–Rh1–N3 165.57(7), C1–Rh1–P1 89.00(8), C1–Rh1–N3 77.7(1), C28–Rh1–N3 102.0(1), C28–Rh1–P1 91.29(9), N1–C1–Rh1 137.8(2); N1–C1–Rh1–P1

7.6(3), N2–C1–Rh1–N3 1.6(2), C1–Rh1–P1–C15 29.7(1) **3.13b**: Rh1–C17 2.005(5), Rh1–P1 2.214(1), Rh1–N3 2.161(3), Rh1–C28 1.874(6); C17–Rh1–C28 172.7(2), N3–Rh1–P1 166.9(1), C17–Rh1–P1 90.0(1), C17–Rh1–N3 77.0(2), N3–Rh1–C28 104.2(2), P1–Rh1–C28 88.7(2); N1–C17–Rh1–P1 -11.4(5), N2–C17–Rh1–N3 -6.4(3), C17–Rh1–P1–C13 -14.6(2)

Powder IR spectroscopic measurements reveal the characteristic CO stretching bands at 2008.7 cm^{-1} for **3.13a** and 2001.7 cm^{-1} for **3.13b**. Such frequency decrease of 7 cm^{-1} discloses the differences in electronic properties of the alkylhalkogen-derivatized $NC^{BIm}P$ ligands. Thus, the tert-butyl thiol-functionalized ligand **3.13b** is slightly more π-basic in comparison to the methoxy-substituted one, owing to more pronounced +M effect of the thiol group on ortho/para-position of pyridine ring.

In order to test catalytic activity of compounds **3.4** and **3.10a**, the hydroboration of phenylacetylene with pinacolborane was performed (Scheme S3.6). Compound **3.10a** catalyzes the borylation reaction affording the β-E-vinylboronate with moderate selectivity (67%, GC-MS). The reaction proceeded untill full consuption of the phenylacetylene within 22 h at 25 °C. GC-MS analysis and ^{1}H NMR monitoring reveal the formation of several by-products, such as α-vinylboronate (28%), β-alkylboronate (3%), and α-alkylboronate (2%) (Figure S3.4). The complex **3.4** is less active and produces β-E-vinylboronate (68%), β-Z-vinylboronate (10%), α-vinylboronate (19%), β-alkylboronate (1%), and α-alkylboronate (2%) within 88 h (Figure S3.3). No conversion to vinylboronates was detected in the absence of rhodium complex (25 °C, 24 h).

Generally, complexes **3.10a**, **3.13a**, and **3.13b**, exhibit nearly regular coordination geometry of the group of atoms C^{BIm}, P, and atoms of monodentate lone-pair donors (see angles: P–Rh–C^{BIm}, N^{CH_3CN}/C^{CO}–Rh–P), while the pyridine rings coordinate at angles of N^{Py}–Rh–C^{BIm} from 77.00(2)° (**3.13b**) to 78.56(6)° (**3.10a**), which reflects a higher rigidity of the five-membered metallacycle in comparison to the six-membered congener.

For the described organometallics, based on rhodium in low oxidation state and containing different donor functionalities, following conclusions can be drawn as to the M–L bonds strength: The pyridine units are weaker bound to the metal than the phosphines and carbenes. As a part of the hybrid ligands they often have a hemilibile character.[75] On the other hand, the NHC moiety is stronger bound to the metal in comparison to the phosphorus atom, due to the thermodynamic instability of the free carbene, which disfavors simple dissociation from the metal.[284] In addition, it is to expect, that the positioning of NHC in the center of the ligands

architecture will suppress its reactivity i.e. liability to reductive elemination through the chelate effect of meridional coordinated pincer.

Experimental Section

1 General

All reactions were carried out under an argon atmosphere, unless noted. Chemicals were purchased from Acros Organics, ABCR, or Sigma-Aldrich and used as received, unless otherwise specified. Glassware was heated and dried under vacuum prior to use. THF, diethyl ether, toluene, and pentane were purified by passing through a solvent purification system MBraun SPS-800. Isopropyl alcohol, CH_3CN, methanol, acetone, chloroform, CH_2Cl_2, and other solvents were dried over 3 Å molecular sieves. The ^{1}H, ^{19}F, ^{13}C, and ^{31}P NMR spectra were recorded on AV-300, AV-360, and AV-500C MHz Bruker spectrometers. Spectroscopic chemical shifts were referenced to the residual proton signal of the deuterated solvents for ^{1}H and ^{13}C NMR spectra. ^{31}P NMR spectra were calibrated to a 85% H_3PO_4 standard solution (internal capillary). Deuterated solvents were purchased from Deutero or Eurisotop and dried over 3 Å molecular sieves. Multiplicity is denoted using the following abbreviations: s, singlet; d, doublet; t, triplet; q, quartet; m, multiplet. Assignment of the signals was based on one-dimensional and two-dimensional COSY, HMBC, and HSQC NMR techniques. EA was measured at the Laboratory for Microanalysis at the Institute of Inorganic Chemistry at Technische Universität München. ESI MS analysis was performed on a Varian 500–MS spectrometer in the positive-ionization mode using undegassed methanol, isopropyl alcohol, THF, or CH_3CN. IR spectra were recorded on a Bruker Vertex 70 spectrometer with a Bruker Platinum ATR setup and an integrated MCT detector. Samples for IR measurements were used in the solid state. For GC analysis, a Varian Saturn 2100T GC MS chromatograph with a 30 m Agilent GC column (P/N: CP8944) and a Varian 490-Micro GC–TCD system (Column 492001450 COX 1m, heated, helium carrier gas, 80 °C) were used. TGA was measured on a TGAQ5000 analyzer from TA Instruments (Waters).

Single-Crystal XRD. Data were collected on a single crystal X-ray diffractometer equipped with a CCD detector (APEX II, κ-CCD), a fine-focused sealed tube with Mo Kα radiation (λ = 0.71073 Å) and a graphite monochromator or a FR591 rotating anode with Mo Kα radiation and a Montel optic, by using the APEX2 software package.[285] The measurements were performed on single crystals coated with perfluorinated ether. The crystals were fixed on the top of a glass fiber and transferred to the diffractometer. Crystals were frozen under a stream of cold nitrogen. A matrix scan was used to determine the initial lattice parameters. Reflections were merged and corrected for Lorenz and polarization effects, scan speed, and background using SAINT.[286] Absorption corrections, including odd and even ordered

spherical harmonics, were performed using SADABS.[286] Space group assignments were based upon systematic absences, E statistics, and successful refinement of the structures. Structures were solved by direct methods with the aid of successive difference Fourier maps,[287] and refined against all data using APEX 2 software[285] in conjunction with SHELXL-97 or SHELXL2014[288] and SHELXLE.[289] Methyl hydrogen atoms were refined as part of rigid rotating groups, with a C–H distance of 0.98 Å and $U_{iso}(H) = 1.5 \bullet U_{eq}$©. Other hydrogen atoms were placed in calculated positions and refined using a riding model, with methylene and aromatic C–H distances of 0.99 and 0.95 Å, respectively, and $U_{iso}(H) = 1.2 \bullet U_{eq}$©. If not mentioned otherwise, non-hydrogen atoms were refined with anisotropic displacement parameters. Full-matrix least-squares refinements were carried out by minimizing Σw(Fo2-Fc2)2 with a SHELXL-97[288] weighting scheme. Neutral atom scattering factors for all atoms and anomalous dispersion corrections for the non-hydrogen atoms were taken from International Tables for Crystallography.[290] Images of the crystal structures were generated by PLATON.[291] Crystallographic data for structures **2.5**, **2.6a**, **2.6b**, **2.7**, **2.8**, **2.10**, **3.10a**, **3.13a**, **3.13b** have also been deposited with the Cambridge Crystallographic Data Centre (CCDC 1405697–1405702). These coordinates can be obtained, upon request, from the Director, Cambridge Crystallographic Data Centre, 12 Union Road, Cambridge CB2 1EZ, U.K. [fax (+44)1223-336-033; e-mail: deposit@ccdc.cam.ac.uk].

2 The Symmetric Carbene-Centered Complexes

Synthesis of Organic and Organometallic Compounds

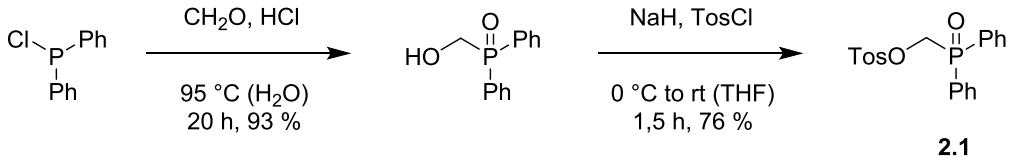

2.1

The intermediate [(diphenylphosphoryl)methylene]hydroxide was synthesized starting from chlorodiphenylphosphine according to a known procedure.[11, 292] This reaction was performed in a pressure vessel according to the safety requirements and the reaction temperature did not exceed 100 °C. Then [(diphenylphosphoryl)methylene]hydroxide (23.6 g, 97.5 mmol, 1.00 equiv) was dissolved in 600 mL (7.4 mol, 76.00 equiv) dry THF in a 1 L three-necked round-bottomed flask equipped with a dropping funnel. Sodium hydride (2.63 g, 107 mmol, 1.10 equiv) was added portionwise to the solution at 0 °C under argon counter-flow and stirred at 25 °C for 1.5 h. Then, the THF solution of 4-toluenesulfonyl chloride (19.9 g, 102.4 mmol, 1.00 equiv) was slowly dropped to the formed colorless precipitate at 0 °C. The reaction mixture was stirred over night at room temperature. Subsequently, all volatiles were removed in vacuo and the remained solid was redissolved in CH_2Cl_2, filtered through Celite® and washed three times with a saturated sodium hydrogen carbonate solution. After the solvent was removed under reduced pressure, the raw product was recrystallized out from a C_2H_5OH/H_2O (1/1) mixture. The method affords 28.8 g (76%) analytically pure 1-[(diphenylphosphoryl)methylene]-4-methylbenzenesulfonate **2.1** as a colorless crystalline material. Anal. Calcd for $C_{20}H_{19}O_4PS$: C, 62.17; H, 4.96; O, 16.56; P, 8.02; S, 8.30. Found: C, 62.61; H, 5.02; P, 8.08; S, 8.36.

The calculated overall yield ($y_{oa} = y_1 \times y_2$), avarage yield ($\bar{y} = \sqrt[n]{y_{oa}}$), and chemical efficiency ($\text{Eff}_{chem} = {}^{y_{oa}}/_{n}$) for two step synthesis of **2.1** are respectively:

$$y_{oa} = 0.93 \times 0.76 = 0.71\ ;\ \bar{y} = \sqrt[2]{0.71} = 0.84\ ;\ Eff_{chem} = {}^{0.71}/_{2} = 0.35$$

1-[(Diphenylphosphoryl)methylene]benzimidazole (2.2)

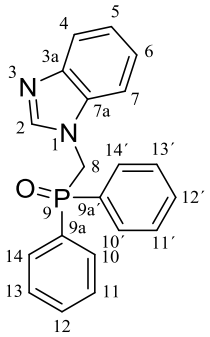

A round-bottomed flask was charged with benzimidazole (1.20 g, 10.0 mmol, 1.00 equiv), [(diphenylphosphoryl)methylene]-4-methylbenzenesulfonate (**2.1**; 4.02 g, 10.0 mmol, 1.00 equiv) and potassium carbonate (9.67 g, 70.0 mmol, 7.00 equiv) under an air atmosphere. After the addition of 40 mL of DMSO, the suspension was intensively stirred at 90 °C for 24 h. The reaction mixture was cooled to 50 °C and the DMSO was removed under reduced pressure. The crude product was isolated by extraction with $CHCl_3/H_2O$ and evaporation of the organic phase. A final washing of the residue with diethyl ether and drying in a vacuum give colorless solid product **2.2** (3.25 g, 97%). Anal. Calcd for $C_{20}H_{17}N_2OP$: C, 72.28; H, 5.16; N, 8.43; P, 9.32. Found: C, 71.88; H, 5.12; N, 8.08; P, 9.15.

^{1}H-NMR ($CDCl_3$, 360 MHz, ref: $CDCl_3$ solvent residual): δ = 7.86 (s, 1H, H-2), 7.67 (m, 5H, H-7,-10,-10',-14,-14'), 7.50 (td, J = 7.4 Hz, 1.5 Hz, 2H, H-12,-12'), 7.39 (td, J = 7.7 Hz, 3.0 Hz, 4H, H-11,-11',-13,-13'), 7.15 (m, 3H, H-4,-5,-6), 4.92 (d, J^{H-P} = 5.9 Hz, 2H, H-8).

^{13}C-NMR ($CDCl_3$, 90 MHz, ref: $CDCl_3$ solvent residual): δ = 143.20 (s, 1C, C-2), 142.94 (s, 1C, C-7a), 134.10 (s, 1C, C-3a), 132.92 (d, $J^{4,C-P}$ = 2.74 Hz, 2C, C-12,-12'), 131.17 (d, $J^{2,C-P}$ = 9.51 Hz, 4C, C-10,-10',-14,-14'), 129.29 (d, $J^{1,C-P}$ = 100.35 Hz, 2C, C-9a,-9a'), 129.05 (d, $J^{3,C-P}$ = 11.91 Hz, 4C, C-11,-11',-13,-13'), 123.22 (s, 1C, C-6), 122.33 (s, 1C, C-5), 120.21 (s, 1C, C-7), 109.76 (s, 1C, C-4), 45.73 (d, $J^{1,C-P}$ = 73.45 Hz, 1C, C-8).

^{31}P-NMR ($CDCl_3$, 146 MHz, ref: 1% H_3PO_4 in D_2O): δ = 25.58 (s, 1 P, P-9).

ESI MS *m/z*: 333.0 ($[C_{20}H_{18}N_2OP]^+$, $[C^{BIm}PO+H]^+$).

1,3-Bis[(diphenylphosphoryl)methylene]benzimidazolium 4-Methylbenzylsulfonate (2.3)

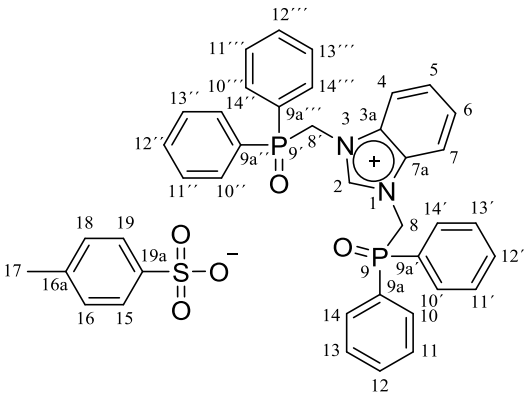

1-[(Diphenylphosphoryl)methylene]benzimidazole **2.2** (1.45 g, 4.3 mmol, 1.00 equiv) and [(diphenylphosphoryl)methylene]-4-methylbenzenesulfonate **2.1** (3.04 g, 7.7 mmol, 1.80 equiv) were ground by stirring under vacuum for 1 h. Thereafter, the flask was backfilled with argon and stirred at 145 °C for 12 h. After the reaction was completed, the solid material was dissolved into CH_2Cl_2, and the product was precipitated from the solution by the addition of toluene, filtered and dried in vacuo. The second product portion was obtained by evaporation of CH_2Cl_2 and multiple extraction of byproducts from the solid crude substance with toluene over prolonged time. Further, the product can be worked up by extraction with a warm H_2O/toluene (3/1) mixture. After water was removed, the residue was redissolved in $CHCl_3$ or CH_2Cl_2 and dried over sodium sulfate. The product (2.87 g, 93% yield) was obtained after evaporation of the organic phase as a colorless solid material. The redundant [(diphenylphosphoryl)methylene]-4-methylbenzenesulfonate can be isolated by evaporation of toluene, recrystallized and reused in synthesis. Anal. Calcd for $C_{39}H_{34}N_2O_5P_2S$: C, 66.47; H, 4.86; N, 3.98; O, 11.35; P, 8.79; S, 4.55. Found: C, 66.59; H, 5.11; N, 3.73; P, 8.62; S, 4.67.

^{1}H-NMR ($CDCl_3$, 360 MHz, ref: $CDCl_3$ solvent residual): δ = 10.69 (s, 1H, H-2), 8.14 (m, 2H, H-5,-6), 7.91 (m, 10H, H-10^{all},-14^{all},-15,-19), 7.55 (m, 2H, H-4,-7), 7.48 (m, 4H, H-12^{all}), 7.40 (m, 8H, H-11^{all},-13^{all}), 7.22 (d, J = 8.0 Hz, 2H, H-16,-18), 5.43 (d, $J^{H\text{-}P}$ = 5.9 Hz, 4H, H-8,-8'), 2.37 (s, 3H, H-17)

^{31}P-NMR ($CDCl_3$, 146 MHz, ref: 1% H_3PO_4 in D_2O): δ = 26.24 (s, 2P, P-9,-9')

^{13}C-NMR ($CDCl_3$, 90 MHz, ref: $CDCl_3$ solvent residual): δ = 144.03 (s, 1C, C-2), 143.01 (s, 1C, C-16a), 140.09 (s, 1C, C-19a), 133.21 (d, $J^{4,C\text{-}P}$ = 2.6 Hz, 4C, C-12^{all}), 131.63 (s, 2C, C-3a,-7a), 133.38 (d, $J^{2,C\text{-}P}$ = 10.0 Hz, 8C, C-10^{all},-14^{all}), 129.37 (d, $J^{3,C\text{-}P}$ = 12.5 Hz, 8C, C-11^{all},-13^{all}), 128.97 (s, 2C, C-16,-18), 127.87 (d, $J^{1,C\text{-}P}$ = 103.0 Hz, 4C, C-9a^{all}), 127.63 (s, 2C, C-4,-

7), 126.14 (s, 2C, C-15,-19), 115.2 (s, 2C, C-5,-6), 48.18 (d, $J^{1,C\text{-}P}$ = 67.2 Hz, 2C, C-8,-8'), 21.52 (s, 1C, C-17)

ESI MS *m/z*: 547.1 $[C_{33}H_{29}N_2O_2P_2]^+$ $[OPC^{BIm}PO]^+$

1,3-Bis(diphenylphosphinomethylene)benzimidazoline (2.4)

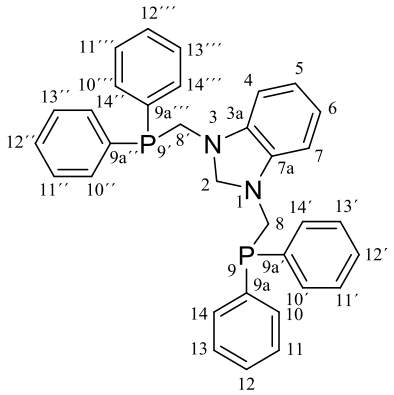

To a suspension of 1,3-bis[(diphenylphosphoryl)methylene]benzimidazolium 4-methylbenzylsulfonate **2.3** (1.30 g, 1.8 mmol, 1.00 equiv) in chlorobenzene (60 mL) were added polymethylhydrosiloxane (1.83 g, 4.4 mmol, 2.50 equiv, M_n = 390 $gmol^{-1}$) and titanium(IV) isopropoxide (1.9 mL, 6.2 mmol, 3.60 equiv) under argon. The reaction mixture was stirred for 2 h at 70 °C. After conversion was complete (^{31}P-NMR monitoring is necessary), the mixture was cooled to 25 °C, and all volatiles were removed in vacuo. Pentane was added to the residue; the suspension formed was stirred for over 3 h and filtered via cannula. Additionally, the crude product was washed three times with a small amount of degassed pentane, dissolved in diethyl ether, filtered, and recrystallized from a concentrated diethyl ether solution at −40 °C. A total of 740.0 mg (82%) of colorless 1,3-bis(diphenylphosphinomethylene)benzimidazoline **2.4** was isolated. Anal. Calcd for $C_{33}H_{30}N_2P_2$: C, 76.73; H, 5.85; N, 5.42; P, 11.99. Found: C, 77.24; H, 5.92; N, 5.45; P, 11.62.

^{1}H-NMR ($CDCl_3$, 500 MHz, ref: $CDCl_3$ solvent residual): δ = 7.46 (m, 8H, H-11^{all},-13^{all}), 7.34 (m, 12H, H-10^{all},-12^{all},-14^{all}), 6.61 (m, 2H, H-5,-6), 6.41 (m, 2H, H-4,-7), 4.66 (s, 2H, H-2), 3.81 (d, $J^{2,H\text{-}P}$ = 5.52 Hz, 4H, H-8,-8').

^{31}P-NMR ($CDCl_3$, 146 MHz, ref: 1% H_3PO_4 in D_2O): δ = -25.00 (s, 2P, P-9, P-9').

^{13}C-NMR ($CDCl_3$, 76 MHz, ref: $CDCl_3$ solvent residual): δ = 142.14 (d, $J^{3,C\text{-}P}$ = 4.77 Hz, 2C, C-3a,-7a), 137.32 (d, *J* = 12.79 Hz, 4C, C-9a^{all}), 132.99 (d, $J^{2,C\text{-}P}$ = 18.10 Hz, 8C, C-10^{all},-14^{all}), 129.08 (s, 4C, C-12^{all}), 128.74 (d, $J^{3,C\text{-}P}$ = 6.60 Hz, 8C, C-11^{all},-13^{all}), 119.18 (s, 2C, C-5,-6), 106.27 (s, 2C, C-4,-7), 77.98 (t, $J^{3,C\text{-}P}$ = 7.02 Hz, 1C, C-2), 50.73 (d, $J^{C\text{-}P}$ = 7.69 Hz, 2C, C-8,-8').

1,3-Bis(diphenylphosphinomethylene)benzimidazolium Hexafluorophosphate (2.5)

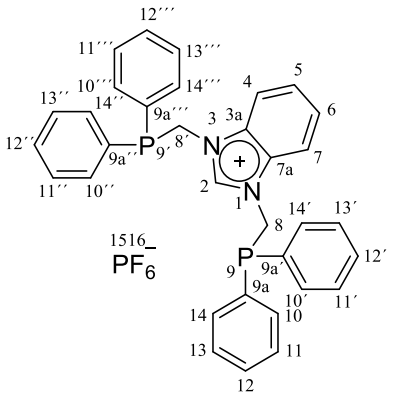

To a colorless solution of 1,3-bis(diphenylphosphinomethylene)benzimidazoline **2.4** (710.0 mg, 1.35 mmol, 1.00 equiv) in 17 mL of degassed dry THF cooled to −78 °C was added in one portion triphenylcarbenium hexafluorophosphate (510.0 mg, 1.31 mmol, 0.97 equiv). The mixture was stirred for 30 min with warming to room temperature. After the reaction was complete, the amount of THF was reduced in vacuo, and the product was precipitated by addition of 15 mL degassed dry toluene. The formed suspension was stirred overnight at room temperature and filtered via cannula. The crude solid product was then redissolved in THF, filtered through syringe filter, and precipitated by the addition of diethyl ether. Recrystallization of this precipitate from THF/Et_2O (2/8) at −40 °C yielded 790.0 mg (86%) of pure colorless crystalline material **2.5**. Anal. Calcd for $C_{33}H_{29}F_6N_2P_3$: C, 60.01; H, 4.43; F, 17.26; N, 4.24; P, 14.07. Found: C, 60.31; H, 4.62; N, 4.38; P, 14.06.

^{1}H-NMR (CD_3CN, 500 MHz, ref: CD_3CN solvent residual): δ = 8.69 (s, 1H, H-2), 7.67 (m, 2H, H-5,-6), 7.53 (m, 2H, H-4,-7), 7.41 (m, 20H, H-10^{all},-11^{all},-12^{all},-13^{all},-14^{all}), 5.15 (d, $J^{2,H\text{-}P}$ = 5.35 Hz, 4H, H-8,-8’).

^{31}P-NMR (CD_3CN, 202 MHz): δ = -14.05 (s, 2P, P-9, P-9’), -144.00 (sept, $J^{P\text{-}F}$ = 706.71 Hz, 1P, P-15).

^{19}F-NMR (CD_3CN, 471 MHz): δ = -72.80 (d, $J^{F\text{-}P}$ = 706.82 Hz, 6F, F-16^{all}).

^{13}C-NMR (CD_3CN, 126 MHz, ref: CD_3CN solvent residual): δ = 140.61 (t, J = 3.91 Hz, 1C, C-2), 134.47 (d, $J^{C\text{-}P}$ = 12.27 Hz, 4C, C-9a^{all}), 133.91 (d, $J^{2,C\text{-}P}$ = 19.87 Hz, 8C, C-10^{all},-14^{all}), 132.30 (s, 2C, C-3a,-7a), 131.24 (s, 4C, C-12^{all}), 130.13 (d, $J^{3,C\text{-}P}$ = 7.18 Hz, 8C, C-11^{all},-13^{all}), 127.90 (s, 2C, C-4,-7), 114.76 (s, 2C, C-5,-6), 47.55 (d, $J^{C\text{-}P}$= 20.95 Hz, 2C, C-8,-8‘).

The calculated overall yield (y_{oa}), avarage yield ($\bar{y}$), and chemical efficiency ($Eff_{\ chem}$) for four step synthesis of **2.5** starting from **2.1** are respectively: $y_{oa} = 0.97 \times 0.93 \times 0.82 \times 0.86 = 0.64$; $\bar{y} = \sqrt[4]{0.64} = 0.89$; $Eff_{\ chem} = {}^{0.64}/_{4} = 0.16$

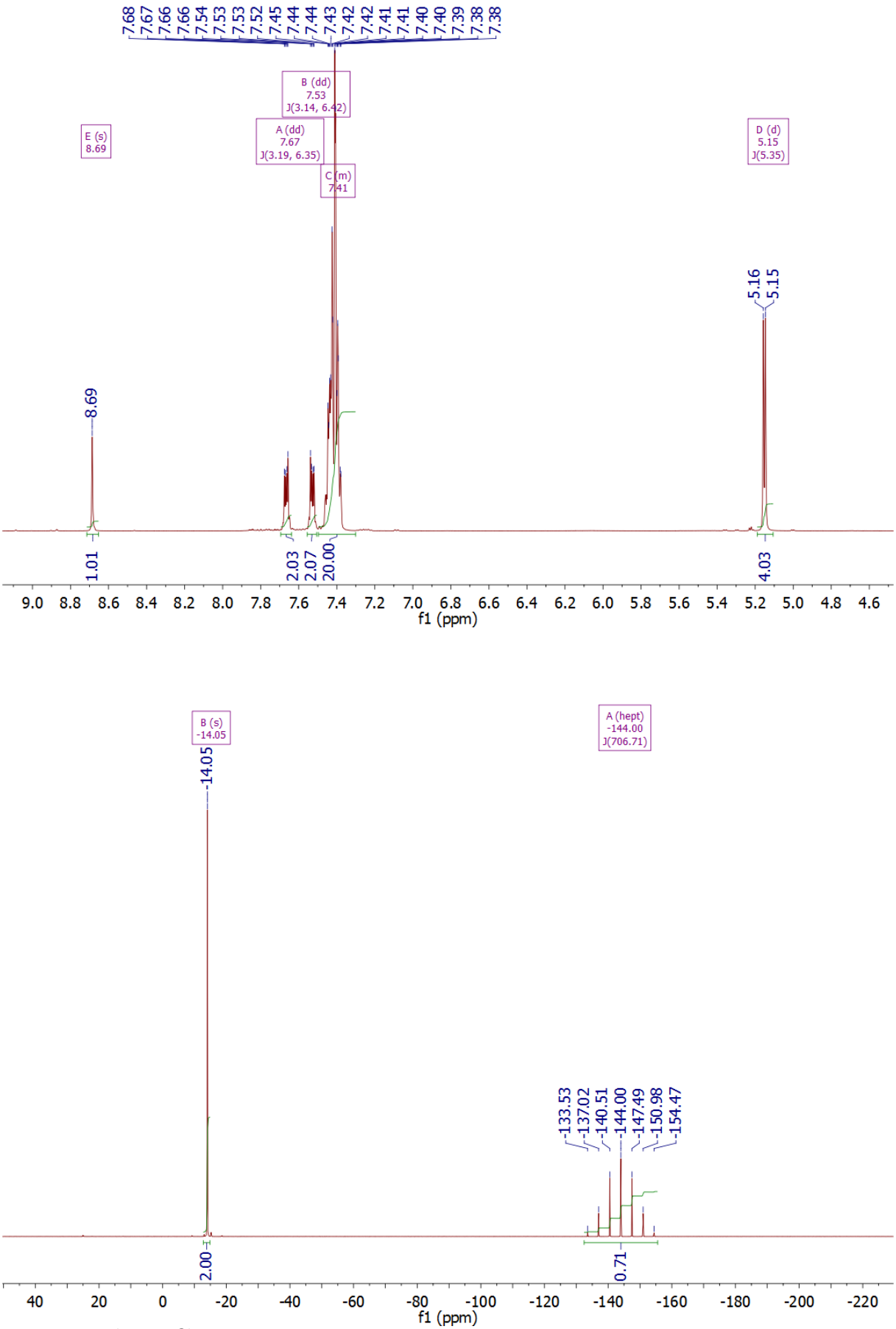

Figure S2.1 ^{1}H and ^{31}P NMR spectra of **2.5**

1,3-Bis(diphenylphosphinomethylene)benzimidazol-2-ylrhodium Acetonitrile/Dimethyl-sulfoxide Hexafluorophosphate (2.6)

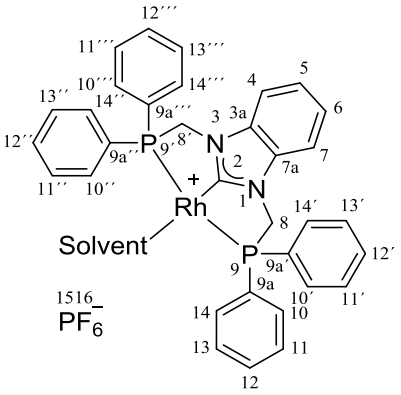

2.6b

2.6a = DMSO
2.6b = CH_3CN

1,3-Bis(diphenylphosphinomethylene)benzimidazolium hexafluorophosphate **5** (480.0 mg, 0.7 mmol, 1.00 equiv) was added to the solution of [μ-$OCH_3Rh(COD)]_2$ (170.0 mg, 0.35 mmol, 0.50 equiv) in 10 mL degassed THF at room temperature and stirred for 17 h. After the reaction was complete, all volatiles were removed in vacuo. The formed amorphous solid was then redissolved in DMSO (for **2.6a**) or in CH_3CN (for **2.6b**) and stirred for 3 h under H_2 atmosphere (0.5 bar over the atmospheric pressure). The reaction mixture was filtered through a 0.20 µm syringe filter and the solvent was partially reduced in vacuo. The yellow needle-shaped crystals of substance **2.6a** (450.0 mg, 76%) were obtained by the addition of diethyl ether after 10 days. The yellow crystals of substance **2.6b** (340.0 mg 61%) were obtained by the addition of diethyl ether. Anal. Calcd for **2.6b** $C_{35}H_{31}F_6N_3P_3Rh$ (+ 0.20 equiv C_2H_3N): C, 53.46; H, 4.00; F, 14.33; N, 5.63; P, 11.68; Rh, 12.94. Found: C, 53.44; H, 4.85; N, 5.24; P, 11.51.

^{1}H-NMR 2.6a: ($(CD_3)_2SO$, 300 MHz, ref: ($(CD_3)_2SO$ solvent residual): δ = 7.89 (m, 8H, H-11^{all},-13^{all}), 7.60 (m, 14H, H-4,-7,-10^{all},-12^{all},-14^{all}), 7.41 (m, 2H, H-5,-6), 5.32 (m, 4H, H-8,-8'). **2.6b**: (CD_3CN, 360 MHz, ref: CD_3CN solvent residual): δ = 7.80 (m, 8H, H-11^{all},-13^{all}), 7.54 (m, 12H, H-10^{all},-12^{all},-14^{all}), 7.40 (m, 2H, H-4,-7), 7.30 (m, 2H, H-5,-6), 4.97 (vt, J^{H-P} = 3.04 Hz, 4H, H-8,-8').

^{31}P-NMR 2.6a: ($(CD_3)_2SO$, 203 MHz): δ = 48.23 (d, J^{P-Rh} = 151.08 Hz, 2P, P-9, P-9'), -144.00 (sept, J^{P-F} = 711.40 Hz, 1P, P-15). **2.6b**: (CD_3CN, 146 MHz): δ = 45.84 (d, J^{P-Rh} = 152.79 Hz, 2P, P-9, P-9'), -144.00 (sept, J^{P-F} = 706.37 Hz, 1P, P-15).

^{19}F-NMR 2.6b: (CD_3CN, 235 MHz): δ = -72.86 (d, J^{F-P} = 706.26 Hz, 6F, F-16^{all}).

^{13}C-NMR 2.6b: (CD_3CN, 126 MHz, ref: CD_3CN solvent residual): δ = 198.96 (dt, $J^{C\text{-}Rh}$ = 51.2 Hz, $J^{2,C\text{-}P}$ = 11.9 Hz, 1C, C-2), 134.93 (t, $J^{C\text{-}P}$ = 6.0 Hz, 2C, C-3a,-7a), 134.25 (t, $J^{C\text{-}P}$ = 20.0 Hz, 4C, C-9a^{all}), 133.76 (vt, $J^{C\text{-}P}$ = 7.7 Hz, 8C, C-10^{all},-14^{all}), 131.97 (s, 4C, C-12^{all}), 130.13 (vt, $J^{C\text{-}P}$ = 4.9 Hz, 8C, C-11^{all},-13^{all}), 124.39 (s, 2C, C-5,-6), 111.97 (s, 2C, C-4,-7), 51.43 (vt, $J^{C\text{-}P}$= 16.77 Hz, 2C, C-8,-8‘).

ESI MS 2.6b: *m/z*: 585.6 ($[C_{33}H_{28}KN_2O_2P_2]^+$, $[OPC^{BIm}POK]^+$), 617.5 ($[C_{33}H_{28}N_2P_2Rh]^+$, $[PC^{BIm}PRh]^+$), 633.4 ($[C_{33}H_{28}N_2OP_2Rh]^+$, $[PC^{BIm}PORh]^+$), 649.4 ($[C_{33}H_{28}N_2O_2P_2Rh]^+$, $[OPC^{BIm}PORh]^+$).

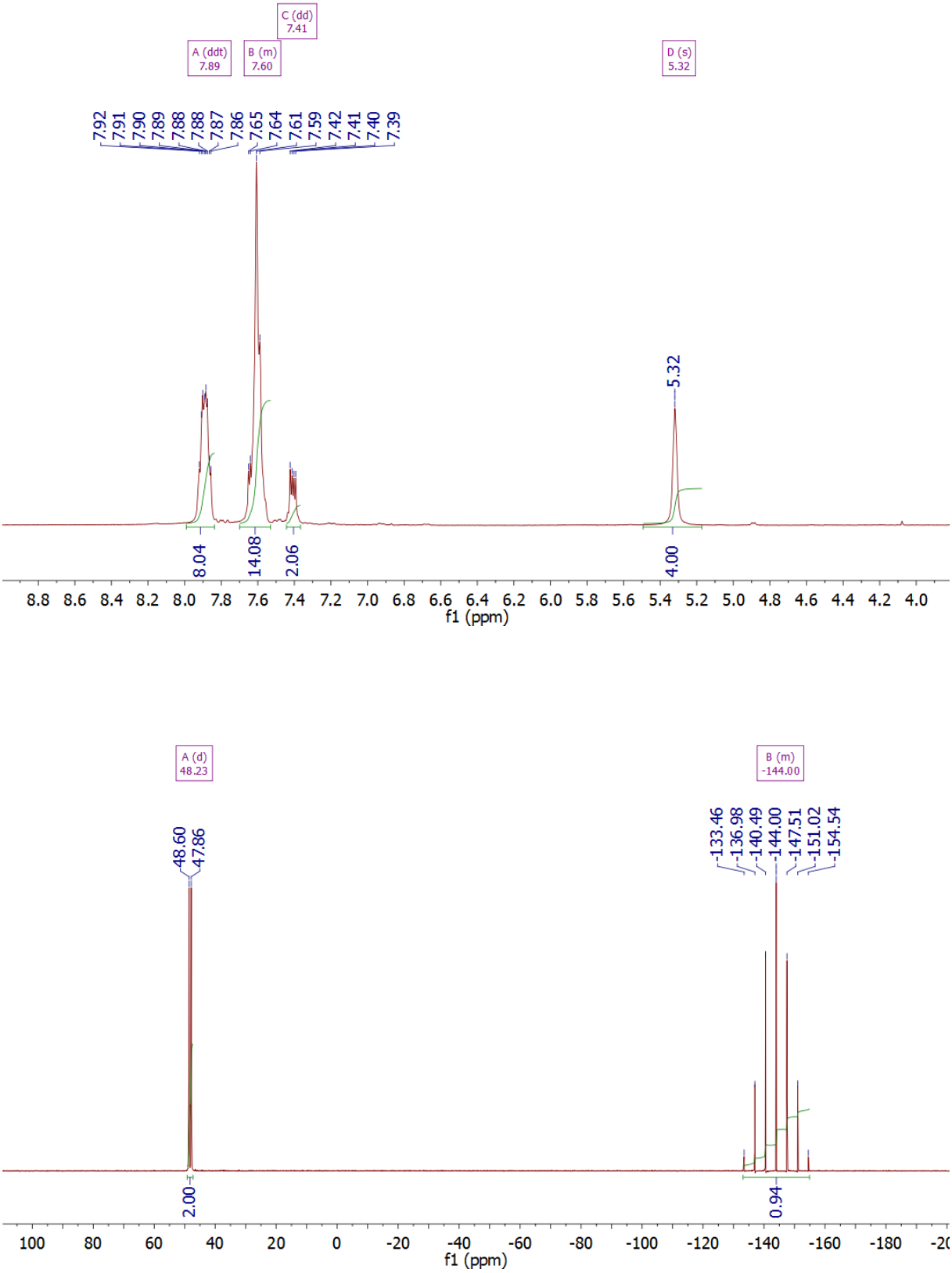

Figure S2.2 (a) ^{1}H and ^{31}P NMR spectra of **2.6a**

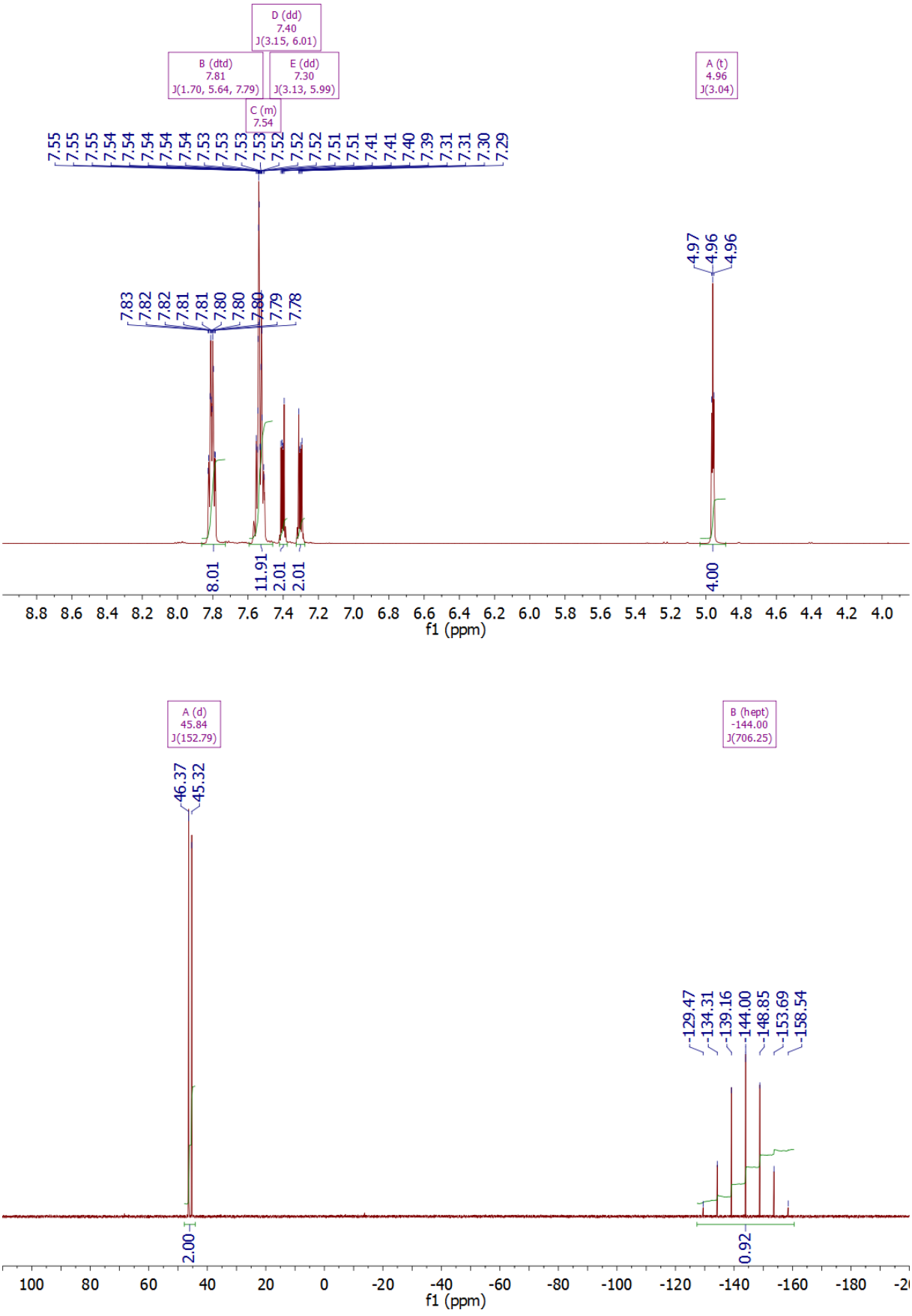

Figure S2.2 (b) ^{1}H and ^{31}P NMR spectra of **2.6b**

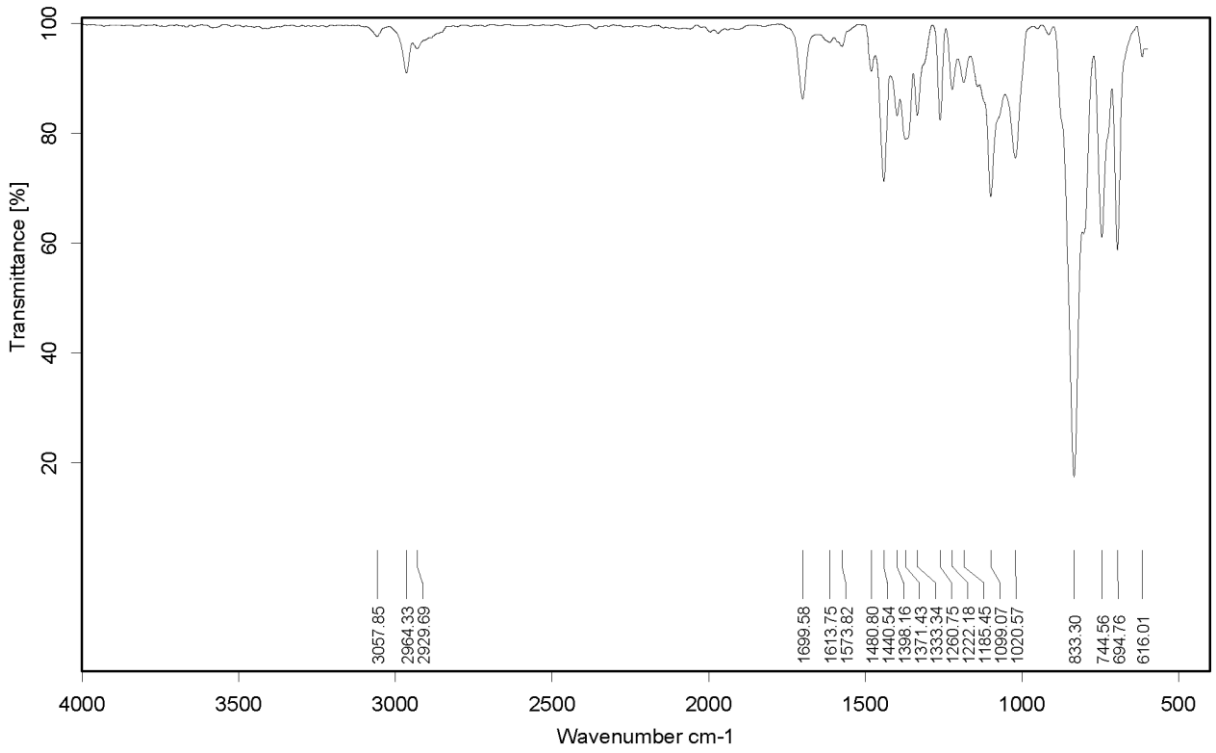

Figure S2.3 IR spectrum of **2.6b**

1,3-Bis(diphenylphosphinomethylene)benzimidazol-2-ylpalladium Chloride Hexafluorophosphate (2.7)

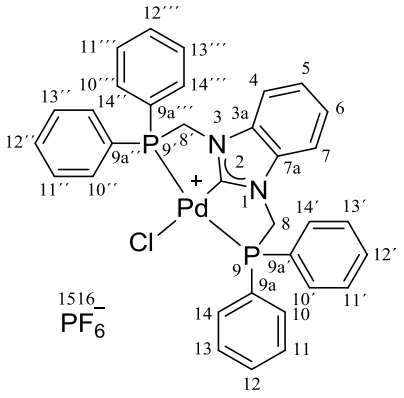

1,3-Bis(diphenylphosphinomethylene)benzimidazolium hexafluorophosphate **2.5** (104.3 mg, 0.15 mmol, 1.00 equiv) was added portionwise to a suspension of $PdCl_2$ (26.9 mg, 0.15 mmol, 1.00 equiv) in 10 mL degassed dry DMF at room temperature and stirred for 8 h at 60 °C. After the reaction was complete, all volatiles were removed in vacuo. The formed amorphous solid was then redissolved in CH_3CN and filtered. The colorless fine crystalline compound **2.7** (41.0 mg, 34%) was obtained after crystallization from CH_3CN/Et_2O mixture. Anal. Calcd for $C_{33}H_{28}ClF_6N_2P_3Pd$: C, 49.46; H, 3.52; Cl, 4.42; F, 14.22; N, 3.50; P, 11.60; Pd, 13.28. Found: C, 49.17; H, 3.75; N, 3.57; P, 11.30.

^{1}H-NMR (CD_3CN, 500 MHz, ref: CD_3CN solvent residual): δ = 7.99 (m, 8H, H-11^{all},-13^{all}), 7.71 (m, 2H, H-4,-7), 7.67 (m, 4H, H-12^{all}), 7.61 (m, 8H, H-10^{all},-14^{all}), 7.58 (m, 2H, H-5,-6), 5.45 (vt, $J^{2,H-P}$ = 3.34 Hz, 4H, H-8,-8').

^{31}P-NMR (CD_3CN, 203 MHz): δ = 38.16 (s, 2P, P-9, P-9'), -144.00 (sept, J^{P-F} = 706.89 Hz, 1P, P-15).

^{19}F-NMR (CD_3CN, 235 MHz): δ = -72.89 (d, J^{F-P} = 706.26 Hz, 6F, F-16^{all}).

^{13}C-NMR (CD_3CN, 126 MHz, ref: CD_3CN solvent residual): δ = 178.82 (t,$J^{2,C-P}$ = 5.78 Hz, 1C, C-2), 134.37 (vt, J^{C-P} = 7.31 Hz, 8C, C-10^{all},-14^{all}), 134.15 (t, J^{C-P} = 6.36 Hz, 2C, C-3a,-7a), 133.68 (s, 4C, C-12^{all}), 130.53 (vt, J^{C-P} = 5.77 Hz, 8C, C-11^{all},-13^{all}), 127.99 (t, J^{C-P} = 25.22 Hz, 4C, C-9a^{all}), 126.63 (s, 2C, C-5,-6), 114.20 (s, 2C, C-4,-7), 52.43 (vt, J^{C-P} = 17.67 Hz, 2C, C-8,-8').

ESI MS *m/z*: 647.3 ($[C_{66}H_{57}ClN_4OP_4Pd_2]^{2+}$, $[(PC^{BIm}P)_2Pd_2Cl(OH)]^{2+}$), 656.2 ($[C_{33}H_{28}ClN_2P_2Pd]^+$, $[PC^{BIm}PPdCl]^+$). **FAB MS** *m/z*: 655.4 ($[C_{33}H_{28}ClN_2P_2Pd]^+$, $[PC^{BIm}PPdCl]^+$).

HRMS *m/z*: Calcd 655.04456, found 655.04491 ([$C_{33}H_{28}ClN_2P_2Pd$]$^+$, [$PC^{BIm}PPdCl$]$^+$).

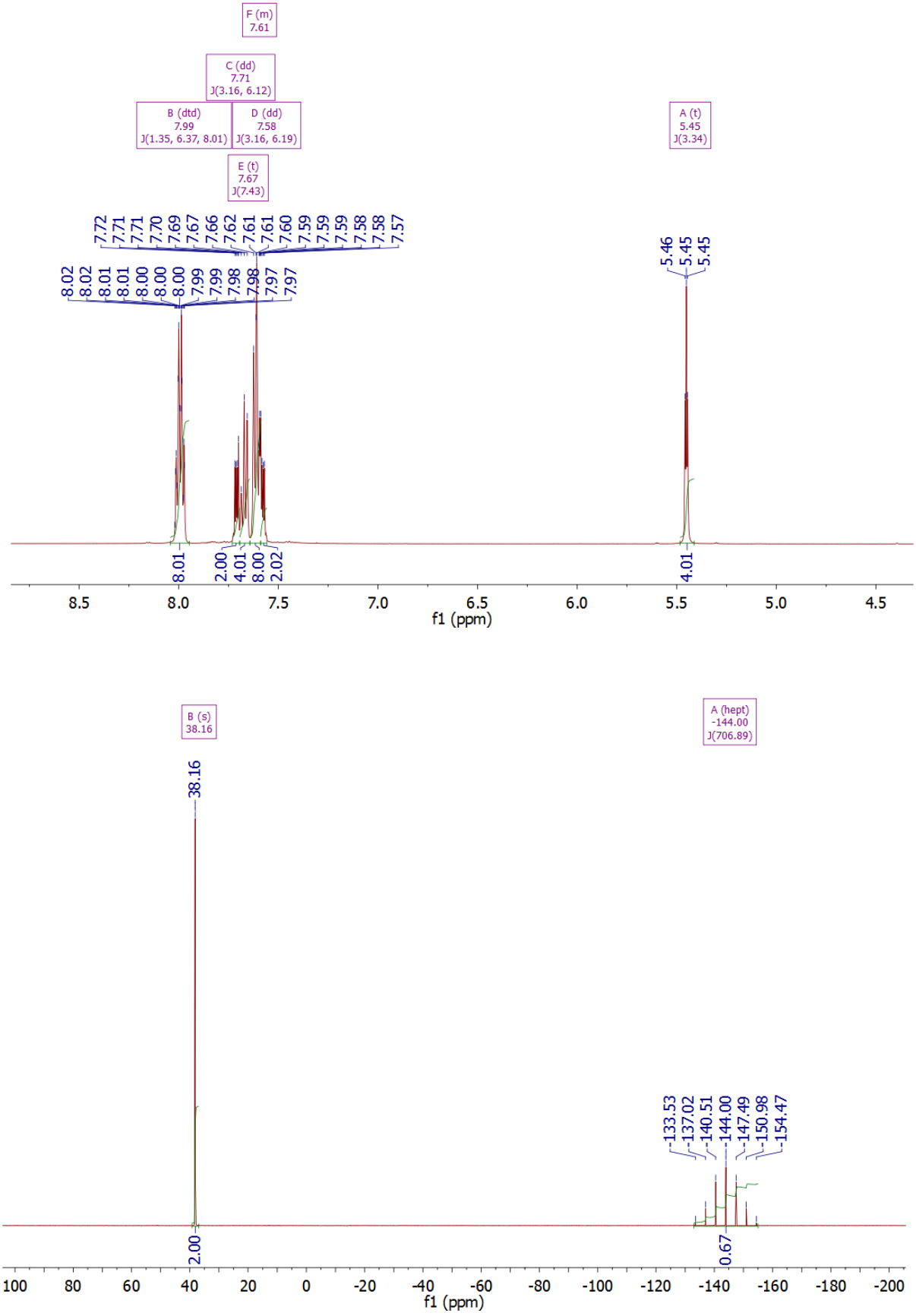

Figure S2.4 ^{1}H and ^{31}P NMR spectra of **2.7**

1,3-Bis(diphenylphosphinomethylene)benzimidazol-2-ylrhodium Carbonyl Hexafluorophosphate (2.8)

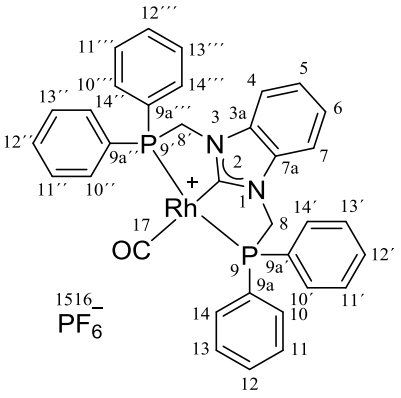

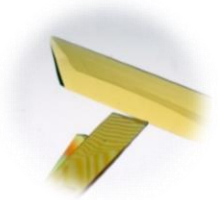

A solution of 1,3-bis(diphenylphosphinomethylene)benzimidazol-2-ylrhodium acetonitrile hexafluorophosphate (**2.6b**, 23.0 mg, 0.03 mmol, 1.00 equiv) in 0.5 mL PO was pressurized with 2 bar ^{13}CO in an young valve NMR tube. After 2 h, the tube containing the reaction mixture was flushed with degassed diethyl ether. Crystallization gave 20.0 mg (98%) of **2.8** in the form of light-yellow needles. Anal. Calcd for $C_{34}H_{28}F_6N_2OP_3Rh$: C, 51.66; H, 3.57; F, 14.42; N, 3.54; O, 2.02; P, 11.76; Rh, 13.02. Found: C, 51.28; H, 4.02; N, 3.21; P, 11.36.

^{1}H-NMR (CD_3CN, 300 MHz, ref: CD_3CN solvent residual): δ = 7.82 (m, 8H, H-11^{all},-13^{all}), 7.65 (m, 2H, H-4,-7), 7.59 (dq, J = 14.30 Hz, 7.27 Hz, 12H, H-10^{all},-12^{all},-14^{all}), 7.50 (m, 2H, H-5,-6), 5.37 (vt, J^{H-P} = 3.14 Hz, 4H, H-8,-8’).

^{31}P-NMR (CD_3CN, 203 MHz): δ = 55.41 (d, J^{P-Rh} = 138.49 Hz, 2P, P-9, P-9’), -144.00 (sept, J^{P-F} = 707.27 Hz, 1P, P-15).

^{19}F-NMR (CD_3CN, 471 MHz): δ = -72.60 (d, J^{F-P} = 706.73 Hz, 6F, F-16^{all}).

^{13}C-NMR (CD_3CN, 126 MHz, ref: CD_3CN solvent residual): δ = 197.21 (dt, J^{C-Rh} = 40.48 Hz, $J^{2,C-P}$ = 12.63 Hz, 1C, C-2), 195.96 (s, 1C, C-17), 134.71 (vt, J^{C-P} = 5.69 Hz, 2C, C-3a,-7a), 134.00 (vt, J^{C-P} = 7.59 Hz, 8C, C-10^{all},-14^{all}), 132.90 (s, 4C, C-12^{all}), 132.01 (vt, J^{C-Ph} = 23.45 Hz, 4C, C-9a^{all}), 130.45 (vt, J^{C-P} = 5.48, 8C, C-11^{all},-13^{all}), 126.09 (s, 2C, C-5,-6), 125.74 (s, C, free ^{13}CO), 113.85 (s, 2C, C-4,-7), 54.31 (vt, J^{C-P}= 17.61 Hz, 2C, C-8,-8‘).

ESI MS *m/z*: 617.4 ([$C_{33}H_{28}N_2P_2Rh$]$^+$, [PC^{BIm}PRh]$^+$), 633.3 ([$C_{33}H_{28}N_2OP_2Rh$]$^+$, [PC^{BIm}PORh]$^+$), 645.4 ([$C_{34}H_{28}N_2OP_2Rh$]$^+$, [PC^{BIm}PRhCO]$^+$), 649.3 ([$C_{33}H_{28}N_2O_2P_2Rh$]$^+$, [OPC^{BIm}PORh]$^+$).

IR: ν_{C-O} = 1995.34 cm^{-1}.

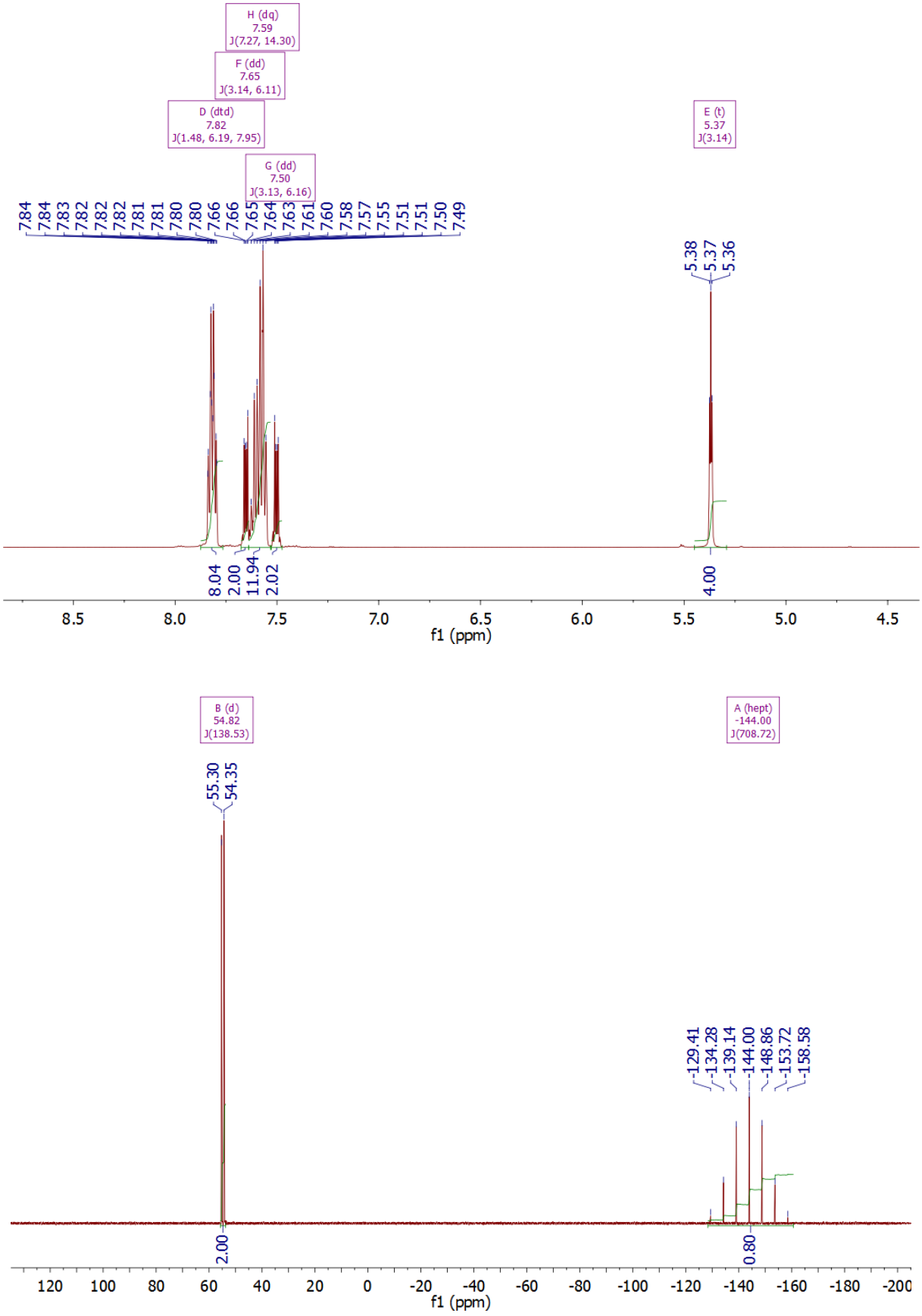

Figure S2.5 ^{1}H and ^{31}P NMR spectra of **2.8**

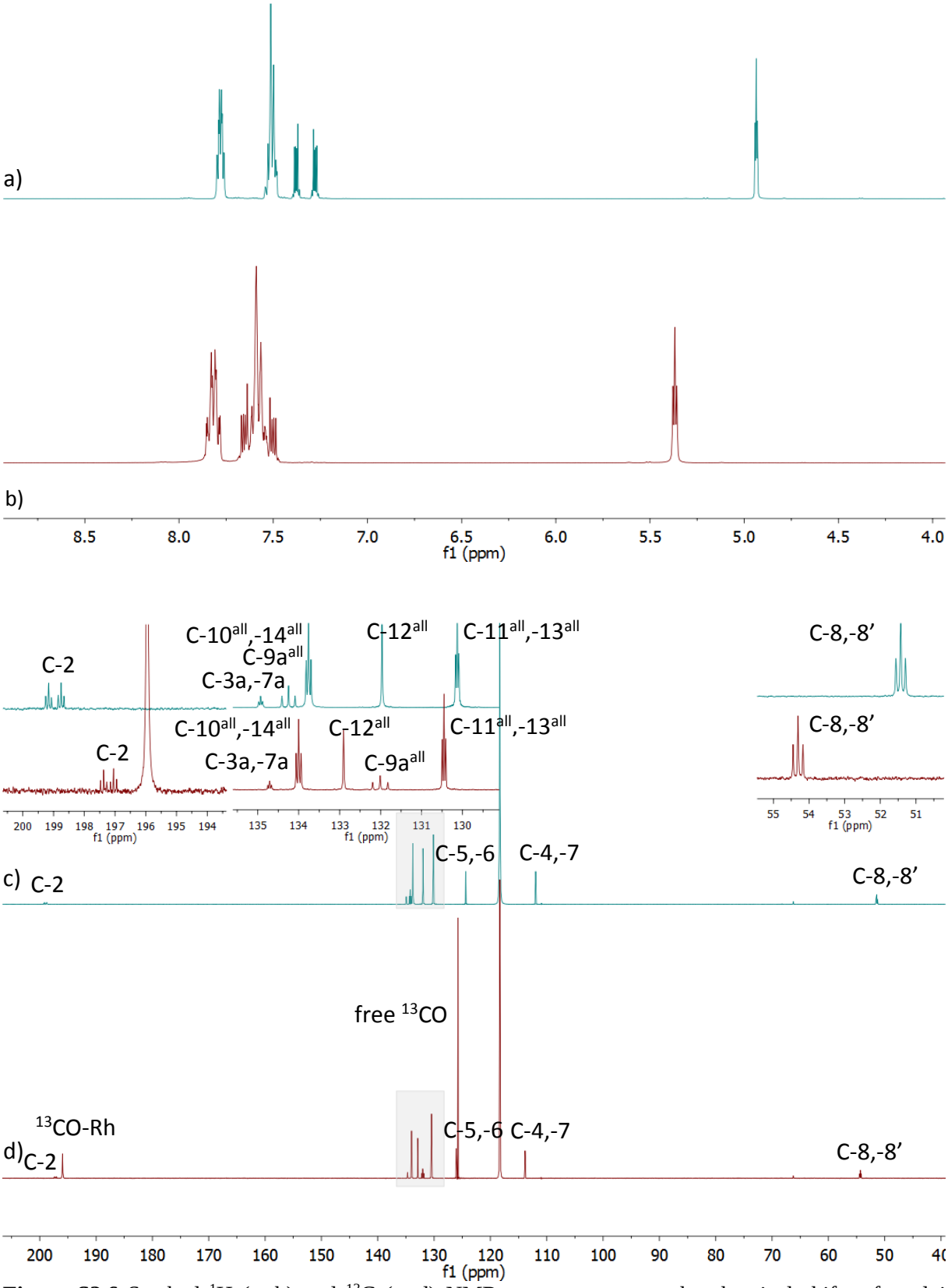

Figure S2.6 Stacked ^{1}H (a, b) and ^{13}C (c, d) NMR spectra represent the chemical shifts of nuclei signals before and after complexation of **2.6b** (a, c) with carbon monoxide leading to **2.8** (b, d)

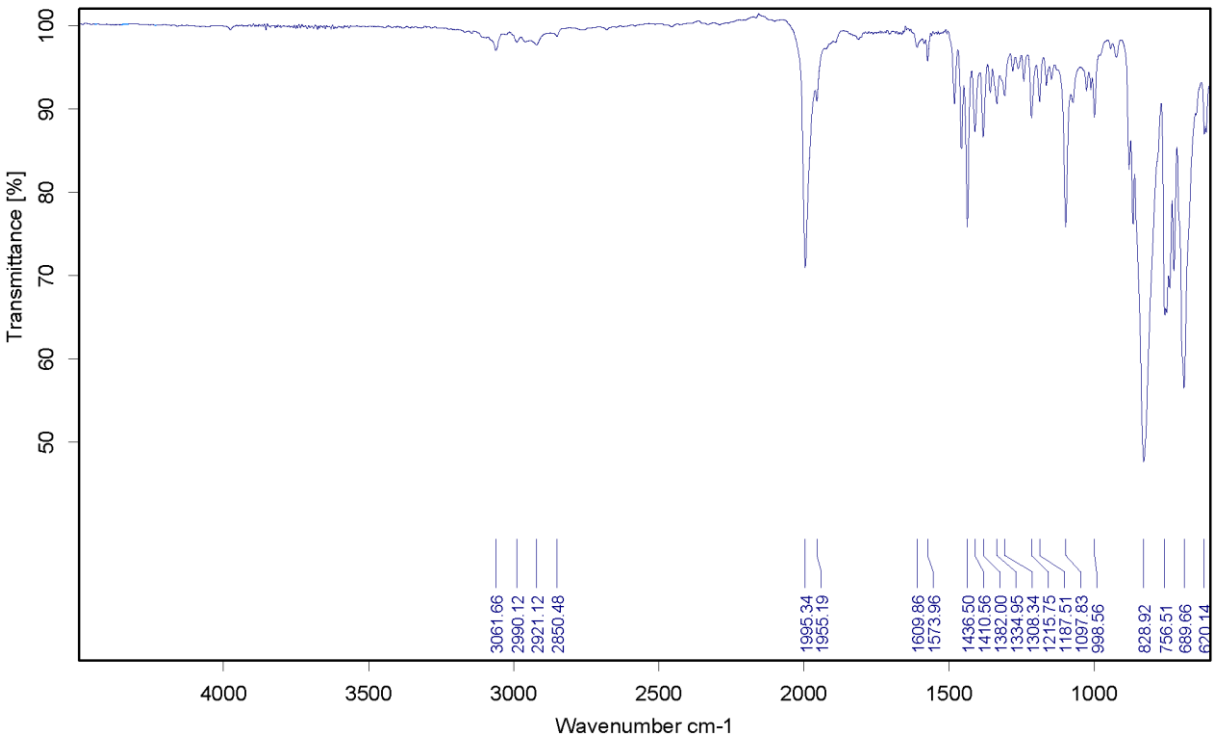

Figure S2.7 IR spectrum of **2.8**

1,3-Bis(diphenylphosphinomethylene)benzimidazol-2-ylrhodium Ethylene Hexafluorophosphate (2.9)

The ethylene gas was introduced to the solution of **2.6b** in a Young-NMR tube. Subsequently, the color of the mixture changed slightly to maize yellow; after 2 h the ^{31}P NMR spectra were recorded. Reaction of **2.6b** with ethylene leads to the reversible formation of $[PC^{BIm}PRhC_2H_4][PF_6]$ **2.9** in PO, CH_2Cl_2, and THF solutions at 25 °C. In all cases, the removal of volatile components led to the formation of **2.6b**, and complex **2.9** could not be isolated. Crystallization directly from the reaction mixture did not give a crystalline product **2.9**.

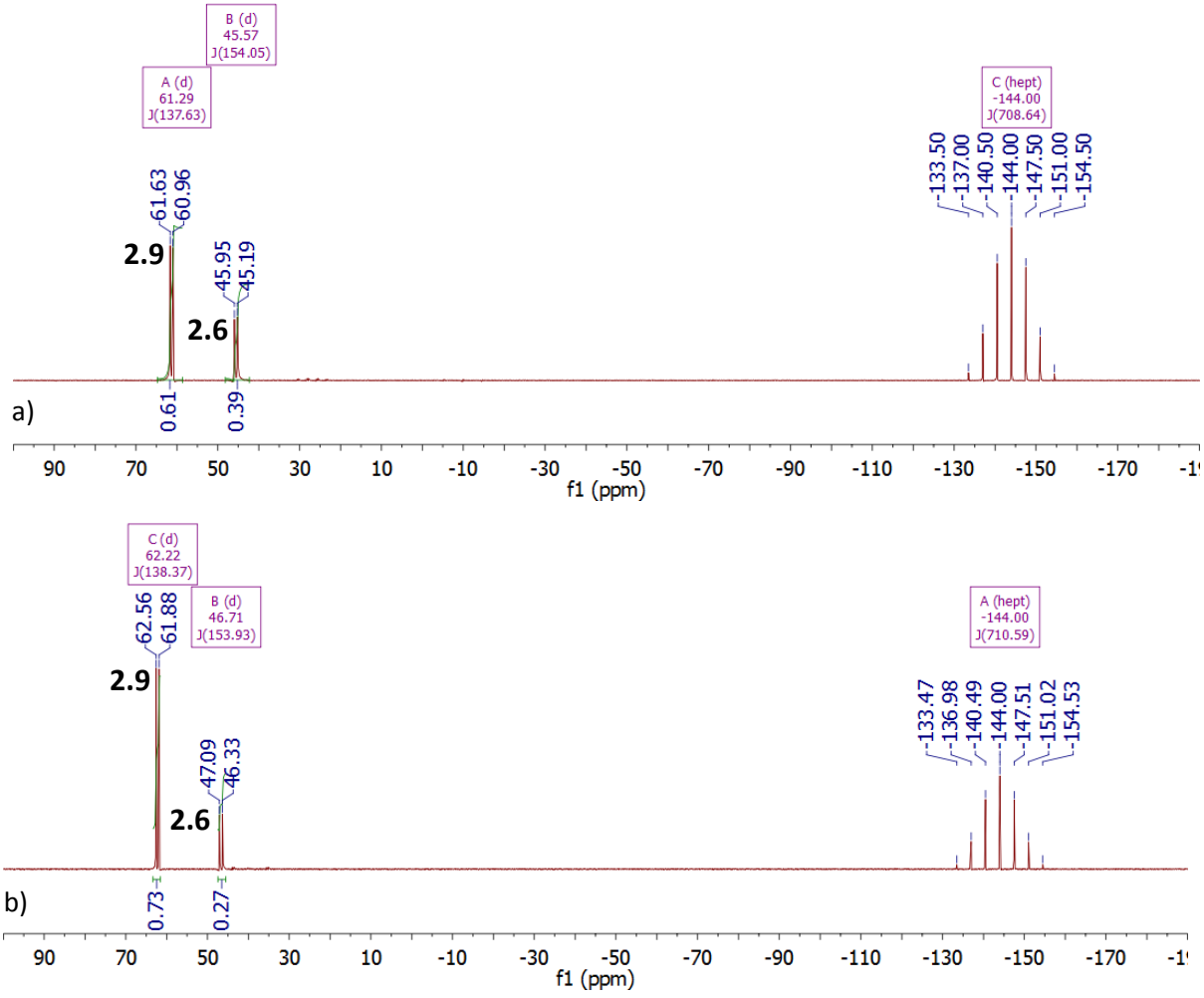

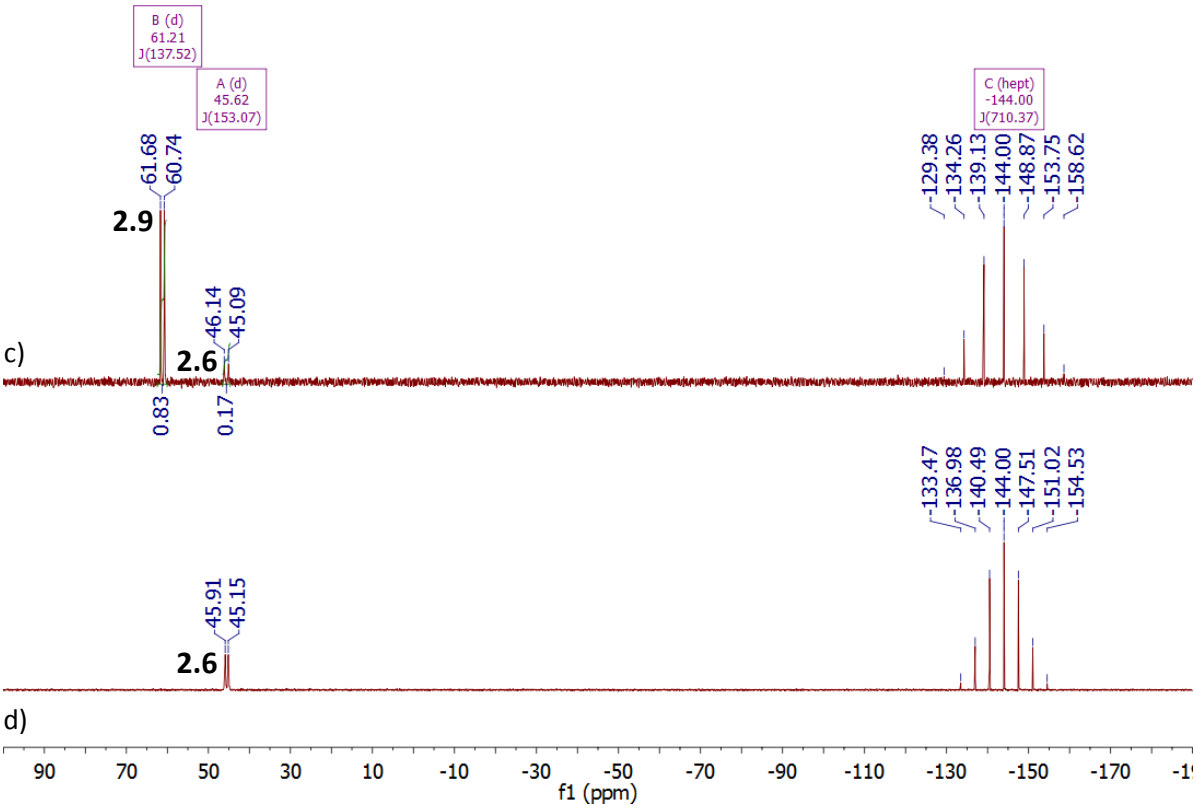

Figure S2.8 Equilibrium between **2.6** and **2.9** under an ethylene atmosphere in a) PO (0.5 bar) CH_2Cl_2 (0.5 bar), c) THF (0.8 bar). All volatiles from the THF solution of **2.6** were removed in vacuo, the solid residue was redissolved again in deuterated THF and measured (d)

Thermal stability in solid state

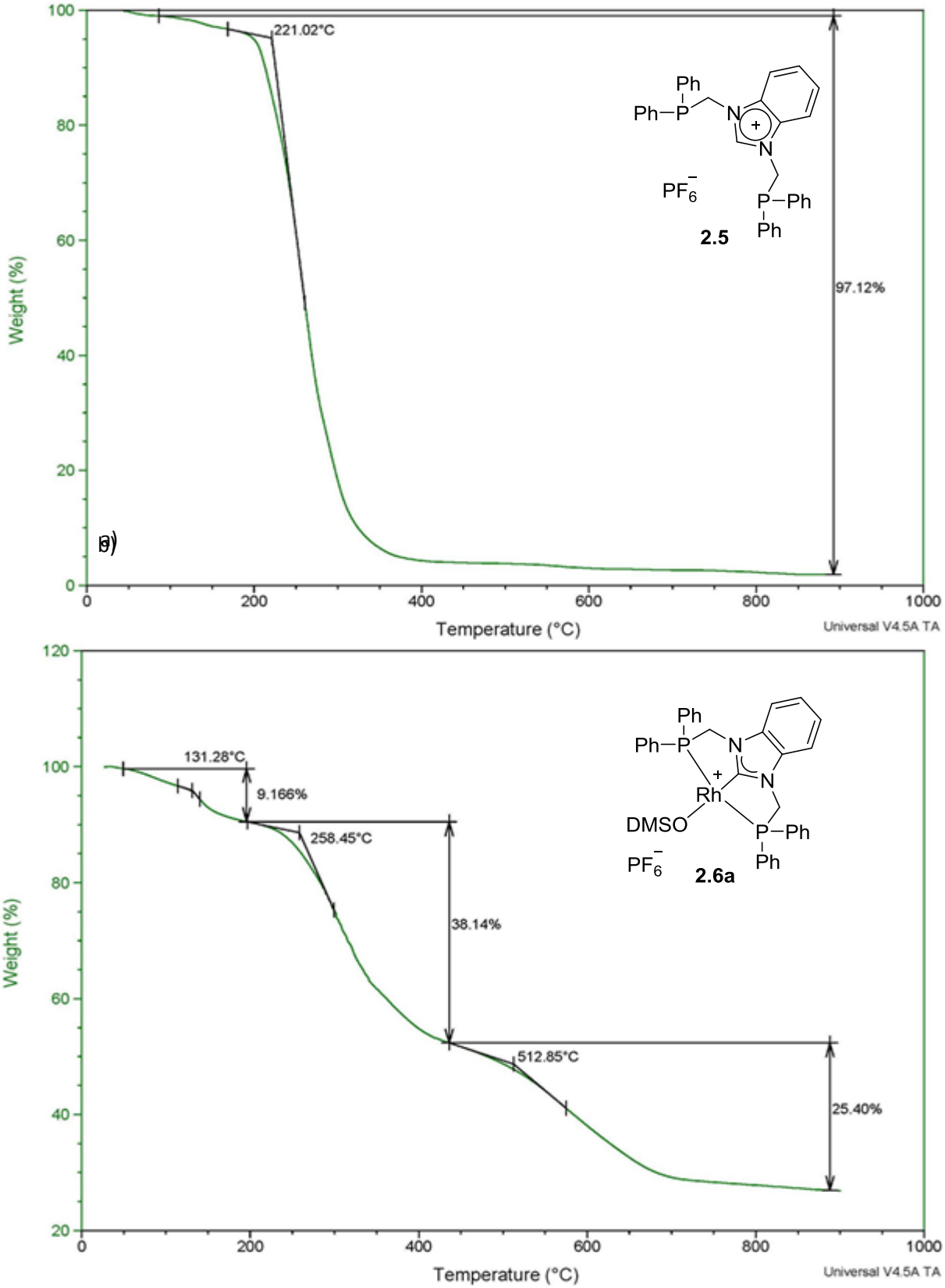

Figure S2.9 Thermogravimetric analysis of a) $PC^{BIm}P$ ligand precursor **2.5** and b) $PC^{BIm}P$ rhodium(I) complex **2.6a**

Thermal stability in solutions

The thermal stability and reactivity of the rhodium complex **2.6b** in various solvents were assessed according to the following procedure.

1,3-Bis(diphenylphosphinomethylene)benzimidazol-2-ylrhodium acetonitrile hexafluorophosphate **2.6b** (3-7 mg) was dissolved in 0.45 mL of a degassed solvent in a NMR tube at room temperature in the glove box. The NMR tube was placed in an oil bath; the tube contents was heated up to a certain temperature, cured at this temperature over a definite period, and analyzed using NMR techniques. After the measurements, the NMR tube was placed back in the oil bath again and the procedure was repeated, reaching another higher temperature limit. Reaction of **2.6b** with hydrogen was performed in a Young NMR tube.

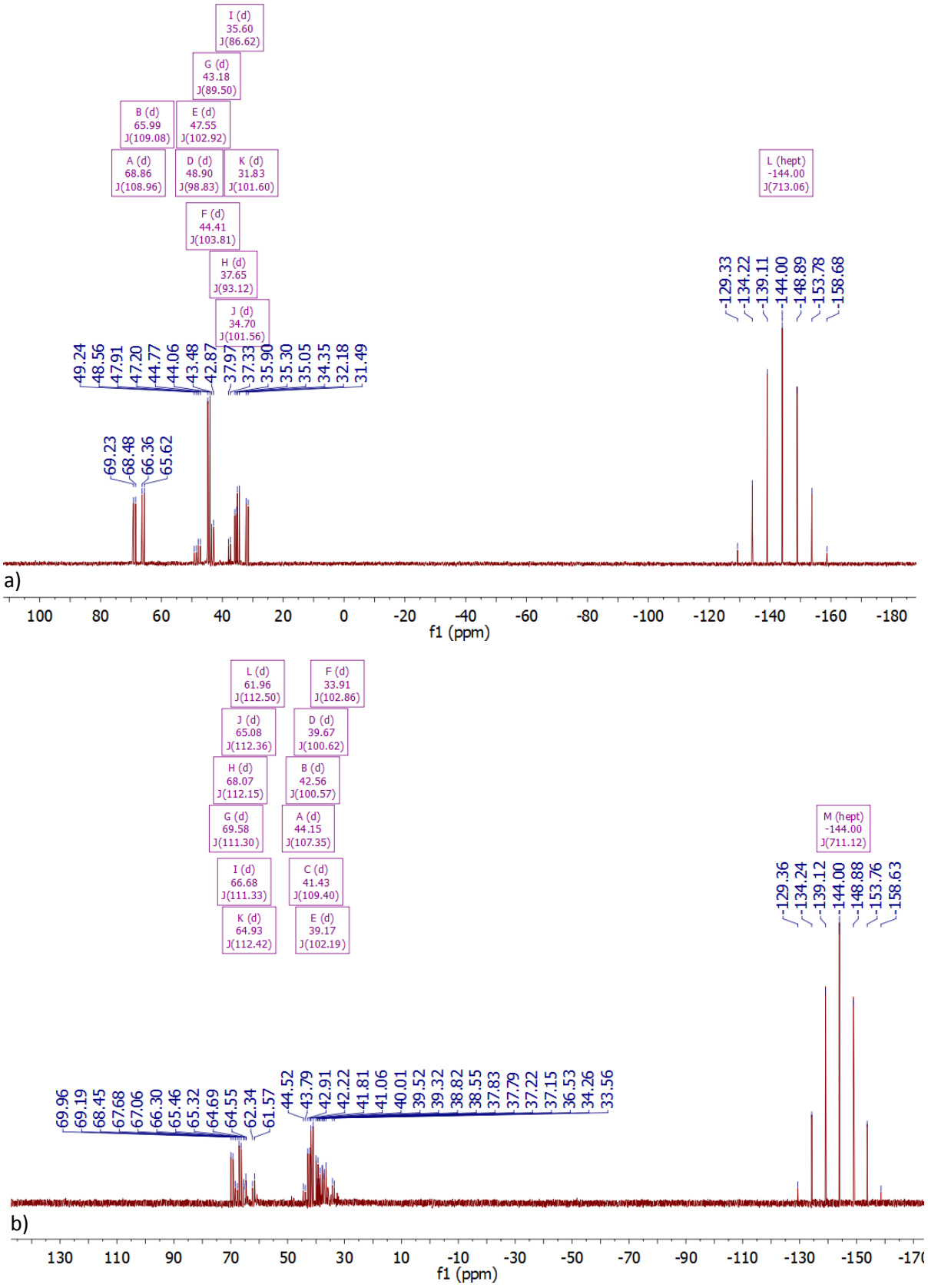

Figure S2.10 Reaction of **2.6b** with a) $CHCl_3$ (0.5 25 °C) and b) CH_2Cl_2 (17 80 °C)

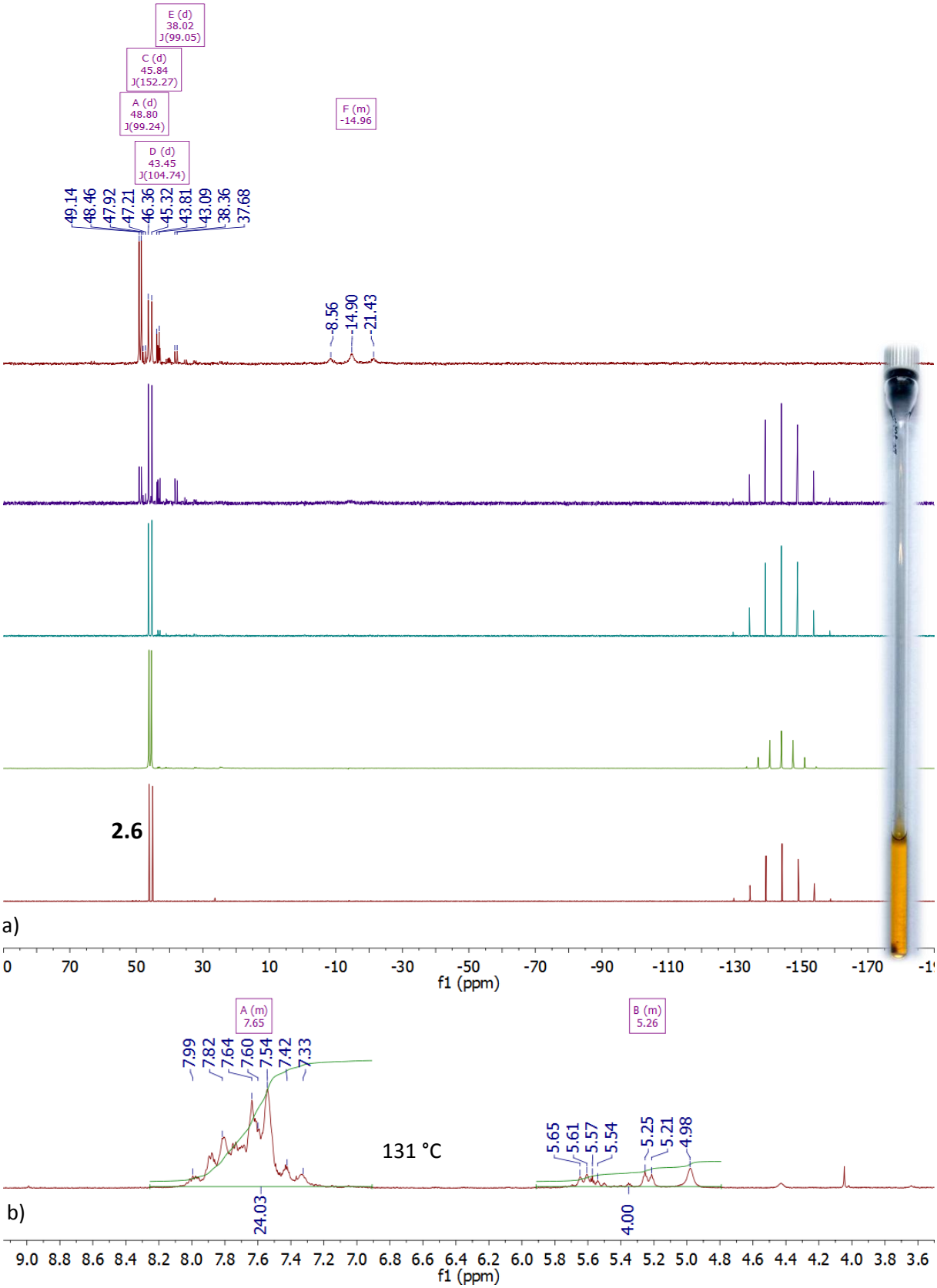

Figure S2.11 Thermal stability of **2.6b** in CH_3CN solution by elevated temperatures under argon atmosphere: a) The ^{31}P NMR monitoring; b) The ^{1}H NMR spectrum: Conversion products of ($PC^{BIm}P$)Rh fragment

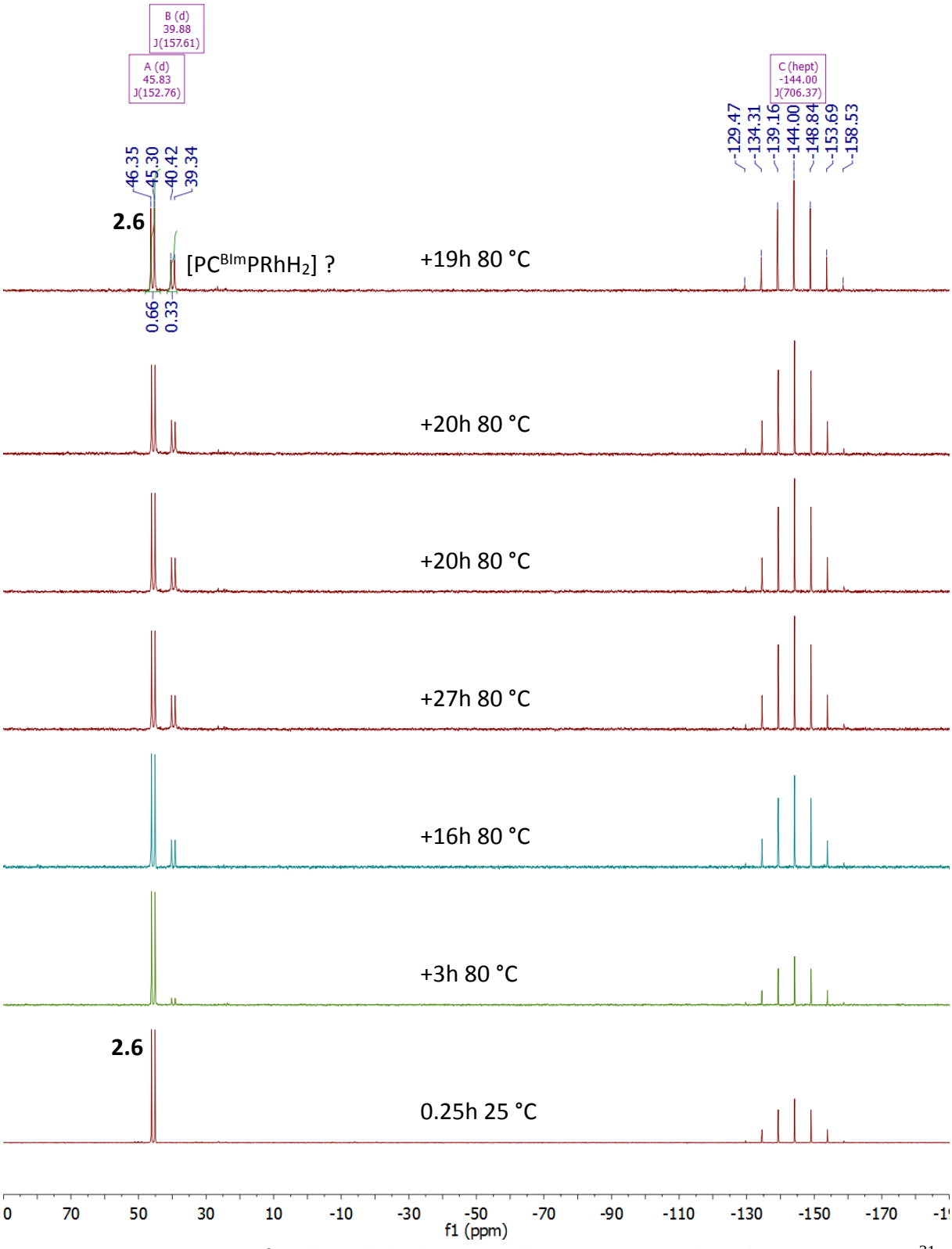

Figure S2.12 Reaction of **2.6b** with hydrogen (1 bar) in acetonitrile solution at 80 °C (^{31}P NMR monitoring)

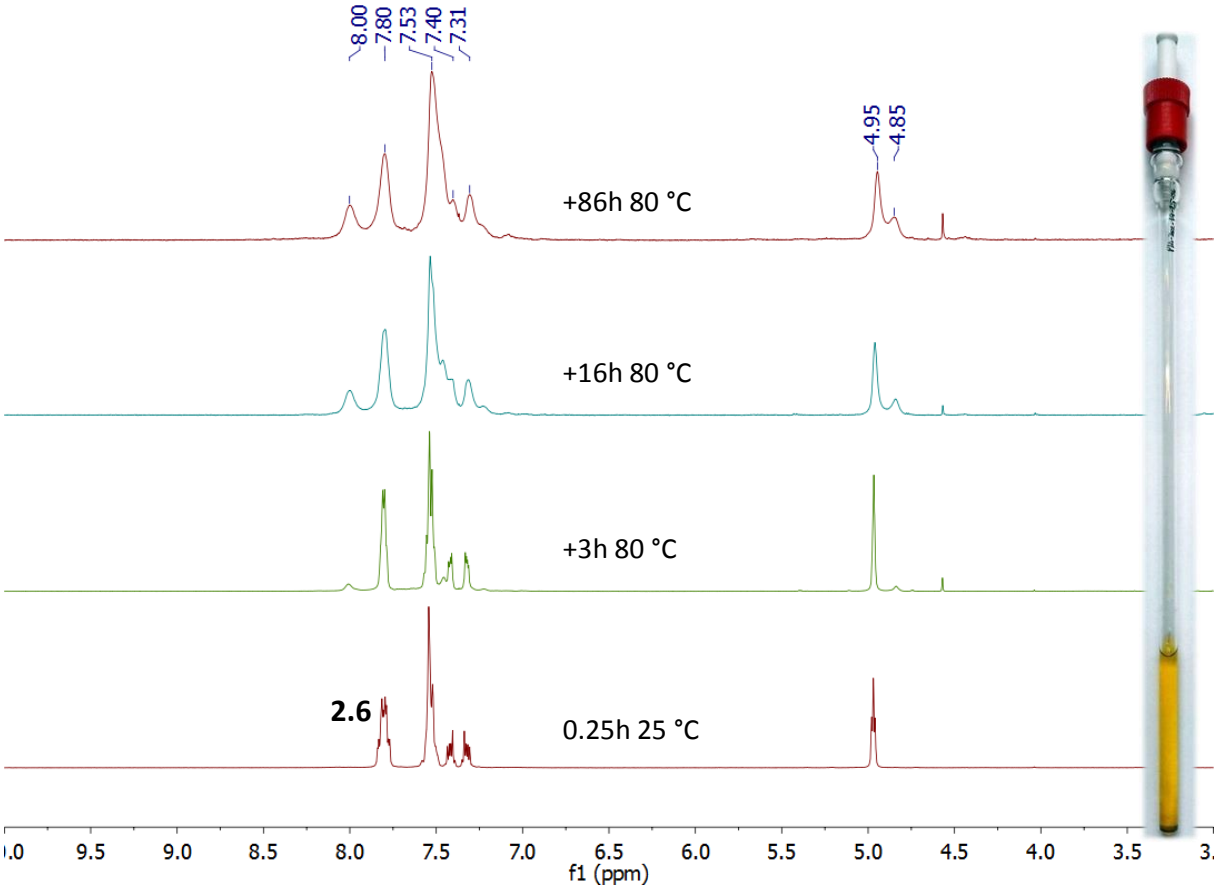

Figure S2.13 Reaction of **2.6b** with hydrogen (1 bar) in CH_3CN solution at 80 °C (^{1}H NMR monitoring)

Decarbonylation of small molecules

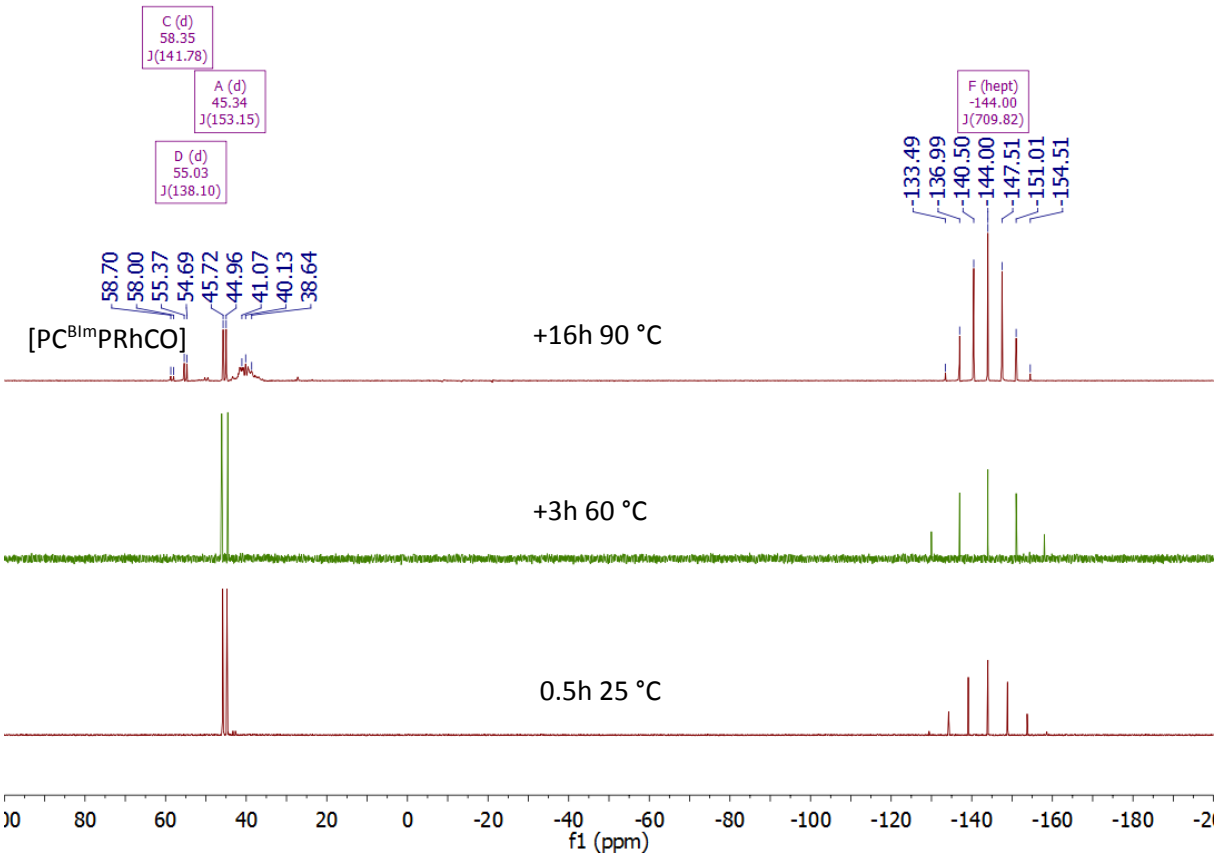

Figure S2.14 The ^{31}P NMR monitoring of **2.6b** in β-Propiolactone by elevated temperatures under argon atmosphere

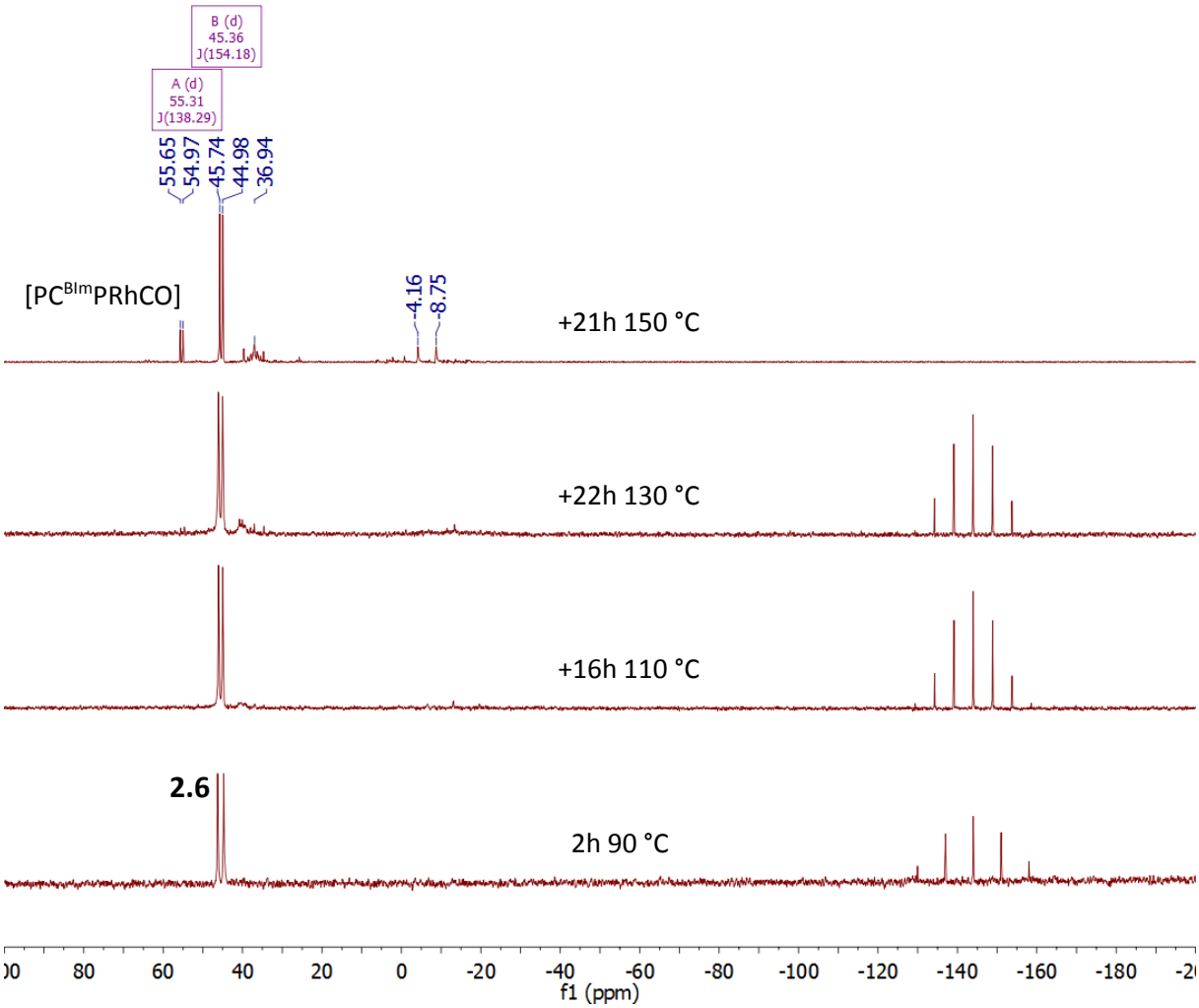

Figure S2.15 Thermal stability of **2.6b** in THF solution by elevated temperatures under argon atmosphere (^{31}P NMR monitoring)

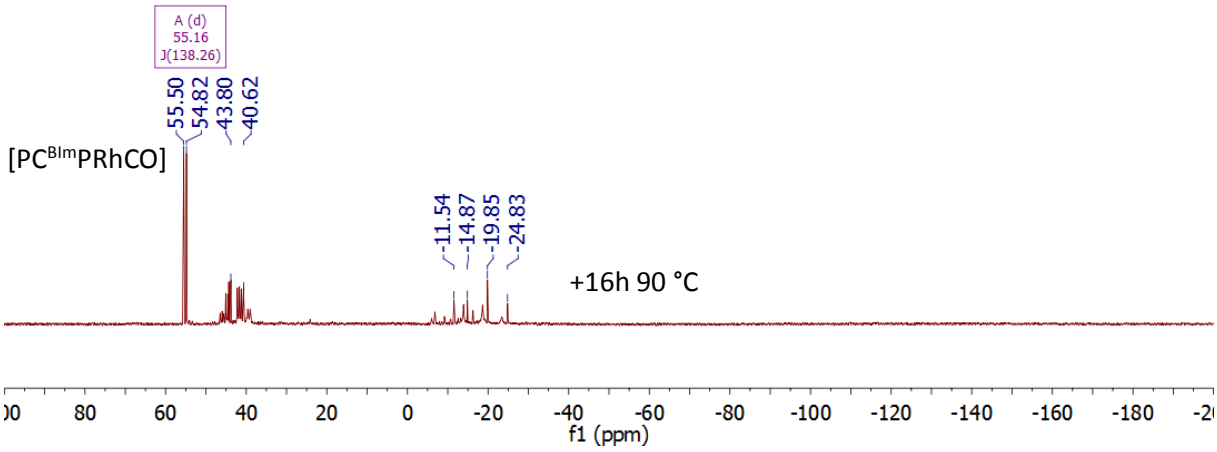

Figure S2.16 Thermal stability of **2.6b** in diethyl carbonate (suspension) by heating at 90 °C under argon atmosphere (^{31}P NMR monitoring)

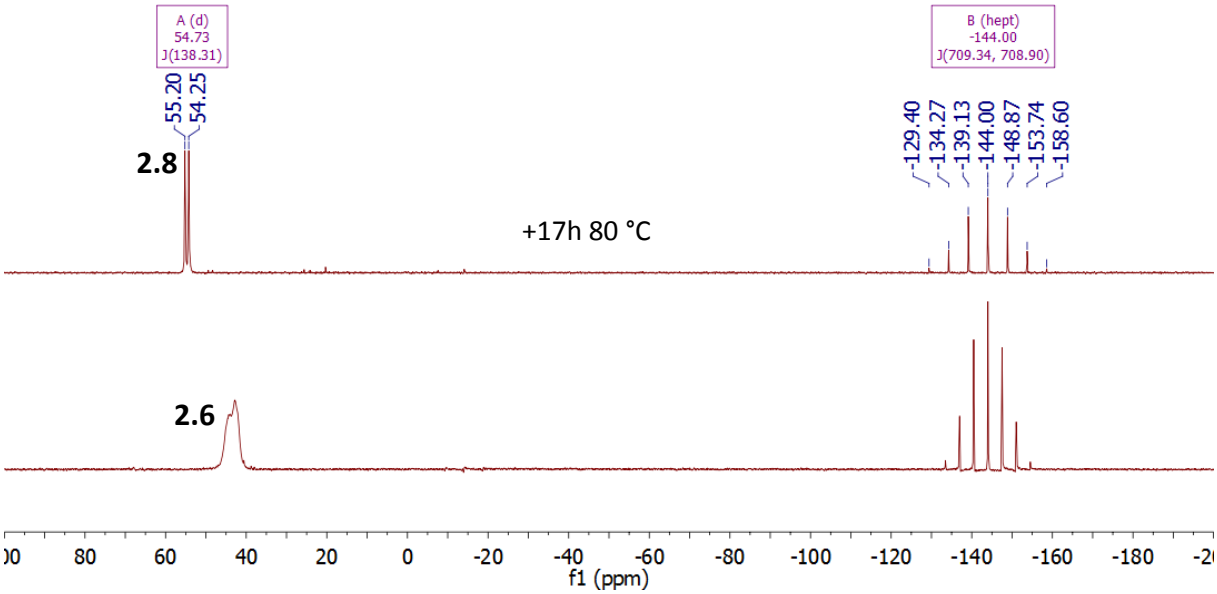

Figure S2.17 Quantitative conversion of **2.6b** to **2.8** through decarbonylation of dimethylformamide at elevated temperatures under argon atmosphere (^{31}P NMR monitoring)

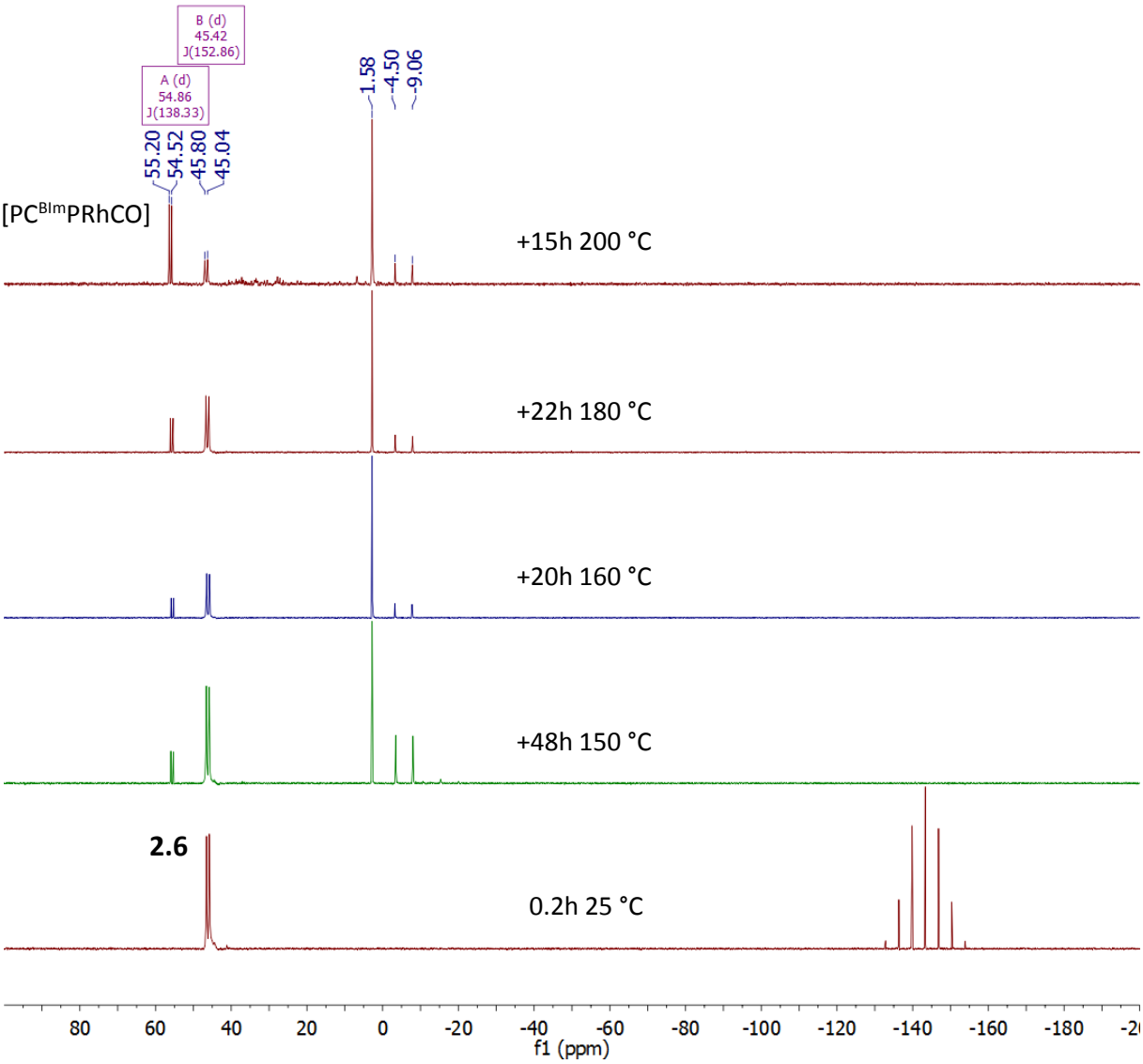

Figure S2.18 Thermal stability of **2.6b** in acetone solution at elevated temperatures under argon atmosphere (^{31}P NMR monitoring)

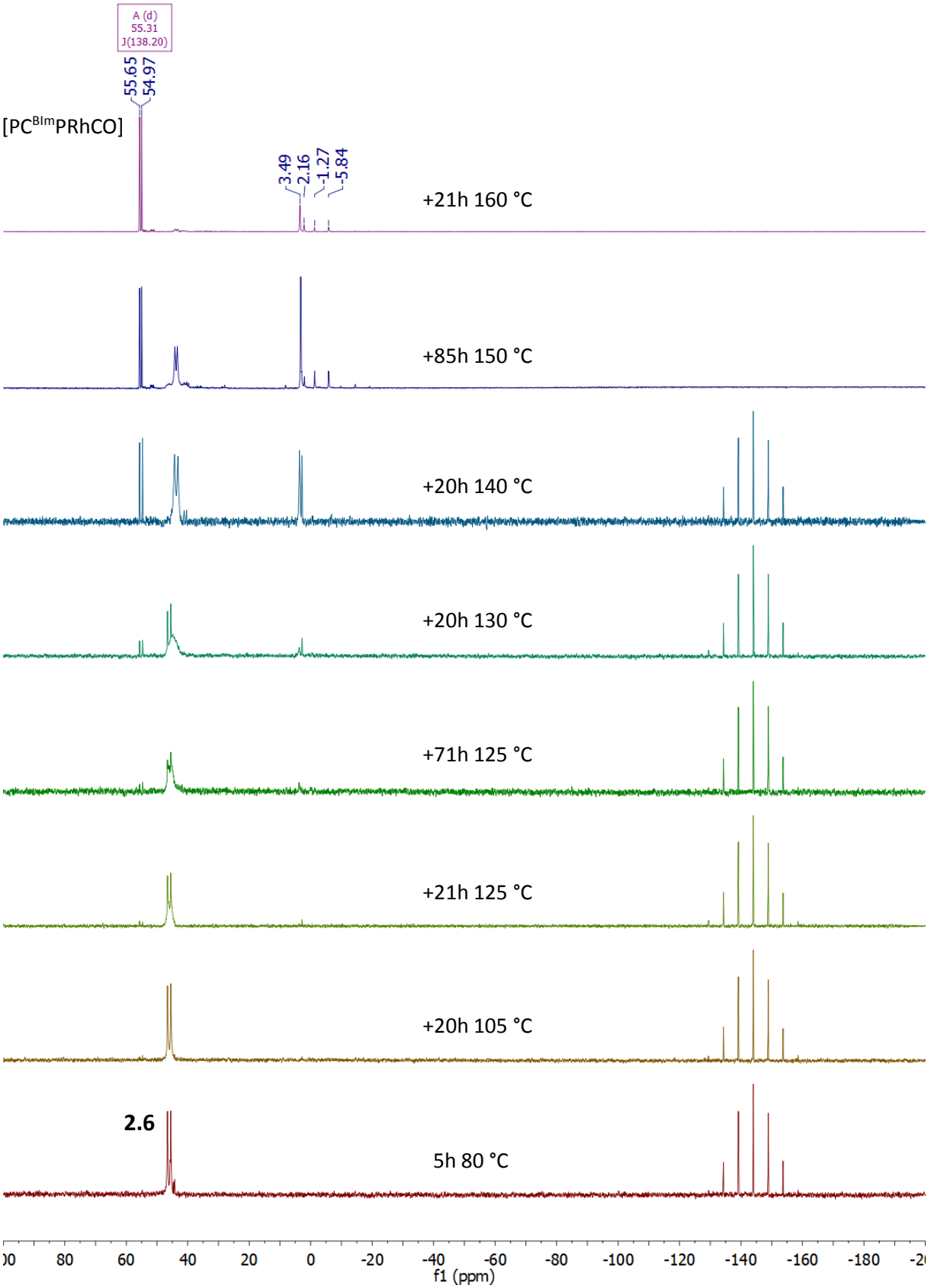

Figure S2.19 Thermal stability of **2.6b** in methanol solution by elevated temperatures under argon atmosphere (^{31}P NMR monitoring)

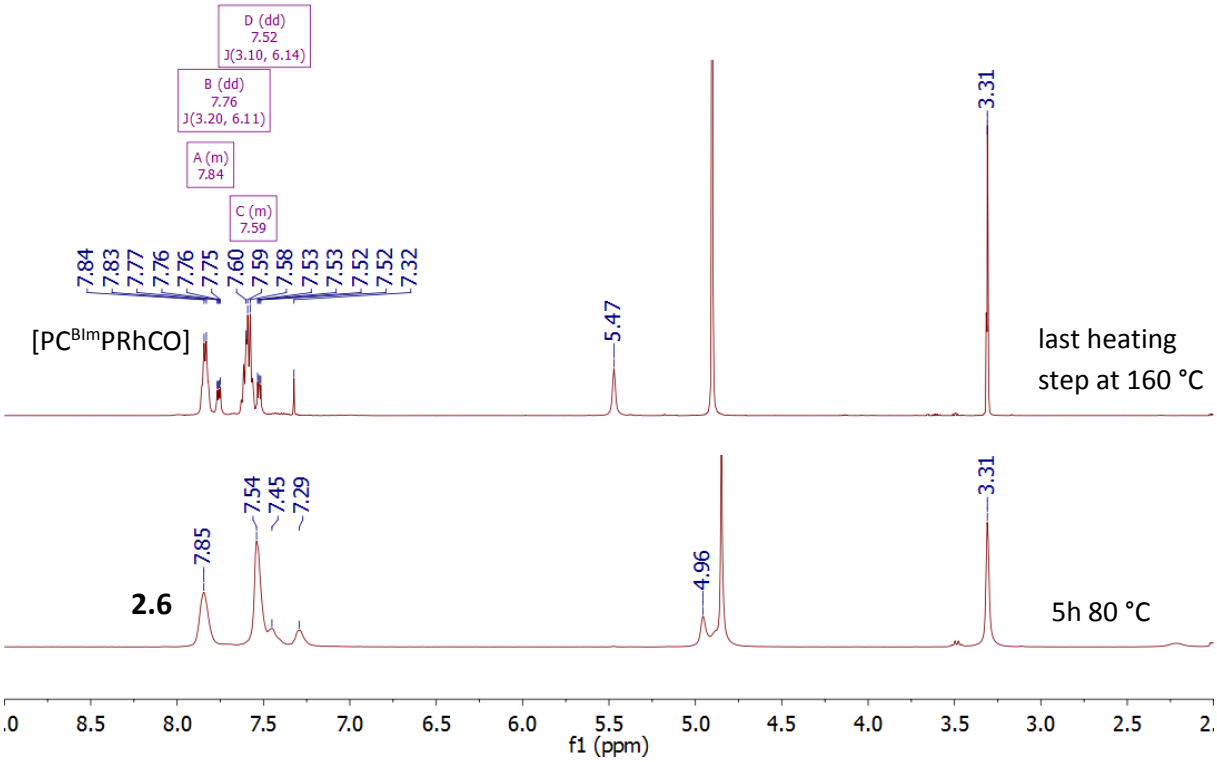

Figure S2.20 Thermal stability of **2.6b** in methanol solution by elevated temperatures under argon atmosphere (^{1}H NMR monitoring)

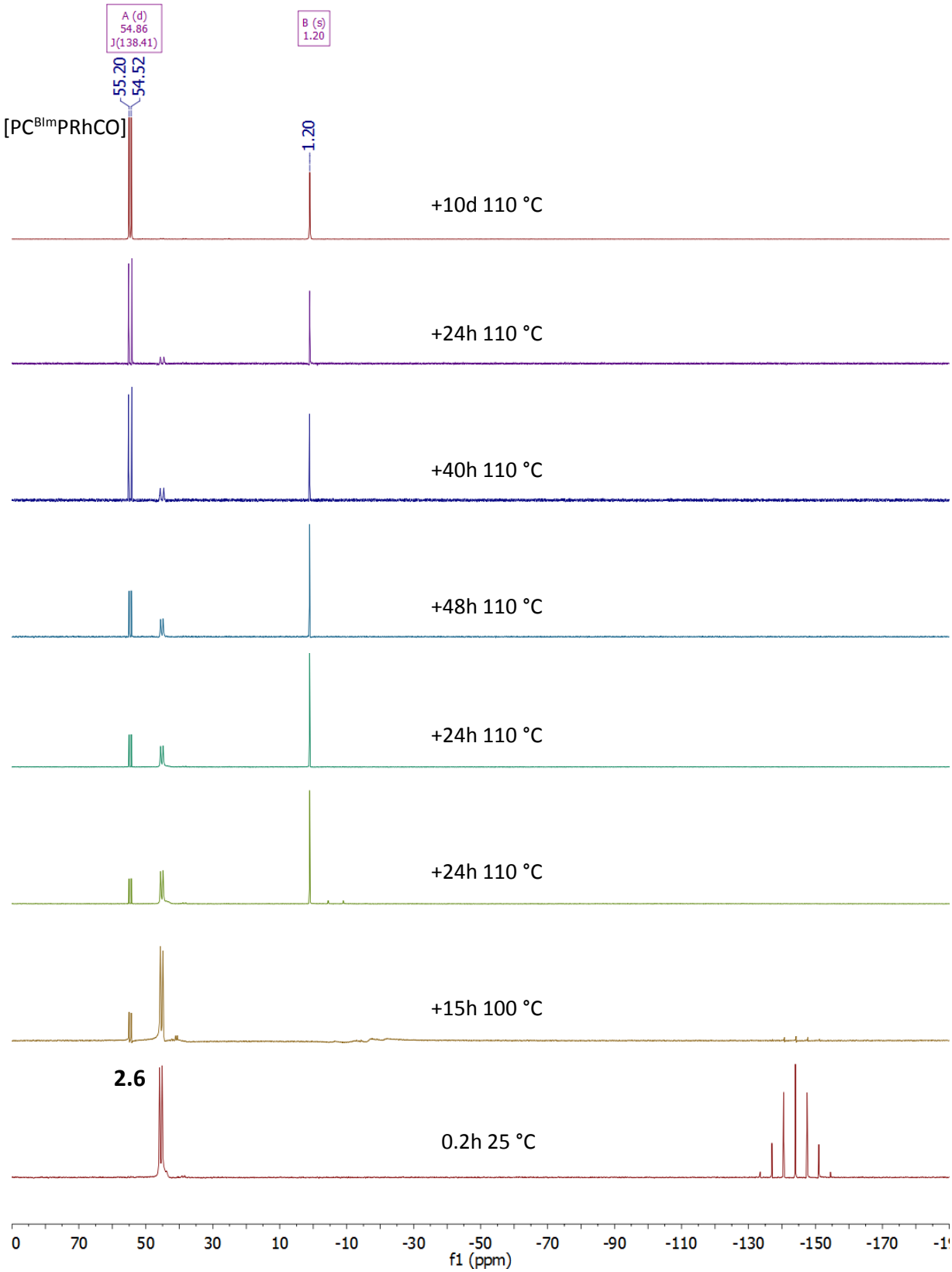

Figure S2.21 Quantitative formation of [(PC^{BIm}P)RhCO] fragment starting from **2.6b** due to the decarbonylation of undecanal in acetone solution at 110 °C under argon atmosphere (^{31}P NMR monitoring)

Bis[1,3-bis(diphenylphosphinomethylene)benzimidazol-2-ylrhodium]-μ-hydride Hexafluoro-phosphate (2.10)

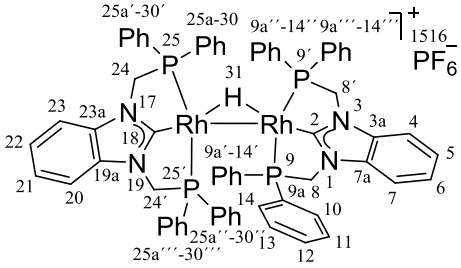

1,3-Bis(diphenylphosphinomethylene)benzimidazol-2-ylrhodium acetonitrile hexafluorophosphate **2.6b** (17.4 mg, 0.02 mmol, 1.00 equiv) was added to a biphasic solution of $KHCO_3$ (62.6 mg, 0.62 mmol, 30.00 equiv) in 0.75 mL degassed water and 3.5 mL degassed THF. The autoclave was pressurized with 10 bar of H_2 and 30 bar of CO_2 and thermostated at 60 °C. After 48 h, all volatiles were removed in vacuo. The product was then redissolved in acetone and filtered via a syringe filter. After the addition of diethyl ether to an acetone solution, filtration, and drying of precipitate, the terra-cotta-colored amorphous compound **2.10** (27.4 mg, 96%) was obtained. Anal. Calcd for $C_{66}H_{57}F_6N_4P_5Rh_2$ (+ 1.00 equiv $C_4H_{10}O$): C, 57.78; H, 4.64; F, 7.83; N, 3.85; O, 1.10; P, 10.64; Rh, 14.15. Found: C, 57.39; H, 5.06; N, 3.49; P, 10.27. Compound **2.10** can also be synthesized by stirring of **2.6b** in a THF suspension containing excess HCOOK within 24 h at 25 °C under an argon atmosphere.

^{1}H-NMR ($(CD_3)_2CO$, 360 MHz, ref: $(CD_3)_2CO$ solvent residual): δ = 7.68 (m, 16H, H-11^{all},-13^{all},-27^{all},-29^{all}), 7.49 (m, 4H, H-4,-7,-20,-23), 7.32 (m, 4H, H-5,-6,-21,-22), 7.24 (vt, J = 7.39 Hz, 8H, H-12^{all},-28^{all}), 7.07 (vt, J = 7.56 Hz, 16H, H-10^{all},-14^{all},-26^{all},-30^{all}), 4.79 (s, 8H, H-8,-8’,-24,-24’), -9.15 (m, 1H, H-31).

^{31}P-NMR ($(CD_3)_2CO$, 146 MHz): δ = 55.90 (d, $J^{P\text{-}Rh}$ = 156.48 Hz, 4P, P-9, P-9’, P-25, P-25’), -144.00 (sept, $J^{P\text{-}F}$ = 706.89 Hz, 1P, P-15).

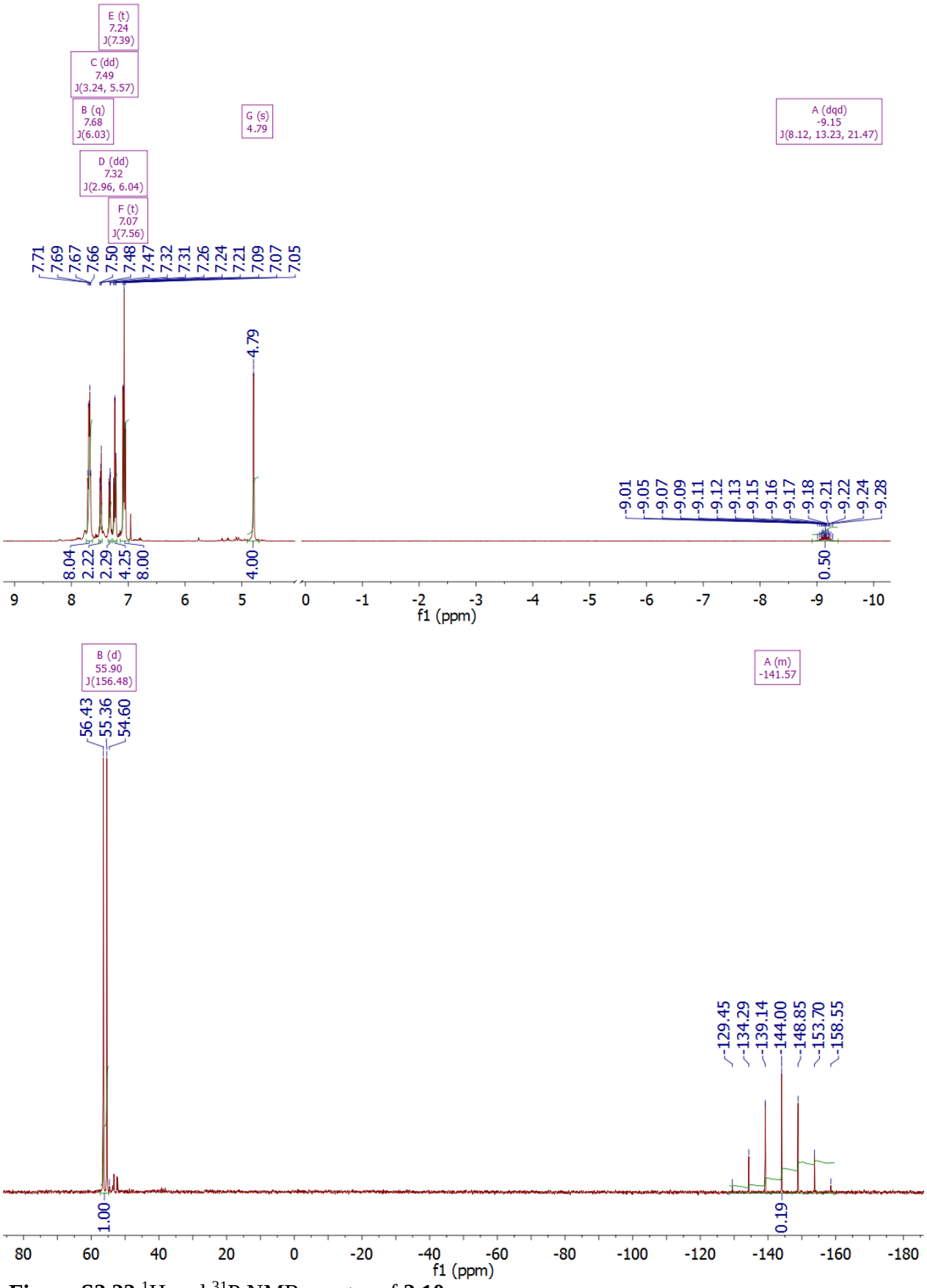

Figure S2.22 ^{1}H and ^{31}P NMR spectra of **2.10**

CO_2 hydrogenation and decarbonylation of acetone-bicarbonate mixture

A solution of $KHCO_3$ (25.3 mg, 0.25 mmol, 100.00 equiv) in 0.5 mL of H_2O and 1.5 mL of organic solvent (THF or acetone) was added to a stainless steel 25 mL high-pressure autoclave containing complex **2.6b** (2.1 mg, 2.50 µmol, 1.00 equiv) and equipped with a magnetic stirring bar. Then the reactor was pressurized with H_2 (10 bar) and CO_2 (10–30 bar) and thermostated at 60 °C. After stirring for 40 h, the vessel was cooled and the excess gases vented. The reaction mixture was analyzed using micro GC–TCD, NMR.

^{1}H-NMR ($(CD_3)_2CO$, 360 MHz, ref: $(CD_3)_2CO$ solvent residual): δ = 8.37 (s, 1H, HCOOK), 4.51 (s, 1H, H_2O).

^{31}P-NMR ($(CD_3)_2CO$, 146 MHz): δ = 55.06 (s, 2P, P-9, P-9'), -144.00 (sept, $J^{P\text{-}F}$ = 706.89 Hz, 1P, P-15).

^{13}C-NMR (D_2O, 126 MHz): δ = 170.95 (s, 1C, HCOOK), 160.45 (s, 1C, $KHCO_3$), 4.51 (s, 1H, H_2O).

IR: no free CO was detected in the gas phase over the reaction mixture.

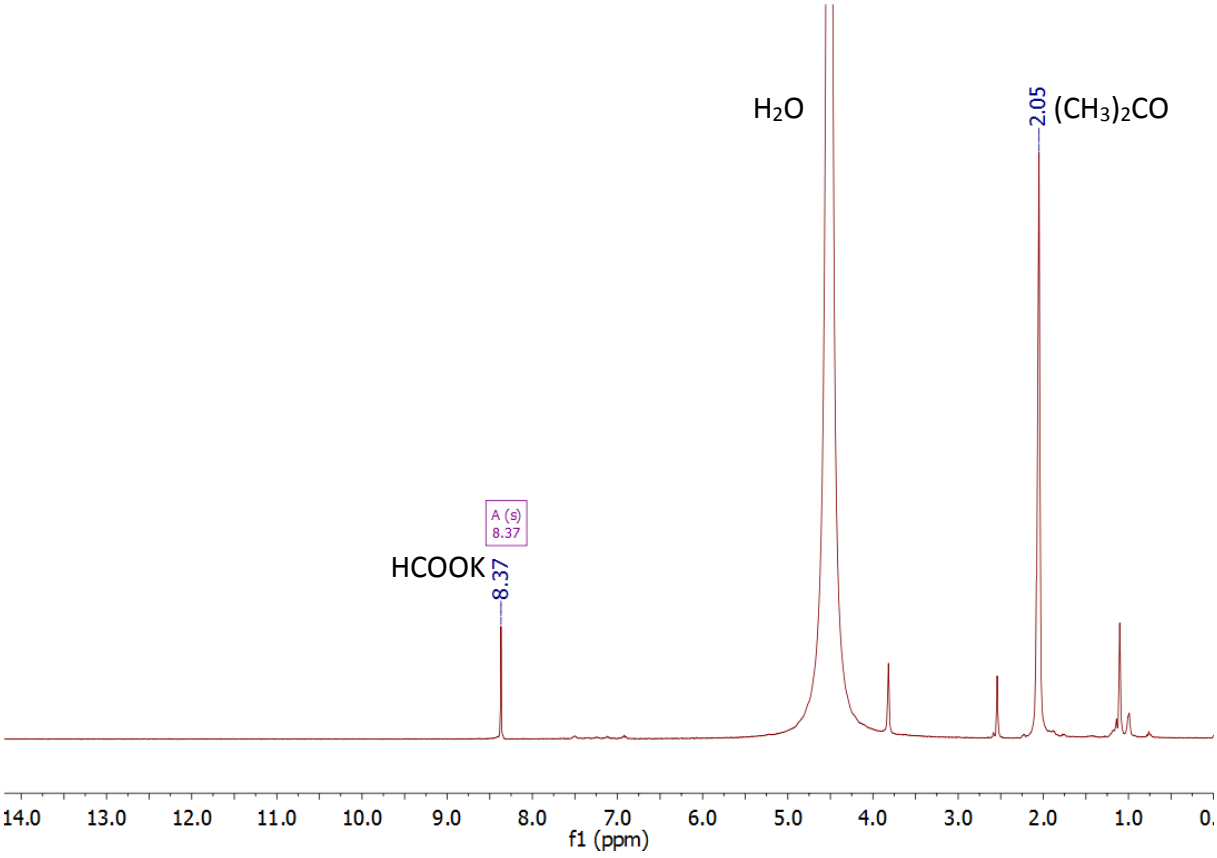

Figure S2.23 ^{1}H NMR spectrum of HCOOK after hydrogenation of CO_2 ($KHCO_3$) in d_6-Aceton/H_2O using **2.6b**

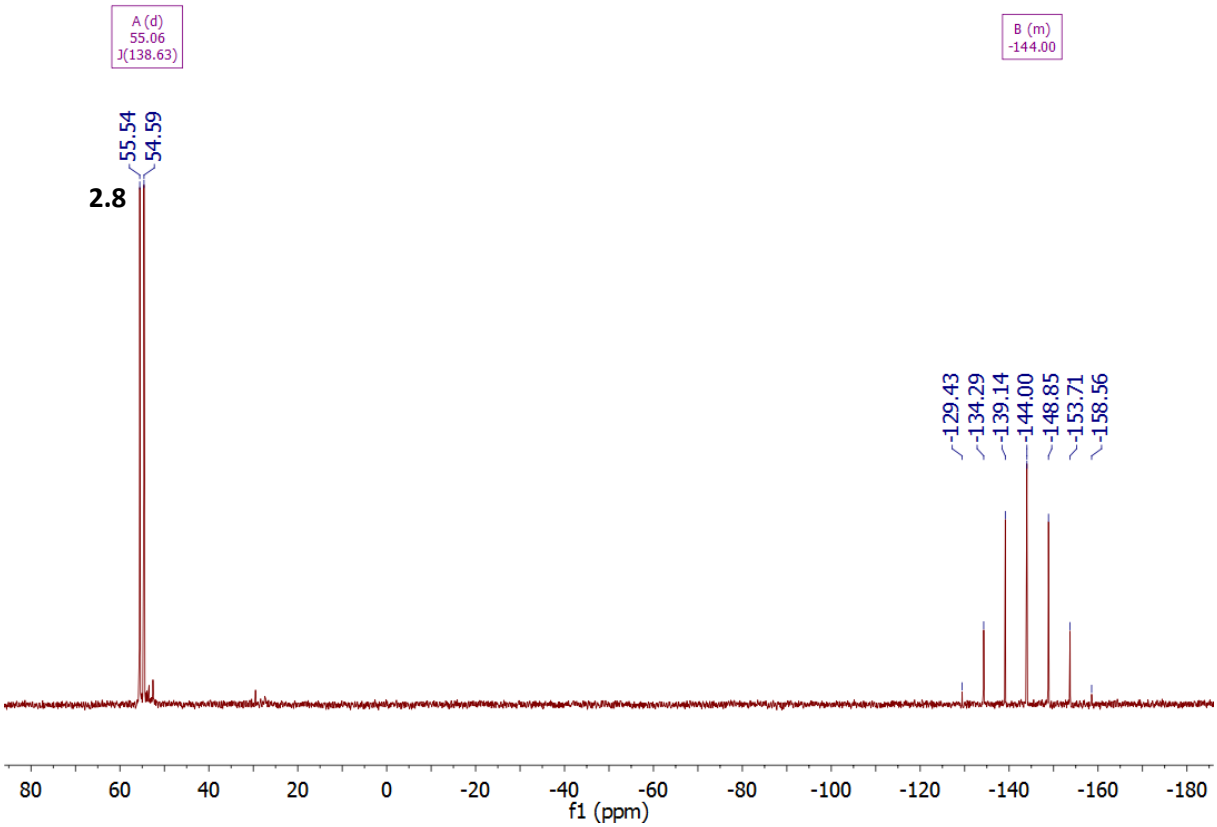

Figure S2.24 ^{31}P NMR spectrum of preconcentrated organometallic compound formed during hydrogenation of CO_2 ($KHCO_3$) in d_6-Aceton/H_2O using **2.6b**

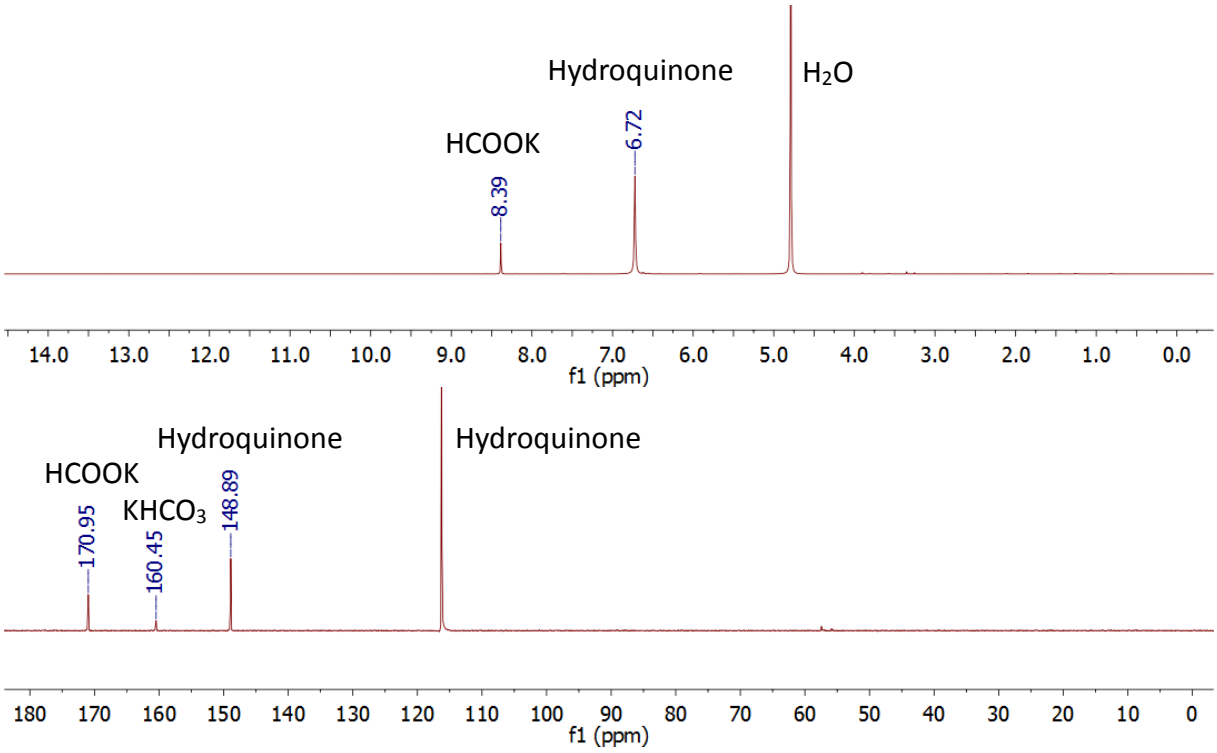

Figure S2.25 ^{1}H and ^{13}C NMR spectra of isolated HCOOK after hydrogenation of CO_2 ($KHCO_3$) in d_6-Aceton/H_2O using **2.6b**

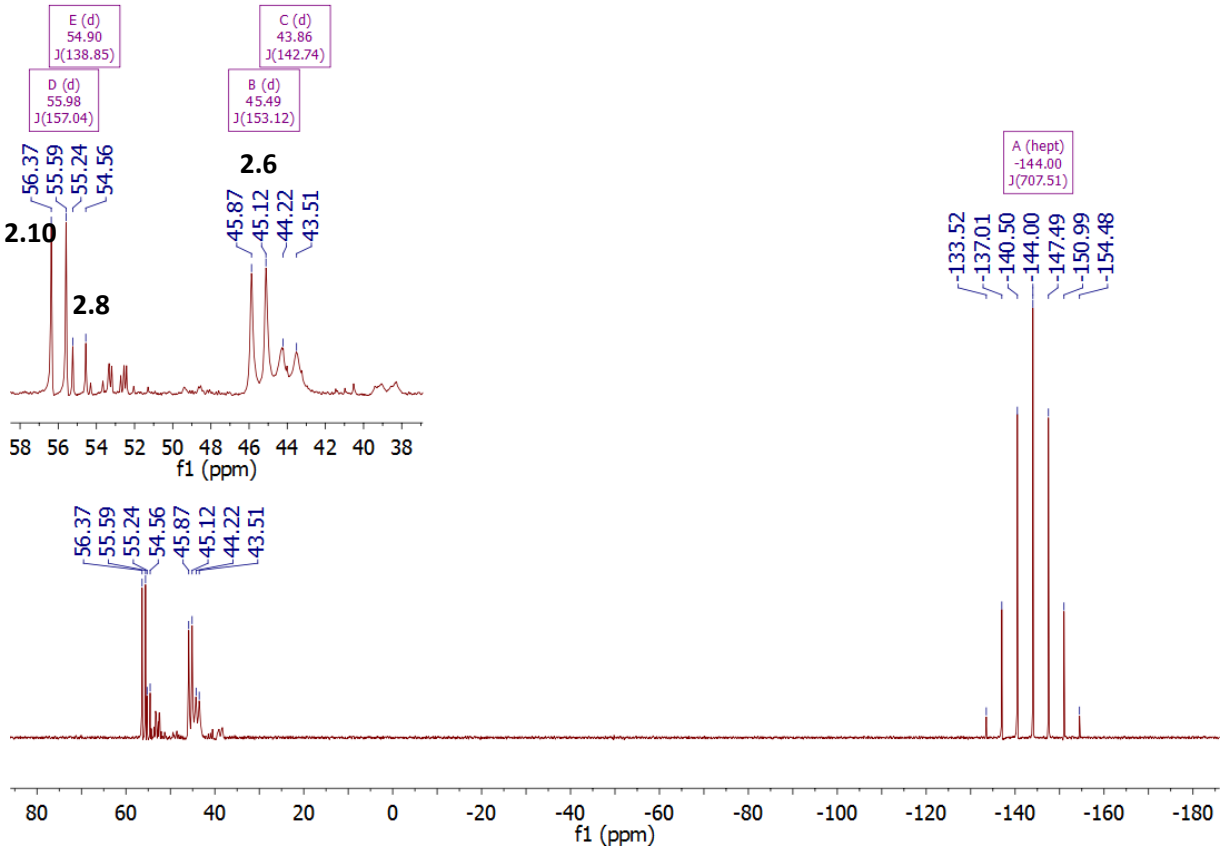

Figure S2.26 ^{31}P NMR spectrum of organometallic compounds formed during hydrogenation of CO_2 in the absence $KHCO_3$ in d_8-THF/H_2O using **2.6b**

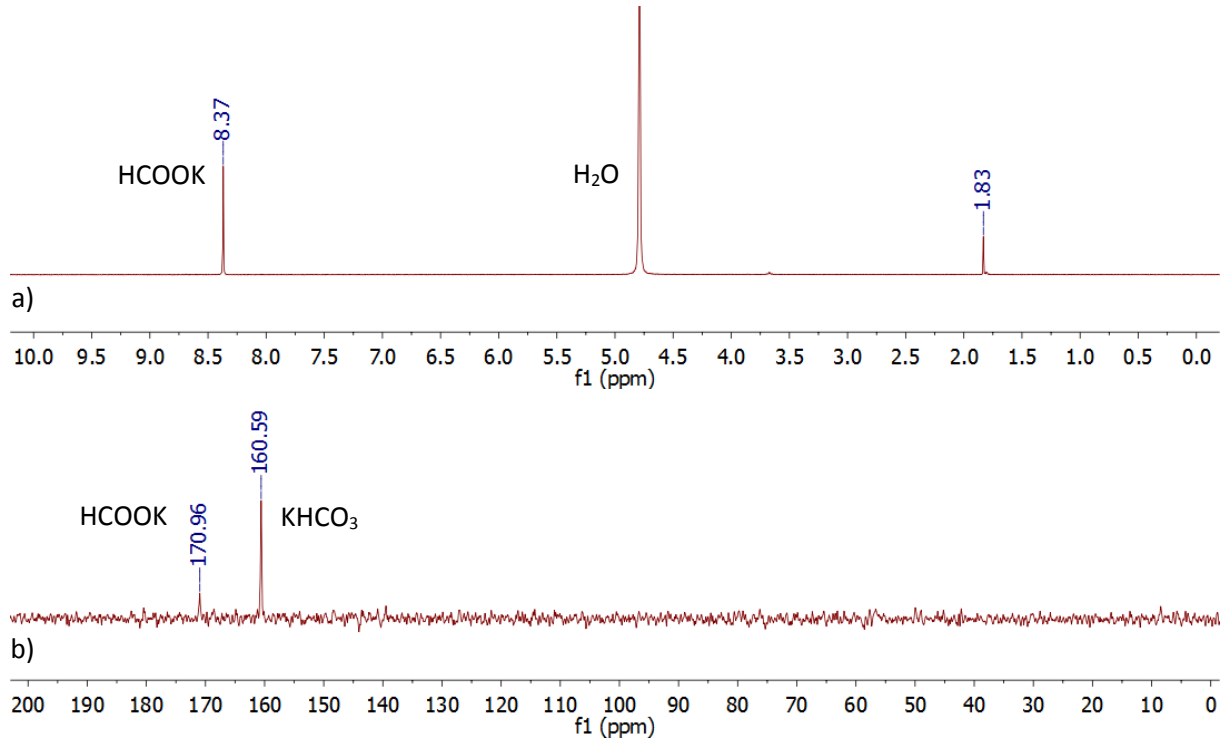

Figure S2.27 Qualitative ^{1}H (a) and ^{13}C NMR (b) analysis of reaction products formed after hydrogenation of CO_2 ($KHCO_3$) using **2.8**

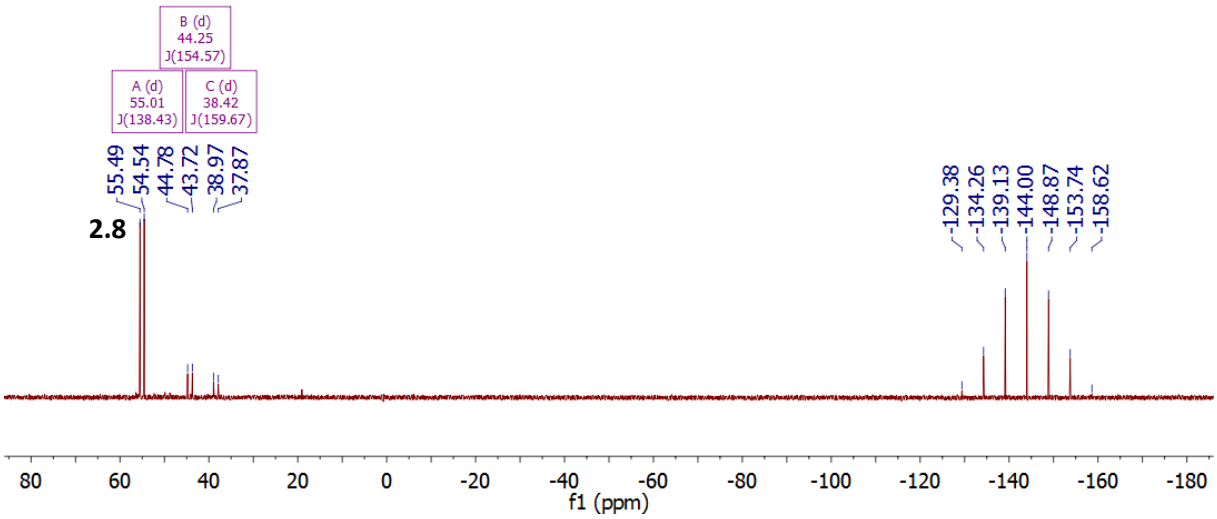

Figure S2.28 ^{31}P NMR spectrum of organometallic products formed after hydrogenation of CO_2 ($KHCO_3$) in d_6-Aceton/H_2O using **2.8**

Reaction of **2.6b** with NaO^tBu:

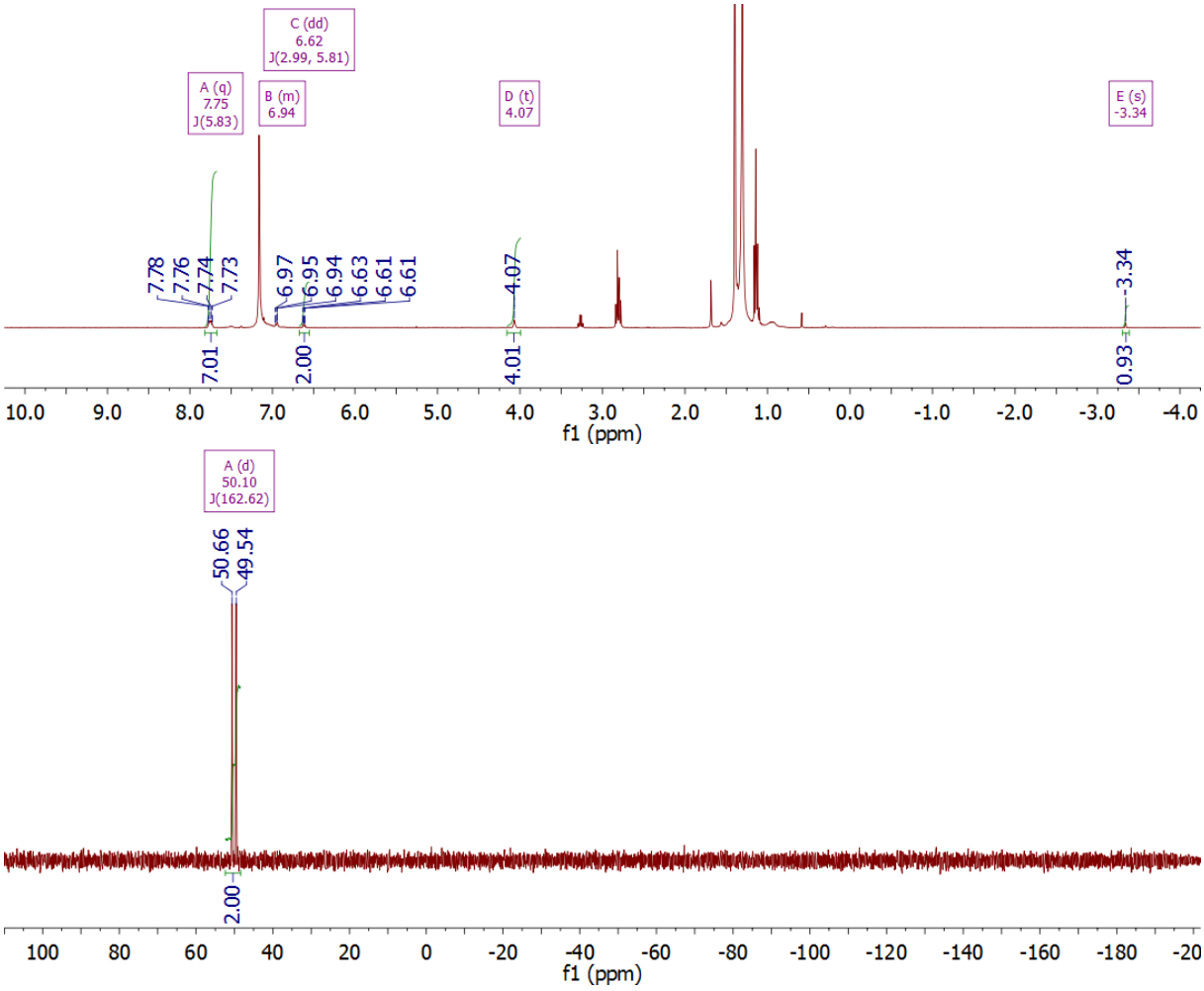

Figure S2.29 ^{1}H and ^{13}C NMR spectra of organometallic product formed after reaction of **2.6b** with NaO^tBu in Toluene

1,3-Bis(diphenylphosphinomethylene)benzimidazol-2-ylrhodium Hydride Derivative (2.11)

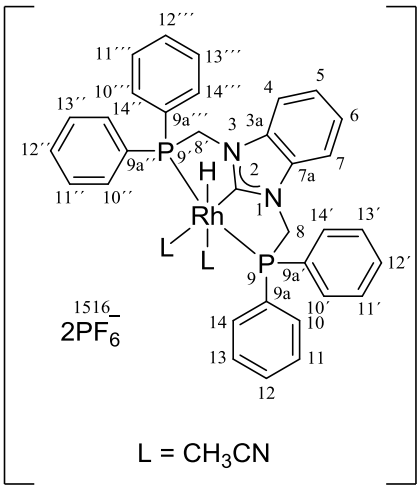

To a suspension of **2.6a** (20.0 mg, 25.0 µmol, 1.00 equiv) in THF (3 mL) was added in one portion $[(C_6H_5)_3C][PF_6]$ (19.0 mg, 50.0 µmol, 2.00 equiv). The reaction mixture was stirred for 15 min at 25 °C. Thereafter all volatiles were removed in vacuo and the formed solid material was redissolved in CD_3CN. The addition of Et_2O to this solution leads to the formation of amorphous compound **2.11**.

^{1}H-NMR: (CD_3CN, 300 MHz, ref: CD_3CN solvent residual): δ = 7.88 (m, 4H, H-12^{all}), 7.68 (m, 22H, H-4,-7,-11^{all},-13^{all},-10^{all},-14^{all},), 7.53 (m, 2H, H-5,-6), 5.62 (vt, J^{H-P} = 3.03 Hz, 1H, H-8), 5.57 (vt, J^{H-P} = 2.96 Hz, 1H, H-8), 5.24 (vt, J^{H-P} = 3.74 Hz, 1H, H-8'), 5.19 (vt, J^{H-P} = 3.75 Hz, 1H, H-8'), -15.22 (dt, J^{H-P} = 9.55 Hz, J^{Rh-P} = 18.36 Hz, 1H, H-2).

^{31}P-NMR: (CD_3CN, 203 MHz): δ = 48.86 (d, J^{P-Rh} = 99.61 Hz, 2P, P-9, P-9'), -144.00 (sept, J^{P-F} = 706.62 Hz, 2P, P-15).

^{19}F-NMR: (CD_3CN, 235 MHz): δ = -72.84 (d, J^{F-P} = 706.69 Hz, F-16^{all}).

ESI MS: *m/z*: 617.4 ($[C_{33}H_{28}N_2P_2Rh]^+$, $[PC^{BIm}PRh]^+$), 633.4 ($[C_{33}H_{28}N_2OP_2Rh]^+$, $[PC^{BIm}PORh]^+$)

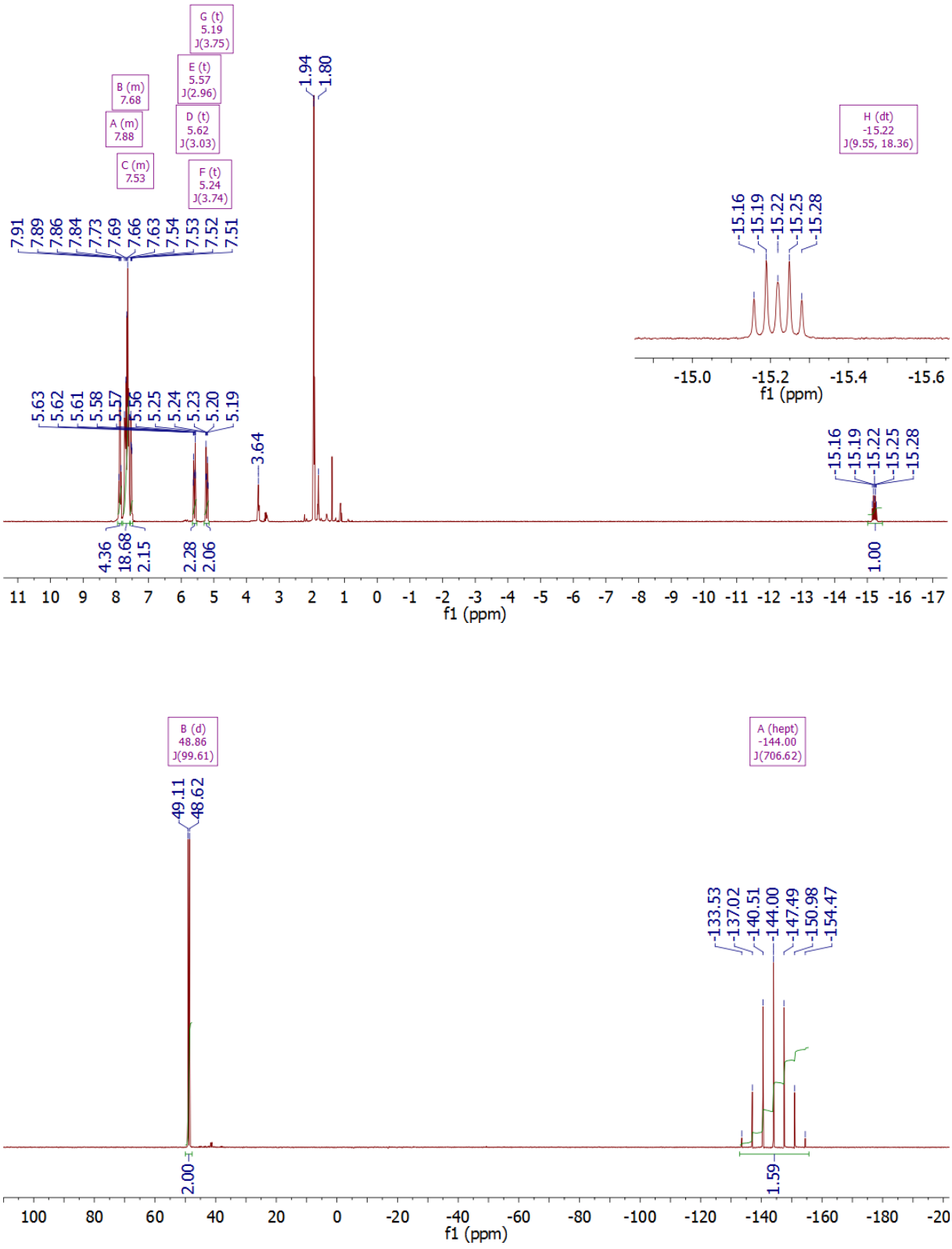

Figure S2.30 ^{1}H and ^{31}P NMR spectra of **2.11**

1,3-Bis(diphenylphosphinomethylene)benzimidazol-2-ylrhodium Tris(Acetonitrile) (Tris)Hexafluorophosphate (2.12)

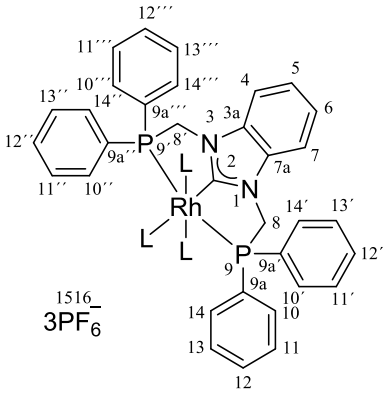

L = CH_3CN

To a suspension of **2.6a** (6.4 mg, 8.0 µmol, 1.00 equiv) in Et_2O (3 mL) was added in one portion $[(C_6H_5)_3C][PF_6]$ (6.2 mg, 16.0 µmol, 2.00 equiv). The reaction mixture was stirred for 2 d at 25 °C. Thereafter all volatiles were removed in vacuo and the formed solid material was redissolved in CD_3CN. The addition of Et_2O to this solution leads to crystallization of compound **2.12** in the form of colorless needles. $C_{39}H_{37}F_{18}N_5P_5Rh$: C, 39.85; H, 3.17; F, 29.09; N, 5.96; P, 13.17; Rh, 8.75. Found: C, 40.35; H, 3.47; N, 5.67.

^{1}H-NMR: (CD_3CN, 500 MHz, ref: CD_3CN solvent residual): δ = 7.98 (m, 2H, H-4,-7), 7.77 (m, 22H, H-11^{all},-13^{all}, H-10^{all},-12^{all},-14^{all}, H-5,-6), 5.89 (vt, $J^{H\text{-}P}$ = 3.38 Hz, 4H, H-8,-8').

^{31}P-NMR: (CD_3CN, 122 MHz): δ = 42.29 (d, $J^{P\text{-}Rh}$ = 74.40 Hz, 2P, P-9, P-9'), -144.00 (sept, $J^{P\text{-}F}$ = 706.55 Hz, 3P, P-15).

ESI MS: *m/z*: 617.4 ($[C_{33}H_{28}N_2P_2Rh]^+$, $[PC^{BIm}PRh]^+$), 633.4 ($[C_{33}H_{28}N_2OP_2Rh]^+$, $[PC^{BIm}PORh]^+$), 649.5 ($[C_{33}H_{28}N_2O_2P_2Rh]^+$, $[OPC^{BIm}PORh]^+$).

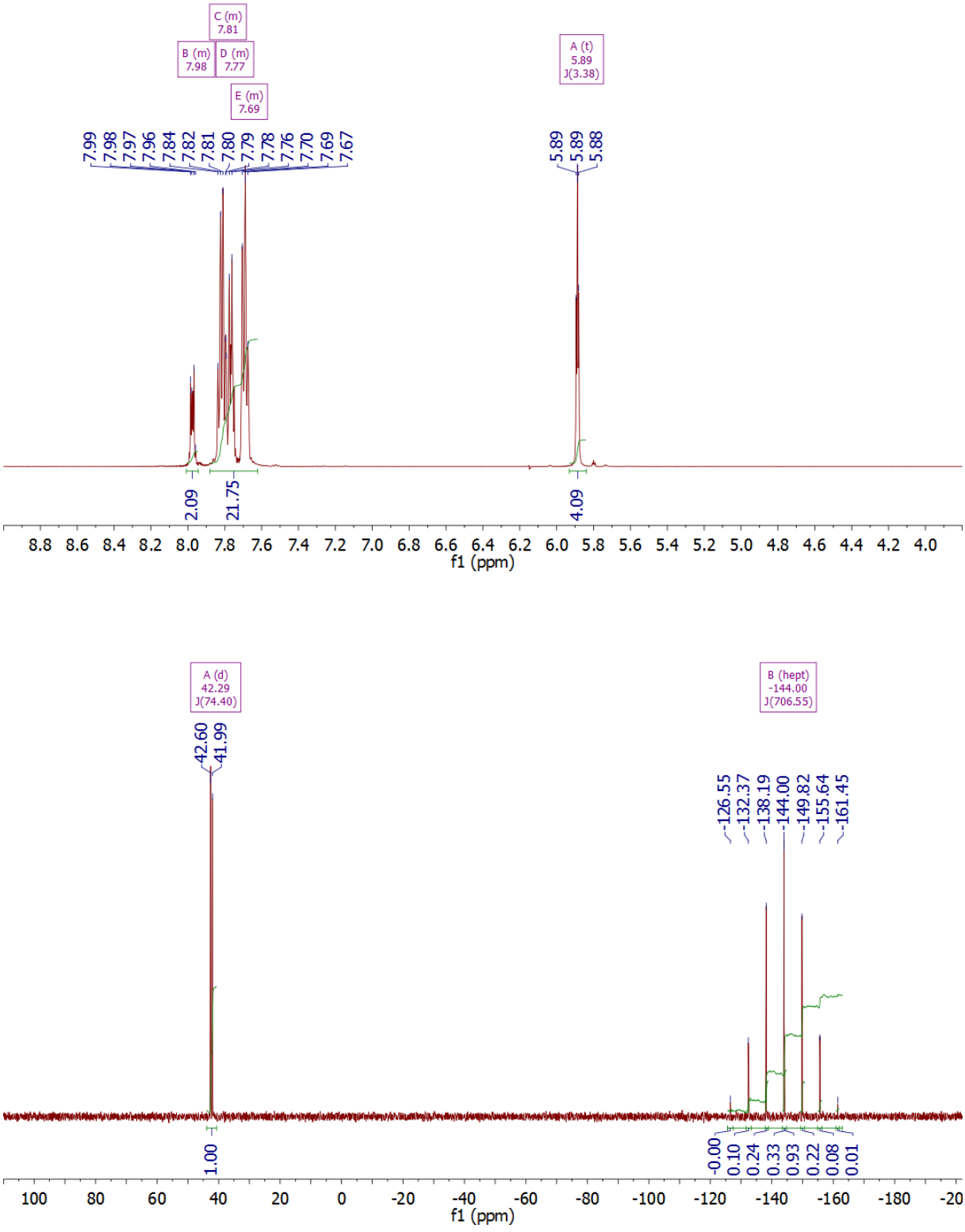

Figure S2.31 ^{1}H and ^{31}P NMR spectra of **2.12**

Hydroboration procedure for 2-[(*E*)-2-phenylethenyl]-4,4,5,5-tetramethyl-1,3,2-dioxaborolane

In a glovebox, phenylacetylene (7.8 µL, 0.07 mmol, 1.00 equiv) and pinacolborane (12.6 µL, 0.08 mmol, 1.20 equiv) were dissolved in 0.45 mL of degassed d_8-THF in a NMR tube. After the addition of 6b (1.1 mg, 1.40 µmol, 0.02 equiv) to the prepared solution, the NMR tube was shaken and placed in a NMR spectrometer. Subsequently, the reaction mixture was analyzed by GC-MS. The reaction was reproduced at least three times.

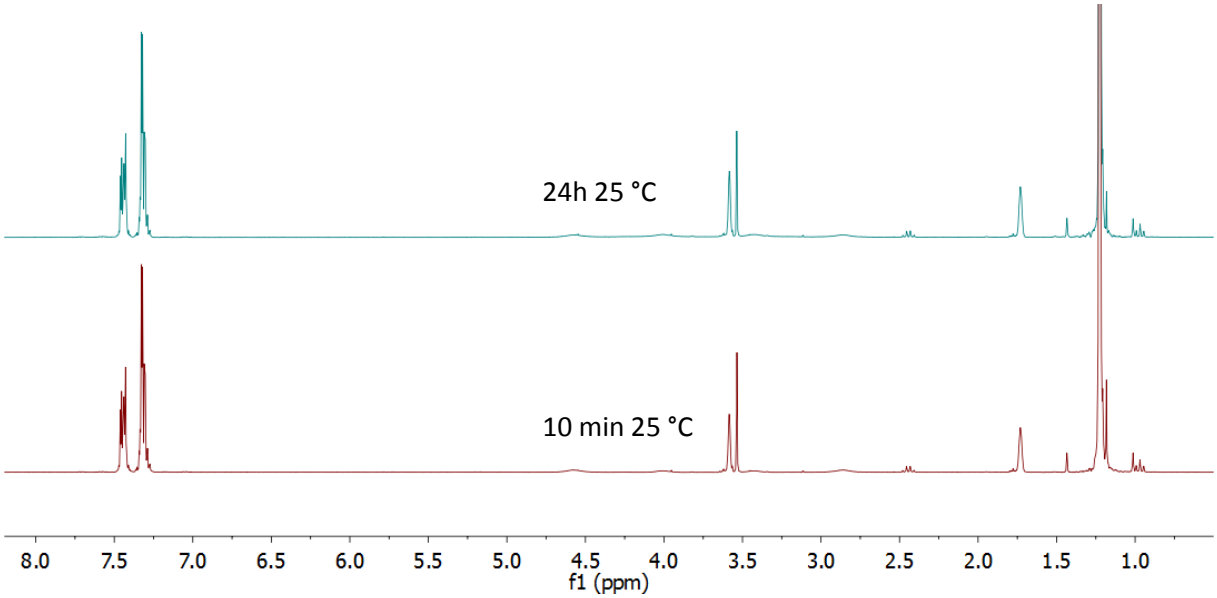

Figure S2.32 ^{1}H NMR measurements show zero reactivity between phenylacetylene and pinacolborane in d_8-THF in the absence of the catalyst

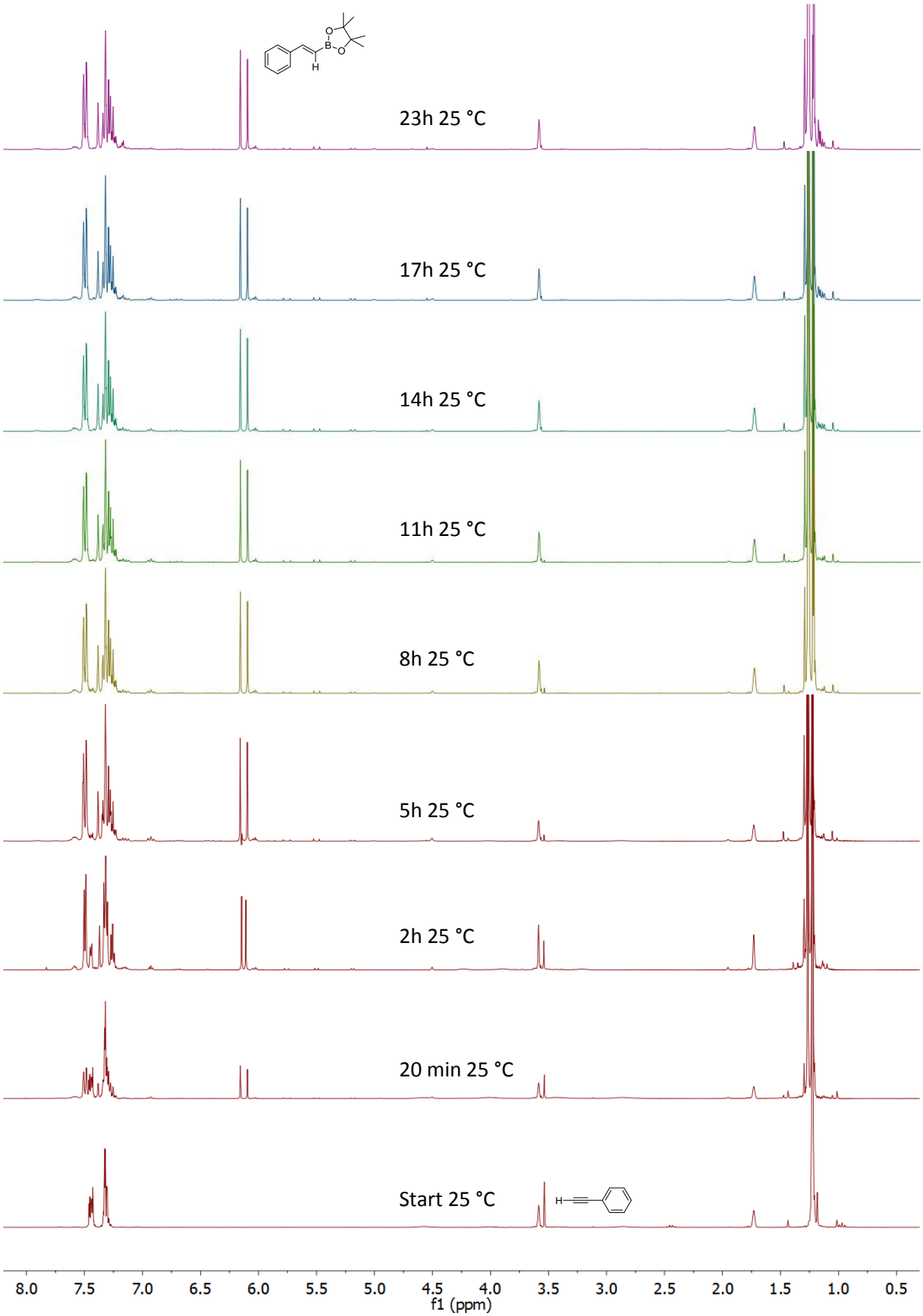

Figure S2.33 Reaction of phenylacetylene and pinacolborane catalyzed by **2.6b** in d_8-THF (^{1}H NMR monitoring)

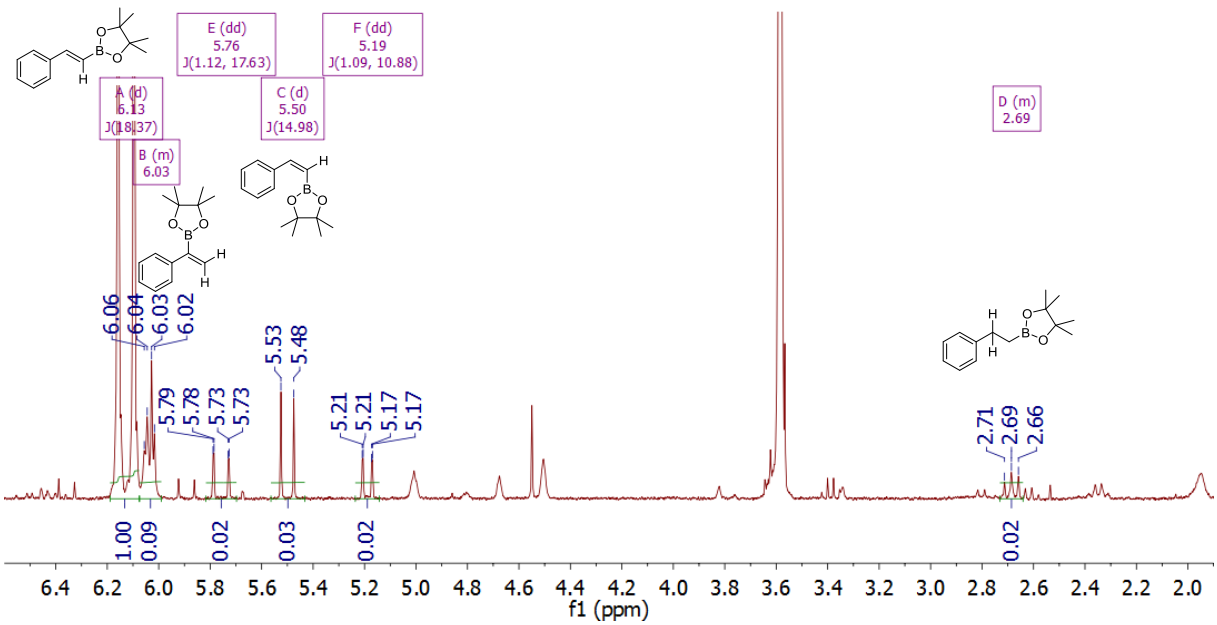

Figure S2.34 Selected characteristic proton signals of *β*-*E*-vinylboronate, δ = 6.13 ppm (d, *J* = 18.4 Hz, 1H), *β*-*Z*-vinylboronate, δ = 5.50 ppm (d, *J* = 14.9 Hz, 1H), *α*-vinylboronate, δ = 6.05 ppm (d, *J* = 3.3 Hz, 1H), δ = 6.02 ppm (d, *J* = 3.3 Hz, 1H), hydrogenated *β*-alkylboronate, δ = 2.69 ppm (m, 2H) in d_8-THF (^{1}H NMR spectrum was recorded after 24 h)

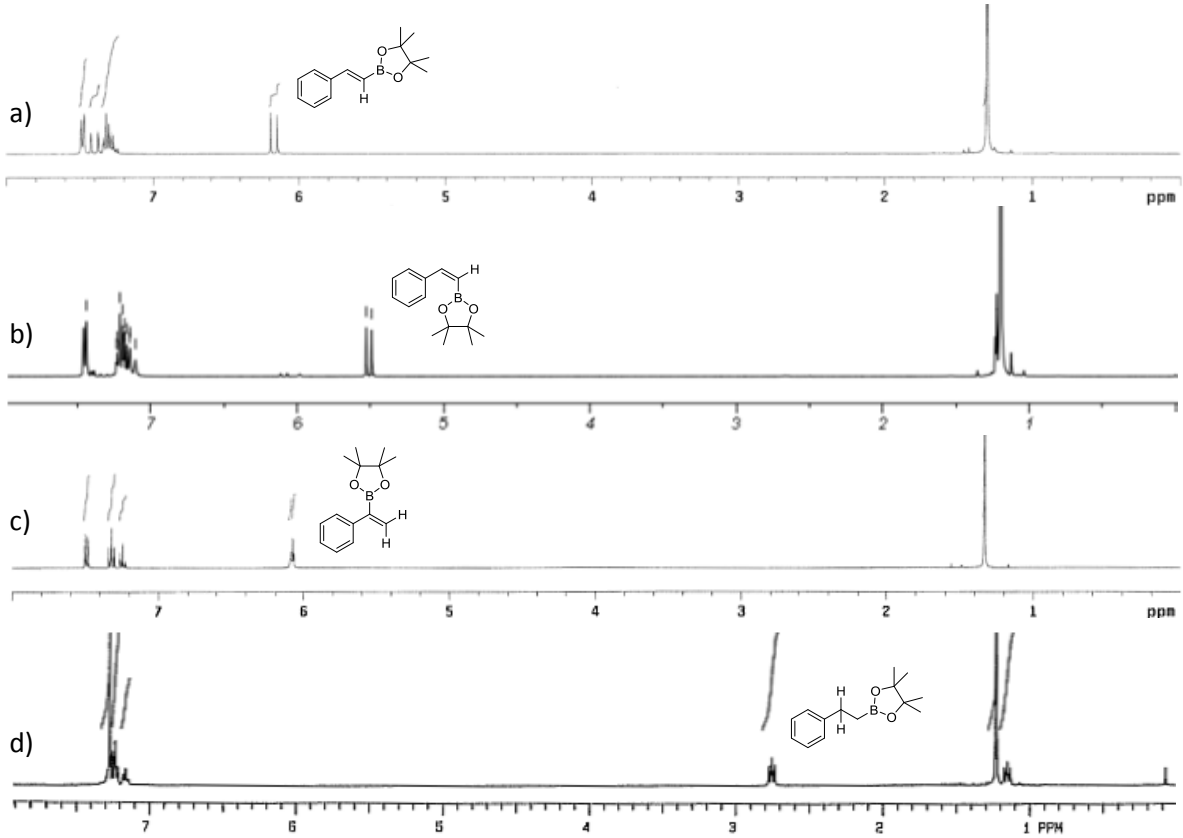

Figure S2.35 Selected characteristic proton signals in reference spectra of *β*-*E*-vinylboronate,[293, 294] δ ($CDCl_3$) = 6.17 ppm (d, *J* = 18.4 Hz, 1H) (a), *β*-*Z*-vinylboronate,[47] δ (CD_2Cl_2) = 5.51 ppm (d, *J* = 14.9 Hz, 1H) (b), *α*-vinylboronate,[294] δ ($CDCl_3$) = 6.09 ppm (d,

J = 2.8 Hz, 1H), 6.07 ppm (d, J = 2.8 Hz, 1H) (c), hydrogenated β-alkylboronate,[295] δ ($CDCl_3$) = 2.76 ppm (t, J = 8.2 Hz, 2H) (d)

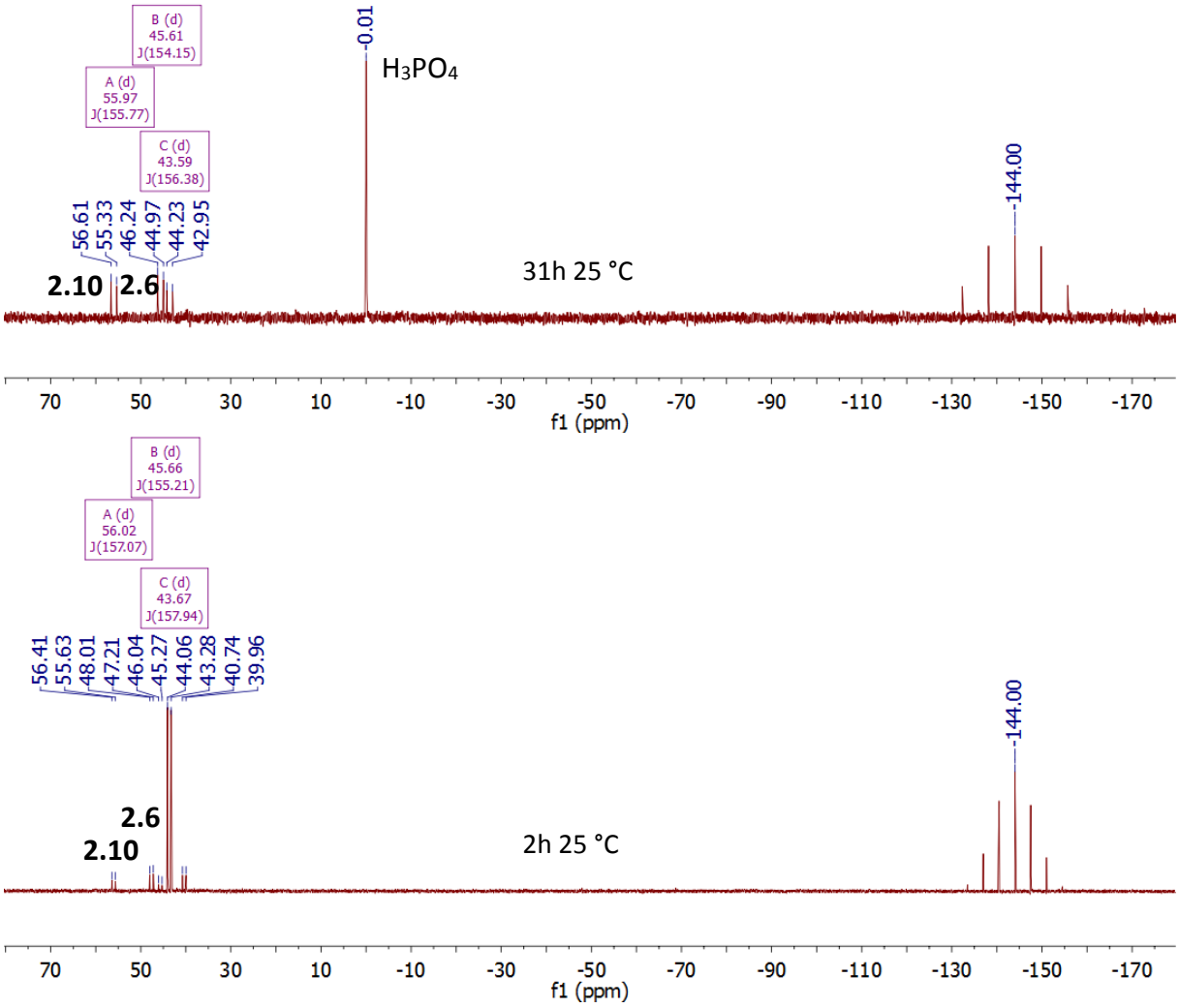

Figure S2.36 Reaction of phenylacetylene and pinacolborane catalyzed by **2.6b** in d_8-THF. ^{31}P NMR spectra were recorded after 2 and 31 h

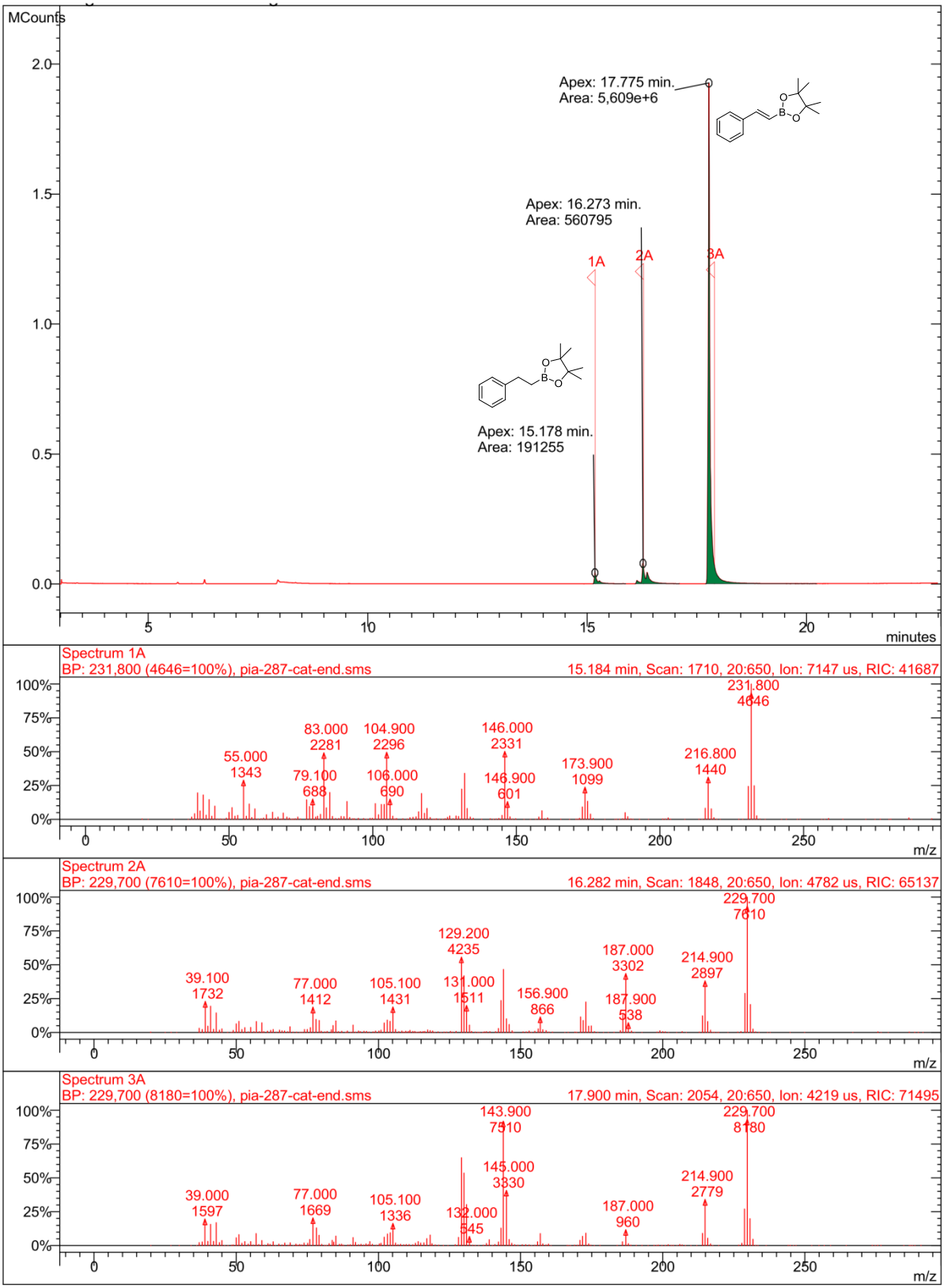

Figure S2.37 GC–MS analysis of the reaction of phenylacetylene and pinacolborane catalyzed by **2.6b** in d_8-THF (measured after 24 h)

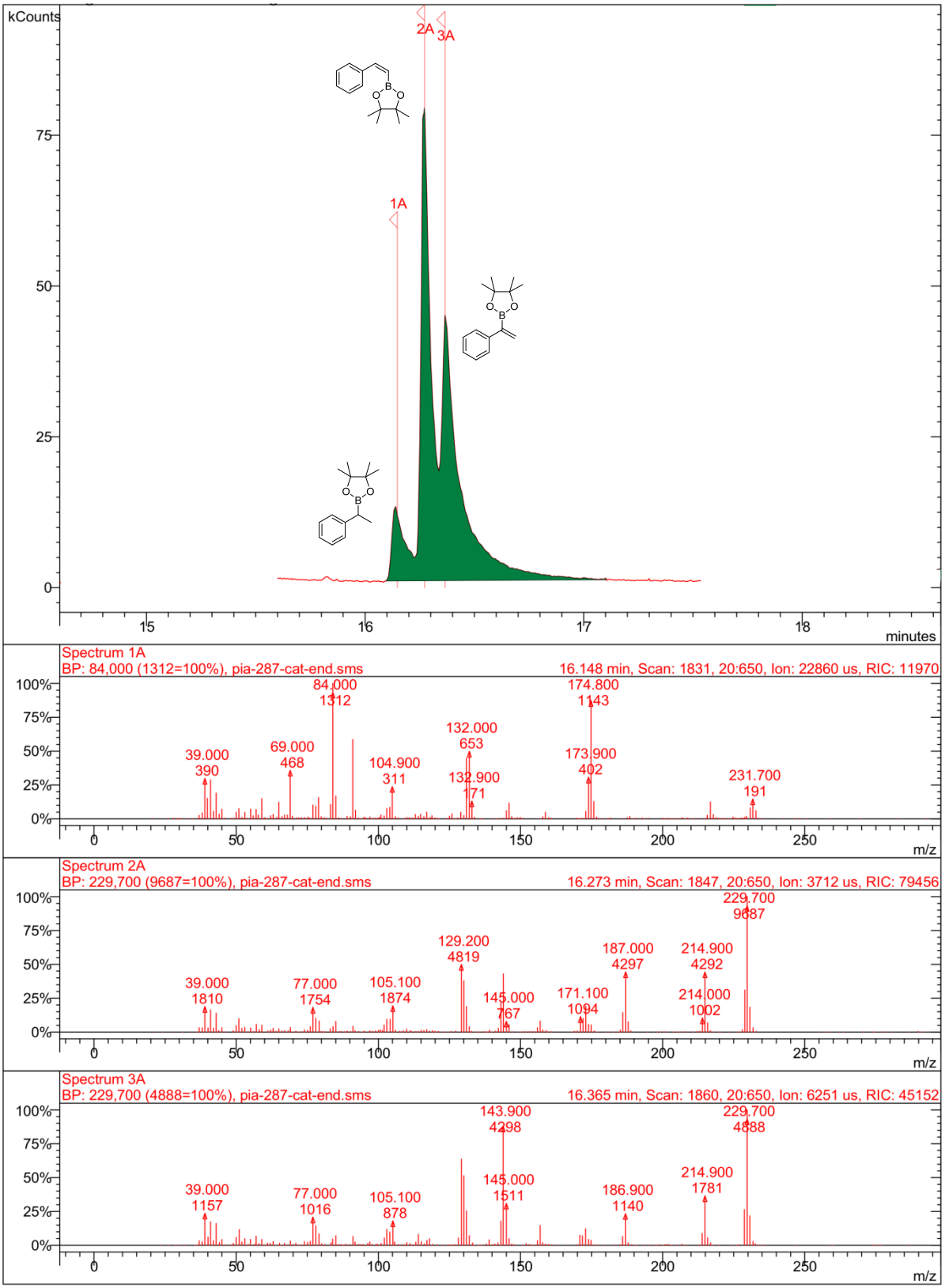

Figure S2.38 GC–MS analysis of the reaction of phenylacetylene and pinacolborane catalyzed by **2.6b** in d_8-THF (measured after 24 h)

3 The Asymmetric Functionalized Carbene-Centered Complexes

Synthesis of organic compounds

1-(6-methoxypyridin-2-yl)benzimidazole (3.1)

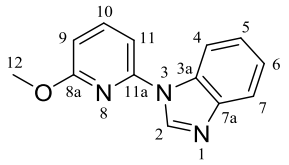

The compound was prepared according to previously published synthetic procedure for pyridine derivatives[296]. Purification method was optimized using a Kugelrohr short-path distillation apparatus.

In a 50 mL Schlenk round-bottom flask, benzimidazole (3.64 g, 30.20 mmol, 1.00 eq, 98%), 2-bromo-6-methoxypyridine (6.73 g, 34.73 mmol, 1.15 eq, 97%), *L*-proline (0.70 g, 6.04 mmol, 0.20 eq, 99%), copper(I) iodide (0.58 g, 3.02 mmol, 0.10 eq, 99%) and potassium carbonate (8.43 g, 60.40 mmol, 2.00 eq, 99%) were suspended in 30 mL dry DMSO under argon. The reaction mixture was then stirred for four days at 130 °C. After the reaction was complete water was added to the suspension. The mixture containing raw product was filtered through Celite® and extracted with a $CH_3COOC_2H_5/NaHCO_{3aq}$ mixture (1/1; 3 x 50 mL). Finally, the colourless compound **3.1** (5.85 g, 86%) was obtained through distillation of the organic phase using a Kugelrohr short-path distillation apparatus at 146 °C ($p = 4.8 \cdot 10^{-2}$ mbar). Anal. calcd. for $C_{13}H_{11}N_3O$: C, 69.32; H, 4.92; N, 18.66; O, 7.10. Found: C, 69.24; H, 4.83; N, 18.60.

^{1}H NMR ($CDCl_3$, 300 MHz): δ = 8.57 (s, 1H, H-2), 8.07 (m, 1H, H-4), 7.87 (m, 1H, H-7), 7.75 (t, J = 7.6 Hz, 1H, H-10), 7.36 (m, 2H, H-5, H-6), 7.11 (d, J = 7,6 Hz, 1H, H-9), 6.73 (d, J = 8.2 Hz, 1H, H-11), 4.03 (s, 3H, H-12).

ESI MS *m/z*: 226.3 $[CH_3O(C_5H_3N)(CHN_2C_6H_4)+H]^+$.

GC-MS: 19.8 min., *m/z*: 225.3 $[CH_3O(C_5H_3N)(CHN_2C_6H_4)]$.

1-(halogenomethylen)-3-(6-methoxypyridin-2-yl)benzimidazolium halogenides

Scheme S3.1. Screening of reaction conditions: alkylation of compound **3.1** using various halogenated methylene synthons.

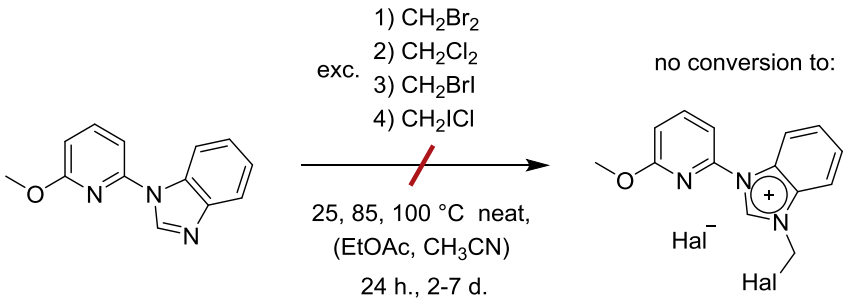

1-((diphenylphopshoryl)methylene)-3-(6-methoxypyridin-2-yl)benzimidazole 4-methylbenzyl-sulfonate (3.2)

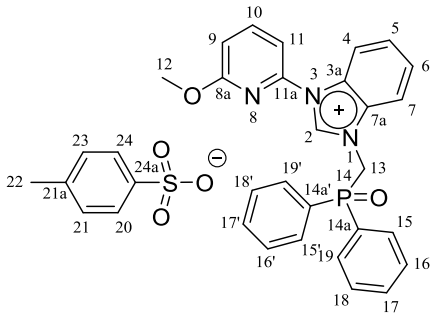

1-(6-methoxypyridin-2-yl)benzimidazole (**3.1**) (4.70 g, 19.41 mmol, 1.00 eq) and 1-(diphenylphosphoryl)methylene-4-methylbenzenesulfonate (11.36 g, 29.11 mmol, 1.50 eq) were placed in a Schlenk-tube, heated up to 127 °C and stirred at this temperature in melt within 3 days. The reaction mixture was then dissolved in dichloromethane. After the solvent was removed under reduced pressure the product was extracted with warm water/toluene mixture. The separated water phase was washed several times with toluene and reduced *in vacuo*. Subsequent filtration of formed precipitate gives 11.47 g (97 %) of colourless amorphous compound **3.2**. Anal. calcd. for $C_{33}H_{30}N_3O_5PS{\cdot}H2O$: C, 62.95; H, 5.12; N, 6.67; O, 15.25; P, 4.92; S, 5.09. Found: C, 62.75; H, 4.95; N, 6.58; P, 4.97; S, 4.7.

^{1}H NMR ($CDCl_3$, 360 MHz): δ = 10.78 (s, 1H, H-2), 8.35 (d, *J* = 7,8 Hz, 1H, H-4), 8.27 (d, *J* = 8,5 Hz, 1H, H-7), 8.11 (m, 4H, H-15,-19,-15‘,-19‘), 7.82 (m, 3H, H-10,-20,-24), 7.67 (m, 2H, H-5,-6), 7.52 (m, 7H, H-9,-16,-17,-18, -16‘,-17‘,-18‘), 7.14 (d, *J* = 8,0 Hz, 2H, H-21,-23), 6.89 (d, *J* = 8,3 Hz, 1H, H-11), 6.03 (d, J^{H-P} = 5,6 Hz, 2H, H-13), 3.99 (s, 3H, H-12), 2.34 (s, 3H, H-22).

^{31}P NMR ($CDCl_3$**,** 146 MHz,): δ = 26.54 (s, 1P, P-14).

ESI MS *m/z*:

439.9 $[CH_3O(C_5H_3N)(CHN_2C_6H_4)CH_2P(O)(C_6H_5)_2]^+$,

461.8 $[CH_3O(C_5H_3N)(CN_2C_6H_4)CH_2P(O)(C_6H_5)_2+Na]^+$.

1-((diphenylphosphino)methylene)-3-(6-methoxypyridin-2-yl)-2-dyhydrobenzimidazole (3.3a)

Scheme S3.2. Hydrogenation of the benzimidazolium molecule fragment of compound **3.2** by $HSiCl_3$.

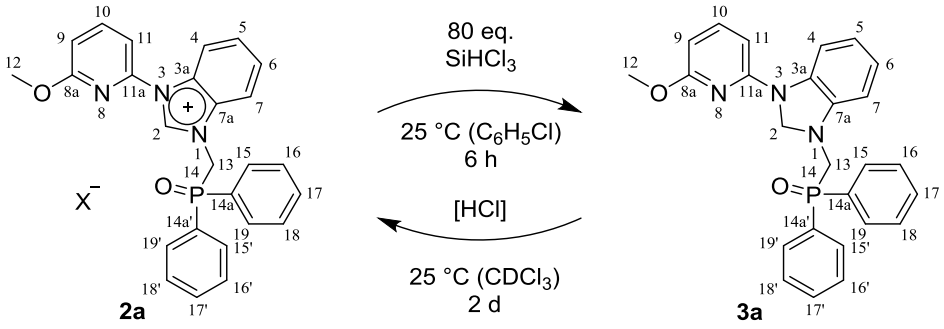

Compound **3.2** (33.0 mg, 0.05 mmol, 1.0 eq) was suspended in 0.4 mL chlorobenzene in a Young-NMR tube. $HSiCl_3$ (542.0 mg, 406.0 µL, 4.00 mmol, 80.00 eq) was added under an argon counter flow. The reaction mixture was then thermostated at 25 °C. After 6 h, all volatiles were removed *in vacuo* and 0.45 mL deuterated chloroform added to the NMR-tube. The ^{1}H and ^{31}P spectra recorded after reaction completion (6 h) represents formation of **3.3a**, as a result of hydrogenation of benzimidazolium fragment by $HSiCl_3$. The spectra of the same probe recorded after 2 d show the hydride abstraction from benzimidazoline derivative leading to organic cation **3.2a**.

3.2a: ^{1}H NMR ($CDCl_3$, 360 MHz): δ = 11.56 (s, 1H, H-2), 8.33 (d, *J* = 8,3 Hz, 1H, H-4), 8.30 (d, *J* = 8,3 Hz, 1H, H-7), 8.18 (m, 4H, H-15,-19,-15‘,-19‘), 7.84 (t, *J* = 7.9 Hz, 1H, H-10), 7.70 (m, 1H, H-6), 7.66 (m, 1H, H-5), 7.53 (m, 7H, H-9,-16,-17,-18, -16‘,-17‘,-18‘), 7.39 (d, *J* = 7,5 Hz, 1H, H-9), 6.91 (d, *J* = 8,3 Hz, 1H, H-11), 6.14 (d, J^{H-P} = 5,7 Hz, 2H, H-13), 4.01 (s, 3H, H-12)

3.3a: ^{1}H NMR ($CDCl_3$, 360 MHz): δ = 7.92 (m, 1H, H-4), 7.86 (m, 4H, H-15,-19,-15‘,-19‘), 7.51 (m, 7H, H-10,-16,-17,-18,-16‘,-17‘,-18‘), 6.74 (m, 2H, H-5,-6), 6.40 (m, 1H, H-7), 6.26 (d, *J* = 8.0 Hz, 1H, H-9), 6.09 (d, *J* = 7.9 Hz, 1H, H-11), 5.21 (s, 2H, H-2), 4.04 (d, *J* = 5.7 Hz, 2H, H-13), 3.95 (s, 3H, H-12)

3.2a: ^{31}**P NMR** ($CDCl_3$**,** 146 MHz,): δ = 26.54 (s, 1P, P-14)

3.3a: ^{31}**P NMR** ($CDCl_3$, 146 MHz) δ = 28.00 (1P, P-14)

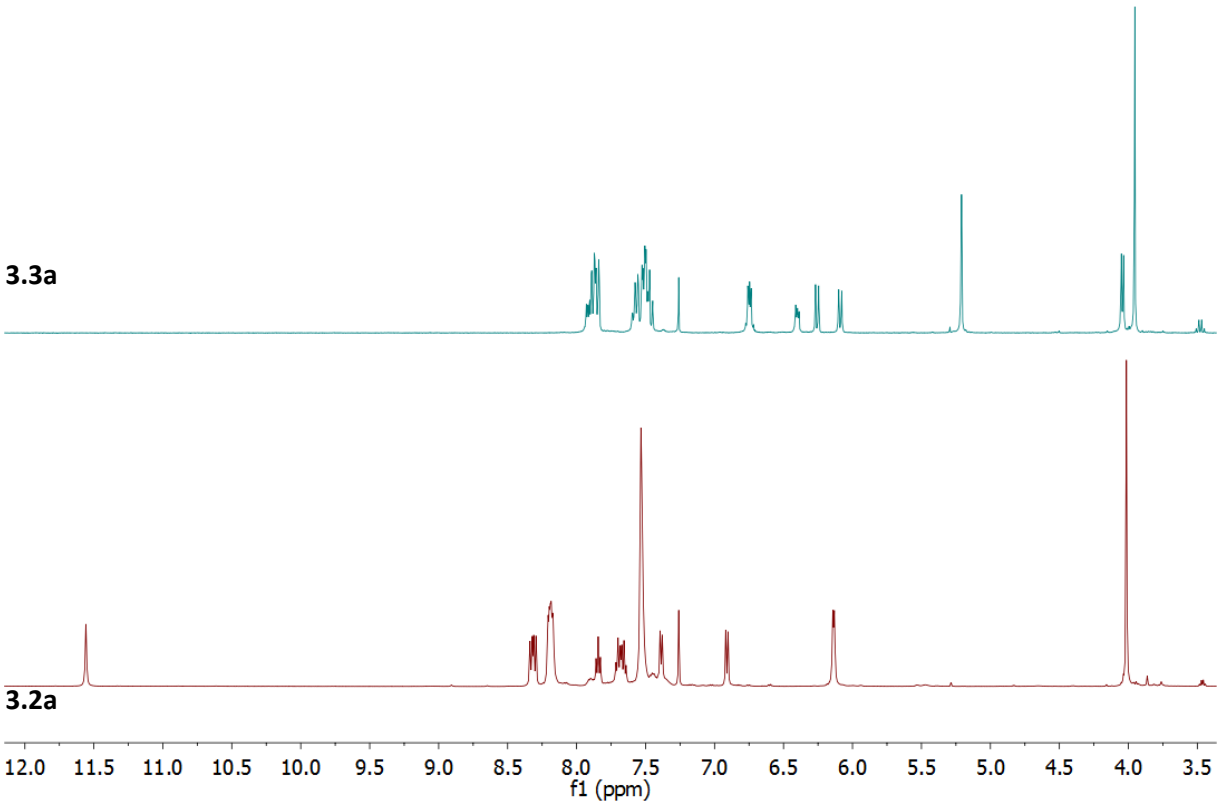

Figure S3.1 Reversible hydrogenation of benzimidazolium molecule fragment **3.2** by $HSiCl_3$ (^{1}H NMR monitoring)

1-((diphenylphopshino)methylene)-3-(6-methoxypyridin-2-yl)benzimidazoline (3.3)

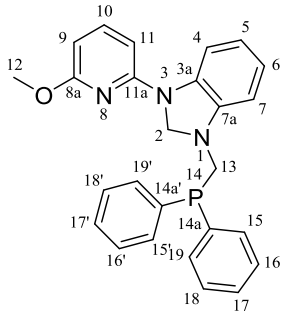

To a suspension of compound **3.2** (2.61 g, 4.06 mmol, 1.00 eq, 95%) in chlorobenzene (40 mL) were added polymethylhydrosiloxane (9.59 g, 24.30 mmol, 6.00 eq, M_n = 390 g/mol, 99%) and titanium(IV) isopropoxide (4.28 g, 4.46 mL, 14.60 mmol, 0.60 eq, 97%) under an argon counter flow. The reaction mixture was stirred for 2 h at 70 °C. After the conversion was completed (^{31}P-NMR monitoring is necessary), the mixture was cooled down to 25 °C and all volatiles were removed *in vacuo*. Pentane was added to the residual, the suspension was stirred over 3 h and filtered *via cannula*. Additionally, the crude product was washed three times with small amount of degassed pentane, dissolved in Et_2O, filtered and precipitated from concentrated Et_2O solution at –40 °C. Finally, the colourless amorphous solid **3.3** (1.61 g, 93%) was isolated. Anal. calcd. for $C_{26}H_{24}N_3OP$: C, 73.40; H, 5.69; N, 9.88; O, 3.76; P, 7.28. Found: C, 72.96; H, 5.69; N, 9.70; P, 7.27.

^{1}H NMR ($CDCl_3$, 360 MHz): δ = 7.87 (d, *J* = 7.5 Hz, 1H, H-4), 7.52 (m, 5H, H-15,-19,-15‘,-19‘,-10), 7.37 (m, 6H, H-16,-17,-18,-16‘,-17‘,-18‘), 6.78 (dt, *J* = 7.6 Hz, 1.2 Hz, 1H, H-6), 6.72 (dt, *J* = 7.6 Hz, 1.2 Hz, 1H, H-5), 6.51 (d, *J* = 7.5 Hz, 1H, H-7), 6.26 (d, *J* = 8.0 Hz, 1H, H-9), 6.09 (d, *J* = 7.9 Hz, 1H, H-11), 5.19 (s, 2H, H-2), 4.00 (d, *J* = 6.0 Hz, 2H, H-13), 3.97 (s, 3H, H-12).

^{31}P NMR ($CDCl_3$, 146 MHz) δ = –25.23 (1P, P-14).

Scheme S3.3. Screening of reaction conditions: hydride abstraction from compound **3.3**

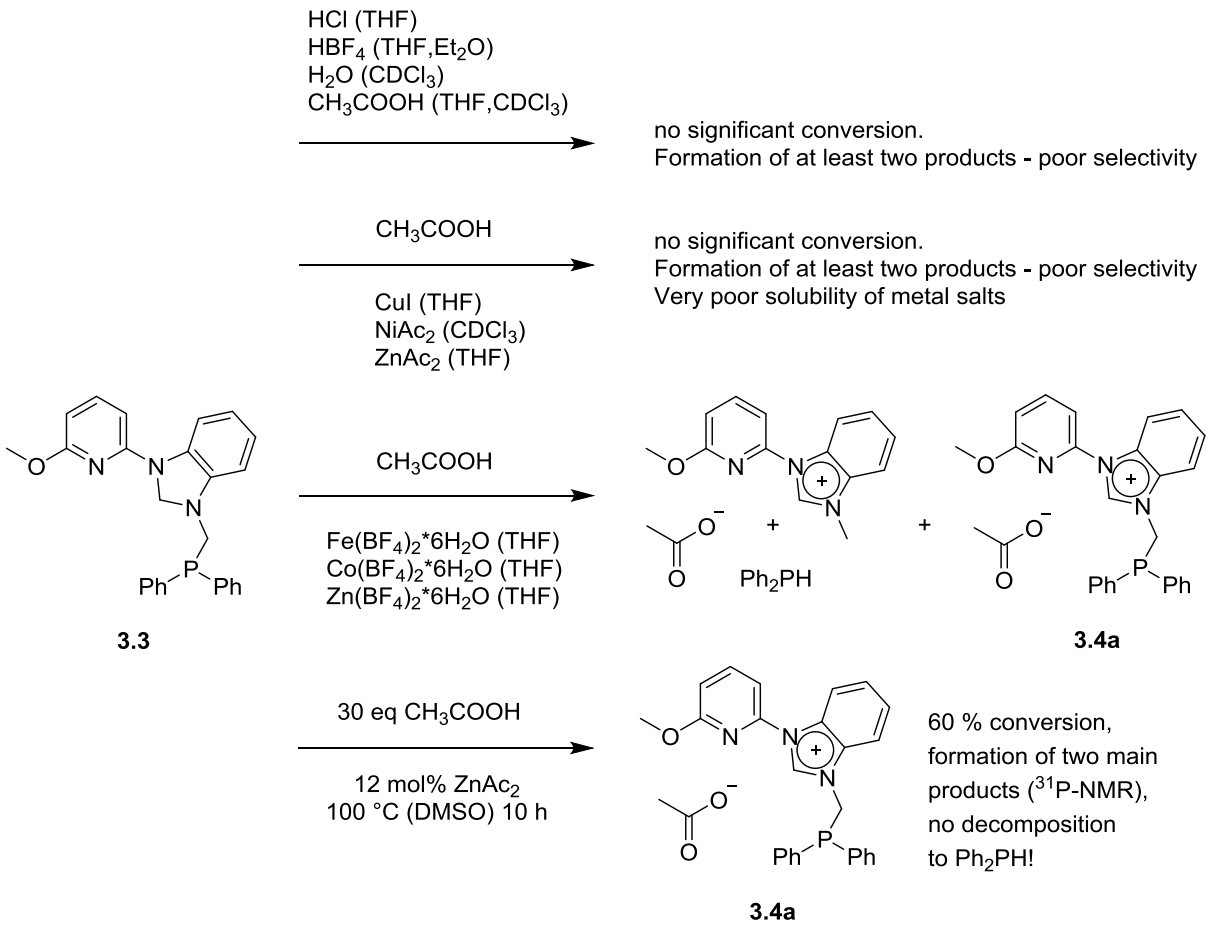

1-((diphenylphopshino)methylene)-3-(6-methoxypyridin-2-yl)benzimidazolium acetate (3.4a)

Scheme S3.4. Hydride abstraction from compound **3.3**

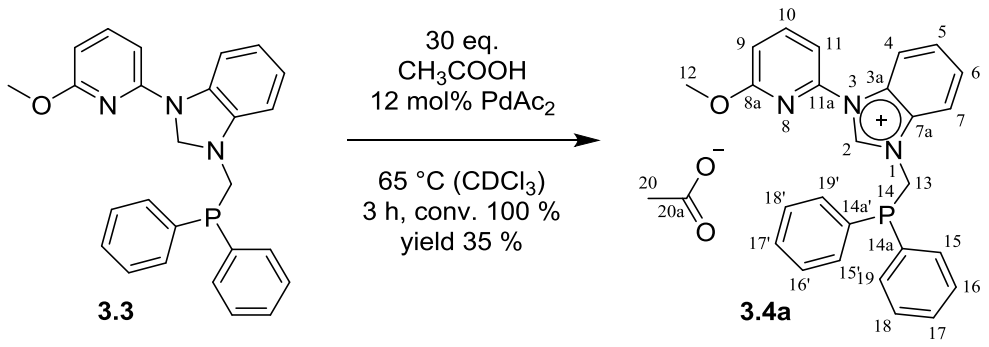

To a colourless solution of benzimidazoline derivative **3.3** (300.0 mg, 0.70 mmol, 1.00 eq, 98%) in 8 mL degassed dry chloroform CH_3COOH (1.36 g, 22.68 mmol, 32.40 eq) and $Pd(CH_3COO)_2$ (19.2 mg, 0.08 mmol, 0.12 eq, 98%) were added. The mixture was stirred at 65 °C within 3h. Subsequently, the solvent and acetic acid were removed *in vacuo*. The product was washed 5 times with cooled dry degassed acetone and filtered. Another portion of **3.4a** was precipitated from acetone filtrate at –30 °C. Finally, the combined fractions of organic salt **3.4a** were dried under reduced pressure and analyzed (Yield: 117.0 mg, 35%).

^{1}H NMR ($CDCl_3$, 500 MHz): δ = 11.98 (s, 1H, H-2), 8.47 (d, *J* = 8,3 Hz, 1H, H-4), 7.85 (t, *J* = 7.9 Hz, 1H, H-10), 7.79 (d, *J* = 7,6 Hz, 1H, H-7), 7.75 (d, *J* = 8,2 Hz, 1H, H-9), 7.69 (t, *J* = 7.3 Hz, 4H, H-15,-19,-15',-19'), 7.63 (t, *J* = 7.4 Hz, 1H, H-6), 7.63 (t, *J* = 7.5 Hz, 1H, H-5), 7.38 (m, 6H, H-16,-17,-18,-16',-17',-18'), 6.87 (d, *J* = 8,2 Hz, 1H, H-11), 5.74 (d, $J^{H\text{-}P}$ = 5,5 Hz, 2H, H-13), 4.02 (s, 3H, H-12), 2.14 (s, 3H, H-20)

^{31}P NMR ($CDCl_3$, 203 MHz): δ = –16.91 (s, 1P, P-14)

ESI MS, *m/z*:

424.1 $[CH_3O(C_5H_3N)(CHN_2C_6H_4)(CH_2)(P(C_5H_6)_2)]^+$;

440.1 $[CH_3O(C_5H_3N)(CHN_2C_6H_4)(CH_2)(PO(C_5H_6)_2)]^+$

1-((diphenylphopshino)methylene)-3-(6-methoxypyridin-2-yl)benzimidazolium hexafluorophosphate (3.4)

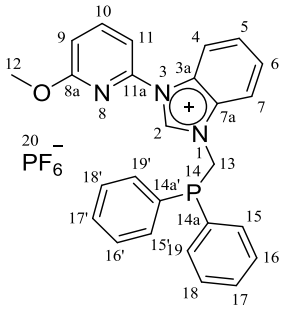

To a colourless solution of benzimidazoline derivative **3.3** (0.50 g, 1.17 mmol, 1.00 eq) in 10 mL degassed dry THF cooled to –78 °C triphenylcarbenium hexafluorophosphate (0.4 g, 1.13 mmol, 0.97 eq, 97%) was added in one portion. The mixture was stirred for 10 min and warm up to room temperature. After the reaction was quenched with 0.5 mL degassed methanol the solution was preconcentrated to 5 mL *in vacuo*. The product was precipitated by addition of 15 mL degassed dry toluene. The formed suspension was stirred then overnight at room temperature and filtered *via cannula*. The crude solid product was then redissolved in THF, filtered through syringe filter (0.2 µm) and isolated by addition of Et_2O to the filtrate phase. The sedimentation from THF/Et_2O (2/8) at –40 °C yielded 0.52 g (79%) of a colourless amorphous substance **3.4**. Anal. calcd. for $C_{26}H_{23}F_6N_3OP_2$: C, 54.84; H, 4.07; F, 20.02; N, 7.38; O, 2.81; P, 10.88. Found: C, 55.31; H, 4.35; N, 7.14; P, 10.53.

^{1}H NMR ($CDCl_3$, 500 MHz) δ = 9.07 (s, 1H, H-2), 8.26 (d, *J* = 8.2 Hz, 1H, H-4), 7.82 (m, 2H, H-7,-10), 7.70 (t, *J* = 7.4 Hz, 1H, H-6), 7.66 (t, *J* = 7.4 Hz, 1H, H-5), 7.52 (m, 4H, H-15,-19,-15',-19'), 7.40 (m, 6H, H-16,-17,-18,-16',-17',-18'), 7.22 (d, *J* = 7,5 Hz, 1H, H-9), 6.91 (d, *J* = 8,3 Hz, 1H, H-11), 5.34 (d, $J^{H\text{-}P}$ = 5,5 Hz, 2H, H-13), 3.98 (s, 3H, H-12)

^{31}P NMR ($CDCl_3$, 203 MHz) δ = –16.35 (1P, P-14), –144.23 (hept, *J* = 713.5 Hz, 1P, P-20)

ESI MS, *m/z*:

424.3 $[CH_3O(C_5H_3N)(CHN_2C_6H_4)(CH_2)(P(C_5H_6)_2)]^+$;

440.3 $[CH_3O(C_5H_3N)(CHN_2C_6H_4)(CH_2)(PO(C_5H_6)_2)]^+$

2-bromo-6-(*tert*-butylthio)pyridine

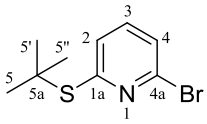

2-bromo-6-(*tert*-butylthio)pyridine was synthesized according to the known procedure from 2,5-dibromopyridine and *tert*-butyl mercaptan.[297] The compound was purified by fractional distillation (60 °C, 0.22 mbar).

^{1}H NMR ($CDCl_3$, 360 MHz): δ = 7.30 (t, *J* = 7.6 Hz, 1H, H-3), 7.17 (d, *J* = 7,8 Hz, 1H, H-2), 7.15 (d, *J* = 7,7 Hz, 1H, H-4) 1.54 (s, 9H, H-5,-5',-5'')

ESI MS, *m/z*: 247.2 $[(CH_3)_3S(C_5H_3N)Br+H]^+$

GC-M S: 15.5 min., *m/z*: 191.3 $[HS(C_5H_3N)Br+H]^+$

1-(6-(*tert*-butylthio)pyridin-2-yl)benzimidazole (3.5)

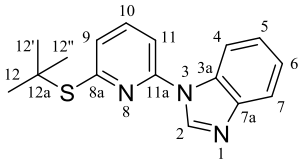

In a 100 mL Schlenk round-bottom flask, benzimidazole (3.58 g, 29.71 mmol, 1.00 eq, 98%), 2-bromo-6-(*tert*-butylthio)pyridine (8.50 g, 34.17 mmol, 1.15 eq), *L*-proline (0.68 g, 5.94 mmol, 0.20 eq, 99%), copper(I) iodide (0. 57 g, 2.97 mmol, 0.10 eq, 99%) and potassium carbonate (8.30 g, 59.42 mmol, 2.00 eq, 99%) were suspended in 60 mL dry DMSO under argon. The reaction mixture was then stirred for 5 days at 130 °C. After this reaction time water was added to the suspension. This biphasic mixture was filtered through Celite® and extracted with a $CH_3COOC_2H_5/NaHCO_{3aq}$ mixture (1/1; 3 x 100 mL). Finally, the colourless compound **3.1** (6.37 g, 76%) was obtained through distillation of the organic phase using a Kugelrohr short-path distillation apparatus at 171 °C ($p = 3.5 \cdot 10^{-2}$ mbar). Anal. calcd. for $C_{16}H_{17}N_3S$: C, 67.81; H, 6.05; N, 14.83; S, 11.31. Found: C, 67.63; H, 5.97; N, 14.74; S, 11.00.

^{1}H NMR ($CDCl_3$, 500 MHz): δ = 8.63 (s, 1H, H-2), 7.89 (m, 2H, H-4, H-7), 7.68 (t, *J* = 7.9 Hz, 1H, H-10), 7.37 (m, 2H, H-5, H-6), 7.32 (d, *J* = 7.9 Hz, 1H, H-9), 7.23 (d, *J* = 7.8 Hz, 1H, H-11), 1.61 (s, 9H, H-12,-12',-12'')

ESI MS, *m/z*: 299.6 $[(CH_3)_3S(C_5H_3N)(CHN_2C_6H_4)+H]^+$

1-(2-bromoethyl)-3-(6-methoxypyridin-2-yl)benzimidazolium bromide (3.6a)

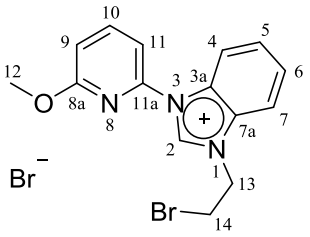

Compound **3.6a** was prepared according to analogous synthetic procedure.[298]
1-(6-methoxypyridin-2-yl)benzimidazole **3.1** (2.36 g, 10.25 mmol, 1.00 eq) was dissolved in 1,2-bromoethane (18 mL, 20.00 eq) in a Schlenk-tube and heated at 85 °C overnight (16 h) under intensive stirring. After the reaction was complete, all volatiles were removed under reduced pressure and 50 mL dichloromethane was added to the solid residue. The formed suspension was stirred for 1 h and filtered over Celite®. After the solvent was removed from the filtrate *in vacuo*, the product was obtained in 68% yield (2.87 g). Anal. calcd. for $C_{15}H_{15}Br_2N_3O$: C, 43.61; H, 3.66; Br, 38.68; N, 10.17; O, 3.87. Found: C, 43.32; H, 3.42; N, 9.85.

^{1}H NMR ($CDCl_3$, 300 MHz): δ = 11.83 (s, 1H, H-2), 8.47 (m, 1H, H-4), 8.01 (m, 1H, H-7), 7.92 (m, 2H, H-9, H-10), 7.69 (m, 2H, H-5, H-6), 6.92 (d, *J* = 7,6 Hz, 1H, H-11), 5.43 (t, *J* = 5.7 Hz, 2H, H-13), 4.16 (t, *J* = 5.8 Hz, 2H, H-14), 4.05 (s, 3H, H-12).

ESI MS, *m/z*: 333.7 $[CH_3O(C_5H_3N)(CHN_2C_6H_4)(C_2H_4Br)]^+$.

1-(2-bromoethyl)-3-(6-(*tert*-butylthio)pyridin-2-yl)benzimidazolium bromide (3.6b)

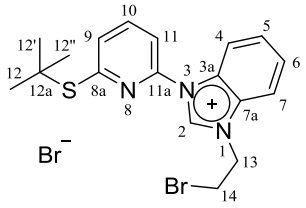

Compound **3.6b** was prepared according to analogous synthetic procedure.[298]
1-(6-(*tert*-butylthio)pyridin-2-yl)benzimidazole **3.5** (1.02 g, 3.55 mmol, 1.00 eq, 98%) was dissolved in 1,2-bromoethane (4.6 mL, 15.00 eq) in a Schlenk-tube and heated at 85 °C overnight (20 h) under intensive stirring. After the reaction was complete, all volatiles were removed under reduced pressure and 30 mL dichloromethane was added to the solid residue. The formed suspension was stirred for 1 h and filtered over Celite®. After the solvent was

removed from the filtrate *in vacuo*, the product was obtained in 78% yield (1.29 g). Anal. calcd. for $C_{18}H_{21}Br_2N_3S$: C, 45.88; H, 4.49; Br, 33.91; N, 8.92; S, 6.80. Found: C, 45.69; H, 4.56; Br, 33.71; N, 9.09; S, 6.66.

^{1}H NMR ($CDCl_3$, 300 MHz): δ = 11.92 (s, 1H, H-2), 8.51 (m, 1H, H-4), 8.27 (d, *J* = 7.9 Hz, 1H, H-7), 7.92 (t, *J* = 7.9 Hz, 1H, H-10), 7.93 (m, 1H, H-9), 7.72 (m, 2H, H-5, H-6), 7.53 (d, *J* = 7.8 Hz, 1H, H-11), 5.40 (t, *J* = 5.6 Hz, 2H, H-13), 4.19 (t, *J* = 5.6 Hz, 2H, H-14), 1.55 (s, 9H, H-12,-12',-12'').

ESI MS, *m/z*: 391.9 $[(CH_3)_3S(C_5H_3N)(CHN_2C_6H_4)(C_2H_4Br)]^+$.

1-(2-(diphenylphopshino)ethyl)-3-(6-methoxypyridin-2-yl)benzimidazolium bromide (3.7a)

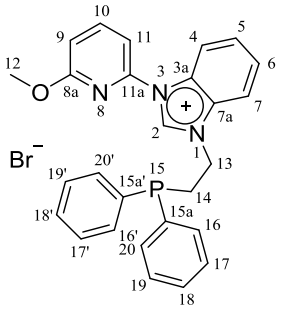

Compound **3.7a** was synthesized according to the previously described method for phosphine-imidazolium salts.[227, 299, 300]

$KPPh_2$ (0.25 g, 1.11 mmol, 1.03 eq), freshly made from $HPPh_2$ and *tert*-BuOK in 5 mL DMSO was slowly dropped to the solution of **3.6a** (461.7 mg, 1.08 mmol, 1.00 eq) in 10 mL DMSO in the glove-box. The mixture was then stirred at 25 °C for 1.5 h and subsequently quenched with degassed methanol. The solvent was then removed *in vacuo*, the residue dissolved in dichloromethane and filtered. The analytically pure compound **3.7a** (0.44 g, 78%) was obtained by its precipitation from THF or CH_2Cl_2/Et_2O mixture (3/7) at -30 °C. Anal. calcd. for $C_{27}H_{25}BrN_3OP$: C, 62.56; H, 4.86; Br, 15.41; N, 8.11; O, 3.09; P, 5.97. Found: C, 62.57; H, 4.96; Br, 15.20; N, 8.17; P, 5.69.

^{1}H NMR ($CDCl_3$, 360 MHz): δ = 11.96 (s, 1H, H-2), 8.37 (m, 1H, H-4), 7.99 (d, *J* = 7.6 Hz, 1H, H-9), 7.88 (t, *J* = 8.0 Hz, 1H, H-10), 7.59 (m, 2H, H-5,-6), 7.47 (m, 1H, H-7), 7.37 (m, 4H, H-17,-17',-19,-19'), 7.20 (m, 6H, H-16,-18,-20,-16',-18',-20'), 6.88 (d, *J* = 6.9 Hz, 1H,

H-11), 5.00 (dt, J^{H-P} = 10.3 Hz, J = 7.3 Hz, 2H, H-14), 4.04 (s, 3H, H-12), 3.07 (t, J = 7.2 Hz, 2H, H-13).

^{31}P-NMR ($CDCl_3$, 146 MHz): δ = –20.81 (s, 1P, P-15)

ESI MS, *m/z*:

438.0 $[CH_3O(C_5H_3N)(CHN_2C_6H_4)(C_2H_4)(P(C_5H_6)_2)]^+$;
454.0 $[CH_3O(C_5H_3N)(CHN_2C_6H_4)(C_2H_4)(PO(C_5H_6)_2)]^+$

1-(2-(diphenylphopshino)ethyl)-3-(6-(*tert*-butylthio)pyridin-2-yl)benzimidazolium bromide (3.7b)

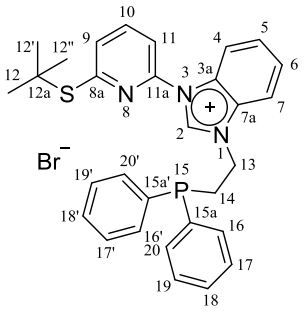

Compound **3.7b** was synthesized according to the previously described method for phosphine-imidazolium salts.[227, 299, 300]

$KPPh_2$ (0.62 g, 1.13 mmol, 1.00 eq), freshly made from $HPPh_2$ and *tert*-BuOK in 12 mL DMSO was slowly dropped to the solution of **3.6b** (309.0 mg, 1.37 mmol, 1.05 eq) in 25 mL DMSO in the glove-box. The mixture was then stirred at 25 °C for 1.5 h and subsequently quenched with degassed methanol. The solvent was then removed *in vacuo*, the residue dissolved in dichloromethane and filtered. The analytically pure compound **3.7b** (0.43 mg, 57%) was obtained by its precipitation from THF or CH_2Cl_2/Et_2O mixture (3/7) at -30 °C. Anal. calcd. for $C_{30}H_{31}BrN_3PS$: C, 62.50; H, 5.42; Br, 13.86; N, 7.29; P, 5.37; S, 5.56. Found: C, 62.80; H, 5.38; Br, 13.82; N, 7.24; P, 5.17; S, 5.38.

^{1}H NMR ($CDCl_3$, 500 MHz): δ = 12.02 (s, 1H, H-2), 8.44 (m, 1H, H-4), 8.38 (d, J = 8.0 Hz, 1H, H-9), 7.89 (t, J = 7.9 Hz, 1H, H-10), 7.60 (m, 2H, H-5,-6), 7.48 (m, 2H, H-7,-11), 7.40 (m, 4H, H-17,-19,-17',-19'), 7.22 (m, 6H, H-16,-18,-20,-16',-18',-20'), 4.97 (dt, J = 7.4 Hz, J^{H-P} = 10.2 Hz, 2H, H-14), 3.10 (t, J = 7.3 Hz, 2H, H-13), 1.51 (s, 9H, H-12,-12',-12'').
^{31}P NMR ($CDCl_3$, 146 MHz): δ = -21.1 (s, 1P, P-15).

ESI MS, *m/z*:

496.7 $[(CH_3)_3S(C_5H_3N)(CHN_2C_6H_4)(C_2H_4)(P(C_5H_6)_2)]^+$;

512.6 $[(CH_3)_3S(C_5H_3N)(CHN_2C_6H_4)(C_2H_4)(PO(C_5H_6)_2)]^+$

1-(2-(diphenylphopshino)ethyl)-3-(6-methoxypyridin-2-yl)benzimidazolium hexafluorophosphate (3.8a)

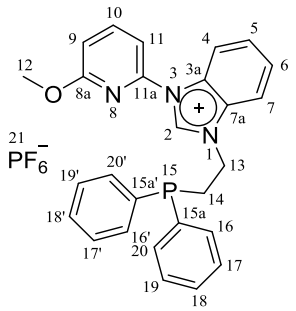

KPF_6 (39.1 mg, 0.21 mmol, 1.10 eq) was added to 5 mL THF solution of **3.7a** (100.0 mg, 0.19 mmol, 1.00 eq) and stirred in the Glove-box. After 1 h THF was removed under reduced pressure and 2 mL dichloromethane was added to the solid. The formed suspension was then stirred for 30 minutes and filtered through a 0.20 μm syringe filter. The product **3.8a** (71.0 mg, 64%) was isolated by evaporation of the solvent as a colourless amorphous compound. Anal. calcd. for $C_{27}H_{25}F_6N_3OP_2$: C, 55.58; H, 4.32; F, 19.54; N, 7.20; O, 2.74; P, 10.62. Found: C, 55.47; H, 4.15; N, 6.97; P, 10.29.

^{1}H NMR (CD_2Cl_2, 300 MHz): δ = 9.61 (s, 1H, H-2), 8.20 (m, 1H, H-4), 7.95 (t, *J* = 7.6 Hz, 1H, H-10), 7.71 (m, 2H, H-5,-6), 7.62 (m, 1H, H-7), 7.38 (d, *J* = 7.6 Hz, 1H, H-9), 7.36 (m, 4H, H-17,-17',-19,-19'), 7.24 (m, 6H, H-16,-18,-20,-16',-18',-20'), 7.01 (d, *J* = 8.3 Hz, 1H, H-11), 4.86 (dt, *J* = 10.9 Hz, *J* = 7.2 Hz, 2H, H-14), 4.06 (s, 3H, H-12), 2.89 (t, *J* = 7.2 Hz, 2H, H-13).

^{31}P NMR ($CDCl_3$, 203 MHz): δ = –20.98 (s, 1P, P-15), –144.00 (hept, *J* = 712.1 Hz, 1P, P-21).

ESI MS, *m/z*:

438.1 $[CH_3O(C_5H_3N)(CHN_2C_6H_4)(C_2H_4)(P(C_5H_6)_2)]^+$;

454.1 $[CH_3O(C_5H_3N)(CHN_2C_6H_4)(C_2H_4)(PO(C_5H_6)_2)]^+$

1-(2-(diphenylphopshino)ethyl)-3-(6-(*tert*-butylthio)pyridin-2-yl)benzimidazolium hexafluorophosphate (3.8b)

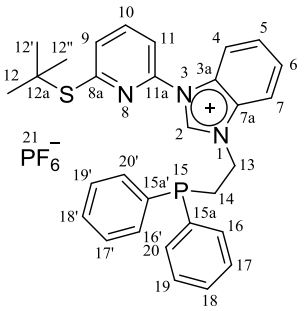

KPF_6 (30.0 mg, 0.16 mmol, 1.02 eq) was added to 5 mL THF solution of **3.7b** (93.2 mg, 0.16 mmol, 1.00 eq) and stirred in the Glove-box. After 2 h THF was removed under reduced pressure and 2 mL dichloromethane was added to the solid residue. The formed suspension was then stirred for 30 minutes and filtered through a 0.20 μm syringe filter. 95.2 mg **3.8b** (93%) was isolated by evaporation of the solvent. Anal. calcd. for $C_{30}H_{31}F_6N_3P_2S$: C, 56.16; H, 4.87; F, 17.77; N, 6.55; P, 9.66; S, 5.00. Found: C, 55.96; H, 4.72; N, 6.37; P, 9.41.

^{1}H NMR (d_8-THF, 500 MHz): δ = 9.91 (s, 1H, H-2), 8.26 (m, 1H, H-4), 8.02 (t, *J* = 8.0 Hz, 1H, H-10), 7.89 (m, 1H, H-7), 7.80 (d, *J* = 7.9 Hz, 1H, H-9), 7.69 (m, 2H, H-5,-6), 7.59 (d, *J* = 7.6 Hz, 1H, H-11), 7.46 (m, 4H, H-17,-17',-19,-19'), 7.28 (m, 6H, H-16,-18,-20,-16',-18',-20'), 4.85 (m, 2H, H-14), 3.00 (t, *J* = 7.2 Hz, 2H, H-13), 1.56 (s, 9H, H-12,-12',-12'')

^{31}P NMR (d_8-THF, 203 MHz): δ = –20.69 (s, 1P, P-15), -144.00 (hept, *J* = 711.6 Hz, 1P, P-21)

ESI MS, *m/z*:

496.7 $[(CH_3)_3S(C_5H_3N)(CHN_2C_6H_4)(C_2H_4)(P(C_5H_6)_2)]^+$;
512.6 $[(CH_3)_3S(C_5H_3N)(CHN_2C_6H_4)(C_2H_4)(PO(C_5H_6)_2)]^+$

Synthesis of organometallic compounds

General procedure for preparation of $[(NC^{BIm}P)Rh(CH_3CN)][PF_6]$ complexes: 1.00 eq of a ligand precursor (**3.4**, **3.8a**, **3.8b**) was added to 0.50 eq $[\mu\text{-}OCH_3Rh(COD)]_2$ dissolved in 10 mL degassed THF and stirred at room temperature for 15 h. After the reaction was complete all volatiles were removed *in vacuo*. The formed amorphous solid was then redissolved in acetonitrile and stirred intensively for 2 h under hydrogen atmosphere (0.5 bar over the atmospheric pressure). The reaction mixture was filtered through a 0.20 µm syringe filter and the solvent was partially reduced *in vacuo*. The complexes (**3.9**, **3.10a**, **3.10b**) were obtained as coloured precipitates by addition of Et_2O. The compound **3.9** was reprecipitated from THF by addition of Et_2O.

1-((diphenylphopshino)methylene)-3-(6-methoxypyridin-2-yl)benzimidazol-2-yl rhodium acetonitrile hexafluorophosphate (3.9)

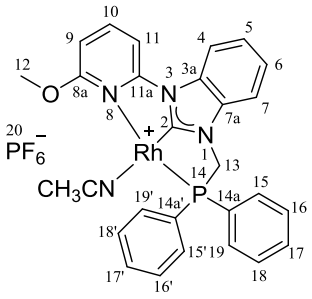

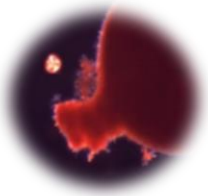

Anal. calcd. for $C_{28}H_{25}F_6N_4OP_2Rh$ (+ 0.50 eq C_4H_8O): C, 48.14; H, 3.91; F, 15.23; N, 7.49; O, 3.21; P, 8.28; Rh, 13.75. Found: C, 47.99; H, 3.78; N, 7.81; P, 7.95.

^{1}H NMR (DMSO, 500 MHz): δ = 8.32 (t, *J* = 8.2 Hz, 1H, H-10), 8.24 (m, 1H, H-4), 7.94 (d, *J* = 8.0 Hz, 1H, H-9), 7.85 (m, 4H, H-15,-19,-15‘,-19‘), 7.55 (m, 7H, H-7,-16,-17,-18,-16‘,-17‘,-18‘), 7.46 (m, 2H, H-5,-6), 7.26 (d, *J* = 8.4 Hz, 1H, H-11), 4.98 (d, *J* = 6.4 Hz, 2H, H-13), 4.06 (s, 3H, H-12).

^{31}P NMR (DMSO, 121 MHz): δ = 60.64 (d, *J* = 222.6 Hz, 1P, P-14), –144.00 (hept, *J* = 711.1 Hz, 1P, P-20).

FAB MS, *m/z*:

525.3 $[(CH_3O(C_5H_3N)(CN_2C_6H_4)(CH_2)(P(C_5H_6)_2))Rh]^+$;

541.3 $[(CH_3O(C_5H_3N)(CN_2C_6H_4)(CH_2)(PO(C_5H_6)_2))Rh]^+$

1-(2-(diphenylphopshino)ethyl)-3-(6-methoxypyridin-2-yl)benzimidazol-2-yl rhodium acetonitrile hexafluorophosphate (3.10a)

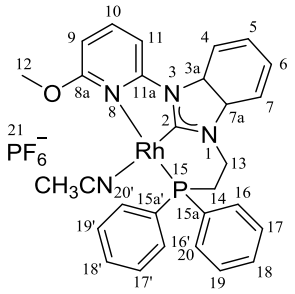

Anal. calcd. for $C_{29}H_{27}F_6N_4OP_2Rh$: C, 47.95; H, 3.75; F, 15.69; N, 7.71; O, 2.20; P, 8.53; Rh, 14.17. Found: C, 48.05; H, 3.81; N, 7.66; P, 8.63.

^{1}H NMR (CD_3CN, 360 MHz): δ = 8.08 (t, *J* = 8.2 Hz, 1H, H-10), 7.82 (m, 5H, H-4,-15,-19,-15',-19'), 7.61 (d, *J* = 8.0 Hz, 1H, H-9), 7.52 (m, 6H, H-16,-17,-18,-16',-17',-18'), 7.37 (m, 1H, H-7), 7.31 (m, 2H, H-5,-6), 6.94 (d, *J* = 8.4 Hz, 1H, H-11), 4.08 (m, 2H, H-14), 3.96 (s, 3H, H-12), 2.83 (ddt, *J* = 11.5 Hz, 5.9 Hz, 2.8 Hz, 2H, H-13).
^{31}P NMR (CD_3CN, 146 MHz): δ = 38.47 (d, *J* = 187.4 Hz, 1P, P-15), –144.00 (hept, *J* = 706.3 Hz, 1P, P-21).

1-(2-(diphenylphopshino)ethyl)-3-(6-(*tert*-butylthio)pyridin-2-yl)benzimidazol-2-yl rhodium acetonitrile hexafluorophosphate (3.10b)

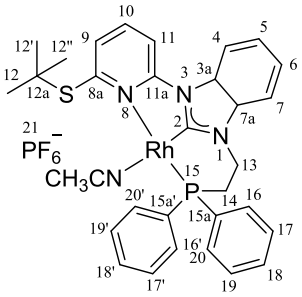

Anal. calcd. for $C_{32}H_{33}F_6N_4P_2RhS$: C, 48.99; H, 4.24; F, 14.53; N, 7.14; P, 7.90; Rh, 13.12; S, 4.09. Found: C, 48.82; H, 4.43; N, 6.33; P, 8.37; S, 3.53. Although these results are outside the range viewed as establishing analytical purity, they are provided to illustrate the best values obtained to date.

^{1}H NMR (d_8-THF, 360 MHz): δ = 8.27 (t, *J* = 8.3 Hz, 1H, H-10), 8.11 (d, *J* = 8.0 Hz, 1H, H-4), 7.90 (m, 4H, H-15,-19,-15',-19'), 7.84 (d, *J* = 7.2 Hz, 1H, H-9), 7.50 (m, 7H, H-7,-16,-17,-

18,-16‘,-17‘,-18‘), 7.38 (m, 2H, H-5,-6), 6.92 (d, *J* = 8.4 Hz, 1H, H-11), 4.21 (dt, *J* = 21.8 Hz, 5.4 Hz, 2H, H-14), 2.91 (m, 2H, H-13), 1.96 (s, 9H, H-12,-12’,-12’’).

^{31}P NMR (CD_3CN, 146 MHz): δ = 39.84 (d, *J* = 189.9 Hz, 1P, P-15), –144.00 (hept, *J* = 708.5 Hz, 1P, P-21).

1-(2-(diphenylphopshino)ethyl)-3-(6-methoxypyridin-2-yl)benzimidazol-2-yl iridium acetonitrile bromide chloride (3.11)

Scheme S3.5. Iridium complexation by [5,6]-membered $NC^{BIm}P$ ligand precursor **3.7a**.

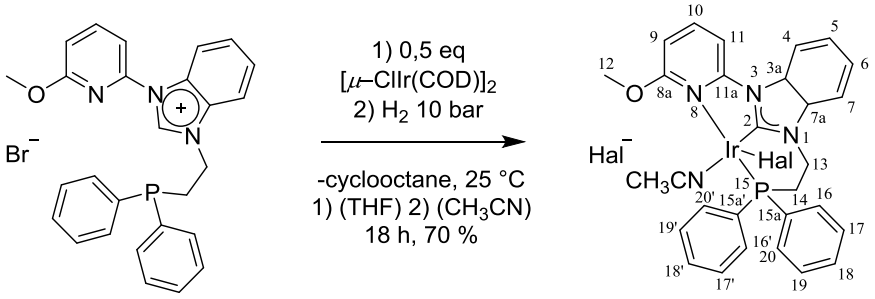

In a 25 mL Schlenk-flask, compound **3.7a** (51.0 mg, 0.10 mmol, 1.00 eq) and [μ-ClIr(COD)]$_2$ (33.4 mg, 0.05 mmol, 0.50 eq, 98%) were dissolved in 10 mL degassed dry THF and stirred for 2 h under argon atmosphere in a glove box. After the solvent was removed, the formed yellow precipitate was suspended in acetonitrile, transferred to a 50 mL autoclave and pressurized with 10 bar hydrogen. The suspension was intensively stirred at room temperature for 16 h. Finally, autoclave was carefully vented and the solvent partially removed *in vacuo*. The residual colourless solution (2 mL) was then transferred to a Schlenk-tube. The colourless crystalline solid material was obtained by addition of Et_2O to this solution. Yield: 51.0 mg, 70%. Anal. calcd. for $C_{29}H_{27}BrClIrN_4OP$: C, 44.31; H, 3.46; Br, 10.16; Cl, 4.51; Ir, 24.45; N, 7.13; O, 2.04; P, 3.94. Found: C, 43.72; H, 3.69; N, 6.95; P, 4.65; Br, 10.70. Although these results are outside the range viewed as establishing analytical purity, they are provided to illustrate the best values obtained to date.

^{1}H NMR (CD_3CN, 360 MHz): δ = 8.24 (t, *J* = 8.1 Hz, 1H, H-10), 8.15 (m, 1H, H-4), 7.90 (m, 4H, H-15,-19,-15’,-19’), 7.69 (m, 2H, H-5,-6), 7.55 (m, 7H, H-7,-9,-16,-17,-18,-16‘,-17‘,-18‘), 7.08 (d, *J* = 8.6 Hz, 1H, H-11), 4.83 (m, 2H, H-14), 4.09 (s, 3H, H-12), 3.27 (m, 2H, H-13).

^{31}P NMR (CD_3CN, 146 MHz): δ = –4.91, –4.78 (s, 1P, P-15).

ESI MS, *m/z*:

628.7 $[(CH_3O(C_5H_2N)(CN_2C_6H_4)(C_2H_4)(P(C_5H_6)_2))Ir]^+$;

666.4 $[(CH_3O(C_5H_3N)(CN_2C_6H_4)(C_2H_4)(P(C_5H_6)_2))IrCl+H]^+$;

710.3 $[(CH_3O(C_5H_3N)(CN_2C_6H_4)(C_2H_4)(P(C_5H_6)_2))\ IrBr+H]^+$

Note: Since the metal precursor contains chloride anion and the organic salt the bromide, the organometallic ($NC^{BIm}P$)Ir substance was obtained in a mixed form, with coordinated chloride and bromide anions to the metal, as revealed by ESI-MS and ^{31}P NMR analysis. This reaction is adduced to demonstrate the formation of first examples of carbene-centered $NC^{BIm}P$ iridium complexes and is a subject of our ongoing experiments.

General procedure for carbonylation of [($NC^{BIm}P$)Rh(CH_3CN)][PF_6] complexes

Solutions containing ($NC^{BIm}P$)Rh complexes (**3.10a**, **3.10b**) 1.00 eq each were dissolved in 0.5 mL propylene oxide and pressurized with 2 bar CO in Young NMR tubes. After 2 h NMR tubes were flushed with degassed diethyl ether for the purpose of product deposition from these solutions. The coloured organometallics were isolated for x-ray single crystal analysis by crystallization from propylene oxide/Et_2O (for **3.13a**) or THF/pentane (for **3.13b**) solutions.

1-(2-(diphenylphopshino)ethyl)-3-(6-methoxypyridin-2-yl)benzimidazol-2-yl rhodium carbonyl hexafluorophosphate (3.13a)

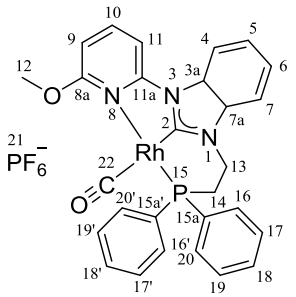

^{1}H NMR (CD_3CN, 500 MHz): δ = 8.16 (t, *J* = 8.3 Hz, 1H, H-10), 7.99 (m, 1H, H-4), 7.81 (m, 4H, H-4,-15,-19,-15',-19'), 7.70 (d, *J* = 8.0 Hz, 1H, H-9), 7.57 (m, 7H, H-7,-16,-17,-18,-16',-17',-18'), 7.49 (m, 2H, H-5,-6), 7.07 (d, *J* = 8.4 Hz, 1H, H-11), 4.37 (m, 2H, H-14), 4.05 (s, 3H, H-12), 3.04 (ddt, *J* = 8.5 Hz, 5.6 Hz, 2.4 Hz, 2H, H-13).

^{31}P NMR (CD_3CN, 203 MHz): δ = 37.26 (d, *J* = 161.71 Hz, 1P, P-15), –144.00 (hept, *J* = 706.6 Hz, 1P, P-21).

IR: $\nu_{C\text{-}O}$ = 2008.74 cm^{-1}

1-(2-(diphenylphopshino)ethyl)-3-(6-(*tert*-butylthio)pyridin-2-yl)benzimidazol-2-yl rhodium carbonyl hexafluorophosphate (3.13b)

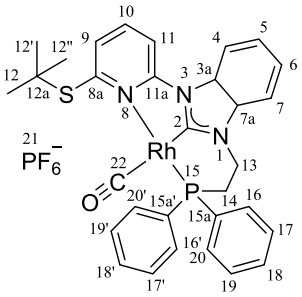

^{1}H NMR (CD_3CN, 250 MHz): δ = 8.23 (t, *J* = 8.3 Hz, 1H, H-10), 8.14 (d, *J* = 8.0 Hz, 1H, H-4), 7.81 (m, 4H, H-15,-19,-15',-19'), 7.97 (d, *J* = 7.2 Hz, 1H, H-9), 7.67 (d, *J* = 7.6 Hz, 1H, H-7), 7.57 (m, 6H, H-16,-17,-18,-16',-17',-18'), 7.52 (m, 2H, H-5,-6), 6.97 (d, *J* = 8.4 Hz, 1H, H-11), 4.42 (m, 2H, H-14), 3.07 (ddt, *J* = 9.0 Hz, 6.1 Hz, 2.8 Hz, 2H, H-13), 1.48 (s, 9H, H-12,-12',-12'').

^{31}P NMR (CD_3CN, 101 MHz): δ = 38.33 (d, *J* = 161.6 Hz, 1P, P-15), –144.00 (hept, *J* = 707.1 Hz, 1P, P-21).

IR: $\nu_{C\text{-}O}$ = 2001.71 cm^{-1}

Hydroboration

Scheme S3.6. Hydroboration of phenylacetylene with pinacolborane using **3.4** and **3.10a**

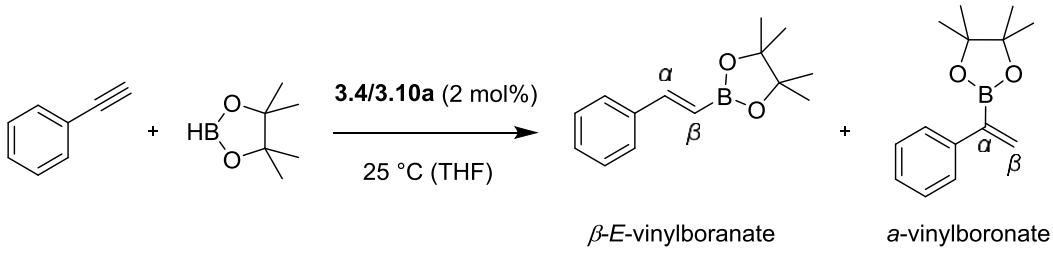

In the glove box, phenyl acetylene (7.8 µL, 0.07 mmol, 1.00 eq), pinacolborane (12.6 µL, 0.08 mmol, 1.20 eq), and mesitylene (1.1 µL, 7.78 µmol, 0.11 eq) were dissolved in 0.45 mL degassed d_8-THF in NMR tube. After addition of the metal complex (**3.4**, **3.10a**) (1.1 mg, 1.40 µmol, 0.02 eq) to the prepared solution the NMR tube was shaked and placed into NMR spectrometer for analysis. Subsequently, the reaction mixture was analyzed by GC-MS.

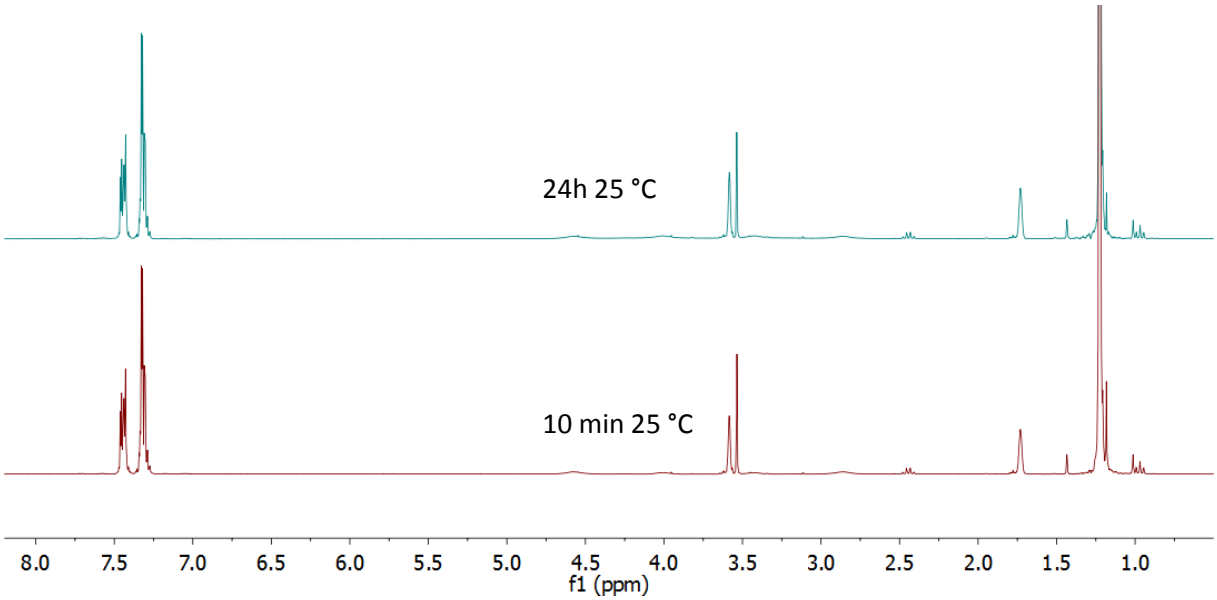

Figure S3.2. Zero reactivity in the reaction of phenylacetylene with pinacolborane in the absence of the catalyst in d_8-THF (^{1}H NMR monitoring)

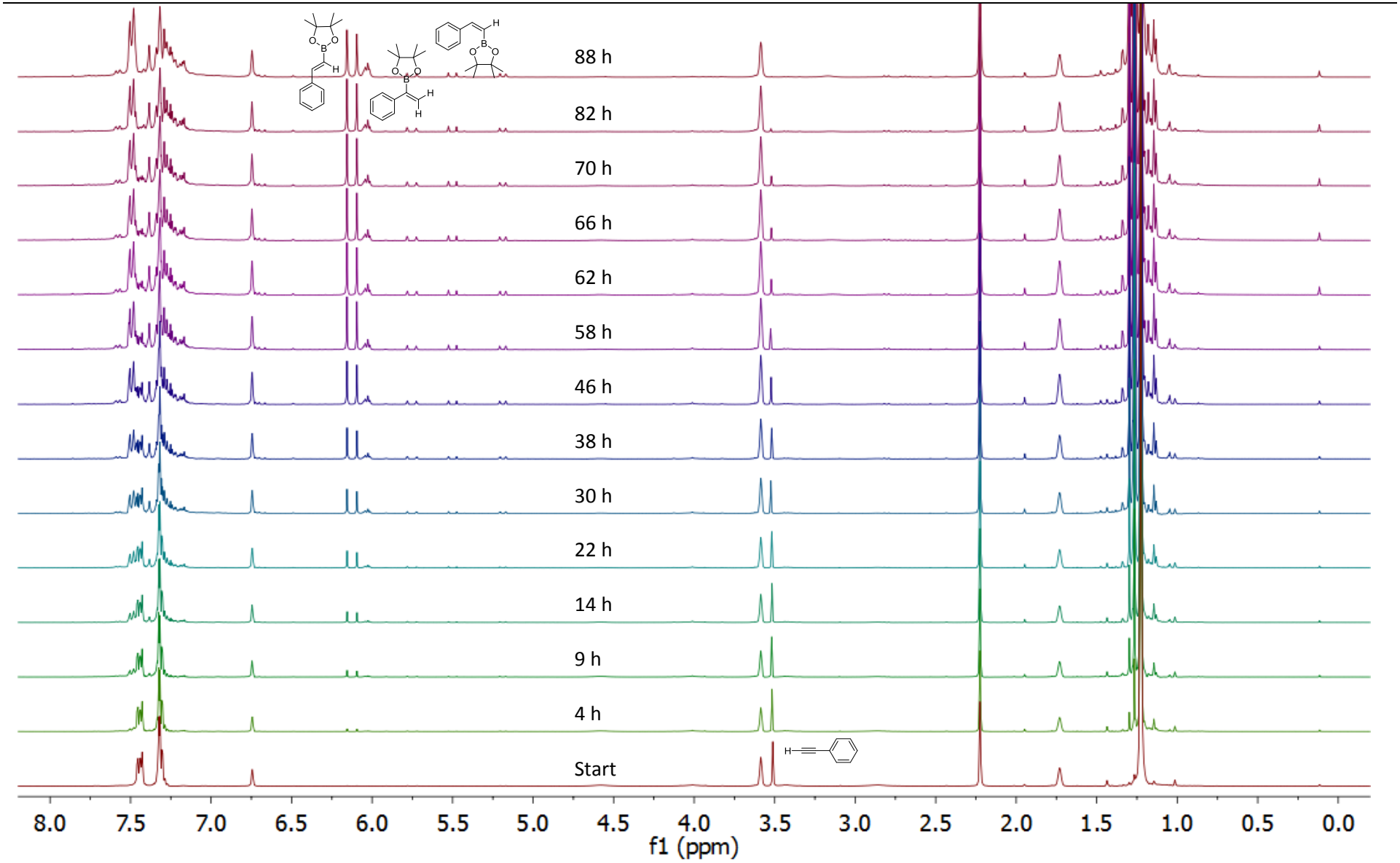

Figure S3.3. Reaction of phenylacetylene and pinacolborane catalyzed by **3.4** in d_8-THF at 25 °C (^{1}H NMR monitoring)

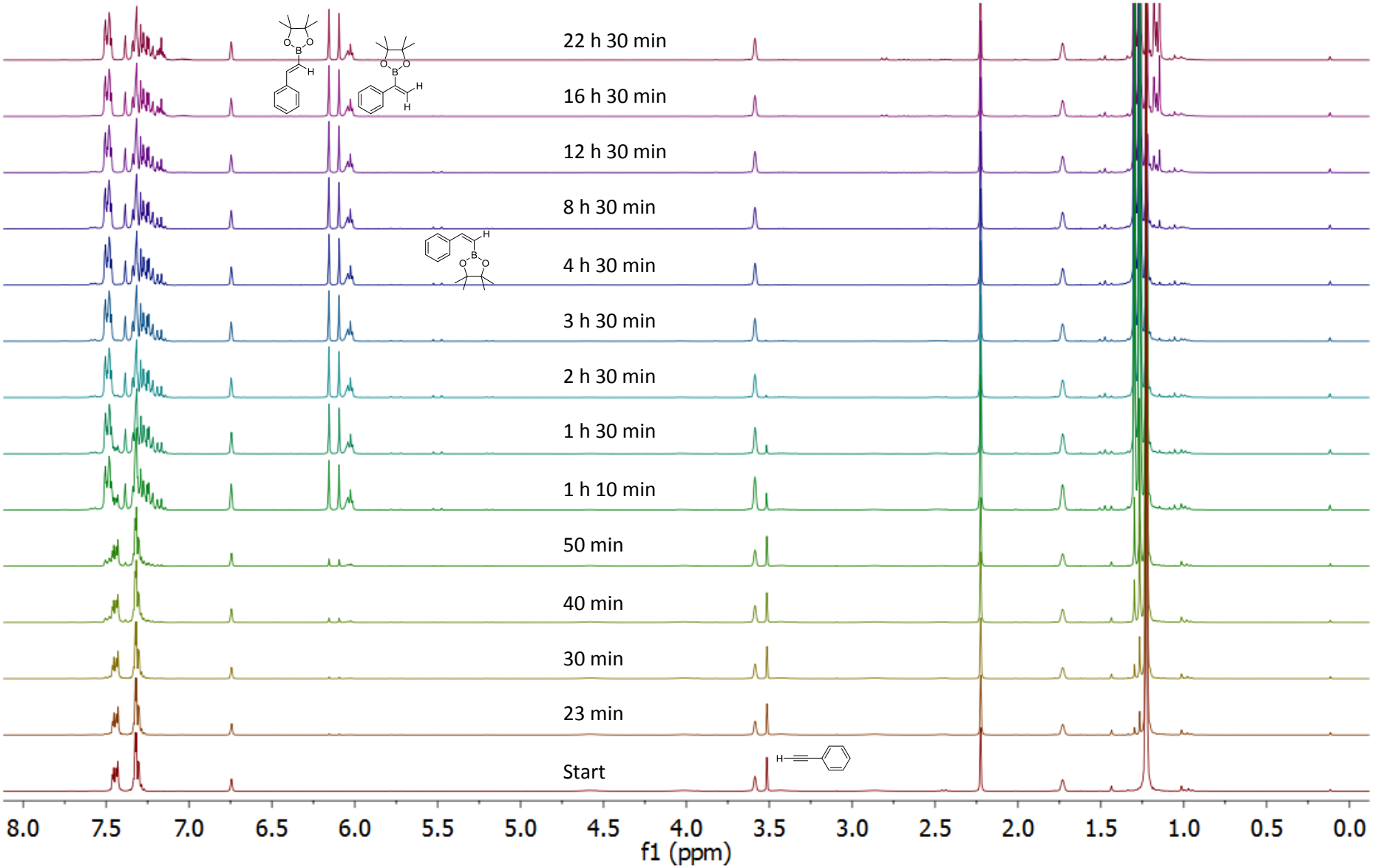

Figure S3.4. Reaction of phenylacetylene and pinacolborane catalyzed by **3.10a** in d_8-THF at 25 °C (^{1}H NMR monitoring)

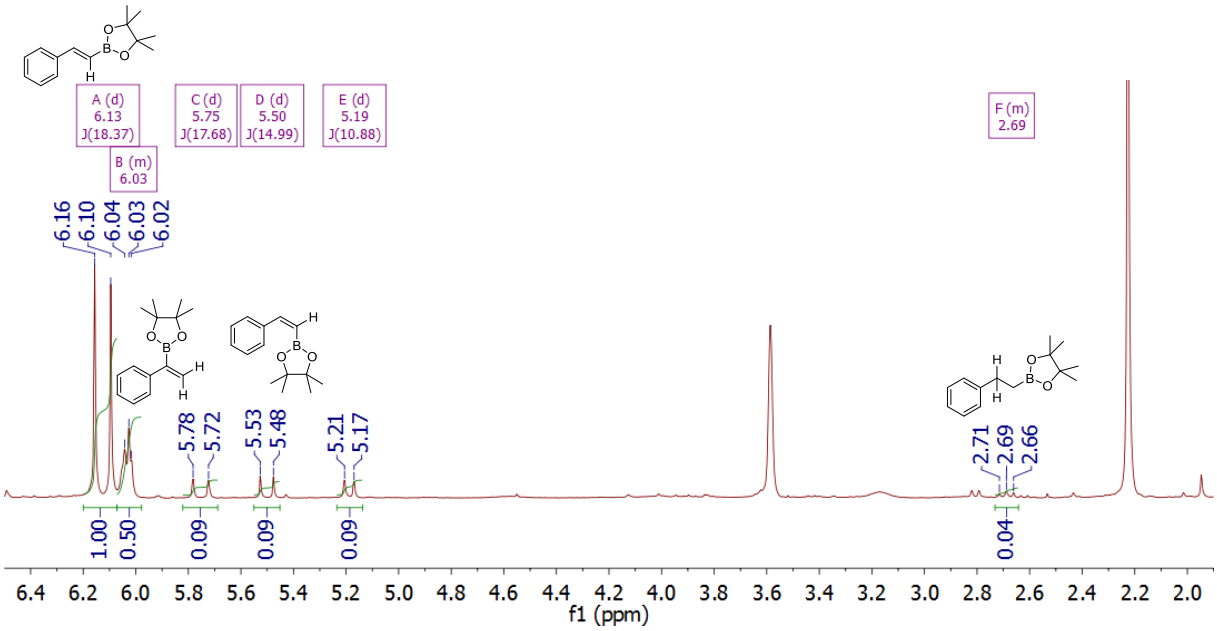

Figure S3.5. Selected characteristic proton signals of *β*-*E*-vinylboronate, δ = 6.13 ppm (d, *J* = 18.4 Hz, 1H); *α*-vinylboronate, δ = 6.03 ppm (m, 2H); *β*-*Z*-vinylboronate, δ = 5.50 ppm (d, *J* = 15.0 Hz, 1H); *β*-ethylboronate, δ = 2.69 ppm (m, 2H) in d_8-THF (^{1}H NMR spectrum was recorded after 88 h)

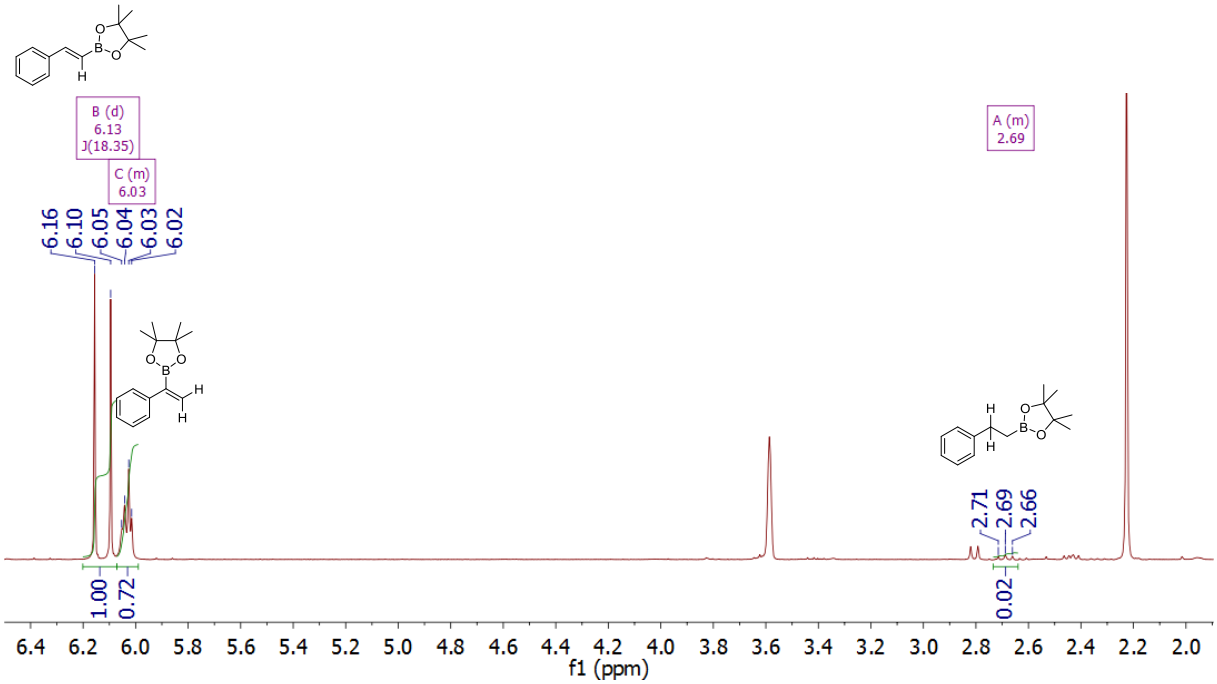

Figure S3.6. Selected characteristic proton signals of *β*-*E*-vinylboronate, δ = 6.13 ppm (d, *J* = 18.4 Hz, 1H); *α*-vinylboronate, δ = 6.03 ppm (m, 2H); *β*-ethylboronate, δ = 2.69 ppm (m, 2H) in d_8-THF (^{1}H NMR spectrum was recorded after 22 h)

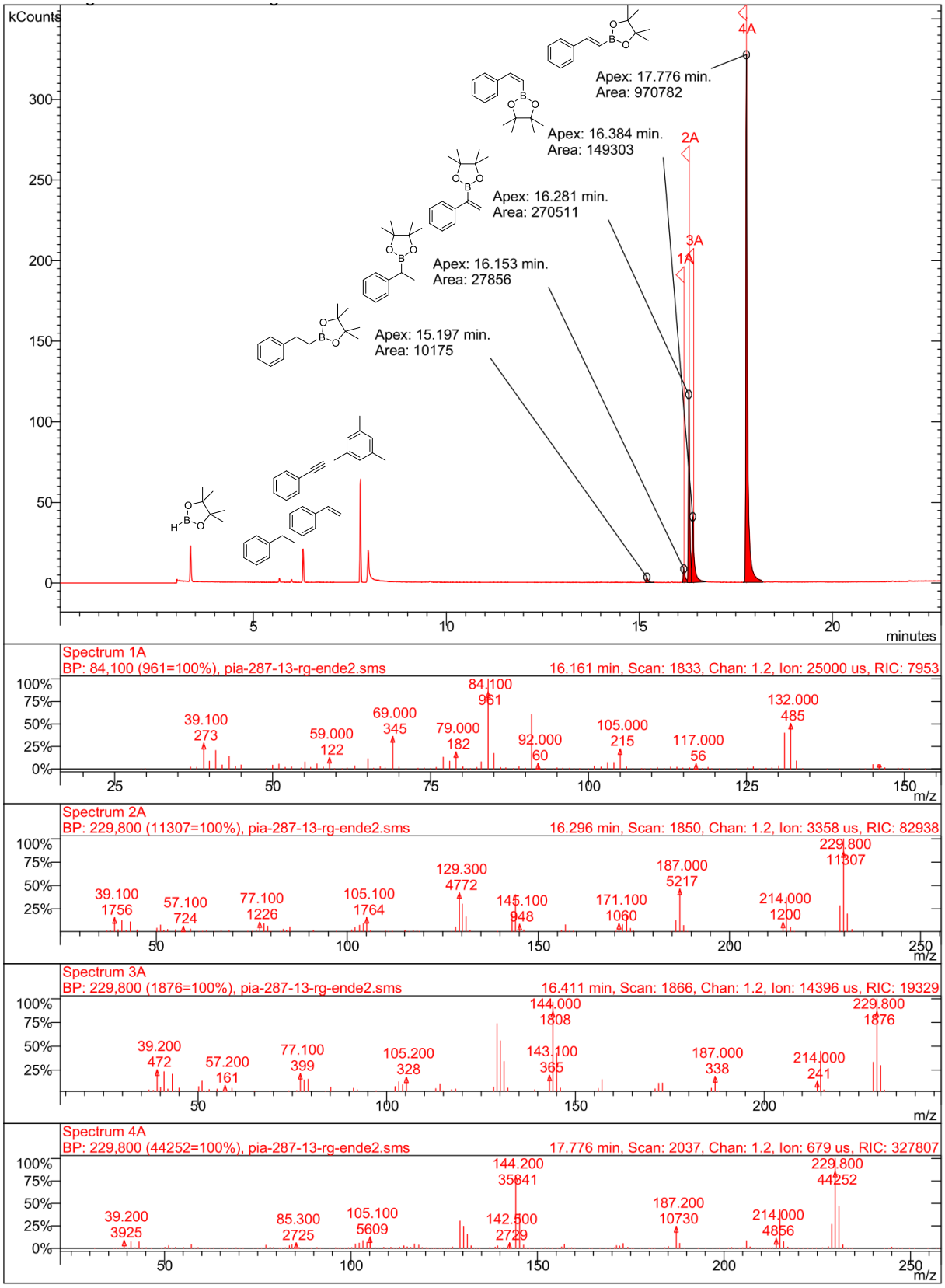

Figure S3.7. Hydroboration of phenylacetylene by pinacolborane using complex **3.4**. GC-MS analysis of the reaction mixture (measured after 88 h)

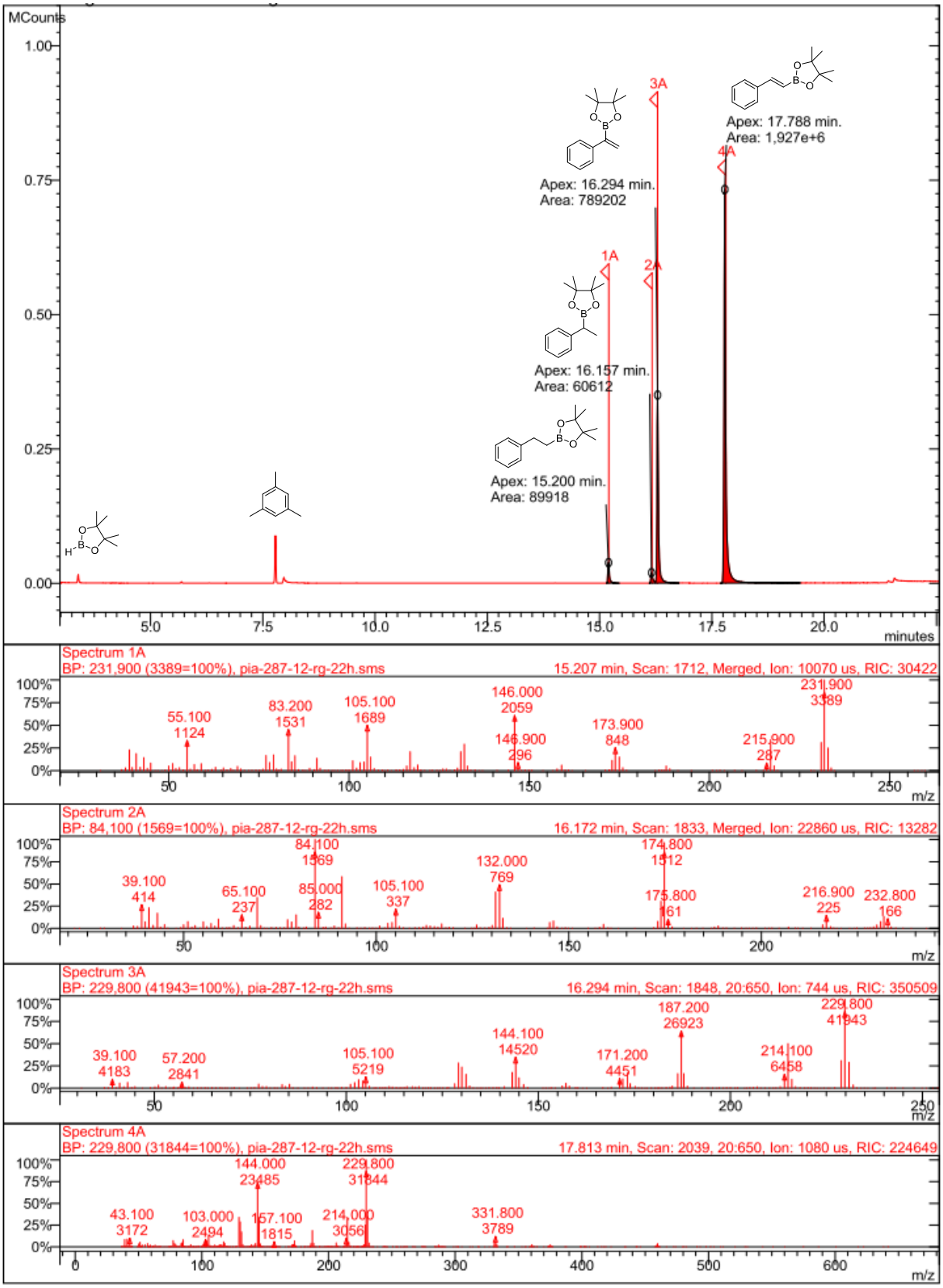

Figure S3.8. Hydroboration of phenylacetylene by pinacolborane using complex **3.10a**. GC-MS analysis of the reaction mixture (measured after 22 h).

4 Crystallographic data

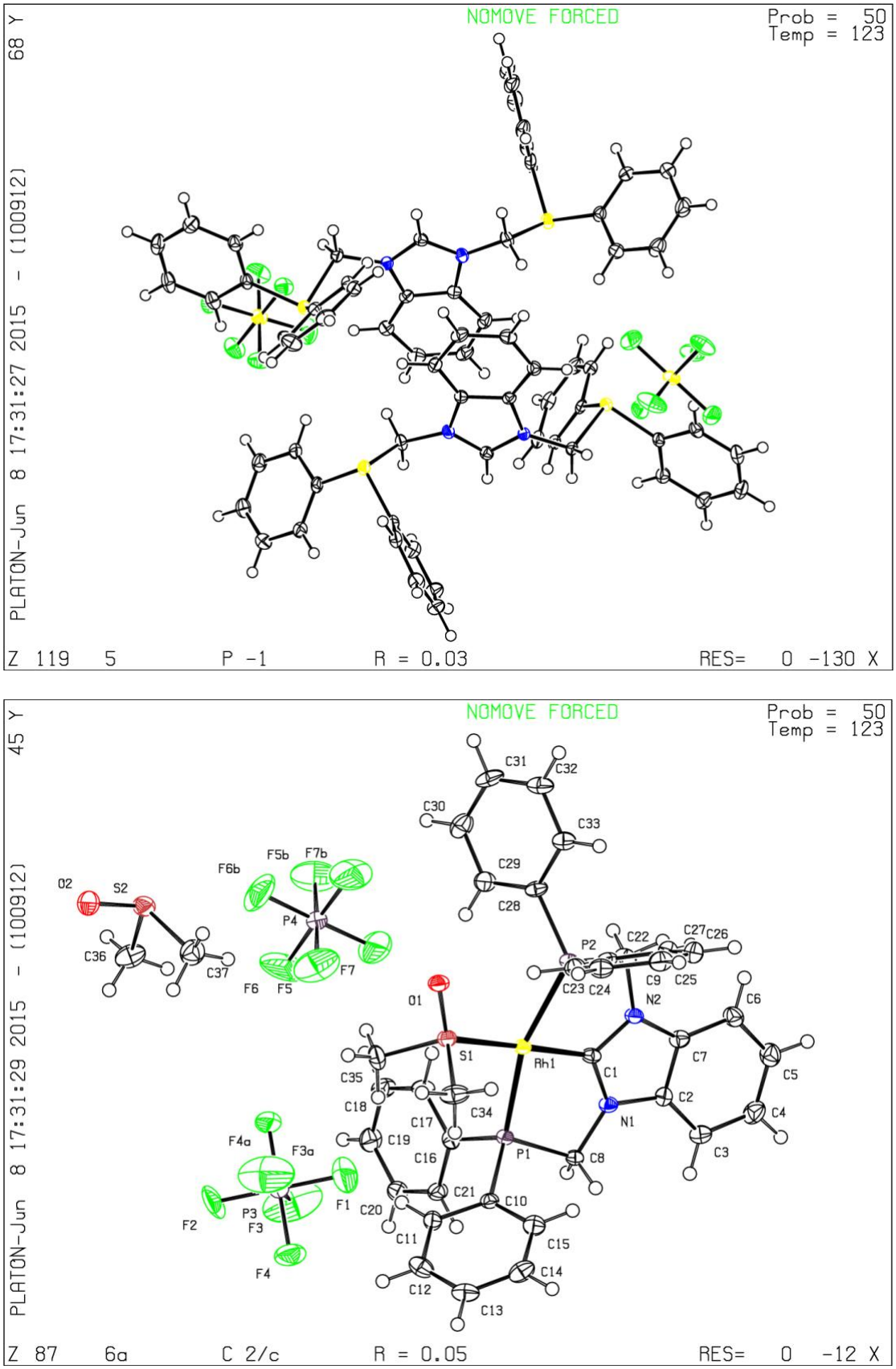

Figure S4.1. Crystal structures **2.5** (at the top) and **2.6a** (at the bottom)

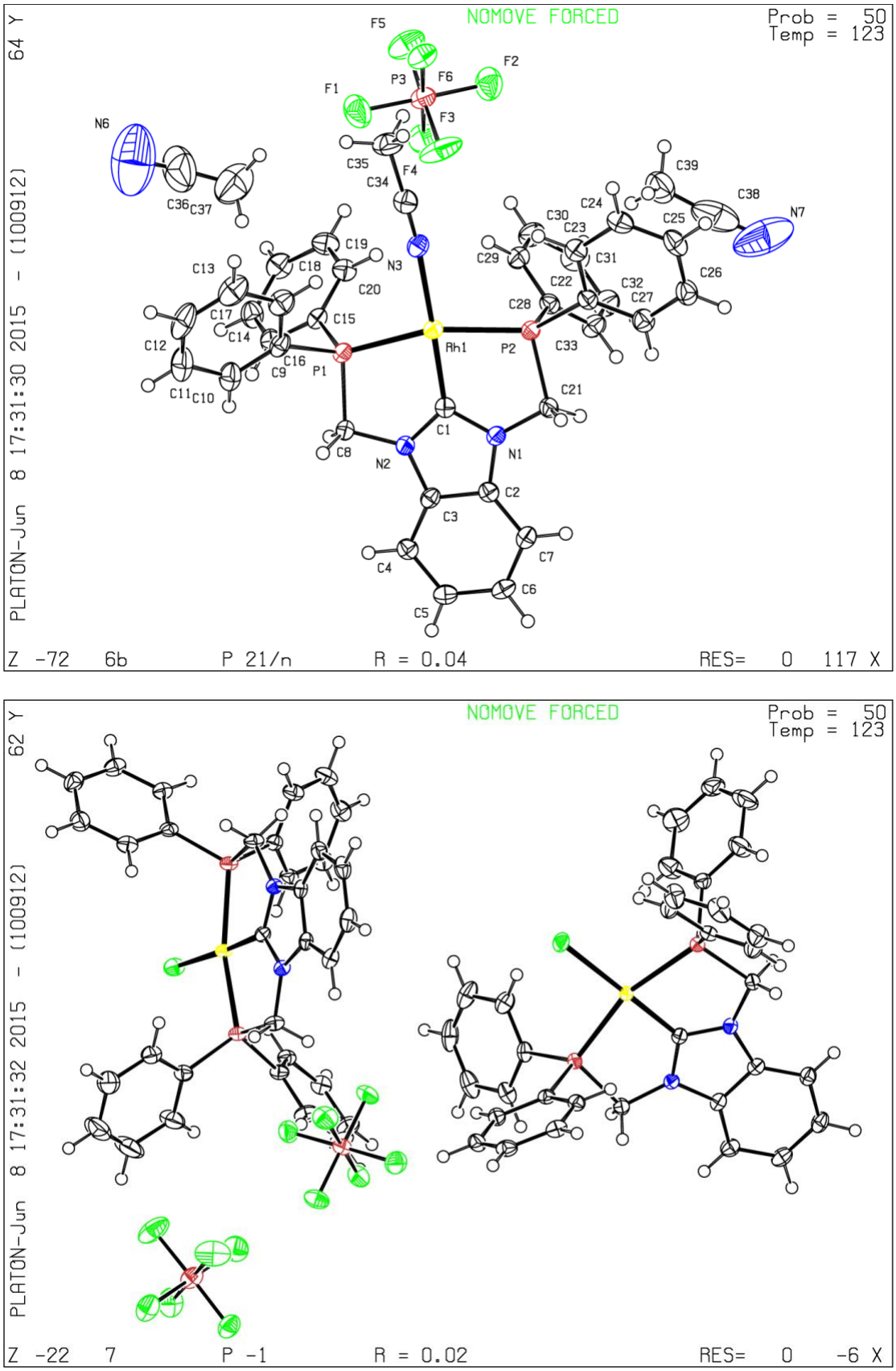

Figure S4.2. Crystal structures of **2.6b** (at the top) and **2.7** (at the bottom)

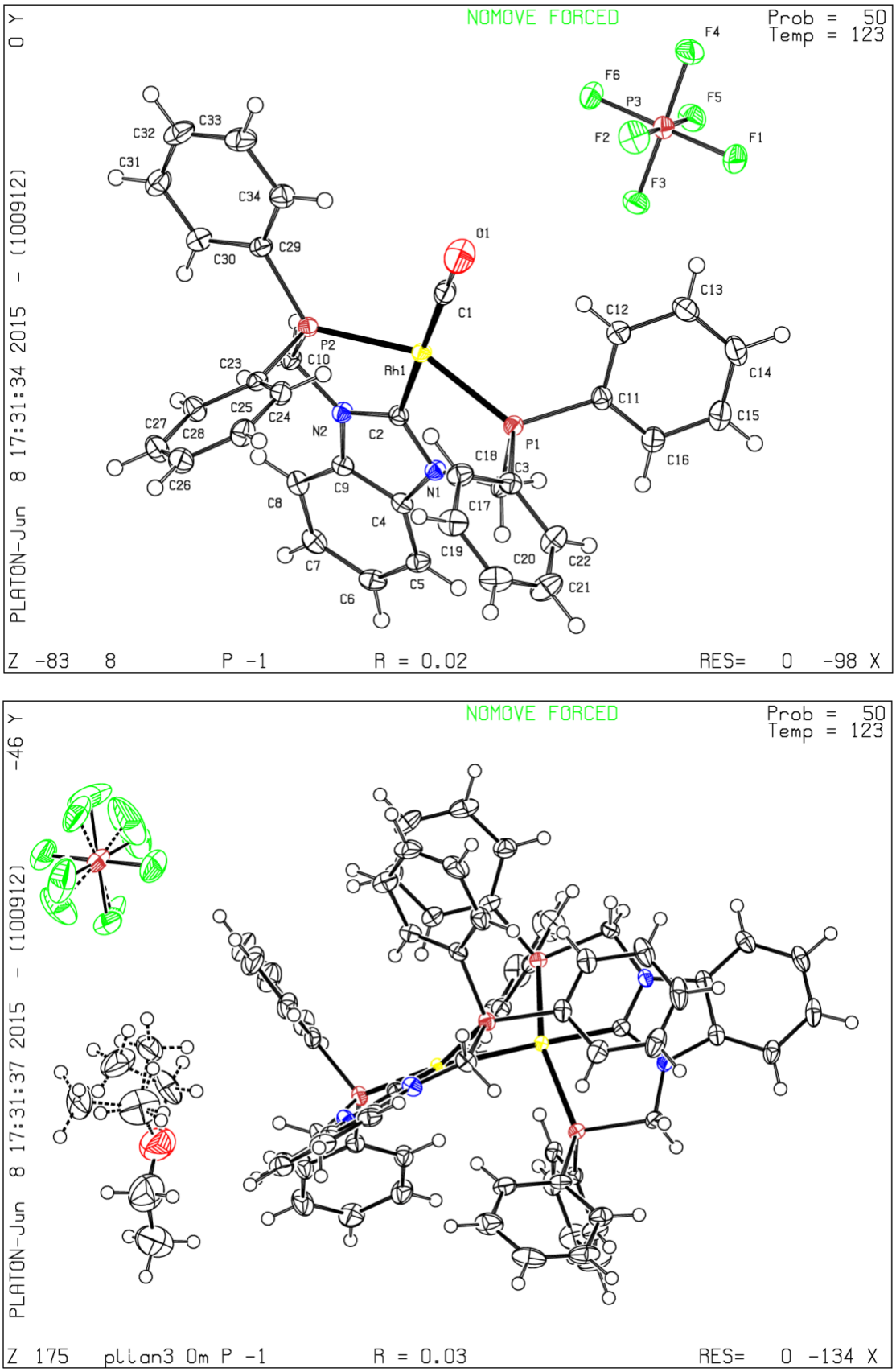

Figure S4.3 Crystal structures of **2.8** (PF_6 were excluded, at the top) and **2.10** (at the bottom).

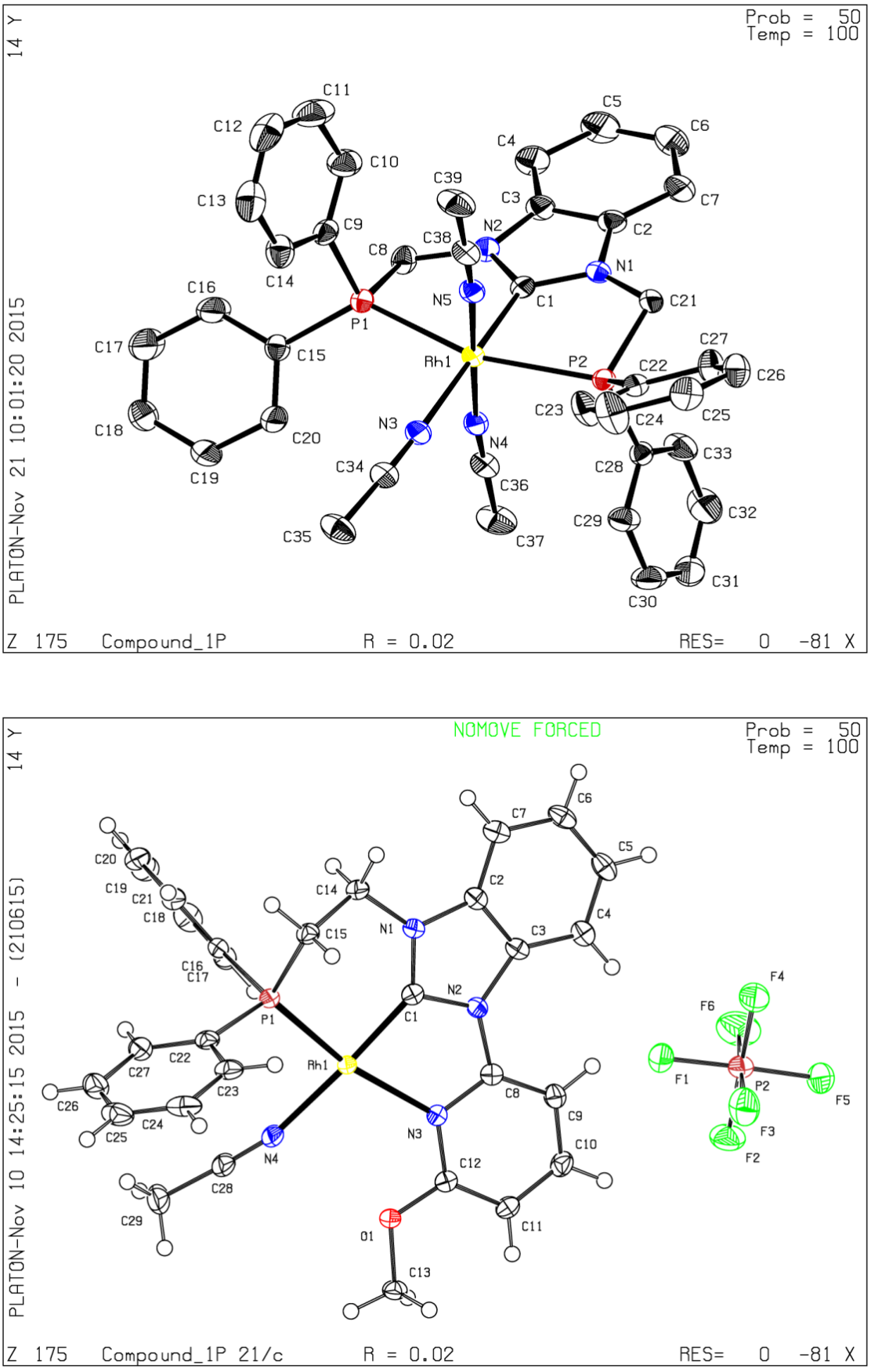

Figure S4.4 Crystal structures of **2.12** (at the top) and **3.10a** (at the bottom).

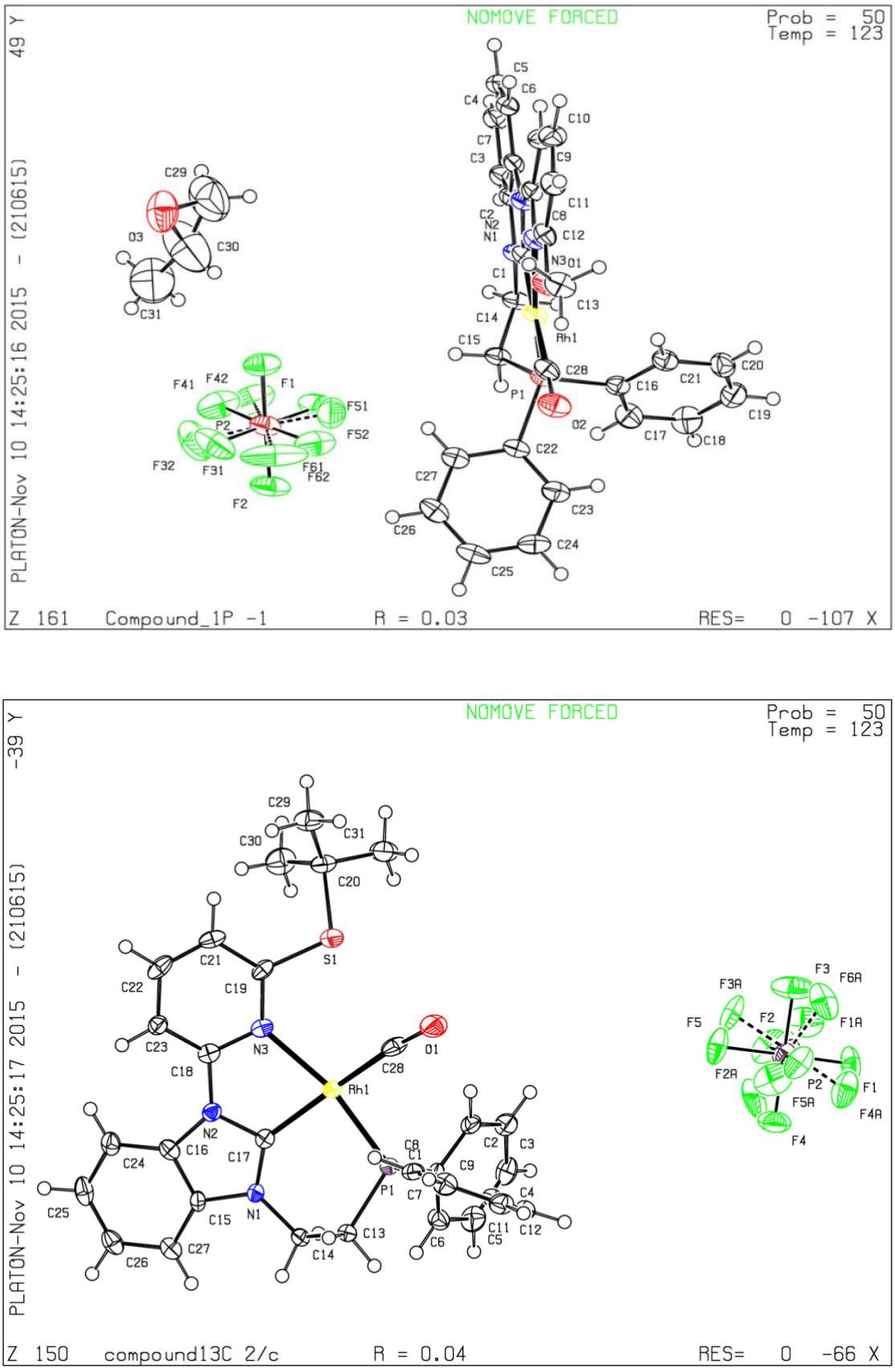

Figure S4.5 Crystal structures of **3.13a** (at the top) and **3.13b** (at the bottom).

Table S4.1. Crystallographic data. [a] R1 = $\sum(||F_o|-|F_c||)/\sum|F_o|$; wR2 = $(\sum [w(F_o^2-F_c^2)^2]/ \sum[w(F_o^2)^2])^{1/2}$; GOF = $(\sum[w(F_o^2-F_c^2)^2]/(n-p))^{1/2}$

	2.5	**2.6b**	**2.6a**	**2.7**	**2.8**
Formula	$C_{33}H_{29}F_6N_2P_3$	$C_{39}H_{37}F_6N_5P_3Rh$	$C_{37}H_{40}F_6N_2O_2P_3RhS_2$	$C_{33}H_{28}ClF_6N_2P_3Pd$	$C_{34}H_{28}F_6N_2OP_3Rh$
Fw	660.49	885.56	918.67	801.33	790.40
Colour/habit	yellow fragment	red-brown fragment	yellow needle	yellow plate	yellow fragment
Cryst. dimensions (mm^3)	0.45 x 0.50 x 0.65	0.17 x 0.23 x 0.28	0.03 x 0.08 x 0.30	0.13 x 0.36 x 0.48	0.13 x 0.15 x 0.51
Crystal system	triclinic	monoclinic	monoclinic	triclinic	triclinic
Space group	*P* -1	*P* $2_1/n$	*C* 2/*c*	*P* -1	*P* -1
a, Å	13.1758(5)	10.2501(7)	16.8923(4)	13.8424(6)	11.0952(5)
b, Å	13.3209(5)	18.5633(13)	23.2464(6)	15.2793(7)	11.8453(5)
c, Å	18.7343(6)	20.8712(14)	19.7992(5)	15.9485(7)	12.5833(6)
α, deg	75.565(2)	90	90	86.477(2)	99.828(2)
β, deg	72.988(1)	101.726(3)	95.9309(12)	89.297(2)	94.714(2)
γ, deg	82.484(2)	90	90	76.105(2)	94.948(2)
V, $Å^3$	3039.04(19)	3888.4(5)	7733.2(3)	3268.2(3)	1615.50(13)
Z	4	4	8	4	2
T, K	123	123	123	123	123
D_{calcd}, g cm^{-3}	1.444	1.513	1.578	1.629	1.625
μ, mm^{-1}	0.260	0.627	0.739	0.858	0.744
F(000)	1360	1800	3744	1608	796
θ range, deg	2.33 – 25.34	1.48 – 25.37	1.50 – 25.45	1.38 – 25.46	1.65 – 25.39
Index ranges (*h*, *k*, *l*)	±15, ±16, ±22	±12, ±22, ±25	±20, ±28, ±23	±16, ±18, ±19	±13, ±14, ±15
No. of rflns collected	142753	89396	71083	114337	45951
No. of independent rflns/R_{int}	11192/0.0362	7110/0.0428	7138/0.0368	12112/0.0200	5924/0.0287
No. of observed rflns ($I>2\sigma(I)$)	9671	6269	6604	11308	5778
No. of data/restraints/parameters	11192/0/ 793	7110 /0/ 490	7138/0/484	12112/0/829	5924/0/424
R1/wR2 ($I>2\sigma(I)$)[a]	0.0294/0.0725	0.0377/0.0973	0.0512/0.1255	0.0189/0.0504	0.0180/0.0466
R1/wR2 (all data)[a]	0.0366/0.0764	0.0451/0.1053	0.0542/0.1271	0.0208/0.0514	0.0186/0.0470
GOF (on F^2)[a]	1.042	1.077	1.207	1.051	1.056
Largest diff peak and hole (e $Å^{-3}$)	0.047/-0.342	1.940/-1.055	4.320/-0.529	0.348/-0.313	0.442/-0.203

	2.10	**2.12b**	**3.10a**	**3.13a**	**3.13b**
Formula	$C_{70}H_{67}F_6N_4OP_5Rh_2$	$C_{39}H_{37}F_{18}N_5P_5Rh$	$C_{29}H_{27}F_6N_4OP_2Rh$	$C_{31}H_{30}F_6N_3O_3P_2Rh$	$C_{31}H_{30}F_6N_3OP_2RhS$
fw	1454.92	1175.49	726.40	771.43	771.49
Colour/habit	orange fragment	clear-colourless fr.	red fragment	orange needle	
Cryst. dimensions (mm^3)	0.16 x 0.19 x 0.27	0.17 x 0.39 x 0.50	0.34 x 0.50 x 0.78	0.08 x 0.08 x 0.61	0.035 x 0.198 x 0.206
Crystal system	triclinic	monoclinic	monoclinic	triclinic	monoclinic
Space group	*P* -1	*C* 1 2/c 1	*P* $2_1/c$	*P* $\bar{1}$	*C 1 2/c 1*
a, Å	12.0213(3)	19.2785(13)	16.4294(4)	9.5361(2)	32.8435(8)
b, Å	15.1548(4)	15.7654(10)	13.4592(3)	13.0869(3)	7.4640(3)
c, Å	18.3327(5)	32.631(2)	13.4920(3)	13.7798(4)	28.2001(8)
α, deg	99.852(2)	90	90	98.9649(13)	90
β, deg	103.228(1)	99.948(3)	104.0655(9)	107.1343(12)	115.383(2)
γ, deg	94.338(1)	90	90	100.1015(12)	90
V, $Å^3$	3180.27(15)	97668.5(11)	2893.99(12)	1578.05(7)	6245.7(4)
Z	2	8	4	2	8
T, K	123	100(2)	100	123	123
D_{calcd}, g cm^{-3}	1.519	1.599	1.667	1.623	1.641
μ, mm^{-1}	0.710	0.617	0.771	0.716	0.784
F(000)	1484	4704	1464	780	3120
θ range, deg	2.32 – 31.45	2.54 – 28.28	1.98 – 25.46	2.00 – 25.43	2.51 – 25.40
Index ranges (*h*, *k*, *l*)	±15, ±18, ±22	±25, ±21, ±43	±19, ±16, ±16	±11, ±15, ±16	±39, -8 – 9, -31 – 33
No. of rflns collected	82566	89396	70451	48206	22734
No. of independent rflns/R_{int}	12981/0.0443	7110/0.0428	5369/0.022	5813/0.027	5717/0.1371
No. of obs. rflns ($I>2\sigma(I)$)	11336	6269	5140	5117	3410
No. of data/restraints/param.	12981/13/868	12118/0/619			5717/27/473
R1/wR2 ($I>2\sigma(I)$)[a]	0.0257/0.0595	0.0397/0.1106	0.0186/0.0468	0.0312/0.0762	0.0423/0.0642
R1/wR2 (all data)[a]	0.0329/0.0621	0.0500/0.1178	0.0198/0.0479	0.0390/0.0825	0.1056/0.0781
GOF (on F^2)[a]	1.035	1.043	1.031	1.035	0.938
Largest peak and hole (e $Å^{-3}$)	0.597/-0.553	0.989/-0.635			0.819/-0.728

Conclusions and Outlook

In chapter I, an introduction is given to rational design, structural peculiarities, and strategies of preparation of pincer complexes as well as their reactivity in conversion of small molecules. Recently, it was highlighted that the participation of ligands in substrate activation often results in extraordinary reactivity of pincer complexes. Therefore, we paid particular attention to principles of cooperative reactivity. This includes a systematic overview of metal ligand cooperative heterolytic substrate activation, hemilability, and furnishing of pincer complexes with pendant heteroatomic centers. The crucial impact of cooperativity on the catalytic performance was elucidated on the example of hydrogenation of CO_2 and CO_2-derived products. Within the framework of the research project, a detailed overview about ionic liquids in transition metal-catalyzed hydroformylation reactions was performed.[128] The uses of CO_2 as chemical C^1 feedstock or *sc*CO_2 as carrier for the reagents and products in the ionic liquid-based hydroformylation complement this chapter.

The results reported in chapter II and III present an extensive work in the field of carbene-centered pincer complexes. In chapter II, a gram-scale synthesis of a benzimidazolium-based pincer ligand precursor is described. The new [5,5]-membered carbene-centered ($PC^{BIm}P$)Rh^{I} and ($PC^{BIm}P$)Pd^{II} complexes were synthesized and fully characterized using NMR, IR, MS, and X-ray techniques. The thermal stability and reactivity of ($PC^{BIm}P$)Rh^{I} complexes were assessed in both the solid state and solution. On the basis of the studied stoichiometric and catalytic transformations, it was clearly shown that the $PC^{BIm}P$-ligated rhodium(I) complex basically tends to decarbonylate the oxygen-containing substrates. It was found that complexes [($PC^{BIm}P$)Rh^{I}(CH_3CN)][PF_6] **2.6b** and [($PC^{BIm}P$)Rh^{I}(CO)][PF_6] **2.8** produce small amounts of potassium formate in acetone/H_2O at 60 °C, 40 h. No decomposition of either [($PC^{BIm}P$)Rh(L)] or [PF_6] was detected under a reducing atmosphere of H_2 in a basic environment. Notably, complex **2.6b** has been converted quantitatively into **2.8** in an acetone/H_2O mixture during the hydrogenation reaction, in accordance with the report made by Ozerov *et al*. The observations that we made on a range of reactions indicate that [($PC^{BIm}P$)Rh^{I}(CH_3CN)][PF_6] **2.6b** undergoes two main conversion pathways, forming more thermodynamically stable species: a carbonyl complex and a hydride-containing dimer. We also describe the synthesis and single-crystal X-ray structural analysis of a dinuclear μ-hydride rhodium cluster as well as the smooth oxidation of [($PC^{BIm}P$)Rh^{I}(CH_3CN)][PF_6] **2.6b** to a new [($PC^{BIm}P$)Rh^{III}(CH_3CN)$_3$][PF_6]$_3$ **2.12** complex using [(C_6H_5)$_3$C][PF_6]. Additionally, it was found that rhodium complex **2.6b** catalyzes the B–H addition on the triple bond of

phenylacetylene, selectively leading to (E)-vinylboronate a through conventional *cis*-hydroboration pathway.

In chapter III, a new series of neutral hybrid ligand systems is presented. The gram-scale synthesis of the methylene- and ethylene-bridged carbene-centered pincer ligand precursors containing both nitrogen and phosphorus donors has been developed. The corresponding mononuclear [5,5]- and [5,6]-membered $NC^{BIm}P$ rhodium complexes were achieved and characterized using common analytical techniques. In addition, the methoxy-derivatized [5,5]- and [5,6]-membered $(NC^{BIm}P)Rh^{I}$ organometallics were explored as catalysts for hydroboration of phenylacetylene. We report herein the isolation and single crystal X-ray structural analysis of acetonitrile and carbonyl coordinated [5,6]-membered $NC^{BIm}P$ rhodium organometallic compounds as well as the first results of iridium coordination. We also were able to furnish the pyridyl moieties of the ligand scaffolds with the pendant oxygen and sulphur atoms protected with alkyl groups. Relying on X-ray single crystal analysis, it was shown that these functional groups are situated in direct proximity to the metals coordination sites. The last are located *trans* to the carbenes and can be potentially opened for substrate coordination by dissociation of weakly bound solvent molecules. The comparative analysis of structures of both [5,6]-membered methoxy and *tert*-butyl thiol-derivatized carbonyl complexes in the solid state shows significant repulsion between bulky thiol group and the strong bound carbonyl. Thus, the increase of steric demand in the *ortho*-position of the pyridyl unit resulted in the in-plane distortion of the complex and, as consequence, the weakening of N–Rh bond.

Although the expected hemilability of types II and III[75, 301] could lead to specific reactivity of such complexes, the on/off coordination of functionalized N^{Py}-auxiliary ligand fragment is rather undesirable in order to ensure the target interactions of pendant heteroatomic groups with the substrates in the second coordination sphere. For implementation of this principle very strong metal-ligand bonding and high rigidity of the ligand scaffold are required. The rational design of the complexes based on pincer ligands furnished with reactive pendant groups would open new catalytic pathways for the cooperative conversion of small molecules through frustrated lewis acid-base interactions.[302] Through this work on the [n,n]-membered carbene-centered complexes we point out the significant interest in synthetic accessibility of heterocyclic pincer ligands and complexes, as well as their potential cooperative reactivity in catalytic processes.

One of the major research priorities in this field to focus is preparation and characterization of ($PC^{BIm}P$)Ru- and ($PC^{BIm}P$)Ir-based organometallic compounds as well as investigation of catalytic reactivity of ($PC^{BIm}P$)Rh^{III}, ($PC^{BIm}P$)Ru^{II}, ($PC^{BIm}P$)$Ir^{I/III}$ in neutral, basic and acidic environments. The stoichiometric reactions of these complexes with LiTMS, $NaBH_4$, $NaEt_3BH$, [mbim][Cl] and CF_3COOAg leading to the substitution of PF_6 anion are also of significant interest. The major issue, which still remains open is an efficient conversion of CO_2 using carbene-centered ($PC^{NHC}P$)M (M = Ru, Ir, Rh, Pd) catalyst motif. Therefore, a special focus should be put on identification of reactive centers of the $PC^{BIm}P$ and $^{FG}NC^{BIm}P$ ligands in these complexes in order to reveal possible cooperativity profiles. In particular, the role and directing character of pendant functional groups of the developed ($^{FG}NC^{BIm}P$)M architectures in the activation of H_2 and CO_2 should be studied in details. Further, the deprotection reactions of pendant methoxy and *tert*-butyl groups should be elaborated. On the other hand, it is also important to understand the main decomposition pathways of the ($PC^{BIm}P$)M systems to achieve robust catalysts.

Zusammenfassung und Ausblick

Kapitel I gibt eine Einführung in das rationelle Design, die strukturellen Besonderheiten und Strategien der Synthese von Pinzerkomplexen sowie ihre Reaktivität bei der Umsetzung kleiner Moleküle, die von großer Bedeutung für die in dieser Arbeit präsentierten Ergebnisse sind. Es wurde vor kurzem festgestellt, dass das Mitwirken der Liganden in der Substrataktivierung eine außergewöhnliche Reaktivität der Pinzerkomplexe resultiert. Aus diesem Grund wurde die Aufmerksamkeit auf die Prinzipien der kooperativen Reaktivität gelenkt. Dies beinhaltet einen systematischen Überblick über die heterolytische Substrataktivierung mithilfe der Metallliganden, Hemilabilität und Derivatisierung der Pinzerkomplexe mit heteroatomaren Domänen. Der wesentliche Einfluss des Zusammenwirkens auf die katalytische Aktivität wurde an dem Beispiel der Hydrierung von CO_2 und den CO_2-abgeleiteten Produkten veranschaulicht. Im Rahmen dieser Forschungsarbeit wurde eine detaillierte Übersicht über ionische Flüssigkeiten in Übergangsmetall-katalysierten Hydroformylierungsreaktionen erstellt.[128] Die Verwendung von CO_2 als chemischen C^1-Ausgangsstoff oder *sc*CO_2 als Träger für Reaktanden und Reaktionsprodukte in der auf ionischen Flüssigkeiten basierenden Hydroformylierung vervollständigt dieses Kapitel.

Die in Kapitel II und III präsentierten Ergebnisse zeigen eine Arbeit in dem Bereich der Carben-zentrierten Pinzerkomplexe. In Kapitel II wird die Synthese von Benzimidazolium-basierten Pinzerligand-Precursoren beschrieben. Die neuen [5,5]-gliedrigen Carben-zentrierten $(PC^{BIm}P)Rh^{I}$ und $(PC^{BIm}P)Pd^{II}$-Komplexe wurden dargestellt und mithilfe von NMR-, IR-, MS- und Röntgenanalysen vollständig charakterisiert. Die thermische Stabilität und Reaktivität der $(PC^{BIm}P)Rh^{I}$-Komplexe wurde sowohl in Lösung als auch im festen Zustand bewertet. An den Beispielen der stöchiometrischen und katalytischen Umsetzungen wurde eindeutig gezeigt, dass der $PC^{BIm}P$-gebundene Rhodium(I)-Komplex grundsätzlich dazu neigt sauerstoffhaltige Substrate zu decarbonylieren. Die Komplexe $[(PC^{BIm}P)Rh^{I}(CH_3CN)][PF_6]$ **2.6b** und $[(PC^{BIm}P)Rh^{I}(CO)][PF_6]$ **2.8** produzieren kleine Mengen an Kaliumformiat in einem Aceton/Wasser-Gemisch bei 60 °C und 40 h. Es wurde keine Zersetzung von $[(PC^{BIm}P)Rh(L)]$ noch von $[PF_6]$ unter reduzierender Wasserstoffatmosphäre in einer basischen Umgebung detektiert. Beachtenswert ist, dass Komplex **2.6b** während der Hydrierugsreaktion in einem Aceton-Wasser-Gemisch, gemäß Ozerov *et al*., quantitativ zu Verbingung **2.8** umgesetzt wird. Eine Reihe von Reaktionen indiziert, dass $[(PC^{BIm}P)Rh^{I}(CH_3CN)][PF_6]$ **2.6b** zwei Hauptreaktionswegen unterliegt, die zu den thermodynamisch stabileren Spezies, einem Carbonylkomplex und einem Hydrid-

haltigen Dimer, führt. Es werden ebenfalls die Synthese und Einkristall-Röntgenstrukturanalyse von dinuklearen μ-Hydrid-Rhodium-Clustern sowie die milde Oxidation von $[(PC^{BIm}P)Rh^{I}(CH_3CN)][PF_6]$ zu einem neuen $[(PC^{BIm}P)Rh^{III}(CH_3CN)_3]3[PF_6]$-Komplex mithilfe von $[(C_6H_5)_3C][PF_6]$ beschrieben. Außerdem wurde gefunden, dass $PC^{BIm}PRh^{I}$ die B–H-Addition an der Dreifachbindung von Phenylacetylen katalysiert und durch eine konventionelle *cis*-Hydroborierung zu (E)-Vinylboronat führt.

In Kapitel III wird eine neue Reihe von neutralen Hybridligand-Systemen vorgestellt. Es wurde Synthesen von Methylen- und Ethylen-verbrückten Carben-zentrierten Pinzerligand-Precursoren entwickelt, die Stickstoff- und Phosphor-Donoren enthalten. Die mononuklearen [5,5]- und [5,6]-gliedrigen $NC^{BIm}P$-Rhodiumkomplexe wurden erhalten und durch gängige analytische Techniken charakterisiert. Außerdem wurden die Methoxy-basierten [5,5]- und [5,6]-gliedrigen $(NC^{BIm}P)Rh^{I}$-Organometalle als Katalysatoren in der Hydroborierung von Phenylacetylen getestet. Neben der Isolierung und Einkristall-Röntgenstrukturanalyse von Acetonitril- und Carbonyl-koordinierten $NC^{BIm}P$-Rhodium-Organometallkomponenten, werden ebenfalls die ersten Ergebnisse der Koordination von Iridium beschrieben. Zudem war es möglich, den Pyridylrest des Ligandengerüsts mit Sauerstoff- und Schwefeleinheiten, die durch Alkylgruppen geschützt sind, auszustatten. Durch die Einkristall-Röntgenstrukturanalyse wurde gezeigt, dass diese Domäne in unmittelbarer Nähe der Koordinationszentren des Metalls liegen. Letztere sind *trans* zu dem Carben angeordnet und können durch die Dissoziation der labilen Lösungsmittelmolekülen für eine Substratkoordination geöffnet werden. Ein Vergleich der Strukturen der [5,6]-gliedrigen Methoxy- und *tert*-Butylthiol-derivatisierten Carbonylkomplexe zeigt eine signifikante Abstoßung der sterisch anspruchsvollen Thiolgruppe und der Carbonylgruppe. Somit resultiert aus der Erhöhung der sterischen Beanspruchung in der *ortho*-Position der Pyridyleinheit eine Verzerrung aus der Ebene des Komplexes und als weitergehende Konsequenz eine Schwächung der N–Rh-Bindung. Obwohl die erwartete Hemilabilität der Typen II und III[75, 301] zu einer spezifischen Reaktivität solcher Komplexe führen kann, ist die on/off-Koordination von funktionalisierten N^{Py}-Hilfsliganden eher unerwünscht, um die Wechselwirkung der gebundenen heteroatomaren Domänen mit Substraten in der zweiten Koordinationssphäre zu gewährleisten. Für die Umsetzung dieses Prinzips werden sehr starke Metall-Ligand-Bindungen und eine hohe Starrheit des Ligandengerüsts benötigt. Das rationelle Design der Komplexe, die sich auf Pinzerliganden mit reaktiven Gruppen basieren, würde neue katalytische Reaktionswege für die kooperative Umsetzung von kleinen Molekülen durch Lewissäure-basierte Wechselwirkungen, eröffnen.[302]

Im Rahmen der Arbeit über [n,n]-gliedrige Carben-zentrierte Komplexe wird das große Interesse an der synthetischen Zugänglichkeit der heterozyklischen Pinzerliganden und –komplexen, sowie an ihrem Potenzial der kooperativen Reaktivität in katalytischen Prozessen hervorgehoben. Die fortdauernde Forschung im Bereich der Carbenkomplexe und die Kommerzialisierung der (Benz)Imidazolium-haltigen ionischen Flüssigkeiten, Feststoffe und Polymere werden die Entwicklung von organometallischer Verbindungnen, die auf einfach zugängliche funktionelle bidentate NHC-Liganden basieren, in der Zukunft intensiv vorantreiben.

Die weitere Entwicklung in diesem Forschungsgebiet liegt sowohl in der Synthese und Charakterisierung von ($PC^{BIm}P$)Ru- und ($PC^{BIm}P$)Ir-basierten Komplexe sowie in der Untersuchung der katalytischen Reaktivität von ($PC^{BIm}P$)Rh^{III}, ($PC^{BIm}P$)Ru^{II}, ($PC^{BIm}P$)$Ir^{I/III}$ in neutraler, basischer und saurer Umgebung. Um Reaktivität und Löslichkeit der Komplexe zu verbessern, sind ihre stöchiometrischen Reaktionen mit LiTMS, $NaBH_4$, $NaEt_3BH$, [mbim][Cl] und CF_3COOAg durch Substitution des PF_6-Anions fertigzustellen. Des Weiteren sollten die reaktiven Zentren von $PC^{BIm}P$- und $^{FG}NC^{BIm}P$-Liganden dieser Komplexe identifiziert werden, um mögliche kooperative Wechselwirkungen aufzudecken. Die Funktion und der dirigierende Charakter der heteroatomaren RY-Domäne von den synthetisierten ($^{RY}NC^{BIm}P$)M-Motiven sollten eingehender in der Aktivierung von H_2 und CO_2 untersucht werden. Außerdem sind die Entschützungsreaktionen der gebundenen Methoxy- und *tert*-Butylgruppen zu vervollständigen. Daneben ist es wichtig, die Hauptreaktionswege der Zersetzung des ($PC^{BIm}P$)M-Systems zu verstehen, um robuste Katalysatoren zu entwickeln. Andererseits bleibt das Thema der effizienten Umsetzung von CO_2 mittels Carben-zentrierter ($PC^{NHC}P$)M (M = Ru, Ir, Rh, Pd) Katalysatorstrukturen weiterhin offen.

References

1. Schüth, F., *Chem. Unserer Zeit* **2006,** *40*, 92-103.

2. In *Organometallic Pincer Chemistry*, Koten, G. v.; Milstein, D., Eds. Springer-Verlag Berlin Heidelberg 2013; p 356.

3. Punji, B.; Emge, T. J.; Goldman, A. S., *Organometallics* **2010,** *29*, 2702-2709.

4. Feller, M.; Iron, M. A.; Shimon, L. J. W.; Diskin-Posner, Y.; Leitus, G.; Milstein, D., *J. Am. Chem. Soc.* **2008,** *130*, 14374-14375.

5. Tulchinsky, Y.; Iron, M. A.; Botoshansky, M.; Gandelman, M., *Nature Chem.* **2011,** *3*, 525-531.

6. Adams, J. J.; Arulsamy, N.; Roddick, D. M., *Organometallics* **2011,** *30*, 697-711.

7. Choi, J.; MacArthur, A. H. R.; Brookhart, M.; Goldman, A. S., *Chem. Rev. (Washington, DC, U. S.)* **2011,** *111*, 1761-1779.

8. Segawa, Y.; Yamashita, M.; Nozaki, K., *J. Am. Chem. Soc.* **2009,** *131*, 9201-9203.

9. Hill, A. F.; McQueen, C. M. A., *Organometallics* **2014,** *33*, 1909-1912.

10. Whited, M. T.; Deetz, A. M.; Boerma, J. W.; DeRosha, D. E.; Janzen, D. E., *Organometallics* **2014,** *33*, 5070-5073.

11. Schuster, E. M.; Botoshansky, M.; Gandelman, M., *Angew. Chem. Int. Ed.* **2008,** *47*, 4555-4558.

12. Schuster, E. M.; Botoshansky, M.; Gandelman, M., *Dalton Transactions* **2011,** *40*, 8764-8767.

13. Kimura, T.; Uozumi, Y., *Organometallics* **2006,** *25*, 4883-4887.

14. Bolliger, J. L.; Blacque, O.; Frech, C. M., *Angew. Chem. Int. Ed.* **2007,** *46*, 6514-6517.

15. Gupta, M.; Hagen, C.; Flesher, R. J.; Kaska, W. C.; Jensen, C. M., *Chem. Commun. (Cambridge, U. K.)* **1996**, 2083-2084.

16. M. Jensen, C., *Chem. Commun. (Cambridge, U. K.)* **1999**, 2443-2449.

17. Xu, W.-w.; P. Rosini, G.; Krogh-Jespersen, K.; S. Goldman, A.; Gupta, M.; M. Jensen, C.; C. Kaska, W., *Chem. Commun. (Cambridge, U. K.)* **1997**, 2273-2274.

18. Allen, K. E.; Heinekey, D. M.; Goldman, A. S.; Goldberg, K. I., *Organometallics* **2013,** *32*, 1579-1582.

19. Ritu Ahuja, B. P., Michael Findlater, Carolyn Supplee, William Schinski,; Goldman, M. B. a. A. S., *Nature Chem.* **2011,** *3*, 167-171.

20. Ahuja, R.; Punji, B.; Findlater, M.; Supplee, C.; Schinski, W.; Brookhart, M.; Goldman, A. S., *Nature Chem.* **2011** *3*, 167-171.

21. Morales-Morales, D.; Redon, R.; Wang, Z.; Lee, D. W.; Yung, C.; Magnuson, K.; Jensen, C. M., *Can. J. Chem.* **2001,** *79*, 823-829.

22. Haibach, M. C.; Kundu, S.; Brookhart, M.; Goldman, A. S., *Acc. Chem. Res.* **2012,** *45* 947-958.

23. Levy, R.; Azerraf, C.; Gelman, D.; Rueck-Braun, K.; Kapoor, P. N., *Catal. Commun.* **2009,** *11*, 298-301.

24. Polukeev, A. V.; Petrovskii, P. V.; Peregudov, A. S.; Ezernitskaya, M. G.; Koridze, A. A., *Organometallics* **2013,** *32*, 1000-1015.

25. Bernskoetter, W. H.; Brookhart, M., *Organometallics* **2008,** *27*, 2036-2045.

26. Clarke, Z. E.; Maragh, P. T.; Dasgupta, T. P.; Gusev, D. G.; Lough, A. J.; Abdur-Rashid, K., *Organometallics* **2006,** *25*, 4113-4117.

27. Zhang, X.; Fried, A.; Knapp, S.; Goldman, A. S., *Chem. Commun. (Cambridge, U. K.)* **2003**, 2060-2061.

28. Milstein, D., *Top. Catal.* **2010,** *53*, 915-923.

29. Filonenko, G. A.; Aguila, M. J. B.; Schulpen, E. N.; van Putten, R.; Wiecko, J.; Müller, C.; Lefort, L.; Hensen, E. J. M.; Pidko, E. A., *J. Am. Chem. Soc.* **2015,** *137*, 7620-7623.

30. Balaraman, E.; Fogler, E.; Milstein, D., *Chem. Commun. (Cambridge, U. K.)* **2012,** *48*, 1111-1113.

31. Hooper, J. F.; Chaplin, A. B.; González-Rodríguez, C.; Thompson, A. L.; Weller, A. S.; Willis, M. C., *J. Am. Chem. Soc.* **2012,** *134*, 2906-2909.

32. Timpa, S. D.; Pell, C. J.; Ozerov, O. V., *J. Am. Chem. Soc.* **2014,** *136*, 14772-14779.

33. Adams, J. J.; Arulsamy, N.; Roddick, D. M., *Organometallics* **2012,** *31*, 1439-1447.

34. Hasegawa, M.; Segawa, Y.; Yamashita, M.; Nozaki, K., *Angew. Chem., Int. Ed.* **2012,** *51*, 6956-6960.

35. Masuda, Y.; Hasegawa, M.; Yamashita, M.; Nozaki, K.; Ishida, N.; Murakami, M., *J. Am. Chem. Soc.* **2013,** *135*, 7142-7145.

36. Kang, P.; Cheng, C.; Chen, Z.; Schauer, C. K.; Meyer, T. J.; Brookhart, M., *J. Am. Chem. Soc.* **2012,** *134*, 5500-5503.

37. Tanaka, R.; Yamashita, M.; Nozaki, K., *J. Am. Chem. Soc.* **2009,** *131*, 14168–14169.

38. Mitton, S. J.; Turculet, L., *Chem. – Eur. J.* **2012,** *18*, 15258-15262.

39. Balaraman, E.; Gunanathan, C.; Zhang, J.; Shimon, L. J. W.; Milstein, D., *Nature Chem.* **2011,** *3*, 609-614.

40. Filonenko, G. A.; van Putten, R.; Schulpen, E. N.; Hensen, E. J. M.; Pidko, E. A., *ChemCatChem* **2014,** *6*, 1526-1530.

41. Zhao, J.; Goldman, A. S.; Hartwig, J. F., *Science* **2005,** *307*, 1080-1082.

42. Feller, M.; Diskin-Posner, Y.; Shimon, L. J. W.; Ben-Ari, E.; Milstein, D., *Organometallics* **2012,** *31*, 4083-4101.

43. Balaraman, E.; Ben-David, Y.; Milstein, D., *Angew. Chem.* **2011,** *123*, 11906-11909.

44. Balaraman, E.; Gnanaprakasam, B.; Shimon, L. J. W.; Milstein, D., *J. Am. Chem. Soc.* **2010,** *132*, 16756-16758.

45. Khusnutdinova, J. R.; Ben-David, Y.; Milstein, D., *Angewandte Chemie International Edition* **2013,** *52*, 6269-6272.

46. Gunanathan, C.; Ben-David, Y.; Milstein, D., *Science* **2007,** *317*, 790-792.

47. Gunanathan, C.; Hölscher, M.; Pan, F.; Leitner, W., *J. Am. Chem. Soc.* **2012,** *134*, 14349-14352.

48. Lee, C.-I.; Zhou, J.; Ozerov, O. V., *J. Am. Chem. Soc.* **2013,** *135*, 3560-3566.

49. Anaby, A.; Butschke, B.; Ben-David, Y.; Shimon, L. J. W.; Leitus, G.; Feller, M.; Milstein, D., *Organometallics* **2014,** *33*, 3716-3726.

50. Zeng, J. Y.; Hsieh, M.-H.; Lee, H. M., *J. Organomet. Chem.* **2005,** *690*, 5662-5671.

51. Calimano, E.; Tilley, T. D., *J. Am. Chem. Soc.* **2009,** *131*, 11161-11173.

52. Serra, D.; Cao, P.; Cabrera, J.; Padilla, R.; Rominger, F.; Limbach, M., *Organometallics* **2011,** *30*, 1885-1895.

53. Morales-Morales, D., *Rev. Soc. Quim. Mex.* **2004,** *48*, 338-346.

54. Selander, N.; J. Szabó, K., *Chem. Rev. (Washington, DC, U. S.)* **2011,** *111*, 2048-2076.

55. Singleton, J. T., *Tetrahedron* **2003,** *59*, 1837-1857.

56. Shaw, B. K.; Patrick, B. O.; Fryzuk, M. D., *Organometallics* **2012,** *31*, 783-786.

57. Kundu, S.; Choliy, Y.; Zhuo, G.; Ahuja, R.; Emge, T. J.; Warmuth, R.; Brookhart, M.; Krogh-Jespersen, K.; Goldman, A. S., *Organometallics* **2009,** *28*, 5432-5444.

58. Steenwinkel, P.; James, S. L.; Gossage, R. A.; Grove, D. M.; Kooijman, H.; Smeets, W. J. J.; Spek, A. L.; van Koten, G., *Organometallics* **1998,** *17*, 4680-4693.

59. Parkin, G., *Chem. Rev. (Washington, DC, U. S.)* **2004,** *104*, 699-768.

60. Palomo, C.; Oiarbide, M.; Garcia, J. M., *Chem. Soc. Rev.* **2004,** *33*, 65-75.

61. Weston, J., *Chem. Rev. (Washington, DC, U. S.)* **2005,** *105*, 2151-2174.

62. Yano, J.; Kern, J.; Sauer, K.; Latimer, M. J.; Pushkar, Y.; Biesiadka, J.; Loll, B.; Saenger, W.; Messinger, J.; Zouni, A.; Yachandra, V. K., *Science* **2006,** *314*, 821-825.

63. Huff, C. A.; Kampf, J. W.; Sanford, M. S., *Organometallics* **2012,** *31*, 4643-4645.

64. Schwartsburd, L.; Iron, M. A.; Konstantinovski, L.; Ben-Ari, E.; Milstein, D., *Organometallics* **2011,** *30*, 2721-2729.

65. Gunanathan, C.; Milstein, D., *Chem. Rev. (Washington, DC, U. S.)* **2014,** *114*, 12024-12087.

66. Li, H.; Zheng, B.; Huang, K.-W., *Coord. Chem. Rev.* **2015,** *293–294*, 116-138.

67. Schneider, S.; Meiners, J.; Askevold, B., *Eur. J. Inorg. Chem.* **2012,** *2012*, 412-429.

68. Gunanathan, C.; Gnanaprakasam, B.; Iron, M. A.; Shimon, L. J. W.; Milstein, D., *J. Am. Chem. Soc.* **2010,** *132*, 14763-14765.

69. Gunanathan, C.; Milstein, D., *Acc. Chem. Res.* **2011,** *44*, 588-602.

70. Musa, S.; Romm, R.; Azerraf, C.; Kozuch, S.; Gelman, D., *Dalton Transactions* **2011,** *40*, 8760-8763.

71. Musa, S.; Fronton, S.; Vaccaro, L.; Gelman, D., *Organometallics* **2013,** *32*, 3069-3073.

72. Poverenov, E.; Leitus, G.; Shimon, L. J. W.; Milstein, D., *Organometallics* **2005,** *24*, 5937-5944.

73. Lindner, R.; van den Bosch, B.; Lutz, M.; Reek, J. N. H.; van der Vlugt, J. I., *Organometallics* **2011,** *30*, 499-510.

74. Frank, N.; Hanau, K.; Langer, R., *Inorg. Chem.* **2014,** *53*, 11335-11343.

75. Braunstein, P.; Naud, F., *Angew. Chem.* **2001,** *113*, 702-722.

76. Haibach, M. C.; Wang, D. Y.; Emge, T. J.; Krogh-Jespersen, K.; Goldman, A. S., *Chemical Science* **2013,** *4*, 3683-3692.

77. Poverenov, E.; Gandelman, M.; Shimon, L. J. W.; Rozenberg, H.; Ben-David, Y.; Milstein, D., *Chemistry – A European Journal* **2004,** *10*, 4673-4684.

78. Akai, N.; Ohno, K.; Aida, M., *Chem. Phys. Lett.* **2005,** *413*, 306-310.

79. Moore, C. M.; Szymczak, N. K., *Chem. Commun. (Cambridge, U. K.)* **2013,** *49*, 400-402.

80. Moore, C. M.; Dahl, E. W.; Szymczak, N. K., *Curr. Opin. Chem. Biol.* **2015,** *25*, 9-17.

81. Blum, Y.; Czarkle, D.; Rahamim, Y.; Shvo, Y., *Organometallics* **1985,** *4*, 1459-1461.

82. Shvo, Y.; Czarkie, D.; Rahamim, Y., *Journal of American Chemical Society* **1986,** *108*, 7400-7402.

83. Comas-Vives, A.; Ujaque, G.; Lledo´s, A., *Organometallics* **2008,** *27*, 4854-4863.

84. Conley, B. L.; Pennington-Boggio, M. K.; Boz, E.; Williams, T. J., *Chem. Rev. (Washington, DC, U. S.)* **2010,** *110*, 2294-2312.

85. Patel, B. P.; Crabtree, R. H., *J. Am. Chem. Soc.* **1996,** *118*, 13105-13106.

86. Lee, D.-H.; Patel, B. P.; Clot, E.; Eisenstein, O.; Crabtree, R. H., *Chem. Commun. (Cambridge, U. K.)* **1999**, 297-298.

87. Hull*, J. F.; Himeda*, Y.; Wang, W.-H.; Hashiguchi, B.; Periana, R.; Szalda, D. J.; Muckerman, J. T.; Fujita*, E., *Nature Chem.* **2012,** *4*, 383-388.

88. Ito, M.; Endo, Y.; Ikariya*, T., *Organometallics* **2008,** *27*, 6053-6055.

89. Chu, H. S.; Lau, C. P.; Wong, K. Y., *Organometallics* **1998,** *17*, 2768-2777.

90. Kawahara, R.; Fujita, K.-i.; Yamaguchi, R., *J. Am. Chem. Soc.* **2012,** *134*, 3643-3646.

91. Ou, W. C.; Cundari, T. R., *ACS Catalysis* **2015,** *5*, 225-232.

92. Casey, C. P.; Vos, T. E.; Singer, S. W.; Guzei, I. A., *Organometallics* **2002,** *21*, 5038-5046.

93. Redmore, S. M.; Rickard, C. E. F.; Webb, S. J.; Wright, L. J., *Inorg. Chem.* **1997,** *36*, 4743-4748.

94. Tutusaus, O.; Ni, C.; Szymczak, N. K., *J. Am. Chem. Soc.* **2013,** *135*, 3403-3406.

95. Moore, C. M.; Szymczak, N. K., Appended Functionality in Pincer Ligands. In *Pincer and Pincer-Type Complexes*, Wiley-VCH Verlag GmbH & Co. KGaA2014; pp 71-94.

96. Taylor, R. A.; Law, D. J.; Sunley, G. J.; White, A. J. P.; Britovsek, G. J. P., *Angew. Chem., Int. Ed.* **2009,** *48*, 5900-5903.

97. Zong, R.; Thummel, R. P., *J. Am. Chem. Soc.* **2005,** *127*, 12802-12803.

98. Kendall, A. J.; Zakharov, L. N.; Gilbertson, J. D., *Inorg. Chem.* **2010,** *49*, 8656-8658.

99. Wang, W.-H.; Himeda, Y., *Recent Advances in Transition Metal-Catalysed Homogeneous Hydrogenation of Carbon Dioxide in Aqueous Media*. 2012.

100. http://www.zsw-bw.de

101. Joo, O.-S.; Jung, K.-D.; Moon, I.; Rozovskii, A. Y.; Lin, G. I.; Han, S.-H.; Uhm, S.-J., *Ind. Eng. Chem. Res.* **1999,** *38*, 1808-1812.

102. Walther, D., *Nachrichten aus der Chemie* **2007,** *55*, 1188-1194.

103. Walther, D.; Ruben, M.; Rau, S., *Coord. Chem. Rev.* **1999,** *182*, 67-100.

104. North, M., *Angew. Chem.* **2009,** *121*, 4166-4168.

105. Yin, X.; Moss, J. R., *Coordination Chemistry Reviews* **1999,** *181*, 27-59.

106. Behr, A., *Angew. Chem.* **1988,** *100*, 681-698.

107. Ostapowicz, T. G.; Hölscher, M.; Leitner, W., *Chem. – Eur. J.* **2011,** *17*, 10329-10338.

108. Tanaka, R.; Yamashita, M.; Nozaki, K., *J. Am. Chem. Soc.* **2009,** *131*, 14168-14169.

109. Schmeier, T. J.; Dobereiner, G. E.; Crabtree, R. H.; Hazari, N., *J. Am. Chem. Soc.* **2011,** *133*, 9274-9277.

110. Jessop, P. G.; Joó, F.; Tai, C.-C., *Coord. Chem. Rev.* **2004,** *248*, 2425-2442.

111. Ohnishi, Y.-y.; Matsunaga, T.; Nakao, Y.; Sato, H.; Sakaki, S., *J. Am. Chem. Soc.* **2005,** *127*, 4021-4032.

112. Creutz, C.; Chou, M. H., *J. Am. Chem. Soc.* **2007,** *129*, 10108-10109.

113. Munshi, P.; Main, A. D.; Linehan, J. C.; Tai, C.-C.; Jessop, P. G., *J. Am. Chem. Soc.* **2002,** *124*, 7963-7971.

114. Hayashi, H.; Ogo, S.; Abura, T.; Fukuzumi, S., *J. Am. Chem. Soc.* **2003,** *125*, 14266-14267.

115. Yin, C.; Xu, Z.; Yang, S.-Y.; Ng, S. M.; Wong, K. Y.; Lin, Z.; Lau, C. P., *Organometallics* **2001,** *20*, 1216-1222.

116. Getty, A. D.; Tai, C.-C.; Linehan, J. C.; Jessop, P. G.; Olmstead, M. M.; Rheingold, A. L., *Organometallics* **2009,** *28*, 5466-5477.

117. Tai, C.-C.; Pitts, J.; Linehan, J. C.; Main, A. D.; Munshi, P.; Jessop, P. G., *Inorg. Chem.* **2002,** *41*, 1606-1614.

118. Himeda, Y.; Onozawa-Komatsuzaki, N.; Sugihara, H.; Kasuga, K., *J. Am. Chem. Soc.* **2005,** *127*, 13118-13119.

119. Musashi, Y.; Sakaki, S., *J. Am. Chem. Soc.* **2002,** *124*, 7588-7603.

120. Federsel, C.; Boddien, A.; Jackstell, R.; Jennerjahn, R.; Dyson, P. J.; Scopelliti, R.; Laurenczy, G.; Beller, M., *Angew. Chem.* **2010,** *122*, 9971-9974.

121. Darensbourg, D. J., *Inorg. Chem.* **2010,** *49*, 10765-10780.

122. Schmeier, T. J.; Hazari, N.; Incarvito, C. D.; Raskatov, J. A., *Chem. Commun. (Cambridge, U. K.)* **2011,** *47*, 1824-1826.

123. Saveant, J.-M., *ChemInform* **2008,** *39*, no-no.

124. Behr, A., *Carbon Dioxide as Chemical Feedstock*. WILEY-VCH Verlag GmbH & Co. KGaA: Weinheim, 2010.

125. Verdejo, B.; Aguilar, J.; García-España, E.; Gaviña, P.; Latorre, J.; Soriano, C.; Llinares, J. M.; Doménech, A., *Inorg. Chem.* **2006,** *45*, 3803-3815.

126. Balaraman, E.; Gunanathan, C.; Zhang, J.; Shimon, L. J. W.; Milstein, D., *Nature Chem.* **2011,** *3*, 609-614.

127. Frade, R. F.; Afonso, C. A., *Hum Exp Toxicol* **2010,** *29*, 1038-1054.

128. Plikhta, A.; Castillo-Molina, D. A.; Rieger, B., Ionic Liquids in Transition Metal-Catalyzed Hydroformylation Reactions. In *Topics in Organometallic Chemistry*, Springer Berlin Heidelberg 2014; pp 1-50.

129. Franke, R.; Selent, D.; Börner, A., *Chem Rev* **2012,** *112*, 5675-5732.

130. Dyson, P.; Tilmann, G., *Metal Catalysed Reactions in Ionic Liquids*. Springer2005; Vol. 29, p 246.

131. Haumann, M.; Riisager, A., *Chem Rev* **2008,** *108*, 1474-1497.

132. Welton, T., *Chem Rev* **1999,** *99*, 2071-2083.

133. Briggs, J. R.; Maher, J. M.; Harrison, A. M. Catalysts for producing 1,3-diols and/or 3-Hydroxyaldehydes, and processes for making and using same. US5225387-A, 1993.

134. Chauvin, Y.; Olivier, H.; Mussmann, L. Process for the hydroformylation of olefinic compounds. EP776880-A, 1997.

135. Keim, W.; Waffenschmidt, H.; Wasserscheid, P. Catalyst stabilization in distillation of products from homogeneous catalysis, e.g. hydroformylation, hydrogenation or oxidation, uses ionic liquid containing quaternary ammonium and/or phosphonium cation. DE19901524-A1, 2000.

136. Valkenberg, M.; Sauvage, E.; Castro-Moriera, C. P.; Hoelderich, W. F. WO 0132308A, 2000.

137. Bahrmann, H.; Bohnen, H. Method for producing aldehydes. EP1177163-B1, 2000.

138. Favre, F.; Commereuc, D.; Olivier-Bourbigou, H. Process for the hydroformylation of olefinically unsaturated compounds in a non-aqueous ionic solvent. US6617474; EP1241156-A1, 2002.

139. Favre, F.; Commereuc, D.; Olivier-Bourbigou, H.; Saussine, L. New non-aqueous ionic liquids, used as catalyst or constituent of transition metal catalyst, e.g. for 2-phase process, are (organic) ammonium salts of sulfonated or carboxylated triester of phosphorous acid. EP1182187-A1, 2002.

140. Hillebrand, G.; Hirschauer, A.; Commereuc, D.; Olivier-Bourbigou, H.; Saussine, L. Improved hydroformylation process with cobalt and/or rhodium based catalysts in a biphasic medium. EP1106595-A, 2004.

141. Bohnen, H.; Herwig, J.; Hoff, D.; Van Hal, R.; Wasserscheid, P.; Hal, R. V. Process for the preparation of aldehydes. EP1400504-A1, 2004.

142. Magna, L.; Olivier Bourbigou, H.; Saussine, L.; Kruger-Tissot, V.; Kruger, T. V. Improved hydroformylation process uses cobalt and-or rhodium-based catalyst dissolved in ionic non-aqueous solvent in which aldehydes are difficultly or not at all soluble. EP1352889-A1, 2003.

143. Magna, L.; Harry, S.; Olivier, B. H.; Saussine, L. Hydroformylation of monoolefin in liquid phase, comprises hydroformylation under pressure in the presence of a catalyst made of

a cobalt compound and a ligand e.g. pyridine compounds using a non-aqueous ionic liquid containing a salt. FR2903686-A1; FR2903686-B1, 2008.

144. Magna, L.; Saussine, L.; Proriol, D.; Olivier-Bourbigou, H. Hydroformylation of olefinically unsaturated compounds in liquid phase, comprises reaction in the presence of non-aqueous ionic liquid comprising a salt and a catalyst comprising a complex of cobalt and a ligand. FR2903687-A1; WO2008006951-A1, 2008.

145. Francio, G.; Klankermayer, J.; Leitner, W.; Schmitkamp, M.; Dianjun, C. Katalysatorzusammensetzung für die enantioselektive Katalyse. DE102007040333-A1, 2009.

146. Wasserscheid, P., *Chem. Unserer Zeit* **2003,** *37*, 52-63.

147. Davis, J. H., *Chem. Lett.* **2004,** *33*, 1072-1077.

148. Welton, T., *Coord. Chem. Rev.* **2004,** *248*, 2459-2477.

149. Plechkova, N. V.; Seddon, K. R., *Chem. Soc. Rev.* **2008,** *37*, 123-150.

150. Dupont, J.; Consorti, C. S.; Spencer, J., *J. Braz. Chem. Soc.* **2000,** *11*, 337-344.

151. Tominaga, K.; Sasaki, Y., *Chem. Lett.* **2004,** *33*, 14-15.

152. Tominaga, K.-i.; Sasaki, Y., *Catal. Commun.* **2000,** *1*, 1-3.

153. Tominaga, K.-i.; Sasaki, Y.; Hagihara, K.; Watanabe, T.; Saito, M., *Chem. Lett.* **1994,** *23*, 1391-1394.

154. Tominaga, K.-i.; Sasaki, Y., *J. Mol. Catal. A: Chem.* **2004,** *220*, 159-165.

155. Srivastava, V. K.; Eilbracht, P., *Catal. Commun.* **2009,** *10*, 1791-1795.

156. Tominaga, K.-i.; Sasaki, Y., *Stud. Surf. Sci. Catal.* **2004,** *153*, 227-232.

157. Tominaga, K., *Catal. Today* **2006,** *115*, 70-72.

158. Mura, M. G.; Luca, L. D.; Giacomelli, G.; Porcheddu, A., *Adv. Synth. Catal.* **2012,** *354*, 3180-3186.

159. Leitner, W., *Acc. Chem. Res.* **2002,** *35*, 746-756.

160. Leitner, W., *Chem. Unserer Zeit* **2003,** *37*, 32-38.

161. Osuna, A. B.; Serbanovic, A.; Nunes da Ponte, M.; Matsubara, H.; Ryu, I.; Dupont, J., Fluid Extraction. In *Green Separation Processes: Fundamentals and Applications*, Afonso, C. A. M.; Crespo, J. G., Eds. Wiley: Weinheim, 2006; pp 207-218.

162. Niessen, H. G.; Woelk, K., *Top. Curr. Chem.* **2007,** *276*, 69-110.

163. Pitter, S.; Dinjus, E.; Ionescu, C.; Maniut, C.; Makarczyk, P.; Patcas, F., *Top Organomet Chem* **2008,** *23*, 109-147.

164. Rathke, J. W.; Klingler, R. J.; Krause, T. R., *Organometallics* **1991,** *10*, 1350-1355.

165. Sellin, M. F.; Cole-Hamilton, D. J., *J Chem Soc Dalton* **2000**, 1681-1683.

166. Blanchard, L. A.; Hancu, D.; Beckman, E. J.; Brennecke, J. F., *Nature* **1999,** *399*, 28-29.

167. Scurto, A. M.; Aki, S. N. V. K.; Brennecke, J. F., *J. Am. Chem. Soc.* **2002,** *124*, 10276-10277.

168. Mellein, B. R.; Brennecke, J. F., *J. Phys. Chem. B* **2007,** *111*, 4837-4843.

169. The high-pressure phase equilibria of CO2 and ionic liquids have been studied by Scurto et al.; see: Ren W, Sensenich B, Scurto AM (2010) J Chem Thermodyn 42: 305-311

170. Blanchard, L. A.; Gu, Z.; Brennecke, J. F., *J. Phys. Chem. B* **2001,** *105*, 2437-2444.

171. Anthony, J. L.; Maginn, E. J.; Brennecke, J. F., *J. Phys. Chem. B* **2002,** *106*, 7315-7320.

172. Cadena, C.; Anthony, J. L.; Shah, J. K.; Morrow, T. I.; Brennecke, J. F.; Maginn, E. J., *J. Am. Chem. Soc.* **2004,** *126*, 5300-5308.

173. Scurto, A. M.; Hutchenson, K.; Subramaniam, B., Gas-Expanded Liquids: Fundamentals and Applications. In *Gas-Expanded Liquids and Near-Critical Media: Green Chemistry and Engineering*, Scurto, A. M.; Hutchenson, K.; Subramaniam, B., Eds. American Chemical Society: Washington, DC, 2009; Vol. 1006, pp 3-37.

174. Scurto, A. M.; Leitner, W., *Chem Commun* **2006**, 3681-3683.

175. Sellin, M. F.; Webb, P. B.; Cole-Hamilton, D. J., *Chem Commun* **2001**, 781-782.

176. Mercer, S. M.; Robert, T.; Dixon, D. V.; Jessop, P. G., *Catal Sci Technol* **2012,** *2*, 1315-1318.

177. Hintermair, U.; Francio, G.; Leitner, W., *Chem. Commun. (Cambridge, U. K.)* **2011,** *47*, 3691-3701.

178. Diao, Y.; Li, J.; Wang, L.; Yang, P.; Yan, R.; Jiang, L.; Zhang, H.; Zhang, S.

179. Scholten, J. D.; Dupont, J., *Organometallics* **2008,** *27*, 4439-4442.

180. Ali, M.; Gual, A.; Ebeling, G.; Dupont, J., *ChemCatChem* **2014,** *6*, 2224-2228.

181. Diez-Gonzalez, S.; Marion, N.; Nolan, S. P., *Chem. Rev. (Washington, DC, U. S.)* **2009,** *109*, 3612-3676.

182. Scholl, M.; Ding, S.; Lee, C. W.; Grubbs, R. H., *Org. Lett.* **1999,** *1*, 953-956.

183. Herrmann, W. A., *Angew. Chem., Int. Ed.* **2002,** *41*, 1290-1309.

184. Casin, C. S. J., *N-Heterocyclic Carbenes in Transition Metal Catalysis and Organocatalysis*. Springer Netherlands 2011; p 340.

185. Díez-González, S., *N-Heterocyclic Carbenes. From Laboratory Curiosities to Efficient Synthetic Tools*. Royal Society of Chemistry 2010; p 442.

186. Schaper, L.-A.; Hock, S. J.; Herrmann, W. A.; Kühn, F. E., *Angew. Chem., Int. Ed.* **2013,** *52*, 270-289.

187. Chang, W.-C.; Chen, H.-S.; Li, T.-Y.; Hsu, N.-M.; Tingare, Y. S.; Li, C.-Y.; Liu, Y.-C.; Su, C.; Li, W.-R., *Angew. Chem., Int. Ed.* **2010,** *49*, 8161-8164.

188. Velazquez, H. D.; Verpoort, F., *Chem. Soc. Rev.* **2012,** *41*, 7032-7060.

189. Melaiye, A.; Simons, R. S.; Milsted, A.; Pingitore, F.; Wesdemiotis, C.; Tessier, C. A.; Youngs, W. J., *J. Med. Chem.* **2004,** *47*, 973-977.

190. Rouhi, A. M., *Chem. Eng. News* **2002,** *80*, 29-38.

191. Gierz, V.; Urbanaite, A.; Seyboldt, A.; Kunz, D., *Organometallics* **2012,** *31*, 7532-7538.

192. Wang, C.-Y.; Fu, C.-F.; Liu, Y.-H.; Peng, S.-M.; Liu, S.-T., *Inorg. Chem.* **2007,** *46*, 5779–5786.

193. Crudden, C. M.; Allen, D. P., *Coord. Chem. Rev.* **2004,** *248*, 2247-2273.

194. Chang, C.-F.; Cheng, Y.-M.; Chi, Y.; Chiu, Y.-C.; Lin, C.-C.; Lee, G.-H.; Chou, P.-T.; Chen, C.-C.; Chang, C.-H.; Wu, C.-C., *Angew. Chem., Int. Ed.* **2008,** *47*, 4542-4545.

195. Reindl, S. A.; Pöthig, A.; Drees, M.; Bechlars, B.; Herdtweck, E.; Herrmann, W. A.; Kühn, F. E., *Organometallics* **2013,** *32*, 4082-4091.

196. Boydston, A. J.; Bielawski, C. W., *Dalton Trans.* **2006**, 4073-4077.

197. Hofmann, P.; Brill, M., NHCP Ligands for Catalysis. In *Molecular Catalysts*, Wiley-VCH Verlag GmbH & Co. KGaA2014; pp 207-234.

198. Pugh, D.; Danopoulos, A. A., *Coord. Chem. Rev.* **2007,** *251*, 610-641.

199. Gaillard, S.; Renaud, J.-L., *Dalton Trans.* **2013,** *42*, 7255-7270.

200. Morales-Morales, D.; Jensen, C. G. M., *The Chemistry of Pincer Compounds*. Elsevier Science B.V.: Amsterdam, 2007; p 450.

201. Chianese, A. R.; Shaner, S. E.; Tendler, J. A.; Pudalov, D. M.; Shopov, D. Y.; Kim, D.; Rogers, S. L.; Mo, A., *Organometallics* **2012,** *31*, 7359-7367.

202. Boom, M. E. v. d.; Milstein, D., *Chem. Rev.* **2003,** *103*, 1759-1792.

203. Gelman, D.; Musa, S., *ACS Catalysis* **2012,** *2*, 2456-2466.

204. van der Vlugt, J. I.; Reek, J. N. H., *Angew. Chem.* **2009,** *121*, 8990-9004.

205. Tian, R.; Ng, Y.; Ganguly, R.; Mathey, F., *Organometallics* **2012,** *31*, 2486-2488.

206. Venkanna, G. T.; Tammineni, S.; Arman, H. D.; Tonzetich, Z. J., *Organometallics* **2013,** *32*, 4656-4663.

207. Dixon, L. S. H.; Hill, A. F.; Sinha, A.; Ward, J. S., *Organometallics* **2014,** *33*, 653-658.

208. Lee, H. M.; Zeng, J. Y.; Hu, C.-H.; Lee, M.-T., *Inorg. Chem.* **2004,** *43*, 6822-6829.

209. Hahn, F. E.; Jahnke, M. C.; Pape, T., *Organometallics* **2006,** *25*, 5927-2936.

210. Plikhta, A.; Rieger, B., Benzimidazolium-based NHC-pincer ligands. In *245th ACS National Meeting & Exposition*: New Orleans, United States, 2013.

211. The grey numbers indicate the size of the metallacylce, as refered in the text.

212. Tsvetkov, E. N.; Tkachenko, S. E.; Yarkevich, A. N., *Zurnal obscej chimii* **1988,** *58*, 531-536.

213. Salem, H.; Schmitt, M.; Herrlich, U.; Kühnel, E.; Brill, M.; Nägele, P.; Bogado, A. L.; Rominger, F.; Hofmann, P., *Organometallics* **2013,** *32*, 29-46.

214. Busacca, C. A.; Raju, R.; Grinberg, N.; Haddad, N.; James-Jones, P.; Lee, H.; Lorenz, J. C.; Saha, A.; Senanayake, C. H., *J. Org. Chem.* **2008,** *73*, 1524-1531.

215. Griffin, S.; Heath, L.; Wyatt, P., *Tetrahedron Lett.* **1998,** *39*, 4405-4406.

216. Imamoto, T.; Kikuchi, S.-i.; Miura, T.; Wada, Y., *Org. Lett.* **2001,** *3*, 87-90.

217. El Moll, H.; Sémeril, D.; Matt, D.; Toupet, L., *Eur. J. Org. Chem.* **2010,** *2010*, 1158-1168.

218. Smith, E. A. S.; Molev, G.; Botoshansky, M.; Gandelman, M., *Chem. Commun. (Cambridge, U. K.)* **2011,** *47*, 319-321.

219. Labrue, F.; Pons, B.; Ricard, L.; Marinetti, A., *J. Organomet. Chem.* **2005,** *690*, 2285-2290.

220. Nilsson, B. L.; Kiessling, L. L.; Raines, R. T., *Org. Lett.* **2001,** *3*, 9-12.

221. Rahman, M. S.; Oliana, M.; Hii, K. K., *Tetrahedron: Asymmetry* **2004,** *15*, 1835-1840.

222. Lemaire, M.; Berthod, M.; Favre-Réguillon, A.; Mohamad, J.; Mignani, G.; Docherty, G., *Synlett* **2007,** *2007*, 1545-1548.

223. Aberdeen Allen, J.; Ma, L.; Lin, W., *Tetrahedron Lett.* **2002,** *43*, 3707-3710.

224. Li, Y.; Das, S.; Zhou, S.; Junge, K.; Beller, M., *J. Am. Chem. Soc.* **2012,** *134*, 9727-9732.

225. Gründemann, S.; Kovacevic, A.; Albrecht, M.; Faller, J. W.; Crabtree, R. H., *J. Am. Chem. Soc.* **2002,** *124*, 10473-10481.

226. Song, G.; Li , X.; Song, Z.; Zhao, J.; Zhang, H., *Chem. – Eur. J.* **2009,** *15*, 5535-5544.

227. Wolf, J.; Labande, A.; Daran, J.-C.; Poli, R., *Eur. J. Inorg. Chem.* **2008**, 3024-3030.

228. Arnold, P. L.; Pearson, S., *Coord. Chem. Rev.* **2007,** *251*, 596-609.

229. Lebel, H.; Janes, M. K.; Charette, A. B.; Nolan, S. P., *J. Am. Chem. Soc.* **2004,** *126*, 5046-5047.

230. Azua, A.; Sanz, S.; Peris, E., *Chem. – Eur. J.* **2011,** *17*, 3963-3967.

231. Coumbe, T.; Lawrence, N. J.; Muhammad, F., *Tetrahedron Lett.* **1994,** *35*, 625-628.

232. Chikashita, H.; Nishida, S.; Miyazaki, M.; Morita, Y.; Itoh, K., *Bull. Chem. Soc. Jpn.* **1987** *60*, 737-746.

233. Montgrain, F.; Ramos, S. M.; Wuest, J. D., *J. Org. Chem.* **1988,** *53*, 1489-1492.

234. Brunet, P.; Wuest, J. D., *Can. J. Chem.* **1996,** *74*, 689-696.

235. Mayr, M.; Buchmeiser, M. R., *Macromol. Rapid Commun.* **2004,** *25*, 231-236.

236. Schwarz, D. E.; Cameron, T. M.; Hay, P. J.; Scott, B. L.; Tumas, W.; Thorn, D. L., *Chem. Commun. (Cambridge, U. K.)* **2005**, 5919-5921.

237. Thorn, D.; Tumas, W.; Hay, J. P.; Schwarz, D.; Cameron, T. M. Method and System for hydrogen Evolution and Storage. WO 2006/009630 A2, 26 January, 2006.

238. Benhamou, L.; Chardon, E.; Lavigne, G.; Bellemin-Laponnaz, S. p.; César, V., *Chem. Rev. (Washington, DC, U. S.)* **2011,** *111*, 2705-2733.

239. Bildstein, B.; Malaun, M.; Kopacka, H.; Ongania, K.-H.; Wurst, K., *J. Organomet. Chem.* **1999,** *572*, 177-187.

240. Frech, C. M.; Shimon, L. J. W.; Milstein, D., *Helv. Chim. Acta* **2006,** *89*, 1730-1739.

241. Swatloski, R. P.; Holbrey, J. D.; Rogers, R. D., *Green Chem.* **2003,** *5*, 361-363.

242. Huddleston, J. G.; Visser, A. E.; Reichert, W. M.; Willauer, H. D.; Broker, G. A.; Rogers, R. D., *Green Chem.* **2001,** *3*, 156-164.

243. Adams, J. J.; Arulsamy, N.; Roddick, D. M., *Organometallics* **2009,** *28*, 1148-1157.

244. Albinati, A.; Chaloupka, S.; Eckert, J.; Venanzi, L. M.; Wolfer, M. K., *Inorg. Chim. Acta* **1997,** *259*, 305-316.

245. Ho, H.-A.; Manna, K.; Sadow, A. D., *Angew. Chem.* **2012,** *124*, 8735-8738.

246. Morales-Morales, D.; Redón, R.; Wang, Z.; Lee, D. W.; Yung, C.; Magnuson, K.; Jensen, C. M., *Can. J. Chem.* **2001,** *79*, 823-829.

247. Kloek, S. M.; Heinekey, D. M.; Goldberg, K. I., *Organometallics* **2006,** *25*, 3007-3011.

248. Çelenligil-Çetin, R.; Watson, L. A.; Guo, C.; Foxman, B. M.; Ozerov, O. V., *Organometallics* **2005,** *24*, 186-189.

249. Huang, K.-W.; Grills, D. C.; Han, J. H.; Szalda, D. J.; Fujita, E., *Inorg. Chim. Acta* **2008,** *361*, 3327-3331.

250. Feller, M.; Ben-Ari, E.; Gupta, T.; Shimon, L. J. W.; Leitus, G.; Diskin-Posner, Y.; Weiner, L.; Milstein, D., *Inorg. Chem.* **2007,** *46*, 10479-10490.

251. Elschenbroich, C., *Organometallchemie*. 4 ed.; Teubner Verlag: Wiesbaden, 2003; p 756.

252. Cid, J.; Carbó, J. J.; Fernández, E., *Chem. – Eur. J.* **2012,** *18*, 1512-1521.

253. Takaya, J.; Kirai, N.; Iwasawa, N., *J. Am. Chem. Soc.* **2011,** *133*, 12980-12983.

254. Zhang, L.; Zuo, Z.; Wan, X.; Huang, Z., *J. Am. Chem. Soc.* **2014,** *136*, 15501-15504.

255. Obligacion, J. V.; Chirik, P. J., *J. Am. Chem. Soc.* **2013,** *135*, 19107-19110.

256. Bruneau, C.; Dixneuf, P. H., *Angew. Chem., Int. Ed.* **2006,** *45*, 2176-2203.

257. Sun, C.; Liu, M.; Sun, H.; Hang, F.; Sun, N.; Chen, D., *Int. J. Quantum Chem.* **2015,** *115*, 59-67.

258. Ruddy, A. J.; Mitton, S. J.; McDonald, R.; Turculet, L., *Chem. Commun. (Cambridge, U. K.)* **2012,** *48*, 1159-1161.

259. Wang, Z.; Eberhard, M. R.; Jensen, C. M.; Matsukawa, S.; Yamamoto, Y., *J. Organomet. Chem.* **2003,** *681*, 189-195.

260. Solé, D.; Solans, X.; Font-Bardia, M., *Dalton Trans.* **2007**, 4286.

261. Poverenov, E.; Gandelman, M.; Shimon, L. J. W.; Rozenberg, H.; Ben-David, Y.; Milstein, D., *Chem. – Eur. J.* **2004,** *10*, 4673-4684.

262. Schneider, N.; César, V.; Bellemin-Laponnaz, S.; Gade, L. H., *Organometallics* **2005,** *24*, 4886-4888.

263. Aleksanyan, D. V.; Kozlov, V. A.; Shevchenko, N. E.; Nenajdenko, V. G.; Vasil'ev, A. A.; Nelyubina, Y. V.; Ananyev, I. V.; Petrovskii, P. V.; Odinets, I. L., *J. Organomet. Chem.* **2012,** *711*, 52-61.

264. Aleksanyan, D. V.; Kozlov, V. A.; Nelyubina, Y. V.; Lyssenko, K. A.; Puntus, L. N.; Gutsul, E. I.; Shepel, N. E.; Vasil'ev, A. A.; Petrovskii, P. V.; Odinets, I. L., *Dalton Trans.* **2011,** *40*, 1535-1546.

265. Kozlov, V. A.; Aleksanyan, D. V.; Nelyubina, Y. V.; Lyssenko, K. A.; Gutsul, E. I.; Vasil'ev, A. A.; Petrovskii, P. V.; Odinets, I. L., *Dalton Trans.* **2009**, 8657.

266. Kozlov, V. A.; Aleksanyan, D. V.; Nelyubina, Y. V.; Lyssenko, K. A.; Vasil'ev, A. A.; Petrovskii, P. V.; Odinets, I. L., *Organometallics* **2010,** *29*, 2054-2062.

267. Gu, S.; Xu, H.; Zhang, N.; Chen, W., *Chem. – Asian J.* **2010,** *5*, 1677-1686.

268. Piers, W. E., *Organometallics* **2011,** *30*, 13-16.

269. Poverenov, E.; Efremenko, I.; Frenkel, A. I.; Ben-David, Y.; Shimon, L. J. W.; Leitus, G.; Konstantinovski, L.; Martin, J. M. L.; Milstein, D., *Nature* **2008,** *455*, 1093-1096.

270. Poverenov, E.; Gandelman, M.; Shimon, L. J. W.; Rozenberg, H.; Ben-David, Y.; Milstein, D., *Organometallics* **2005,** *24*, 1082-1090.

271. Liu, X.; Braunstein, P., *Inorg. Chem.* **2013,** *52*, 7367-7379.

272. Yoo, K. S.; O'Neill, J.; Sakaguchi, S.; Giles, R.; Lee, J. H.; Jung, K. W., *J. Org. Chem.* **2010,** *75*, 95-101.

273. Fogler, E.; Balaraman, E.; Ben-David, Y.; Leitus, G.; Shimon, L. J. W.; Milstein, D., *Organometallics* **2011,** *30*, 3826-3833.

274. Vabre, B.; Canac, Y.; Duhayon, C.; Chauvin, R.; Zargarian, D., *Chem. Commun. (Cambridge, U. K.)* **2012,** *48*, 10446-10448.

275. Fuchs, D.; Rousseau, G.; Diab, L.; Gellrich, U.; Breit, B., *Angew. Chem., Int. Ed.* **2012,** *51*, 2178-2182.

276. Kaim, W., *Eur. J. Inorg. Chem.* **2012,** *2012*, 343-348.

277. van der Vlugt, J. I., *Eur. J. Inorg. Chem.* **2012,** *2012*, 363-375.

278. Grützmacher, H., *Angew. Chem., Int. Ed.* **2008,** *47*, 1814-1818.

279. Becker, J.; Modl, T.; Gessner, V. H., *Chem. – Eur. J.* **2014,** *20*, 11295-11299.

280. Friedrich, A.; Drees, M.; Schmedt auf der Günne, J.; Schneider, S., *J. Am. Chem. Soc.* **2009,** *131*, 17552-17553.

281. Plikhta, A.; Pöthig, A.; Herdtweck, E.; Rieger, B., *Inorg. Chem.* **2015,** *54*, 9517-9528.

282. Valyaev, D. A.; Filippov, O. A.; Lugan, N.; Lavigne, G.; Ustynyuk, N. A., *Angew. Chem. Int. Ed.* **2015,** *54*, 6315-6319.

283. Chiu, P. L.; Lee, H. M., *Organometallics* **2005,** *24*, 1692-1702.

284. Crabtree, R. H., *The Organometallic Chemistry of the Transition Metals*. forth ed.; John Wiley & Sons, Inc.2005; p 546.

285. APEX suite of crystallographic software. APEX 2 Version 2008.4. Bruker AXS Inc.: Madison, Wisconsin, USA, **2008**.

286. SAINT Version 7.56a and SADABS Version 2008/1. Bruker AXS Inc.: Madison, Wisconsin, USA, **2008**.

287. Sheldrick, G. M., "**SHELXS-97**", Program for Crystal Structure Solution, Göttingen, **1997**.

288. Sheldrick, G. M.: "**SHELXL-97**", University of Göttingen, Göttingen, Germany, **1997**.

289. Huebschle, C. B.; Sheldrick, G. M.; Dittrich, B.; "**SHELXLE**", *J. Appl. Cryst.* **2011,** *44*, 1281-1284.

290. International Tables for Crystallography: Vol. C, Tables 6.1.1.4 (pp. 500-502), 4.2.6.8 (pp. 219-222), and 4.2.4.2 (pp. 193-199), Wilson, A. J. C., Ed., Kluwer Academic Publishers, Dordrecht, The Netherlands, **1992**.

291. Spek, A. L.: "**PLATON**", A Multipurpose Crystallographic Tool, Utrecht University, Utrecht, The Netherlands, **2010**.

292. Lawrence, N. J.; Liddle, J.; Jackson, D., *J. Chem. Soc., Perkin Trans. 1* **2002**, 2260-2267.

293. Tucker, C. E.; Davidson, J.; Knochel, P., *J. Org. Chem.* **1992,** *57*, 3482-3485.

294. Jang, H.; Zhugralin, A. R.; Lee, Y.; Hoveyda, A. H., *J. Am. Chem. Soc.* **2011,** *133*, 7859-7871.

295. Pereira, S.; Srebnik, M., *J. Am. Chem. Soc.* **1996,** *118*, 909-910.

296. Peters, M.; Breinbauer, R., *Tetrahedron Lett.* **2010,** *51*, 6622-6625.

297. Tiecco, M.; Tingoli, M.; Testaferri, L.; Bartoli, D.; Chianelli, D., *Tetrahedron* **1989,** *45*, 2857-2868.

298. Huynh, H. V.; Yuan, D.; Han, Y., *Dalton Trans.* **2009**, 7262-7268.

299. Wolf, J.; Labande, A.; Daran, J.-C.; Poli, R., *J. Organomet. Chem.* **2006,** *691*, 433-443.

300. Wolf, J.; Labande, A.; Natella, M.; Daran, J.-C.; Poli, R., *J. Mol. Catal. A: Chem.* **2006,** *259*, 205-212.

301. Riener, K.; Bitzer, M. J.; Pöthig, A.; Raba, A.; Cokoja, M.; Herrmann, W. A.; Kühn, F. E., *Inorg. Chem.* **2014,** *53*, 12767-12777.

302. Forrest, S. J. K.; Clifton, J.; Fey, N.; Pringle, P. G.; Sparkes, H. A.; Wass, D. F., *Angew. Chem.* **2015,** *127*, 2251-2255.